Formalization, Analysis, and Sampled-Data Design of Hybrid Integrator-Gain Systems

Formalization, Analysis, and Sampled-Data Design of Hybrid Integrator-Gain Systems

Bardia Sharif

The work described in this thesis was carried out at the Eindhoven University of Technology and is part of the project "From PID to Complex Order Control (CLOC)" with project number 16335, which is financed by the Netherlands orgnization for scientific research (NWO).

A catalogue record is available from the Eindhoven University of Technology Library.
ISBN: 978-90-386-5693-9

Typeset by the author using the pdf LaTeX documentation system.
Cover design: Negar Amani, Bardia Sharif
Reproduction: Ipskamp Printing, Enschede, the Netherlands

Formalization, Analysis, and Sampled-Data Design of Hybrid Integrator-Gain Systems

Proefschrift

ter verkrijging van de graad van doctor aan de
Technische Universiteit Eindhoven, op gezag van de
rector magnificus prof.dr.ir. F.P.T. Baaijens, voor een
commissie aangewezen door het College voor
Promoties, in het openbaar te verdedigen
op Dinsdag 28 Maart 2023 om 16.00 uur

door

Bardia Sharif

geboren te Esfahan, Iran

Dit proefschrift is goedgekeurd door de promotoren en de samenstelling van de promotiecommissie is als volgt:

voorzitter:	prof.dr.ir. P.D. Anderson
1^e promotor:	prof.dr.ir. M.F. Heertjes
2^e promotor:	prof.dr.ir. W.P.M.H. Heemels
co-promotor:	prof.dr. H. Nijmeijer
leden:	prof.dr. S. Weiland
	prof.dr. L. Zaccarian (LAAS-CNRS and University of Trento)
	prof.dr. A. R. Teel (University of California, Santa Barbara)
	dr. S. H. Hossein Nia Kani (Technische Universiteit Delft)

Het onderzoek dat in dit proefschrift wordt beschreven is uitgevoerd in overeenstemming met de TU/e Gedragscode Wetenschapsbeoefening.

Dedicated to Baba, Maman, Negar and Khashayar

Summary

Formalization, Analysis, and Sampled-Data Design of Hybrid Integrator-Gain Systems

Control engineering is one of the main enablers of technological innovations that are at the heart of our modern way of life. Some example technologies include wafer scanners that are used for manufacturing electronic chips, satellites orbiting the earth, large-scale chemical processes that are used for production of food, pharmaceuticals, and energy, as well as autonomous vehicles and surgical robots. As a result, automatic control is a ubiquitous technology in the contemporary world. Over the years, the backbone of control engineering has become the Linear Time-Invariant (LTI) framework, which has formed an essential part in many industries. However, as powerful as LTI control techniques are, they come with fundamental limitations, thereby limiting the performance of many engineered systems. In view of the ever increasing performance expectations of high-tech engineering systems, nonlinear and hybrid control strategies have gained attention as potential solutions for realizing performance beyond the limitations of LTI control. In this dissertation, a particular, recently introduced, class of hybrid controllers called hybrid integrator-gain systems (HIGS) are considered, which have an operational philosophy inspired by reset integrators. As in the case of reset integrators, HIGS have phase advantages over LTI integrators that can be potentially exploited to realize performance objectives that are unattainable with LTI control. Contrary to reset integrators, HIGS achieve this advantage by generating continuous control signals which, depending on the engineering application under consideration, may be highly beneficial. The work presented in this thesis contributes to the study of HIGS and HIGS-controlled systems with respect to various topics, as summarized in the following paragraphs.

To formally study HIGS and HIGS-controlled systems, in this thesis, we present a new class of discontinuous dynamical systems called extended projected dynamical systems (ePDS), based on extensions of so called projected dynamical systems (PDS). This new ePDS framework, naturally captures (among others) the design

philosophy and the working principle of HIGS and is therefore used for mathematical formalization of HIGS-controlled systems. Furthermore, we establish the important property of well-posedness in the sense of existence and forward completeness of solutions for HIGS-controlled systems, thereby laying down an appropriate mathematical groundwork for formal studies of HIGS-controlled systems. We also establish conditions under which the introduced ePDS are equivalent to other variants of PDS thereby enabling the transfer of system theoretical properties and tools from one system class to the other. We provide examples of the transfer system theoretical results for properties such as (incremental) stability for ePDS in general and use the established equivalence to propose conditions that can be used to verify the important property of incremental stability of HIGS-controlled systems, in particular.

In practice, automatic control is utilized for the control of physical systems which naturally exhibit continuous time (CT) dynamics. Controllers are designed to stabilize, regulate and optimize the behavior of such systems. Nowadays, the implementation of these controllers are done in a digital environment and thus in discrete time (DT). Consequently, the overall control system is a sampled-data (SD) system consisting of the CT plant dynamics and DT controller dynamics. As another part of this thesis, we consider the analysis of sampled-data HIGS-controlled systems. Particularly, we present DT versions of HIGS which preserve the main philosophy and working principle of CT HIGS. Additionally, stability criteria are presented that can be used to certify stability of DT and SD HIGS-controlled systems based on both frequency domain response data, as well as linear matrix inequalities (LMIs). While the frequency-domain results can be more easily applied in practice, the LMI-based stability analysis provides one with less conservative conclusions regarding stability.

To illustrate the strength of HIGS and HIGS-based control design, this thesis also investigates whether it is possible to obtain performance beyond fundamental limitations of LTI control by utilizing HIGS-based control. In particular, we consider various scenarios wherein it is impossible to obtain certain performance objectives using any LTI controller. In each case, we ask the question whether it would be possible to achieve such objectives by HIGS-based control, to which an affirmative answer is found. In fact, we show that it is possible to overcome all fundamental limitations of LTI control which have been previously overcome by other hybrid/nonlinear control strategies, using HIGS-based control.

At last, in this dissertation results are also presented of HIGS-based control for industrial application, in particular for active vibration isolation. Vibration isolation systems are widely used in high-precision mechatronic systems examples of which include wafer scanners and electron microscopes. In such applications linear band-pass filters are widely used since they allow for active isolation in a limited frequency band while avoiding isolation performance deterioration outside this band. In this thesis, we present a novel HIGS-based bandpass filter that can be used in such applications to enable superior active vibration isolation as

well as improved transient performance. The effectiveness of the novel control design is shown by means of experimental results obtained from an industrial active vibration isolation system.

Contents

1 Introduction

In this introductory chapter, we start by motivating the work presented in this thesis. In particular, we start by noting the important role of automatic control as an indispensable technology at the heart of many of the innovations that are crucial in keeping up with socioeconomic needs of the modern society. Subsequently, the widespread utilization of linear time-invariant control techniques in different industries is recalled, while noting their main strengths and weaknesses. The latter is then used to motivate the use of hybrid control strategies, and in particular, hybrid integrator gain-systems, which form the central focus of the work presented in this dissertation. Subsequently, an overview of the research objectives pursued in this work is provided. Upon stating the main objectives of the thesis, we describe the contributions of this work towards addressing them. Lastly, we end this chapter by providing an outline of the remainder of the thesis.

1.1 Automatic Control: A Vital Technology in an Increasingly Complex World

Throughout history, systems and control engineering has played a major role in many technological innovations and breakthroughs made by mankind. In particular, the first known examples of control systems are water clocks built in ancient Egypt, as shown in Fig. 1.1a, and date back to 1500BC [87]. Centuries later, in 1788, James Watt built one of the first well-known feedback control systems, as shown in Fig. 1.1b known as the flyball governor, used to regulate the speed of the celebrated steam engine. Nowadays, automatic control is a ubiquitous technology, used to stabilize, regulate and optimize the operation of many of the processes

(a) **(b)**

Figure 1.1. (a) an Egyptian water clock, **(b)** the flyball governor used for speed regulation of the steam engine.

and devices that are key to modern life [91]. Some examples, as shown in Fig. 1.2 include smart agriculture used to ensure efficient and sustainable food production, smart power grids that generate and distribute energy, space crafts used for space exploration, lithography machines that are utilized in the production of integrated circuits, and many more. In the contemporary world, technological progress remains a strong determining factor for economic growth and plays a crucial role in addressing current worldwide problems such as climate change and ageing populations [32, 53, 101]. Concurrently, many societal, economical and technological trends are pushing the performance requirements (accuracy, throughput and resilience) for future technologies to unprecedented levels, leading to increasing levels of complexity in engineered systems surrounding us. As a result, automatic control, being the hidden technology that ensures desired operation of the engineered systems around us [10], is expected to play a crucial role in fulfilment of the needs of modern society.

1.2 Linear Time-Invariant Control

Over the years, the backbone of industrial control remains to be Linear Time-Invariant (LTI) control [46]. Several LTI control techniques have been developed ranging from the well-known and widely used proportional-integral-derivative (PID) control [46, 157], to the more advanced H_∞-optimal control techniques [49, 127, 138] making LTI control the bread and butter of automatic control [157]. The widespread adoption of LTI control by industry can be attributed to, among others, the possibility of designing LTI controllers by means of easy to use and computationally efficient loop-shaping techniques [46, 127], which can be done

(a)

(b)

(c)

(d)

Figure 1.2. Some examples of modern process and devices that rely on automatic control: **(a)** smart farming © [2022] iberdrola.com, **(b)** Power grid © [2022] interestingengineering.com, **(c)** Space crafts used for space exploration © [2022] spacex.com, **(d)** lithography machines used in the prodcution of integrated circuits © [2022] ASML.com

based on easy to measure and accurate frequency-domain data [133]. In addition, vast industrial experiences have been acquired with respect to the application of LTI techniques in different industrial sectors [133, 136].

In spite of the widespread use of LTI control techniques in different industries, all LTI controllers are bound to fundamental limitations [21, 48, 100, 119, 127], which in turn result in design trade-offs with compromising implications for performance both in frequency-domain as well as in time-domain. As a first limitation of LTI control, consider the "waterbed effect" due to Bode's sensitivity integral [47]. Due to this limitation, while low frequency disturbance suppression properties of a linear control system can be enhanced by inclusion of integral action or increasing the bandwidth of the controller, this will necessarily deteriorate sensitivity of the system to high frequency disturbances and noise (see Fig.1.3 for a graphical illustration). Another limitation of LTI control is the so-called Bode gain-phase

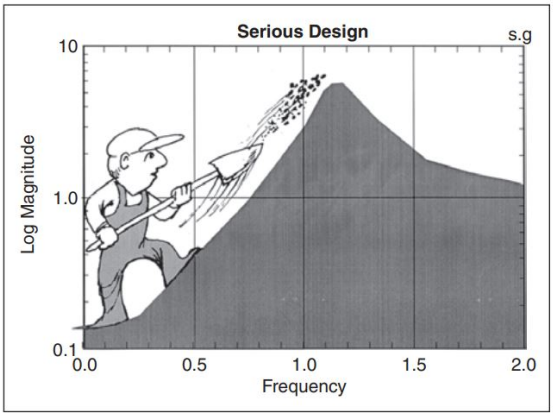

Figure 1.3. Reduction of sensitivity at low frequencies comes at the cost of inevitable increase of sensitivity at high frequencies (picture taken from [132]).

relationship [118], due to which for a linear, minimum phase and stable system, the phase properties of the system are directly related to the slope of the magnitude response. This in turn poses restrictions on the achievable linear control designs, as phase and gain properties cannot be tuned independently. An integrator is a good example of a linear control element subject to this performance trade-off. It is common to use an integrator to ensure a zero steady-state tracking error in the presence of (constant) disturbances. However, this typically results in overshoot in the step-response of the system and therefore a decreased transient performance [6]. To understand why this is the case, consider the closed-loop system in Fig. 1.4. Here, the output $y(t)$ of the system P to be controlled, at time t, is subtracted from a desired reference signal $r(t)$, resulting in the error $e(t)$, which is fed back to the controller C that in turn produces an output $u(t)$ to steer $y(t)$ towards $r(t)$, to

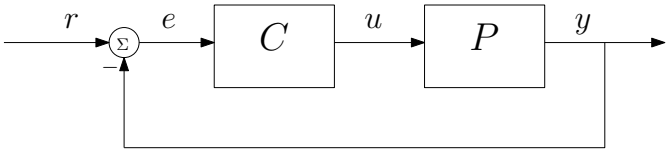

Figure 1.4. Linear closed-loop system configuration.

obtain a tracking error $e(t) = 0$, when $t \to \infty$. Typically, the controller C contains an integrator in order to ensure a steady-state tracking error $e(t) = 0$, when the reference signal $r(t)$ is constant. The integrator builds up a buffer of the integrated error in the time domain, i.e., it "sums" error over time and stores it in its state. In particular, when a step-reference is applied to such a system, the integral buffer builds up throughout the time of rise. At the moment when there is a sign change in the error e, the buffer still enforces an integrator action directed away from the reference as it is not emptied instantaneously (the integrator still has the summed error stored in its state). A schematic representation of this scenario is given in Fig. 1.5. The green dashed surfaces depict areas where the error $e = r - y$ is positive valued, whereas the orange dotted surfaces depict areas where the error is negative valued. The surface represents the buffer of the integrator, which, as can be seen in the bottom half of the graph, does not change sign when the error does. The delayed behaviour of the integral buffer is due to the $-90°$ phase of the integrator, which is inevitably present due to the aforementioned Bode's gain-phase relation. As a result of this $90°$ of phase lag of an integrator, integral control can result in overshoot in the step-response of the closed-loop system. In addition to its detrimental effects on transient performance, frequency domain characteristics of the closed-loop system such as bandwidth are also limited by the $90°$ phase lag of a linear integrator.

Due to the fundamental limitations of LTI control, there are inevitable performance compromising design trade-offs, when designing LTI controllers.

1.3 Hybrid and Nonlinear Control

In view of the ever-increasing demands on the performance of modern engineering systems, and, as a potential solution to realize performance beyond the limitations of LTI control, hybrid and nonlinear control strategies have received attention by the systems and control community [82, 149]. This has led to the development of control elements such as switching controllers [43, 69], variable gain controllers (VGC) [70, 80], split-path nonlinear integrators (SPANI) [45, 151], filtered split-path nonlinear integrators (F-SPANI) [126, 146], sliding mode controllers [3, 116, 137], and reset controllers [2, 19, 31, 35, 60, 107, 115, 155]. In fact, as shown in [18, 81, 156] some of these control strategies have been shown to overcome some

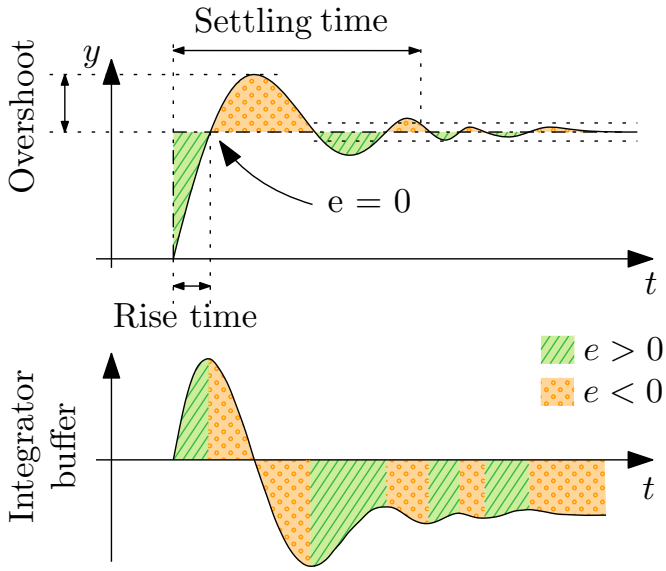

Figure 1.5. Transient performance with linear integral action.

of the fundamental limitations of LTI control. In this thesis, the focus is on a particular class of hybrid control elements, referred to as *hybrid integrator-gain systems* (HIGS). The underlying philosophy of HIGS is inspired by the main ideas that led to reset control [12], which will be shortly recalled in Section 1.4 below.

1.4 Reset Control

A particularly interesting hybrid control strategy, aiming to realize performance beyond the limitations of LTI control is reset control [1, 12, 31, 104]. Reset control started with the introduction of the Clegg integrator [31], being an integrator that resets its state to zero upon zero input crossings. As a result, the input and output of a Clegg integrator have the same sign at all times, and therefore, the output generated by the Clegg integrator always pushes the system to be controlled towards zero error, which is not the case in the case of an LTI integrator (see Fig. 1.5 and related discussion). As a result of this construction, the describing function [51] of a Clegg integrator has similar magnitude characteristics as an LTI integrator, while having 38.15° of phase lag (as opposed to the 90° of phase lag in the LTI case). The development of reset control progressed with generalizations including the first-order reset element [19, 29, 79, 89, 156], the second-order reset element [60], and, generalized fractional order reset elements [115]. Extensive research on reset control systems has led to various fruitful results regarding

stability analysis [14, 19, 27, 56, 103, 104, 154], beating fundamental time-domain performance limitations of LTI control [18, 156], hybrid formulations [155], and experimental demonstration of reset control systems achieving improved performance [13, 15, 16, 55, 60, 71, 72, 115, 153].

Generally speaking, the favorable phase properties of reset control systems suggest the possibility of designing a controller capable of achieving the required bandwidth, with a reduced gain at high frequencies. However, these favorable properties of reset control systems are achieved by hard resets of the controller's state, thereby generating discontinuous control signals. Such control signals can potentially have negative impact on performance by excitation of high-frequency (un-modelled) dynamics of the plant. As a result, recently in the literature, there have been efforts to propose hybrid/nonlinear control elements that offer the same phase advantage as reset control systems while avoiding the need for hard resets of the state of the controller. This has led to the recent development of soft-reset elements [20, 94, 135], as well as the creation of HIGS [37], the latter being shortly discussed in Section 1.5 below.

1.5 Hybrid Integrator-Gain Systems

Hybrid integrator-gain systems (HIGS) were introduced in [37], with the aim of proposing a nonlinear integrator with the same phase advantage of reset controllers while avoiding the need for discontinuous control signals. In particular, HIGS are designed to primarily operate as a linear integrator, while producing input-output trajectories that are constrained to a particular sector, such that the input and output of a HIGS element have the same sign at all times, which in turn results in inheriting the phase advantage of reset control elements. More specifically, a HIGS element acts as a linear integrator as long as its input-output pair satisfies the above-mentioned sector boundedness property. At moments when the integrator dynamics would result in trajectories that tend to violate this sector constraint, HIGS switch to another mode of operation such that the resulting trajectories remain on the boundary of the sector. This switching is done in a manner that ensures the sector boundedness of the input-output pair of a HIGS element, while generating *continuous* control signals as opposed to the *discontinuous* ones generated by a reset controller. In Fig. 1.6, typical responses of a linear integrator, a reset integrator and a HIGS element to a sinusoidal input are shown.

As it can be seen in Fig. 1.6, while the output of the linear integrator would result in pushing the system in the wrong direction (away from zero error), both the reset controller and the HIGS element produce outputs with the same sign as the input, at all times, and thus towards zero error. However, while the reset controller achieves this by resetting its output to zero as soon as the input crosses zero, and, therefore, with a discontinuous control signal, a HIGS element does so while generating a continuous output. Additionally, it is worth noting that,

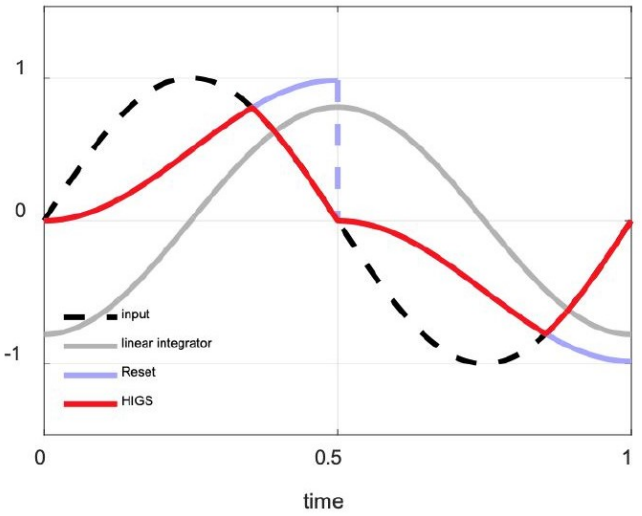

Figure 1.6. Typical response of a linear integrator, reset integrator and a HIGS element, to a sinusoidal input.

as shown in Fig. 1.7 the describing function of a HIGS element exhibits a 20 dB/decade amplitude decay similar to that of a linear integrator, however induces only 38.15° of phase lag, as in the case of the Clegg integrator [31].

This thesis is dedicated to the study of HIGS and HIGS-controlled systems, addressing important topics on their formalization, analysis and design, as outlined in Section 1.6 below.

1.6 Research objectives

In this thesis, the aim is to address a number of important open problems related to HIGS and HIGS-based control. These open problems have a wide scope and vary in nature from fundamental system theoretical ones to more applied and engineering problems. In this section, we provide a list of the main research objectives pursued in the thesis.

Mathematical systems and control theory is an area of applied mathematics concerned with the underlying principles of analysis and design of control systems [131]. As a result, to influence the behavior of dynamical systems in the desired fashion, engineers employ several mathematical techniques [131]. In order to further aid the study of HIGS and HIGS-based control systems using principles of mathematical control theory, a mathematical framework capable of explaining the engineering philosophy underlying this new control element is required. This leads

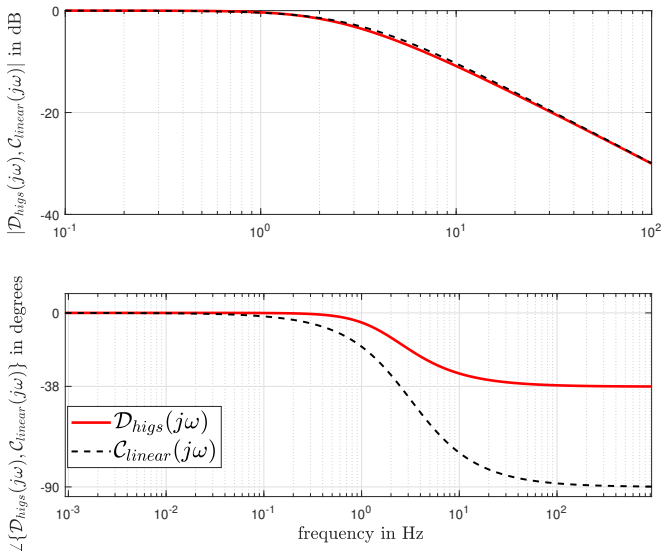

Figure 1.7. Bode plot of describing function $\mathcal{D}_{higs}$ of a HIGS element and a linear lowpass filter $\mathcal{C}_{linear}$.

us to the first research objective of this thesis.

Research objective I. *Develop a mathematical framework that captures the engineering philosophy of HIGS and can be used for the formalization of HIGS-controlled systems.*

For a mathematical model to be sound, a crucial property is the so-called well-posedness property [34, 61]. Given initial conditions (and possibly external signals), well-posedness is often defined as existence and uniqueness of solutions [83, 112], although in the literature related to hybrid systems requiring the solutions to be unique is sometimes viewed as restrictive [52, 63]. Another research objective pursued in this thesis is to provide conditions for well-posedness of HIGS-controlled systems.

Research objective II. *Establish conditions under which HIGS-controlled systems are well-posed.*

As explained in Section 1.2, LTI control techniques are widely adopted by control practitioners in the full industrial spectrum. In order for HIGS-based control techniques to be taken up in practice, they should offer clear performance enhancing benefits, by enabling one to achieve performance beyond the limitations of LTI control [119].

Research objective III. *Show rigorously that HIGS-based control is capable of obtaining performance levels that are impossible with LTI control techniques.*

Nowadays, almost all controllers are implemented on a digital platform [9] and thus have dynamics that evolve in discrete time. As a result, digital implementation of controllers requires discrete-time versions of them [30]. In addition, the interconnection of the discrete-time controllers and the continuous-time plants to be controlled, results in an overall sampled-data control system, for which dedicated analysis and design tools should be developed.

Research objective IV. *Develop discrete-time HIGS elements, which preserve the main properties and the engineering philosophy of HIGS, in order to facilitate the digital implementation of HIGS-based controllers in practice. In addition, provide a framework for analysis of sampled-data HIGS-controlled systems.*

For a new control element to be utilized by control engineers in practice, showing promise in theory and based on simulations is a good start. However, it is also important to provide experimental demonstrations that illustrate the power of the newly proposed control techniques on industrially relevant applications to further aid the adoption of the proposed techniques by control practitioners.

Research objective V. *Illustrate the power of HIGS-based control through experimental validation, and show the performance-enhancing benefits of HIGS compared to LTI controllers on industrially relevant applications.*

In the next section we provide a high-level overview of the main contributions of the thesis that aim to address the research objectives outlined above.

1.7 Contributions

In addressing the research objectives discussed in Section 1.6, we present six main contributions in this thesis, each of which is directly linked to one or more of the objectives above.

In addressing Research objective I, in Chapter 2 we introduce a new class of discontinuous dynamical systems based on extensions of projected dynamical systems (PDS) [102]. PDS are a class of discontinuous dynamical systems introduced in the early 1990s. While the PDS philosophy resembles that of the HIGS, there are essential differences that prevent direct formalization of HIGS-controlled systems in the PDS framework. Therefore, in Chapter 2 we present the required extensions to PDS, leading to the introduction of *extended projected dynamical systems* (ePDS), and subsequently formalize HIGS in the presented framework. Note that the introduction of ePDS is of interest beyond the study of HIGS and HIGS-controlled systems, as it supplements PDS with unprecedented features, and thus, can be used in other areas where PDS are considered.

Contribution I. *Introduction of a new class of discontinuous dynamical systems called ePDS, used for mathematical formalization of HIGS-controlled systems.*

Research objective II is also pursued in Chapter 2. In particular, upon formalizing HIGS in the newly introduced ePDS framework, under certain regularity conditions on the exogenous input signals entering the closed-loop HIGS-controlled systems, we prove existence and forward completeness of solutions.

Contribution II. *A proof of well-posedness of HIGS-controlled systems in the sense of existence and forward completeness of solutions.*

Chapter 3 is concerned with providing conditions under which the introduced class of ePDS are equivalent to another variant of PDS, namely *oblique projected dynamical systems* (oPDS) [57], which have been widely used in the context of feedback-based optimisation. This is done in order to allow for the transfer of system theoretical tools and properties between the two system classes. Upon establishing conditions of equivalence, the results are used to also obtain a description of HIGS-controlled system as an oPDS. In addition, we use these equivalence results to propose conditions for incremental stability [7] and convergence [110] of ePDS and HIGS-controlled systems. The results in Chapter 3 are also related to Research objective I as they show how the formalization of HIGS-controlled systems as ePDS can be used to obtain, new (non-obvious) descriptions of these systems,

and additionally demonstrate the benefits of doing so by proposing new analysis tools for them. In addition, these results are also related to Research objective II, since under the satisfaction of the proposed conditions for incremental stability, one may also conclude uniqueness of solutions of HIGS-controlled systems.

Contribution III. *Sufficient conditions for the equivalence of the introduced class of ePDS to other variants of PDS, namely oPDS, which can be used for the transfer of system theoretical tools and properties from one class to the other. This transfer of system theoretical properties is highlighted for properties such as incremental stability and convergence for ePDS in general, and for HIGS-controlled systems in particular.*

In Chapter 4, we consider fundamental performance limitations of LTI control [119]. In particular, scenarios wherein certain performance objectives are impossible to achieve with any LTI controller are considered. In each scenario, we show that by employing a well-crafted HIGS-based controller one can achieve these performance objectives. This, thus, shows rigorously that HIGS-based control can overcome well-known fundamental limitations of LTI control. The results presented in Chapter 4 address Research objective III, as they clearly show that one may push the performance of control systems beyond the limitations of LTI control, by employing HIGS-based control. That is, beyond performance accessible to any LTI controller irrespective of the order or tuning.

Contribution IV. *Demonstration of the possibility of overcoming time-domain performance limitations of LTI feedback control by using HIGS-based control in an otherwise LTI closed-loop system.*

In addressing Research objective IV, in Chapter 5, discrete-time versions of HIGS are presented. The proposed discrete-time HIGS elements share the same philosophy of operation as continuous-time HIGS and preserve important properties of continuous-time HIGS, namely sector boundedness of their input-output pair, in discrete time. We also present two sets of results for stability analysis of discrete-time HIGS controlled systems, based on (i) frequency-domain conditions and (ii) feasibility of a set of linear matrix inequalities (LMIs). It is also shown, that the stability certificates obtained in discrete time, can also be used to conclude stability of sampled-data HIGS-controlled systems consisting of the discrete-time controller dynamics as well as the continuous-time dynamics of the

plant to be controlled.

Contribution V. *Development of discrete-time HIGS elements that share the same philosophy of operation as continuous-time HIGS and stability analysis tools for discrete-time and sampled-data HIGS-controlled systems using (i) (measured) frequency domain data and (ii) solving a set of LMIs.*

The sixth contribution of this dissertation, addressing Research objective V and presented in Chapter 6, is the experimental demonstration of HIGS-based control on an industrial active vibration isolation system, widely used in high-precision motion industries. We show, by means of experiments, that the novel HIGS-based control strategy outperforms its linear counterpart. In particular, the HIGS-based control strategy allows for superior active vibration isolation compared to LTI control and improves system's performance with respect to metrics that are typically considered in the context of active vibration isolation.

Contribution VI. *Development of a HIGS-based controller that can be used for active vibration isolation with superior performance when compared to its linear counterpart, as demonstrated by experimental results obtained from an industrial active vibration isolation system.*

Next, we describe the outline and structure of this dissertation.

1.8 Outline of the thesis

Including this introductory chapter, this thesis consists of seven chapters. With the exception of Chapter 7, where conclusions and recommendations are provided, each chapter is based on one or multiple research papers and is self-contained.

To be more specific, Chapters 2-3 are related to Contributions I, II and III and are based on

- B. Sharif, M.F. Heertjes, and W.P.M.H. Heemels. Extended projected dynamical systems with applications to hybrid integrator-gain systems. In *2019 IEEE Conference on Decision and Control (CDC)*, pages 5773–5778, 2019.

- B. Sharif, M. Heertjes, H. Nijmeijer, and W.P.M.H. Heemels. On the equivalence of extended and oblique projected dynamics with applications to hybrid integrator-gain systems. In *2021 American Control Conference (ACC)*, New Orleans, USA, pages 3434–3439, 2021.

- D.A. Deenen, B. Sharif, S.J.A.M. van den Eijnden, H. Nijmeijer, W.P.M.H. Heemels, and M.F. Heertjes. Projection-Based Integrators for Improved Motion Control: Formalization, Well-posedness and Stability of Hybrid Integrator-Gain Systems. *Automatica*, Volume 133, 109830, 2021.

- B. Sharif, M.F. Heertjes, H. Nijmeijer, and W.P.M.H. Heemels. Extended projected dynamical systems. *In preparation for journal submission*

Chapter 4 corresponds to Contribution IV and is based on

- D. van Dinther, B. Sharif, S. J. A. M. van den Eijnden, H. Nijmeijer, M. F. Heertjes, and W. P. M. H. Heemels. Overcoming performance limitations of linear control with hybrid integrator-gain systems. In *IFAC-Papers OnLine,* volume 54, issue 5, pages 289-294, 2021.

The work presented in Chapter 5 corresponds to Contribution V and is based on

- B. Sharif, D.W.T. Alferink, M.F. Heertjes, H. Nijmeijer, and W.P.M.H. Heemels. A discrete-time approach to analysis of sampled-data hybrid integrator-gain systems. In *2022 IEEE Conference On Decision and Control (CDC)*, pages 7612-7617, 2022.

- B. Sharif, D.W.T. Alferink, M.F. Heertjes, H. Nijmeijer, and W.P.M.H. Heemels. Analysis of sampled-data hybrid integrator-gain systems: A discrete-time approach. *Submitted for publication in journal.*

Chapter 6 corresponds to Contribution VI and is based on

- M.F. Heertjes, S.J.A.M. van den Eijnden, B. Sharif, W.P.M.H. Heemels, and H. Nijmeijer. Hybrid integrator-gain system for active vibration isolation with improved transient response. *IFAC-PapersOnLine*, volume 52, issue 15, pages 454–459, 2019

- B. Sharif, S.J.A.M. van den Eijnden, M. Beijen, S.P. Achten, H. Nijmeijer, W.P.M.H. Heemels, and M.F. Heertjes. A hybrid integrator-gain based bandpass filter for active vibration isolation with improved skyhook damping. *In prepration for journal submission.*

Finally, in Chapter 7, a summary of the results obtained in the thesis and recommendations for future work are provided.

2

Projection-Based Formalization and Well-posedness of Hybrid Integrator-Gain-based control systems

Abstract - *The class of projected dynamical systems (PDS) has proven to be a powerful framework for modeling dynamical systems of which the trajectories are constrained to a set by means of projection. However, PDS fall short in modeling systems in which the constraint set does not satisfy certain regularity conditions and only part of the dynamics can be projected. This poses limitations in terms of the phenomena that can be described in this framework especially in the context of systems and control. Motivated by hybrid integrator-gain systems (HIGS), which are recently proposed control elements in the literature that aim at overcoming fundamental limitations of linear time-invariant feedback control, a new class of discontinuous dynamical systems referred to as extended projected dynamical systems (ePDS) is introduced in this chapter. Extended projected dynamical systems include PDS as a special case and can accommodate constraint sets not considered in the PDS literature so far, as well as partial projections of the dynamics. In this*

This chapter is based on [38, 123, 124].

work, the ePDS framework is connected to the classical PDS literature and is subsequently used to provide a formal mathematical description of a HIGS-controlled system. Based on the latter result, a proof of well-posedness, in the sense of existence of and forward completeness of solutions, for the formalized HIGS-controlled system is provided.

2.1 Introduction

Nonlinear and hybrid control strategies have been demonstrated to be effective tools in dealing with the well-known and classical trade-off in linear time-invariant (LTI) control systems between (i) low frequency disturbance suppression by means of integral control and (ii) desired transient performance. A well-known example of such a nonlinear control technique is reset control initially proposed by Clegg [31] and later developed into the first-order reset element (FORE) [97]. A reset controller is a linear time-invariant (LTI) system whose states, or part of the states, are reset to zero (or some other value) whenever its input and output signals meet certain conditions [2, 150]. More specifically, the reset generally happens to enforce that the input and output signals of the reset element have the same sign. The development of reset control continued with generalizations such as the first-order reset element [19, 29, 79, 156], the second-order reset element [60] and generalized fractional-order reset elements [115]. Extensive research on reset control systems has led to various fruitful results regarding stability analysis [14, 19, 27, 56, 103, 104, 154], beating fundamental time-domain performance limitations of LTI control [18, 156], hybrid formulations [155] using temporal regularization to avoid Zeno phenomena, and experimental demonstration of reset control systems achieving improved performance [13, 60, 115, 153]. A desirable feature typical of reset controllers is characterized by the Clegg integrator's describing function, which exhibits a 20 dB/decade amplitude decay similar to that of a linear integrator, however induces only 38.15 degrees of phase lag (as opposed to 90 degrees for the linear integrator). The latter is a result of the reset forcing the integrator's input and output to always be of equal sign. This is a general feature of many reset controllers, in which the resetting mechanism leads to an improvement in phase lag over its linear counterpart, which in turn suggests the possibility of designing a compensator capable of supplying the required bandwidth with a reduced gain at high frequencies [29]. Clearly, this favorable phase behavior hints towards the possibility of significantly improving closed-loop performance of the reset control system.

In spite of the design advantages that reset control systems offer when compared to linear control methods, there are also some features that might limit the performance obtained by controllers designed with such techniques. More specifically, by resetting (part of) the states, reset controllers produce discontinuous control signals that can potentially excite high-frequency plant dynamics or amplify high-frequency noise, which can be highly undesirable. For these reasons, a novel hybrid integrator-gain system (HIGS) was presented in [37] that aims at overcoming the above mentioned design limitation of reset controllers while offering the same promising features regarding phase by keeping the sign of its input and output the same. In particular, HIGS are hybrid, sector bounded integrators that avoid explicit reset of the integrator state by switching to a so-called gain mode when the sector conditions tend to be violated, see [37]. As a result, unlike

2

a reset element, the output of a HIGS element is a *continuous* signal that has the potential to considerably reduce the excitation of high-frequency dynamics. Moreover, the switching between the integrator and the gain mode is performed in such a way that the input and output of a HIGS element always have equal sign. More specifically, a HIGS element $\mathscr{H}$ in its preferred mode of operation is described by an integrator element

$$\dot{x}_h(t) = \omega_h e(t), \tag{2.1a}$$

$$u(t) = x_h(t), \tag{2.1b}$$

where $x_h(t) \in \mathbb{R}$, $e(t) \in \mathbb{R}$ and $u(t) \in \mathbb{R}$ denote the state, input and output of $\mathscr{H}$, respectively, at time $t \in \mathbb{R}_{\geq 0}$ and $\omega_h \in (0, \infty)$ is the integrator frequency. However, the integrator mode (2.1) can only be used as long as the input-output pair $(e(t), u(t))$ remains inside the sector $\mathcal{F}$:

$$\mathcal{F} := \left\{ (e, u) \in \mathbb{R}^2 \mid eu \geq \frac{1}{k_h} u^2 \right\}, \tag{2.2}$$

with $k_h \in \mathbb{R}_{>0}$, the so called gain parameter. At moments when the input-output pair $(e(t), u(t))$ of $\mathscr{H}$ tends to leave the sector $\mathcal{F}$ which can happen when $u(t) = k_h e(t)$, the vector field of $\mathscr{H}$ is changed to $\dot{x}_h(t) = k_h \dot{e}(t)$ so that the trajectories remain on the sector boundary, where $u(t) = k_h e(t)$, until the integrator mode can be used again (See Fig. 2.1 for a graphical interpretation). This second mode of operation where $\dot{x}_h(t) = k_h \dot{e}(t)$, is called the gain mode of HIGS. As a consequence, the switching operation of HIGS is such that its input-output $(e(t), u(t))$ are always contained in $\mathcal{F}$ and thus always have the same sign. This explains why the HIGS

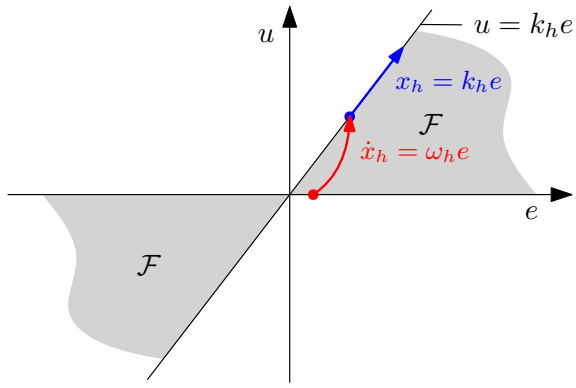

Figure 2.1. An example of HIGS in operation.

element offers similar advantages as reset control elements while overcoming their

potential shortcomings related to discontinuous control signals, making HIGS a powerful control element for high-performance control. The strength of HIGS in terms of improving the closed-loop performance of control systems (mainly in applications to high-precision mechatronics) as well as frequency domain tools for design/analysis of HIGS-controlled systems have been portrayed in [37, 73, 145].

Despite the engineering success of HIGS, up to now a formal mathematical description and well-posedness analysis of HIGS have not been provided. Addressing these open issues may prove instrumental for gaining further insight into the operation of HIGS and paving the way for further developments with this control element. This forms one of the main objectives of this chapter.

When considering a HIGS element with state $x_h(t) \in \mathbb{R}$ in feedback interconnection with a linear physical plant with state $x_p(t) \in \mathbb{R}^{n_p}$, as previously explained, the intended operation of HIGS is to use integrator dynamics as long as its input signal, being a function of $x = [x_h^\top, x_p^\top]^\top$ (plus possible external exogenous signals such as disturbance and references), and output signal, lie within a set S (related to the sector $\mathcal{F}$, cf. (2.2)), such that the input and output of the controller have the same sign. At moments when the sector condition tends to be violated by following integrator dynamics, the vector field of the controller changes by switching to gain mode thereby enforcing the input-output signals to stay within the sector. Similar dynamics are observed in the literature in the class of projected dynamical systems (PDS), where the trajectories of the system are ensured to be within a given constraint set at all times by means of projection. However, the PDS literature (see, e.g., [11, 40, 57, 102]) is limited to cases where the full state vector x is projected onto a constraint set, which is generally assumed to satisfy certain regularity conditions. More specifically, in [76] PDS are shown to be well-defined for convex constraint sets. Weaker conditions are required in [33] where Clarke regularity and prox-regularity (see [114]) of constraint sets are required for existence and uniqueness of solutions, respectively. In the case of HIGS, however, the constraint set S does not satisfy any of these regularity conditions. Moreover, in the context of control, one can only project the controller (x_h) dynamics while the plant (x_p) dynamics cannot be projected, as these are related to the physics of the underlying plant that can not be altered. As a consequence, for the mathematical formalization of HIGS (and related systems), the PDS framework should be generalized to accommodate for *partial* projections onto a wider range of constraint sets. Motivated by these arguments, as a first contribution in this chapter, we introduce a new class of dynamical systems, which we refer to as extended projected dynamical systems (ePDS). This class of systems includes as a special case the classical PDS available in the literature. As a second contribution, the introduced ePDS framework is used for formalizing HIGS. As it turns out, ePDS indeed provides the appropriate tool set to consider HIGS, and in fact connects well to the engineering "philosophy" underlying this new control element, as indicated in [37, 73, 145]. In fact, the ePDS-based representation of HIGS-controlled systems can be used to obtain the other representations of HIGS

as used in. e.g., [37, 73, 145]. As a third contribution, this chapter gives a proof of well-posedness in terms of global existence and forward completeness of solutions (in the Carathéodry sense) for the feedback interconnection of an LTI system with a HIGS element. It should be noted that well-posedness analysis of HIGS is a challenging task as the dynamics of HIGS lack the (continuity) properties typically used in the literature related to hybrid systems and differential inclusions such as [11, 52, 117], for proving well-posedness of hybrid systems.

The remainder of this chapter is organized as follows. Section 2.2 contains the preliminary material used in the subsequent sections. In Section 2.3 the ePDS framework is introduced and is shown to be well-defined. This is followed by Section 2.4 where our formulation in Section 2.3 is linked to components of alternative formulations frequently encountered in the PDS literature. A HIGS-controlled system is described and formalized in the ePDS framework in Section 2.5. Subsequently, local well-posedness of the HIGS-controlled system, is presented in Section 2.6.1. Building on the developments in Section 2.6.1, the proof of forward completeness of all the solutions to the HIGS-controlled system is presented in Section 2.6.2. Section 2.7 contains concluding remarks and future directions of research.

2.2 Preliminary definitions

In this section, we present the preliminary material and definitions, which are used in the sections to follow.

2.2.1 Definitions

Definition 2.2.1. *The Euclidean inner product between two vectors $a \in \mathbb{R}^n$ and $b \in \mathbb{R}^n$, denoted by $\langle a, b\rangle$ is defined as*

$$\langle a, b\rangle = a^\top b.$$

Definition 2.2.2. *A sequence of scalars $(u^1, u^2, ..., u^k)$ with $k \in \mathbb{N}$, is called lexicographically non-negative (non-positive), written as $(u^1, u^2, ..., u^k) \geq_l 0$ $(\leq_l 0)$, if $(u^1, u^2, ..., u^k) = (0, 0, ..., 0)$ or $u^j > 0$ (< 0) where $j = \min\{p \in \{1, \ldots, k\} \mid u^p \neq 0\}$.*

Definition 2.2.3. *A polyhedral set in $\mathbb{R}^n$ is a set given by the intersection of a finite number of closed half-spaces.*

As a particular polyhedral set, consider $G = [g_1 \ g_2 \ldots g_m] \in \mathbb{R}^{n\times m}$, where $g_i \in \mathbb{R}^n$, $i = 1, 2, \ldots, m$ are the columns of G. Then the polyhedral set $\operatorname{pos} G$ is the convex cone consisting of all positive combinations of the columns of G given by [78]

$$\operatorname{pos} G = \{\sum_{i=1}^{m} \alpha_i g_i \mid \alpha_i \geq 0, \quad i = 1, 2, \ldots, m\}$$

Definition 2.2.4. *A function $w : \mathcal{I} \to \mathbb{R}^{n_w}$, with $\mathcal{I} \subseteq \mathbb{R}$ is called a Bohl function, denoted by $w \in B_{\mathcal{I}}$, if there exist matrices $H \in \mathbb{R}^{n_w \times n_F}$, $F \in \mathbb{R}^{n_F \times n_F}$, and a vector $v \in \mathbb{R}^{n_F}$ such that $w(t) = He^{Ft}v$ for all $t \in \mathcal{I}$.*

Definition 2.2.5. *A function $w : \mathbb{R}_{\geq 0} \to \mathbb{R}^{n_w}$ is called a piecewise Bohl function, denoted by $w \in PB$, if there exists a sequence $\{t_i\}_{i\in\mathbb{N}}$ with $0 = t_0 < t_i < t_{i+1}$ for all $i \in \mathbb{N}$ and $t_i \to \infty$ when $i \to \infty$ such that $w : [t_i, t_{i+1}) \to \mathbb{R}^{n_w}$ is a Bohl function for each $i \in \mathbb{N}$.*

Note that piecewise Bohl functions can be discontinuous, but they are continuous from the right in the sense that for each $T \in \mathbb{R}_{\geq 0}$ it holds that $w(T) = \lim_{t \downarrow T} w(t)$.

Definition 2.2.6. *An absolutely continuous (AC) function $f : [a, b] \to \mathbb{R}^n$ is a function that can be written as $f(t) - f(a) = \int_a^t \dot{f}(\tau)d\tau$ for any $t \in [a, b]$ for a Lebesgue integrable function $\dot{f} \in \mathcal{L}^1([a, b], \mathbb{R}^n)$, which is considered as its derivative. A function $f : \mathcal{I} \to \mathbb{R}^n$ is locally AC, if it is AC for any bounded interval $[a, b] \subset \mathcal{I}$.*

Definition 2.2.7. *For the column space of a matrix $H \in \mathbb{R}^{n\times m}$ we write*

$$imH = \{Hx \mid x \in \mathbb{R}^m\}. \tag{2.3}$$

Definition 2.2.8. *The tangent cone to a set $K \subset \mathbb{R}^n$ at a point $x \in K$, denoted by $T_K(x)$, is the set of all vectors $w \in \mathbb{R}^n$ for which there exist sequences $\{x_i\}_{i\in\mathbb{N}} \in K$ and $\{\tau_i\}_{i\in\mathbb{N}}$, $\tau_i > 0$ with $x_i \to x$, $\tau_i \downarrow 0$ and $i \to \infty$, such that*

$$w = \lim_{i\to\infty} \frac{x_i - x}{\tau_i}. \tag{2.4}$$

When K is a closed convex cone, we have $T_K(x) = \bigcup_{t>0} \frac{K-x}{t}$ (see Remark 5.2.2. in III, [78]). In fact, due to convexity, it holds that for $x \in K$

$$\frac{K - x}{t_2} \subseteq \frac{K - x}{t_1} \text{ when } 0 < t_1 \leq t_2. \tag{2.5}$$

Definition 2.2.9. *[78], The projection of a vector $x \in \mathbb{R}^n$ onto a closed, nonempty set $S \in \mathbb{R}^n$, denoted by $P_S(x)$, is defined as*

$$P_S(x) = \text{argmin}_{s\in S} \|s - x\|. \tag{2.6}$$

2.2.2 Projected dynamical systems

To introduce the "classical" projected dynamical systems (PDS) [40, 67, 102], consider a differential equation

$$\dot{x}(t) = f(x(t), u(t)), \tag{2.7}$$

in which $x(t) \in \mathbb{R}^n$ denotes the state at time $t \in \mathbb{R}_{\geq 0}$, and $u(t) \in \mathbb{R}^{n_u}$ is the external input. There is a restriction on the state of the system in the sense that $x(t)$ has to remain inside a set $S \subseteq \mathbb{R}^n$, which in PDS is ensured by redirecting the vector field at the boundary of S. Formally, a PDS is given for a continuous vector field $f : \mathbb{R}^{n+n_u} \to \mathbb{R}^n$ and a set $S \subseteq \mathbb{R}^n$ (with further additional conditions to make the definitions below meaningful) by

$$\dot{x}(t) = \Pi_S(x(t), f(x(t), u(t))), \tag{2.8}$$

with

$$\Pi_S(x, v) = \operatorname{argmin}_{w \in T_S(x)} \|w - v\|, \tag{2.9}$$

for $x \in S$ and $v \in \mathbb{R}^n$. Based on this formulation, $\Pi_S(x, v)$ can be interpreted as an operator that selects the vector closest to v, which lies in the set of admissible velocities at x. An equivalent characterization of $\Pi_S(x, v)$, (see Proposition 5.3.5 in III, [78]) is

$$\Pi_S(x, v) = \lim_{\delta \downarrow 0} \frac{P_S(x + \delta v) - x}{\delta}, \tag{2.10}$$

when S is a closed, convex and non-empty set. In fact, in many works on PDS (see for example [24, 40, 102]) the expression (2.10) is used to define PDS.

2.3 Extended projected dynamical systems

Inspired by the philosophy behind the HIGS element discussed in the introduction, we present in this section a generalization to PDS.

2.3.1 Model representation

Let $S \subseteq \mathbb{R}^n$ be a given non-empty closed set, on which we impose additional conditions later to obtain a well-posed system. We are interested in dynamical systems of the form

$$\dot{x}(t) = f(x(t), u(t)), \tag{2.11}$$

in which the state of the system has to reside inside the set S. In classical PDS, as recalled in Subsection 2.2.2, the latter is ensured by "projecting" the complete vector field on the tangent cone of the set S, cf. (2.8) and (2.9). This projection is along *all* possible directions of the state in the sense that it just takes the vector $\Pi_S(x, v) \in T_S(x)$ that is "closest" to $v = f(x, u)$, irrespective of the direction $\Pi_S(x, v) - v$. Therefore, it is allowed to alter the complete vector field and thus the velocities of all the states x in (2.11). Clearly, if (2.11) is a closed-loop system in the sense of an interconnection of a physical plant and a controller (and thus the state x consists of physical plant states x_p and controller states x_c), one cannot project in all directions (see the discussion in the introduction). Indeed, the physical state

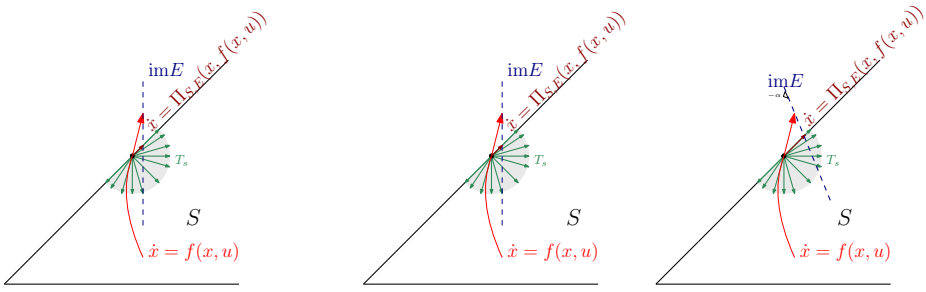

Figure 2.2. Examples of (a) Projected dynamical system $\dot{x} = \Pi_S(x, f(x,u))$, or equivalently the ePDS $\dot{x} = \Pi_{S,E}(x, f(x,u))$ with $\mathrm{im}E = \mathbb{R}^2$, (b) extended projected dynamical system $\dot{x} = \Pi_{S,E}(x, f(x,u))$, with $E = [0,1]^\top$, and (c) extended projected dynamical system $\dot{x} = \Pi_{S,E}(x, f(x,u))$, with $E = [\alpha, 1]^\top$, $\alpha \in \mathbb{R}_{>0}$, where the primary mode of operation is given by $\dot{x} = f(x,u)$, with $x \in \mathbb{R}^2$, and constraint set $S \subseteq \mathbb{R}^2$.

dynamics cannot be modified by straightforward projection. It is only possible to "project" the controller (x_c-)dynamics and possibly a part of the plant states (x_p-)dynamics in which the control input appears explicitly. Hence, in contrast to PDS, we only have limited directions by which we can "correct" the vector field $f(x)$ at the boundary, if needed, to keep the state trajectories inside S. To formalize this, we model the restricted "correction / projection" directions by the image of a matrix $E \in \mathbb{R}^{n \times n_E}$, which is assumed, without loss of generality, to have full column rank. Formally,

$$\dot{x}(t) = \Pi_{S,E}(x(t), f(x(t), u(t))) \tag{2.12}$$

with

$$\Pi_{S,E}(x, v) = \mathrm{argmin}_{w \in T_S(x), w - v \in \mathrm{Im}\, E} \|w - v\|, \tag{2.13}$$

for $x \in S$ and $v \in \mathbb{R}^n$. Hence, the projection operator Π projects the velocity v at $x \in S$ onto the set of admissible velocities (tangent cone) along $\mathrm{Im}\, E$ in such a way that the correction $w - v$ is minimal in norm. For these systems, we coin the term *extended Projected Dynamical Systems* (ePDS), as they include the classical PDS (2.8) as a special case by taking $\mathrm{Im}\, E = \mathbb{R}^n$ (and restricting S such that required regularity conditions are satisfied). Graphical illustrations of examples of PDS and ePDS are provided in Fig. 2.2.

2.3.2 Well-posed projection operator $\Pi_{S,E}$

Clearly, we have to show that the introduced projection $\Pi_{S,E}(x, v)$ is well-defined in the sense that it provides a unique outcome for each $x \in S$ and each $v \in \mathbb{R}^n$. As

in the case of classical PDS, this requires conditions on the set S and, in this case, also on E. Although we envision that we can work under more general conditions, for the sake of setting the scene in this chapter and inspired by the application of HIGS (see Fig. 2.1), we focus on the setting below.

Assumption 2.3.1. *The set $S \subseteq \mathbb{R}^n$ and $E \in \mathbb{R}^{n\times n_E}$ satisfy*

- *$S = K \cup -K$ in which K is a convex polyhedral cone given*

$$K := \{x \in \mathbb{R}^n \mid Fx \geq 0\}, \tag{2.14}$$

  for some matrix $F \in \mathbb{R}^{n_f \times n}$ of full rank.

- *E has full column rank.*

- *$\operatorname{Im} E \cap S = \{0\}$ and $S + \operatorname{Im} E = \mathbb{R}^n$.*

We are particularly interested in this setup as it can describe *sector conditions* as are used in reset controllers and HIGS cf. (2.2), e.g., describing that the input and output of a controller have the same sign. Sector conditions also appear in circle and Popov criteria for the analysis of Lur'e type of systems, see e.g., [88].

To prove the well-posedness of (2.13), observe first that

$$T_S(x) = \begin{cases} T_K(x), & \text{if } x \in K \setminus -K \\ K \cup -K, & \text{if } x \in K \cap -K \\ -T_K(-x), & \text{if } x \in -K \setminus K \end{cases} \tag{2.15}$$

with

$$T_K(x) = \{w \in \mathbb{R}^n \mid F_{I(x)} w \geq 0\}, \tag{2.16}$$

where

$$I(x) = \{i \in \{1, 2, \ldots, n_f\} \mid F_i x = 0\}$$

is the set of active constraints at x. We used here the notation F_J for $J \subseteq \{1, \ldots, n_f\}$ to denote the matrix consisting of the rows of F with row numbers in J. Also observe that we can rewrite (2.13) as

$$\Pi_{S,E}(x, v) = v + E\eta^*(x, v) \tag{2.17}$$

with

$$\eta^*(x, v) = \operatorname{argmin}_{\eta \in \Lambda(x,v)} \|E\eta\| \tag{2.18}$$

and

$$\Lambda(x, v) = \{\eta \in \mathbb{R}^{n_E} \mid v + E\eta \in T_S(x)\}. \tag{2.19}$$

Lemma 2.3.1. *Under Assumption 2.3.1, it holds for each $x \in S$ and each $v \in \mathbb{R}^n$ that $\Lambda(x, v)$ is a non-empty closed polyhedral set.*

Proof. Let $x \in S$ and $v \in \mathbb{R}^n$ be given. First note that due to $S + \operatorname{Im} E = \mathbb{R}^n$ it follows that $\Lambda(x, v)$ is non-empty. Clearly, when $x \notin K \cap -K$ it follows that $T_S(x)$, as given in (2.15), is a closed polyhedral cone and then also $\Lambda(x, v)$ is a polyhedral set. So, let us turn our attention to $x \in K \cap -K$ in which $T_S(x) = K \cup -K$ and thus $\Lambda(x, v) = \{\eta \in \mathbb{R}^{n_E} \mid v + E\eta \in K \cup -K\}$. We now claim that $v + E\eta \in K$ and $v + E\bar{\eta} \in -K$ imply that $\eta = \bar{\eta}$. Note that such a claim would show that if there is η with $v + E\eta \in K$ then $\Lambda(x, v) = \{\eta \in \mathbb{R}^{n_E} \mid v + E\eta \in K\}$ (as any η in $\{\eta \in \mathbb{R}^{n_E} \mid v + E\eta \in -K\}$ would also be contained in $\{\eta \in \mathbb{R}^{n_E} \mid v + E\eta \in K\}$, and similarly if there is $\bar{\eta}$ with $v + E\bar{\eta} \in -K$ then $\Lambda(x, v) = \{\eta \in \mathbb{R}^{n_E} \mid v + E\eta \in -K\}$. As the sets $\{\eta \in \mathbb{R}^{n_E} \mid v + E\eta \in K\}$ and $\{\eta \in \mathbb{R}^{n_E} \mid v + E\eta \in -K\}$ are both closed polyhedral sets, so is $\Lambda(x, v)$. To prove the claim, observe that due to K being a convex cone and $-v - E\bar{\eta} \in K$, we get that

$$E(\eta - \bar{\eta}) = (v + E\eta) - v - E\bar{\eta} \in K.$$

Since $\operatorname{Im} E \cap S = \{0\}$ and E has full column rank, this shows that $\eta = \bar{\eta}$ and the result follows. □

Due to the fact that the constraint set of (2.18) is a non-empty, closed polyhedral set and that the square of the cost function of (2.17) being $\eta^\top E^\top E\eta$ is a quadratic positive definite function (as E has full column rank), a unique minimizer exists, showing the well-posedness of (2.17) and thus (2.13).

2.4 Connecting to alternative PDS representations

As already indicated in Subsection 2.2.2, there is an equivalence for classical PDS between the representations (2.9) and (2.10) under certain regularity conditions imposed on the set S. In this section, the objective is to establish a similar equivalence for ePDS. To do so, let us first introduce

$$P_{S,E}(x) = \operatorname{argmin}_{s \in S, s - x \in \operatorname{Im} E} \|s - x\|. \tag{2.20}$$

Clearly, we can rewrite (2.20) as

$$P_{S,E}(x) = \operatorname{argmin}_{s \in C_x} \|s - x\| \text{ with } C_x := \{s \in S \mid s - x \in \operatorname{Im} E\}. \tag{2.21}$$

Note that, although this formulation has similarities with (2.9), the set $C_x = S \cap (x + \operatorname{Im} E)$ is dependent on x, which is not the case in (2.9). Observe that C_x is a non-empty closed and convex set, following from a similar reasoning as in the proof of Lemma 2.3.1. In fact, this yields that C_x is equal to $\{s \in K \mid s - x \in \operatorname{Im} E\}$ or $\{s \in -K \mid s - x \in \operatorname{Im} E\}$ due to the following implication

$$\left.\begin{array}{c} s - x \in \operatorname{Im} E,\ s \in K \\ \bar{s} - x \in \operatorname{Im} E,\ \bar{s} \in -K \end{array}\right\} \text{ imply } s = \bar{s}.$$

Hence, $P_{S,E}(x) = P_{K,E}(x)$ (if $x \in K + \operatorname{Im} E$) or $P_{S,E}(x) = P_{-K,E}(x)$ (if $x \in -K + \operatorname{Im} E$) and thus $P_{S,E}(x)$ gives a unique outcome, see, e.g., the reasoning on page 116 of [78]. Note that based on Theorem 3.1.1 in III, [78] and using the previous observation, we have that $P_{S,E}(x)$ is characterized by the following *variational inequalities*:
s_x is equal to $P_{S,E}(x)$ if and only if

$$\langle x - s_x, s - s_x \rangle \leq 0 \text{ for all } s \in S \cap (x + \operatorname{Im} E). \tag{2.22}$$

In line with (2.10) for classical PDS, we consider

$$\tilde{\Pi}_{S,E}(x, v) = \lim_{\delta \downarrow 0} \frac{P_{S,E}(x + \delta v) - x}{\delta}. \tag{2.23}$$

Theorem 2.4.1. *Under Assumption 2.3.1, it holds that* $\tilde{\Pi}_{S,E}(x, v) = \Pi_{S,E}(x, v)$ *for all* $x \in S$ *and* $v \in \mathbb{R}^n$.

Proof. Following the arguments of the proof of Proposition 5.3.5, [78], we can obtain that $\frac{P_{S,E}(x+\delta v)-x}{\delta}$ is equal to $P_{\frac{S-x}{\delta},E}(v)$. Indeed, using the variational inequalities characterisation of projections, we have that (2.22) for $s_\delta := P_{S,E}(x + \delta v)$ gives

$$\langle x + \delta v - s_\delta, s - s_\delta \rangle \leq 0 \text{ for all } s \in S,\ s - (x + \delta v) \in \operatorname{Im} E.$$

Straightforward algebraic manipulations give for $\delta > 0$ that

$$\langle v - \frac{s_\delta - x}{\delta}, \frac{s - x}{\delta} - \frac{s_\delta - x}{\delta} \rangle \leq 0 \ \text{ for all } s \in S,\ s - (x + \delta v) \in \operatorname{Im} E,$$

and thus

$$\langle v - \frac{s_\delta - x}{\delta}, \tilde{s} - \frac{s_\delta - x}{\delta} \rangle \leq 0 \ \text{ for all } \tilde{s} \in \frac{S - x}{\delta},\ \tilde{s} - v \in \operatorname{Im} E,$$

where we took $\tilde{s} = \frac{s-x}{\delta}$. From this we conclude indeed that $\frac{P_{S,E}(x+\delta v)-x}{\delta} = \frac{s_\delta - x}{\delta} = P_{\frac{S-x}{\delta},E}(v)$.

Now we use the fact that $T_S(x) = \lim_{\delta \downarrow 0} \frac{S-x}{\delta}$ (and the monotonicity of $\delta \mapsto \frac{S-x}{\delta}$ as in (2.5)) together with the fact that $\frac{S-x}{\delta}$ and the limit $T_S(x)$ are (the union of) convex closed sets, to obtain that $\tilde{\Pi}_{S,E}(x, v) = P_{T_S(x),E}(v) = \Pi_{S,E}(x, v)$. □

Hence, also for ePDS we have the equivalence between (2.13) and (2.23).

Remark 2.4.1. *Note that we could extend the dynamics* (2.12) *that work for initial states* $x(0) \in S$*, such that they are also defined for* $x(0) \notin S$*. Indeed, in case* $x(0) \notin S$*, we can use* $x(0^+) = P_{S,E}(x(0), u(0))$ *to reset the state to a state inside* S*. Note that this reset only occurs at the initial time and not afterwards, as the state never leaves* S *for time* $t \in \mathbb{R}_{>0}$*. Moreover, also note that this is typically a reset of only (part of) the "controller states" (*x_c*) and not the full state vector. Therefore, this reset is feasible to implement.*

Remark 2.4.2. *In [57], the authors treat oblique projections by formulating PDS as*

$$\begin{aligned}\dot{x} = \Pi_S^g(x, f(x)) &= \operatorname{argmin}_{w \in T_S(x)} \|w - f(x)\|^2_{g(x)} \\ &= \operatorname{argmin}_{w \in T_S(x)} (w - f(x))^\top \mathcal{G}(x)(w - f(x)),\end{aligned} \tag{2.24}$$

where $\mathcal{G}(x)$ is a symmetric, positive definite matrix of appropriate dimensions, for all $x \in S$. This is a generalization of the classical PDS that correspond to (2.24) *with $\mathcal{G}(x)$ equal to the identity matrix. The connection between* (2.12) *and* (2.24) *will be studied in detail in Chapter 3.*

2.5 Description of HIGS-controlled systems

In this section we consider the closed-loop system setup in Fig. 2.3, consisting of a linear time-invariant (LTI), single-input single-output (SISO) plant $\mathscr{G}$ interconnected with a (SISO) HIGS element $\mathscr{H}$. The plant $\mathscr{G}$ contains the linear part of the closed-loop system including the plant to be controlled and possibly an LTI controller, given by the state-space representation

$$\mathscr{G}: \begin{cases} \dot{x}_g(t) = A_g x_g(t) + B_{gv} v(t) + B_{gw} w(t), & \text{(2.25a)} \\ e(t) = C_g x_g(t), & \text{(2.25b)} \end{cases}$$

with states $x_g(t)$ taking values in $\mathbb{R}^{n_g}$, performance output $e(t)$ in $\mathbb{R}$, control input $v(t)$ in $\mathbb{R}$ and exogenous disturbances and references denoted by $w(t)$ taking values in $\mathbb{R}^{n_w}$, at time $t \in \mathbb{R}_{\geq 0}$. Moreover, the realization (A_g, B_{gv}, C_g) is assumed to be minimal. As our key area of application involves motion systems containing

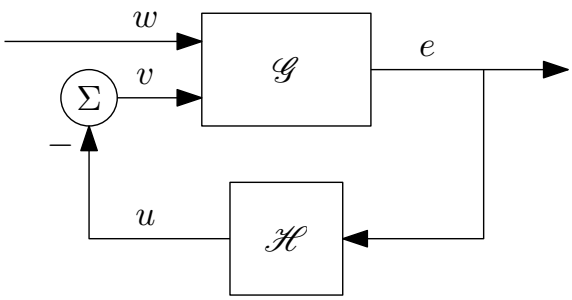

Figure 2.3. Closed-loop HIGS-controlled system.

moving masses, the following assumption is typically satisfied.

Assumption 2.5.1. *The LTI system $\mathscr{G}$ as in Fig. 2.3 is such that $C_g B_{gw} = 0$ and $C_g B_{gv} = 0$.*

As previously explained, the HIGS element $\mathscr{H}$ has as its preferred mode of operation the linear integrator dynamics

$$\begin{aligned} \dot{x}_h(t) &= \omega_h e(t), \\ u(t) &= x_h(t), \end{aligned} \tag{2.26}$$

where the state $x_h(t)$ takes values in $\mathbb{R}$, the (HIGS) input $e(t)$ and the (HIGS) output $u(t)$ both take values in $\mathbb{R}$ and $\omega_h \in [0, \infty)$ denotes the integrator frequency. This mode of operation of the HIGS element is referred to as the *integrator mode*. The integrator mode (2.26) can only be used as long as the input-output pair (e, u) of $\mathscr{H}$ remains inside the set

$$\mathcal{F} := \left\{ (e, u) \in \mathbb{R}^2 \mid eu \geq \frac{1}{k_h} u^2 \right\}, \tag{2.27}$$

where $k_h \in (0, \infty)$ denotes the gain parameter of $\mathscr{H}$. Note that $(e, u) \in \mathcal{F}$ implies equal sign of the input e and the output u of the HIGS element as $eu \geq 0$, see Fig. 2.1. At moments when the input-output pair (e, u) of $\mathscr{H}$ tends to leave the sector $\mathcal{F}$ we will "project" the integrator dynamics in (2.26) such that $(e, u) \in \mathcal{F}$ remains true along the trajectories of the system. Using the ePDS framework presented in Section 2.3, we will formalize this operation of the HIGS in the upcoming subsections.

2.5.1 Projection-based representation

To mathematically introduce the operation of HIGS, we directly use the interconnection of the HIGS element $\mathscr{H}$ and the linear system $\mathscr{G}$ described by (2.25), resulting in a closed-loop system as in Fig. 2.3, with state $x = \begin{bmatrix} x_g^\top & x_h^\top \end{bmatrix}^\top$ taking values in $\mathbb{R}^n$, where x_g and x_h are the states of $\mathscr{G}$ and $\mathscr{H}$, respectively and thus $n = n_g + 1$. Note that the constraint $(e, u) \in \mathcal{F}$ translates to $x \in \mathcal{S}$ with

$$\mathcal{S} = \mathscr{K} \cup -\mathscr{K}, \tag{2.28}$$

where $\mathscr{K}$ is a polyhedral cone given by

$$\mathscr{K} := \{x \in \mathbb{R}^n \mid Fx \geq 0\}, \tag{2.29}$$

where $F = \begin{bmatrix} F_1^\top & F_2^\top \end{bmatrix}^\top$ with $F_1 = \begin{bmatrix} k_h C_g & -1 \end{bmatrix}$, and $F_2 = \begin{bmatrix} 0_{n_g \times 1} & 1 \end{bmatrix}$. In fact, $F_1 x = k_h e - u$ and $F_2 x = u$ such that $(e, u) \in \mathcal{F}$ if and only if $x \in \mathcal{S}$. When $\mathscr{H}$ operates in the integrator mode, by combining (2.25) and (2.26) we obtain the state space representation for the HIGS-controlled system in Fig. 2.3, given by

$$\begin{aligned} \dot{x} &= A_1 x(t) + B w(t), \\ y(t) &= C x(t), \end{aligned} \tag{2.30}$$

where $y = [e \;\; u]^\top$, and

$$\left[\begin{array}{c|c} A_1 & B \\ \hline C & \end{array}\right] = \left[\begin{array}{ccc} A_g & -B_{gv} & B_{gw} \\ \omega_h C_g & 0 & 0_{1\times n_w} \\ \hline C_g & 0 & \\ 0_{1\times n_g} & 1 & \end{array}\right]. \tag{2.31}$$

As indicated above, when the state trajectory tends to leave the set $\mathcal{S}$, which in terms of Definition 2.2.8 happens when

$$A_1 x(t) + Bw(t) \notin T_{\mathcal{S}}(x(t)), \tag{2.32}$$

for $x(t) \in \mathcal{S}$, the vector field of (2.30), is altered by partial projection such that the resulting trajectory remains inside $\mathcal{S}$. Using this perspective, we can formally introduce the HIGS-controlled system as the ePDS

$$\Sigma := \begin{cases} \dot{x}(t) = \Pi_{\mathcal{S},E}(x(t), A_1 x(t) + Bw(t)), \\ y = Cx(t), \end{cases} \tag{2.33}$$

with $\Pi_{\mathcal{S},E} : \mathcal{S} \times \mathbb{R}^n \to \mathbb{R}^n$ an operator, which projects the dynamics $A_1 x + Bw$ onto the tangent cone of the set $\mathcal{S}$ at point x, in the direction im$E$. In the case of (2.33), $E = [0_{n_p\times 1}^\top \;\; 1]^\top$ such that the correction of the dynamics (2.30) is only possible for the dynamics of the HIGS element and not for the (physical) plant dynamics (2.25). Note that as the set $\mathcal{S}$ (2.28) and the matrix E are such that Assumption 2.3.1 is satisfied, it follows from the results in Subsection 2.3.2 that the projection operator $\Pi_{\mathcal{S},E}$, is well-defined in the sense that it provides a unique outcome for every $x \in \mathcal{S}$ and each vector field $A_1 x + Bw$.

Remark 2.5.1. *It is easy to see that* (2.33) *satisfies*

$$\Pi_{\mathcal{S},E}(x, A_1 x + Bw) = -\Pi_{\mathcal{S},E}(-x, -(A_1 x + Bw)).$$

This symmetry property will prove to be useful in Section 2.6, in showing well-posedness of the system.

2.5.2 Discontinuous PWL model

In this subsection we reformulate (2.33) as an equivalent piecewise linear (PWL) model. To explicitly compute (2.33), we first note that

$$T_{\mathcal{S}}(x) = \begin{cases} T_{\mathscr{K}}(x), & \text{if } x \in \mathscr{K} \setminus -\mathscr{K}, \\ \mathscr{K} \cup -\mathscr{K}, & \text{if } x \in \mathscr{K} \cap -\mathscr{K}, \\ -T_{\mathscr{K}}(-x), & \text{if } x \in -\mathscr{K} \setminus \mathscr{K}, \end{cases} \tag{2.34}$$

where $T_{\mathscr{K}}(x) = \{a \in \mathbb{R}^n \mid F_{I(x)}a \geq 0\}$, with $I(x) = \{i \in \{1,2\} \mid F_i x = 0\}$. Based on (2.31), (2.34), and Assumption 2.5.1, we obtain that $A_1x + Bw \in T_{\mathcal{S}}(x)$ if and only if $x \in \mathcal{S}_1$ with

$$\begin{aligned}\mathcal{S}_1 = \{x \in \mathbb{R}^n \mid F_2x \geq 0 \wedge (F_1x, F_1(A_1x)) \geq_l 0\} \cup \\ \{x \in \mathbb{R}^n \mid F_2x \leq 0 \wedge (F_1x, F_1(A_1x)) \leq_l 0\}.\end{aligned} \tag{2.35}$$

The proof of the statement above can be established by comparing the algebraic expressions of (2.34) and (2.35) for states lying in the interior of $\mathcal{S}$ where $F_1x > (<)0$ and $F_2x > (<)0$, and its boundaries where $F_1x = 0$ or $F_2x = 0$. As a result of the discussion above, $\mathcal{S}_1$ is the region where the integrator mode of $\mathscr{H}$ is active. Moreover, when

$$\begin{aligned}&x \in \mathcal{S}_2 := \{x \in \mathcal{S} \mid x \notin \mathcal{S}_1\} \\ &= \underbrace{\{x \in \mathcal{S} \mid F_2x \geq 0 \wedge F_1x = 0 \wedge F_1(A_1x) < 0\}}_{\mathcal{S}_2^+} \cup \\ &\underbrace{\{x \in S \mid F_2x \leq 0 \wedge F_1x = 0 \wedge F_1(A_1x) > 0\}}_{\mathcal{S}_2^-},\end{aligned} \tag{2.36}$$

(2.32) holds. To solve (2.33) when $x \in \mathcal{S}_2$, we use the representation (2.17) of ePDS. As such, one has

$$\dot{x}(t) = A_1x(t) + Bw(t) + E\eta^\star \tag{2.37}$$

with $\eta^\star$ as in (2.18). By resorting to the Karush-Kuhn-Tucker (KKT) optimality conditions for constrained optimization one finds that when $x \in \mathcal{S}_2$, then $\eta^\star = -(F_1E)^{-1}F_1A_1x - F_1Bw$, and thus

$$\begin{aligned}\dot{x} &= A_1x + Bw + E((F_1E)^{-1}(-F_1A_1x - F_1Bw)), \\ &= \underbrace{(I - E((F_1E)^{-1}F_1)(A_1x)}_{A_2x} + Bw =: A_2x + Bw,\end{aligned} \tag{2.38}$$

where we have used that $F_1B = 0$, due to Assumption 2.5.1. We refer to (2.38) as the gain mode dynamics.

By considering both modes of operation (given by (2.30) and (2.38)) and their corresponding regions, we obtain the explicit *discontinuous* PWL model

$$\begin{aligned}\dot{x} &= \Pi_{\mathcal{S},E}(x, A_1x + Bw) = \begin{cases} A_1x + Bw, & \text{if } x \in \mathcal{S}_1, \\ A_2x + Bw, & \text{if } x \in \mathcal{S}_2, \end{cases} \\ y &= Cx,\end{aligned} \tag{2.39}$$

for (2.33). Note that $\mathcal{S}_1$ has a non-empty interior while $\mathcal{S}_2$ does not (it is part of the lower-dimensional sub-space $\ker F_1$). The matrices A_1, B and, C have been explicitly computed in (2.31). We can also compute A_2 from (2.38) as

$$\begin{aligned}\dot{x} &= A_1x + Bw + E((F_1E)^{-1}(-F_1A_1x - F_1Bw)) \\ &= \begin{bmatrix} A_gx_g - B_{gv}x_h \\ \omega_h C_g x_g \end{bmatrix} + \begin{bmatrix} B_{gw}w \\ 0 \end{bmatrix} + \\ &\quad \begin{bmatrix} 0 \\ k_hC_gA_gx_g - \omega_hC_gx_g + k_hC_gB_{gv}x_h + k_hC_gB_{gw}w \end{bmatrix}.\end{aligned}$$

As a result of Assumption 2.5.1, this simplifies to

$$\dot{x} = \begin{bmatrix} A_gx_g - B_{gv}x_h \\ k_hC_gA_gx_g \end{bmatrix} + \begin{bmatrix} B_{gw}w \\ 0 \end{bmatrix}, \tag{2.40}$$

and thus for (2.39) we have

$$\left[\begin{array}{c|c} A_2 & B \\ \hline C & \end{array}\right] = \left[\begin{array}{cc|c} A_g & -B_{gv} & B_{gw} \\ k_hC_gA_g & 0 & 0_{1\times n_w} \\ \hline C_g & 0 & \\ 0_{1\times n_g} & 1 & \end{array}\right]. \tag{2.41}$$

Hence, (2.39) with (2.31) and (2.41) is an explicit PWL formulation of the HIGS controlled system in Fig. 2.3.

Remark 2.5.2. *As observed from the expressions of $\mathcal{S}_1$ and $\mathcal{S}_2$ the switching in* (2.39) *is based on*

$$F_2x,\ F_1x,\ \text{and } F_1(A_1x),$$

where $F_2x = x_h = u$ is the output of the HIGS element (input u to the linear system $\mathscr{G}$ in Fig. 2.3) and $F_1x = k_hC_gx_g - x_h = k_he - u$, which is a function of e (output of the linear plant) and u (output of $\mathscr{H}$). Lastly, $F_1(A_1x) = k_h\dot{e} - \omega_he$ is a function of $\dot{e}$, the first derivative of the plant output, and the plant output e. Hence, the regions $\mathcal{S}_1$ and $\mathcal{S}_2$ can be fully described in terms of $e, \dot{e}$ and u. Indeed, one has $x \in \mathcal{S}_2$ when $(\dot{e}, e, u) \in \mathcal{F}_2$, where

$$\begin{aligned}\mathcal{F}_2 = \Big\{(\dot{e}, e, u) \in &\mathbb{R}^3 \mid (e, u) \in \mathcal{F} \wedge \\ &u = k_he \wedge w_he^2 > k_h\dot{e}e\Big\},\end{aligned} \tag{2.42}$$

where $\mathcal{F}$ is as defined in (2.27). *Moreover, $x \in \mathcal{S}_1$ when $(\dot{e}, e, u) \in \mathcal{F}_1$ with*

$$\mathcal{F}_1 = \{(\dot{e}, e, u) \in \mathbb{R}^3 \mid (e, u) \in \mathcal{F}\} \setminus \mathcal{F}_2. \tag{2.43}$$

A graphical illustration of the regions $\mathcal{F}_1$ and $\mathcal{F}_2$ is provided in Fig. 2.4. As a

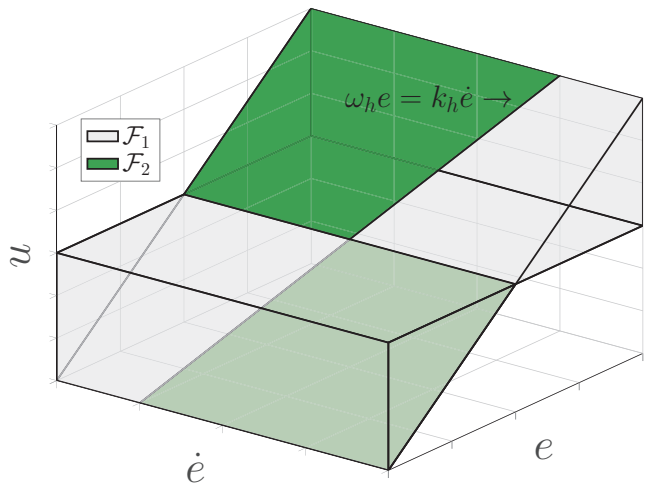

Figure 2.4. Regions $\mathcal{F}_1$ and $\mathcal{F}_2$ in $(\dot{e}, e, u)$-space.

result, an (internally) equivalent representation of (2.39) *is given by*

$$\Sigma : \begin{cases} \dot{x} = A_q x + Bw, \quad \text{if } z \in \mathcal{F}_q,\ q = 1, 2, & \text{(2.44a)} \\ z = \tilde{C}x, & \text{(2.44b)} \end{cases}$$

with augmented output signal $z = [\dot{e}\ \ e\ \ u]^\top \in \mathbb{R}^3$, *and*

$$\left[\begin{array}{c|c} A_q & B \\ \hline \tilde{C} & \end{array}\right] = \left[\begin{array}{cc|c} A_g & -B_{gv} & B_{gw} \\ \tilde{B}_{h,q}\tilde{C}_g & 0 & 0_{1\times n_w} \\ \hline \tilde{C}_g & 0_{2\times 1} & \\ 0_{1\times n_g} & 1 & \end{array}\right], \tag{2.44c}$$

with matrices $\tilde{B}_{h,1} = [0\ \ \omega_h]$, $\tilde{B}_{h,2} = [k_h\ \ 0]$, *and* $\tilde{C}_g = \left[(C_g A_g)^\top\ \ C_g^\top\right]^\top$.

Each of the different representations of the closed-loop system in Fig. 2.3 as presented above, offers advantages of their own, and can be used interchangeably for different analysis purposes.

From (2.39), we also see that we are dealing with a *discontinuous* differential equation, which makes proving (global) existence of solutions, given an initial state x_0 and external signal w, a difficult problem, since typical continuity properties used for studying differential equations/inclusions (such as upper-semicontinuity

of the right-hand side cf. [11]) are not fulfilled, see also [34] for further in-depth discussions on well-posedness of discontinuous differential equations and its related subtleties.

2.6 Well-posedness Analysis

In this section we show that the HIGS-controlled system (2.39) is well-posed in the sense of global existence and forward completeness of solutions. To this end, we first prove in Subsection 2.6.1 that (2.39) is locally well-posed, i.e., for each initial state $x(0) \in \mathcal{S}$ and exogenous signal of interest w, the system admits a solution on $[0, \epsilon]$ for some $\epsilon > 0$. We select here the class of exogenous signals (disturbances, references, etc.) to be of piecewise Bohl (PB) nature (see Definition 2.2.5). Note that sines, cosines, exponentials, polynomials, and their sums are all Bohl functions, thereby showing that the class of PB functions is sufficiently rich to accurately describe (deterministic) disturbances frequently encountered in practice. In particular, any piecewise constant signal is PB, and thus this class of functions can approximate any measurable function arbitrarily closely. An interesting future research direction is establishing the existence of solutions for larger classes of input signals. Building on the local existence results of Subsection 2.6.1, in Subsection 2.6.2 we prove that all (maximal) solutions are forward complete, i.e., are defined for all times $t \in \mathbb{R}_{\geq 0}$. To make this discussion precise, we will formalize the solution concept.

Definition 2.6.1. *Let $\mathbb{T} \subset \mathbb{R}_{\geq 0}$ be an interval of the form $[0, T]$ or $[0, T)$ with $T \in \mathbb{R}_{\geq 0}$ a finite number, or $\mathbb{T} = \mathbb{R}_{\geq 0}$. A locally AC function $x : \mathbb{T} \to \mathbb{R}^n$ is called a solution to the HIGS-controlled system* (2.39) *on $\mathbb{T}$ with initial state $x_0 \in \mathcal{S}$ and $w \in PB$, if $x(0) = x_0$, $x(t) \in \mathcal{S}$ for all $t \in \mathbb{T}$, and* (2.39) *holds almost everywhere in $\mathbb{T}$.*

The solutions in Definition 2.6.1 are *Carathéodory*-type solutions, see also [34] for more details regarding solution concepts for discontinuous dynamical systems.

2.6.1 Local Well-Posedness

Definition 2.6.2. *We call the HIGS-controlled system* (2.39) *locally well-posed if for all $x_0 \in \mathcal{S}$ and $w \in PB$, there exists an $\epsilon > 0$ such that the system admits a solution on $[0, \epsilon]$ with initial state x_0 and input w.*

Theorem 2.6.1. *The HIGS-controlled system* (2.39) *is locally well-posed.*

Proof. Take $x_0 \in \mathcal{S}$ and $w \in PB$. Without loss of generality we can take $w \in B_{[0,\tilde{\epsilon}]}$ by selecting $\tilde{\epsilon} > 0$ sufficiently small. Hence, w can be represented as

$$w(t) = H_w e^{F_w t} v_w, \quad t \in [0, \tilde{\epsilon}], \tag{2.45}$$

for some matrices $H_w \in \mathbb{R}^{n_w \times n_{F_w}}$, $F_w \in \mathbb{R}^{n_{F_w} \times n_{F_w}}$ and a vector $v_w \in \mathbb{R}^{n_{F_w}}$. In other words, w is generated (on $[0, \bar{\epsilon}]$) by the exo-system

$$\dot{x}_w = F_w x_w, \quad w = H_w x_w \quad x_w(0) = v_w, \tag{2.46}$$

Combining this exo-system with (2.39) yields

$$\begin{aligned} \dot{\hat{x}} &= \Pi_{\hat{\mathcal{S}},\hat{E}}(\hat{x}, \hat{A}_1\hat{x}) = \begin{cases} \hat{A}_1\hat{x}, & \text{if } \hat{x} \in \hat{\mathcal{S}}_1, \\ \hat{A}_2\hat{x}, & \text{if } \hat{x} \in \hat{\mathcal{S}}_2, \end{cases} \\ z &= \hat{C}\hat{x}, \end{aligned} \tag{2.47}$$

where $\hat{x} = \begin{bmatrix} x^\top & x_w^\top \end{bmatrix}^\top$ and

$$\hat{A}_1 = \begin{bmatrix} A_1 & BH_w \\ 0 & F_w \end{bmatrix}, \quad \hat{A}_2 = \begin{bmatrix} A_2 & BH_w \\ 0 & F_w \end{bmatrix}, \quad \hat{C} = \begin{bmatrix} C & 0 \end{bmatrix},$$

as an equivalent description of (2.39) with w as in (2.45) on $[0, \bar{\epsilon}]$. Here, $\hat{E} = \begin{bmatrix} E^\top & 0^\top \end{bmatrix}^\top$, and $\hat{\mathcal{S}} = \hat{\mathscr{H}} \cup -\hat{\mathscr{H}}$ with $\hat{\mathscr{H}} = \{\hat{x} \in \mathbb{R}^{n+n_{F_w}} \mid \hat{F}\hat{x} \geq 0\}$, where $\hat{F} = \begin{bmatrix} \hat{F}_1^\top & \hat{F}_2^\top \end{bmatrix}^\top$ with $\hat{F}_1 = [F_1 \;\; 0]$ and $\hat{F}_2 = [F_2 \;\; 0]$. Furthermore, the regions $\hat{\mathcal{S}}_1$ and $\hat{\mathcal{S}}_2$ are given by

$$\begin{aligned} \hat{\mathcal{S}}_1 = \{&\hat{x} \in \mathbb{R}^{n+n_{F_w}} \mid \hat{F}_2\hat{x} \geq 0 \wedge (\hat{F}_1\hat{x}, \hat{F}_1(\hat{A}_1\hat{x})) \geq_l 0\} \cup \\ &\{\hat{x} \in \mathbb{R}^{n+n_{F_w}} \mid \hat{F}_2\hat{x} \leq 0 \wedge (\hat{F}_1\hat{x}, \hat{F}_1(\hat{A}_1\hat{x})) \leq_l 0\}, \\ \hat{\mathcal{S}}_2 = \{&\hat{x} \in \hat{\mathcal{S}} \mid \hat{F}_2\hat{x} \geq 0 \wedge \hat{F}_1\hat{x} = 0 \wedge \hat{F}_1(\hat{A}_1\hat{x}) < 0\} \cup \\ &\{\hat{x} \in \hat{\mathcal{S}} \mid \hat{F}_2\hat{x} \leq 0 \wedge \hat{F}_1\hat{x} = 0 \wedge \hat{F}_1(\hat{A}_1\hat{x}) > 0\}. \end{aligned}$$

For proving local well-posedness of (2.47) (and thus of (2.39) with w as in (2.45)), we define the set

$$\hat{\mathcal{S}}_{\text{int}} := \{\hat{x}_0 \in \hat{\mathcal{S}} \mid \exists \epsilon > 0, \; \forall t \in [0, \epsilon], \; e^{\hat{A}_1 t}\hat{x}_0 \in \hat{\mathcal{S}}\}. \tag{2.48}$$

In fact, since $\hat{\mathcal{S}}_{\text{int}} \subseteq \hat{\mathcal{S}}_1$, we conclude that $e^{\hat{A}_1 t}\hat{x}_0$ is also a solution to (2.47) on a non-trivial time window $[0, \varepsilon]$ for some $0 < \varepsilon \leq \bar{\varepsilon}$. Next, we will also show that for each $\hat{x}_0 \in \hat{\mathcal{S}} \setminus \hat{\mathcal{S}}_{\text{int}}$, a local solution to (2.47) exists, so that it is established that for all $\hat{x}_0 \in \hat{\mathcal{S}}$ a local solution exists. In order to do so, we first rewrite (2.48) in a more algebraic form. Using the definition of $\hat{\mathcal{S}}$, one can rewrite (2.48) as

$$\begin{aligned} &\hat{\mathcal{S}}_{\text{int}} = \\ &\{\hat{x}_0 \mid \exists \epsilon > 0, \; \forall t \in [0, \epsilon), \; \hat{F}_1 e^{\hat{A}_1 t}\hat{x}_0 \geq 0 \wedge \hat{F}_2 e^{\hat{A}_1 t}\hat{x}_0 \geq 0\} \cup \\ &\{\hat{x}_0 \mid \exists \epsilon > 0, \; \forall t \in [0, \epsilon), \; \hat{F}_1 e^{\hat{A}_1 t}\hat{x}_0 \leq 0 \wedge \hat{F}_2 e^{\hat{A}_1 t}\hat{x}_0 \leq 0\}. \end{aligned}$$

By using the Taylor series expansion of $e^{\hat{A}_1 t}$ together with the Cayley-Hamilton theorem, the characterization $\hat{\mathcal{S}}_{\text{int}} = \hat{\mathcal{S}}^+_{\text{int}} \cup -\hat{\mathcal{S}}^+_{\text{int}}$ is obtained with

$$\begin{aligned}\hat{\mathcal{S}}^+_{\text{int}} = \\ \Big\{\hat{x} \in \mathbb{R}^{n+n_{F_w}} \mid &\begin{pmatrix}\hat{F}_1\hat{x}, \hat{F}_1\hat{A}_1\hat{x}, \dots, \hat{F}_1\hat{A}_1^{n+n_{F_w}-1}\hat{x}\end{pmatrix} \geq_l 0 \\ \wedge &\begin{pmatrix}\hat{F}_2\hat{x}, \hat{F}_2\hat{A}_1\hat{x}, \dots, \hat{F}_2\hat{A}_1^{n+n_{F_w}-1}\hat{x}\end{pmatrix} \geq_l 0\Big\},\end{aligned}$$

Claim: $\hat{x}_0 \in \hat{\mathcal{S}} \setminus \hat{\mathcal{S}}_{\text{int}}$ implies that $\hat{F}_1\hat{x}_0 = 0 \wedge \hat{F}_2\hat{x}_0 \neq 0$. To prove the claim, note that when $\hat{x}_0$ lies in the interior of $\hat{\mathcal{S}}$, then $\hat{x}_0 \in \hat{\mathcal{S}}_{\text{int}}$ since $(\hat{F}_1\hat{x}_0 > 0 \wedge \hat{F}_2\hat{x}_0 > 0)$ or $(\hat{F}_1\hat{x}_0 < 0 \wedge \hat{F}_2\hat{x}_0 < 0)$. Moreover, $\hat{F}_2\hat{x}_0 = 0$ and $\hat{x}_0 \in \hat{\mathcal{S}}$ also imply $\hat{x}_0 \in \hat{\mathcal{S}}_{\text{int}}$. To show this, we use

$$\hat{F}_2\hat{A}_1 = \frac{\omega_h}{k_h}(\hat{F}_1 + \hat{F}_2), \tag{2.49}$$

which can be verified based on the expressions of $\hat{F}_2$, $\hat{A}_1$, and $\hat{F}_1$. Consider the sequence $(\hat{F}_1\hat{x}_0, \hat{F}_1\hat{A}_1\hat{x}_0, \hat{F}_1\hat{A}_1^2\hat{x}_0, \dots)$ and let $\hat{F}_1\hat{A}_1^\rho\hat{x}_0$ be the first nonzero element of the sequence for $\rho \in \mathbb{N}$. Then, it follows from (2.49) that $\hat{F}_2\hat{A}_1^k\hat{x}_0 = 0$ for $k = 0, 1, \dots, \rho$, and $\hat{F}_2\hat{A}_1^{\rho+1}\hat{x}_0 = \frac{\omega_h}{k_h}\hat{F}_1\hat{A}_1^\rho\hat{x}_0$. This shows that if $\hat{F}_2\hat{x}_0 = 0$ and $\hat{x}_0 \in \hat{\mathcal{S}}$, then $\hat{x}_0 \in \hat{\mathcal{S}}_{\text{int}}$ (using the lexicographic inequalities in $\hat{\mathcal{S}}^+_{\text{int}}$ and $(-\hat{\mathcal{S}}^+_{\text{int}})$). This proves the claim.

Additionally, let us make the observation that if for some $\hat{x} \in \mathbb{R}^{n+n_w}$ and some $N \in \mathbb{N}$ one has $\hat{F}_1\hat{A}_1^k\hat{x} = 0$, $k = 0, 1, 2, \dots, N$, then

$$\hat{F}_1\hat{A}_1\hat{A}_2^k\hat{x} = 0, \qquad k = 0, 1, 2, \dots, N-1, \tag{2.50}$$

$$\hat{F}_1\hat{A}_1\hat{A}_2^N\hat{x} = \hat{F}_1\hat{A}_1^{N+1}\hat{x}. \tag{2.51}$$

This identity can be easily verified by substituting the expression (2.38) for $\hat{A}_2$ in (2.50) and (2.51).

In case $\hat{x}_0 \in \hat{\mathcal{S}} \setminus \hat{\mathcal{S}}_{\text{int}}$, and thus $\hat{F}_1\hat{x}_0 = 0$ and $\hat{F}_2\hat{x}_0 \neq 0$, we will show that a solution of the form $\bar{x}(t) = e^{\hat{A}_2 t}\hat{x}_0 \in \hat{\mathcal{S}}_2$ exists and is a local solution to (2.47). For the case where $\hat{F}_2\hat{x}_0 > 0$. To show $\bar{x}(t) \in \hat{\mathcal{S}}_2$, let us note that since $\hat{F}_2\hat{x}_0 > 0$, the constraint $\hat{F}_2\bar{x}(t) \geq 0$ is satisfied by continuity for $t \in (0, \epsilon]$, with $\epsilon > 0$ sufficiently small. Thus it is sufficient to show that

$$\hat{F}_1\bar{x}(t) = 0 \wedge \hat{F}_1\hat{A}_1\bar{x}(t) < 0, \quad t \in (0, \epsilon],$$

due to the definition of $\hat{\mathcal{S}}_2$. Since we know that $\hat{F}_1\bar{x}(t) = 0$ for all t, it suffices to show that

$$\hat{F}_1\hat{A}_1\bar{x}(t) < 0, \text{ for } t \in (0, \epsilon]. \tag{2.52}$$

To prove this, we use the fact that $\hat{x}_0 \in \hat{\mathcal{S}} \setminus \hat{\mathcal{S}}_{\text{int}}$ implies

$$(\hat{F}_1\hat{A}_1\hat{x}_0, \hat{F}_1\hat{A}_1^2\hat{x}_0, \dots, \hat{F}_1\hat{A}_1^{n+n_{F_w}}\hat{x}_0) <_l 0. \tag{2.53}$$

By using (2.50) and (2.51), (2.53) implies

$$(\hat{F}_1\hat{A}_1\hat{x}_0, \hat{F}_1\hat{A}_1A_2\hat{x}_0, \ldots, \hat{F}_1\hat{A}_1\hat{A}_2^{n+n_{F_w}-1}\hat{x}_0) <_l 0, \tag{2.54}$$

which indeed implies (2.52) for some $\epsilon > 0$, and thus

$$\bar{x}(t) = e^{\hat{A}_2 t}\hat{x}_0 \in \hat{\mathcal{S}}_2 \text{ for } t \in (0, \epsilon],$$

for some $\epsilon > 0$. Therefore, $\bar{x}(t)$ is a solution to (2.47). As a result of the symmetry property shown in Remark 2.5.1, this also proves local existence of solutions when $\hat{F}\hat{x}_0 < 0$. Hence, we conclude local well-posedness. □

2.6.2 Forward completeness

Definition 2.6.3. *Let $\mathbb{T} \subset \mathbb{R}_{\geq 0}$ be an interval of the form $[0, T]$ or $[0, T)$ with $T \in \mathbb{R}_{\geq 0}$ a finite number, or $\mathbb{T} = \mathbb{R}_{\geq 0}$. A solution $x : \mathbb{T} \to \mathbb{R}^n$ to (2.39) with $w \in PB$ on $\mathbb{T}$ is called maximal, if there does not exist a solution $x' : \mathbb{T}' \to \mathbb{R}^n$ with $w \in PB$ on $\mathbb{T}'$, where $\mathbb{T}' = [0, T')$ with $T' \in \mathbb{R}_{\geq T}$, that satisfies $x(t) = x'(t)$ for $t \in \mathbb{T}$. A solution $x : \mathbb{T} \to \mathbb{R}^n$ is forward complete, if $\mathbb{T} = \mathbb{R}_{\geq 0}$.*

Hence, a maximal solution is a solution that cannot be prolonged (is not a strict prefix of another "larger" solution for the same input).

Theorem 2.6.2. *All maximal solutions to HIGS-controlled system (2.39) for $w \in PB$ are forward complete.*

Proof. Consider a maximal solution $x : \mathbb{T} \to \mathbb{R}^n$ of (2.39) for initial state $x_0 \in \mathcal{S}$ and $w \in PB$. We will show that if $\mathbb{T}$ is equal to $[0, T]$ or $[0, T)$ with $T \in \mathbb{R}_{\geq 0}$ a finite number, the left-limit $x(T) := \lim_{t \uparrow T} x(t) \in \mathcal{S}$ exists, and we can exploit the local existence result to prolong x to a solution on $[0, T + \varepsilon)$. This would contradict the maximality of the solution and thus $\mathbb{T} = \mathbb{R}_{\geq 0}$, hence x has to be forward complete.
To show the existence of $\lim_{t \uparrow T} x(t)$, let us remark that if $\mathbb{T}$ is equal to $[0, T]$, the solution is AC on $[0, T]$ and thus the left-limit trivially exists. So, the exciting case to handle is $[0, T)$. By Definition 2.2.5, w can be represented on $[t_i, T]$ as in (2.45) for some $t_i < T$ (in fact, t_i is the largest value in the set $\{t_k\}_{k \in \mathbb{N}}$, which is strictly smaller than T). Thus, (2.39) can be equivalently written as (2.47) on $[t_i, T]$. This implies the existence of a constant $M \in \mathbb{R}$ such that the vector field of (2.47) satisfies the linear growth condition

$$\|\Pi_{\hat{\mathcal{S}}, \hat{E}}(\hat{x}, \hat{A}_1\hat{x})\| \leq M\|\hat{x}\|, \text{ for all } \hat{x} \in \mathbb{R}^{n+n_{F_w}}, \tag{2.55}$$

because $\Pi_{\hat{\mathcal{S}}, \hat{E}}(\hat{x}, \hat{A}_1\hat{x}) \in \{\hat{A}_1\hat{x}, \hat{A}_2\hat{x}\}$. As a result of (2.55),

$$\begin{aligned}\|\hat{x}(t)\| &\leq \|\hat{x}_0\| + \int_0^t \|\Pi_{\hat{\mathcal{S}}, \hat{E}}(\hat{x}(\tau), \hat{A}_1\hat{x}(\tau))\| d\tau \\ &\leq \|\hat{x}_0\| + M\int_0^t \|\hat{x}(\tau)\| d\tau, \qquad \text{for } t \in [t_i, T].\end{aligned}$$

By applying Gronwall's Lemma [88], one concludes that $\|\hat{x}(t)\| \leq L$ for some constant $L > 0$ and $t \in [0, T)$. Moreover, for $t \in [t_i, T]$ one has

$$\|\hat{x}(s) - \hat{x}(t)\| \leq \int_t^s \|\Pi_{\hat{\mathcal{S}},\hat{E}}(\hat{x}(\tau), \hat{A}_1\hat{x}(\tau))\| d\tau.$$

Once again we use (2.55) together with $\|\hat{x}(t)\| \leq L$ to conclude $\|\hat{x}(s) - \hat{x}(t)\| \leq M\int_t^s \|\hat{x}(\tau)\| d\tau \leq ML(s-t)$. Hence, the solution $\hat{x}(t)$ is Lipschitz continuous on $t \in [t_i, T]$, and thus also absolutely continuous and uniformly continuous. Thereby, the limit $\hat{x}(T) := \lim_{t\uparrow T} \hat{x}(t)$ exists, as required. □

Since we proved local existence of solutions and forward completeness of all maximal solutions, it is concluded that for each initial state $x_0 \in \mathcal{S}$ and $w \in PB$ a global solution exists on $[0, \infty)$ and all solutions can be extended to be defined on $[0, \infty)$.

Remark 2.6.1. *In this chapter, we have provided a proof of existence and forward completeness of so-called Carathéodry solutions to HIGS-controlled systems. When analyzing properties of discontinuous dynamical systems in general and HIGS-controlled systems in particular, as pointed out in [52], it is of interest to also consider Krasovskii solutions (see e.g. [34]) in order to ensure robustness of stability guarantees with respect to small state perturbations due to measurement errors. In [38], stability analysis tools are presented that guarantee input-to-state stability of Carathéodry solutions to HIGS-controlled systems. Furthermore, it is also shown that the stability guarantees obtained by the methods presented in [38] also extend to stability guarantees for Krasovskii solutions to the system, thereby ensuring robustness with respect to small state perturbations.*

2.7 Summary and Conclusions

In this chapter we introduced the class of extended projected dynamical systems (ePDS). This class includes as a special case the well-established PDS and extends their usage to accommodate for partial projections on a larger range of constraint sets. We have established a connection between our representation of ePDS and representations that resemble those frequently utilized in the PDS literature, cf. (2.23). The extension of PDS to ePDS was instrumental in (and, in fact, motivated by) the mathematical formalization of HIGS-controlled systems, which was lacking in the literature so far. Additionally, we have proven the fundamental property of well-posedness of HIGS-controlled systems [37, 73, 145], in the sense of existence and forward completeness of solutions.

Future research directions include the relaxation of the conditions in Assumption 2.3.1 in order to enable the modeling of a larger variety of systems in the ePDS framework. Moreover, well-posedness analysis of ePDS in general, and

HIGS-controlled systems in particular, beyond references and disturbances being piece-wise Bohl functions as well as proving uniqueness of solutions are open issues. In addition, the study of multiple HIGS elements in a control loop and connections to other classes of dynamical systems including complementarity systems (see e.g., [66, 147]), are of special interest.

3

On the Equivalence of Extended and Oblique Projected Dynamics with Applications to Hybrid Integrator-Gain Systems

Abstract - *The class of projected dynamical systems (PDS) provides a powerful framework for modeling dynamical systems of which the trajectories are constrained to a set by means of projection. This chapter is concerned with establishing equivalence results among two variations of PDS. These are (i) extended PDS (ePDS), which enable partial projection of dynamics, and (ii) oblique PDS, (oPDS) where projections can be done with respect to non-Euclidean norms. We present two sets of sufficient conditions for equivalence among these two system classes. These results enable the transfer of system theoretic properties and tools from one class to the other, which we illustrate in this chapter. As an application, we study hybrid integrator-gain systems (HIGS), which are hybrid control elements aiming at overcoming fundamental limitations of linear time-invariant control, and are formally described in the ePDS framework. We use our results to also describe these control elements as oPDS, thereby enabling the study of HIGS-controlled systems in this*

This chapter is based on [122, 124].

framework. Using the oPDS representation of HIGS-controlled systems, sufficient conditions for incremental stability of these systems are presented.

3.1 Introduction

Projected dynamical systems (PDS) [40, 102] form an important class of discontinuous dynamical systems, which have proven to be useful in the study of many different applications. Examples include control and optimisation [24, 57, 67, 86, 123] as well as the study of oligopolistic markets, urban transportation networks, traffic networks, international trade, agricultural and energy markets [102]. PDS are particularly useful in describing constrained dynamical systems, where the trajectories are ensured to be within a given constraint set at all times by means of projection.

In this chapter, we are interested in two recent variations of PDS. One variation is formed by *extended projected dynamical systems* (ePDS), which were introduced in [123] and extend the class of PDS in two essential ways. Firstly, while PDS have been shown to be well-defined for constraint sets that satisfy certain regularity conditions (convexity in [11, 102] and Clarke regularity and prox-regularity (see [114]) in [33]), ePDS are well-defined for other constraint sets not satisfying these conditions. Secondly, while in the PDS literature the complete vector field is projected onto the constraint set, the ePDS framework considers the possibility of partial projection of dynamics (see Chapter 2 for details). This feature of ePDS is particularly useful in the context of systems and control, where one can only modify (and thus project) the controller dynamics and not the plant dynamics, which abide the laws of physics and can not be altered by means of projections.

The other class consists of so-called *oblique projected dynamical systems* (oPDS) [57] which are extensions of PDS in the sense that in contrast to the PDS literature, where projections are performed with respect to the standard Euclidean norm, oPDS provide the possibility of having projections with respect to (varying) non-Euclidean norms. The class of oPDS are particularly interesting in the context of feedback-based optimization [58, 59].

The main contributions of this chapter are establishing conditions under which ePDS and oPDS are equivalent in the sense that they lead to same system trajectories. In particular, we provide two sets of sufficient conditions under which ePDS can be written as oPDS and vice versa. These results are motivated by the fact that while many constrained systems (especially in the context of systems and control, such as HIGS-based controllers [38] discussed later) are naturally modelled in the ePDS framework, the PDS and oPDS frameworks are currently much more extensively studied. In particular, there exists many results on existence and uniqueness of solutions [11, 33, 57, 102], stability analysis [57, 102] and equivalence to other classes of discontinuous dynamical systems [24, 66] for PDS and oPDS. As such, establishing an equivalence would be useful as it facilitates transferring existing theoretical properties and tools between the classes of oPDS and ePDS. In this work, we particularly highlight this transfer of system-theoretic results, for properties such as (incremental) stability.

As an interesting case study, we consider *hybrid integrator-gain systems* (HIGS)

[37, 38, 75, 123, 145], which are recently introduced hybrid control elements aiming at overcoming fundamental limitations of linear time-invariant (LTI) control and, as reported in [37, 38, 73, 75, 145], have enjoyed considerable engineering success, particularly in the field of high-precision mechatronics. In [38, 123], HIGS-controlled systems are formally described in the ePDS framework, which turns out to be the natural framework for their formalization. As another contribution of this work, we use our equivalence results to obtain a mathematical description of HIGS-controlled systems in the oPDS framework, which in turn, provides the possibility of analyzing HIGS-controlled systems based on existing results available in the PDS and oPDS literature. In particular, we showcase the strength of this result by using the oPDS representation of HIGS-controlled systems to study properties such as incremental stability of these systems, building on results available for oPDS (see, e.g., [64]).

The remainder of this chapter is organized as follows. Section 3.2 contains preliminary definitions and notation. In Section 3.3, the system classes considered in this chapter are described. Sufficient conditions for establishing equivalence between ePDS and oPDS are presented in Section 3.4. In Section 3.5 we present some implications of the equivalence results. Section 3.6 is concerned with HIGS-controlled systems and their oPDS description. Based on the obtained oPDS representation of HIGS-controlled systems, sufficient conditions for their incremental stability are presented in Section 3.7. The chapter is concluded in Section 3.8, where conclusions and future directions of research are provided.

3.2 Preliminaries and notation

We say that a matrix $A \in \mathbb{R}^{n\times n}$ is positive definite, denoted by $A \succ 0$ if it is symmetric and $x^\top Ax > 0$ for all $x \in \mathbb{R}^n \setminus \{0\}$. The Euclidean inner product between two vectors $a \in \mathbb{R}^n$ and $b \in \mathbb{R}^n$, denoted by $\langle a, b\rangle$, is defined as $\langle a, b\rangle = a^\top b$. We will also use a "weighted" inner product based on a symmetric positive definite matrix G, denoted by $\langle ., .\rangle_G$ and given by $\langle a, b\rangle_G = a^\top Gb$. For the null space (or kernel) of a matrix $H \in \mathbb{R}^{n\times m}$ we write $\ker H = \{x \in \mathbb{R}^m \mid Hx = 0\}$, and for its column space (or image) we write $\mathrm{im} H = \{Hx \mid x \in \mathbb{R}^m\}$. Moreover, for $J \subseteq \{1, \dots, n\}$, we denote by H_J the matrix of size $|J|\times m$, with $|J|$ the cardinality of set J, consisting of the rows of H with indices in J. The tangent cone to a set $K \subset \mathbb{R}^n$ at a point $x \in K$, denoted by $T_K(x)$, is the set of all vectors $w \in \mathbb{R}^n$ for which there exist sequences $\{x_i\}_{i\in\mathbb{N}} \in K$ and $\{\tau_i\}_{i\in\mathbb{N}}$, $\tau_i > 0$ with $x_i \to x$, $\tau_i \downarrow 0$ and $i \to \infty$, such that $w = \lim_{i\to\infty} \frac{x_i - x}{\tau_i}$. Given a set $K \subseteq \mathbb{R}^n$, for $x \in K$, we define the normal cone of K at x as $N_K(x) = \{s \in \mathbb{R}^n \mid \langle s \mid k - x\rangle \leq 0 \text{ for all } k \in K\}$. A continuous function $\alpha : [0, a) \to [0, \infty)$ is said to belong to class $\mathcal{K}$ if it is strictly increasing and $\alpha(0) = 0$. A continuous function $\alpha : [0, a) \to [0, \infty)$ is said to belong to class $\mathcal{K}_\infty$, if $\alpha \in \mathcal{K}$ and $\alpha(s) \to \infty$, as $s \to \infty$. A continuous function $\beta : [0, a) \times [0, \infty) \to [0, \infty)$ is said to belong to class $\mathcal{KL}$ if, for each fixed s,

the mapping $r \mapsto \beta(r,s)$ belongs to class $\mathcal{K}$ with respect to r and, for each fixed r, the mapping $s \mapsto \beta(r,s)$ is decreasing with respect to s and $\beta(r,s) \to 0$ as $s \to \infty$. Finally, L_∞^{loc} denotes the set of locally essentially bounded functions on $\mathbb{R}_{\geq 0} := [0,\infty)$. A function $w : \mathcal{I} \to \mathbb{R}^{n_w}$, with $\mathcal{I} \subseteq \mathbb{R}$ is called a Bohl function, denoted by $w \in B_{\mathcal{I}}$, if there exist matrices $H \in \mathbb{R}^{n_w \times n_F}$, $F \in \mathbb{R}^{n_F \times n_F}$, and a vector $v \in \mathbb{R}^{n_F}$ such that $w(t) = He^{Ft}v$ for all $t \in \mathcal{I}$. A function $w : \mathbb{R}_{\geq 0} \to \mathbb{R}^{n_w}$ is called a piecewise Bohl function, denoted by $w \in PB$, if there exists a sequence $\{t_i\}_{i\in\mathbb{N}}$ with $0 = t_0 < t_i < t_{i+1}$ for all $i \in \mathbb{N}$ and $t_i \to \infty$ when $i \to \infty$ such that $w : [t_i, t_{i+1}) \to \mathbb{R}^{n_w}$ is a Bohl function for each $i \in \mathbb{N}$.

3.3 System Classes

In this section we describe the classes of discontinuous dynamical systems considered in this chapter. Both the system classes are variations of so-called Projected dynamical systems (PDS) [24, 40, 64, 102], which are described by differential equations of the form

$$\dot{x}(t) = \Pi_S(x(t), f(x(t), w(t))), \tag{3.1}$$

where $x(t) \in \mathbb{R}^n$ and $w(t) \in \mathbb{R}^{n_w}$ denote the state and exogenous (disturbances) inputs at time $t \in \mathbb{R}_{\geq 0}$, $f : \mathbb{R}^n \times \mathbb{R}^{n_w} \to \mathbb{R}^n$ is a vector field and Π_S is a projection operator that projects the dynamics onto the tangent cone of the constraint set $S \subseteq \mathbb{R}^n$. A more detailed description of PDS can be found in Chapter 2.

3.3.1 Extended Projected Dynamical Systems

Extended projected dynamical systems (ePDS) are discontinuous dynamical systems introduced in [123] and given by

$$\dot{x}(t) = \Pi_{S,E}(x(t), f(x(t), w(t))), \tag{3.2}$$

where $x(t) \in \mathbb{R}^n$ and $w(t) \in \mathbb{R}^{n_w}$ denote the state and exogenous (disturbances) inputs at time $t \in \mathbb{R}_{\geq 0}$, $f : \mathbb{R}^n \times \mathbb{R}^{n_w} \to \mathbb{R}^n$ is a vector field and $\Pi_{S,E}$ is a projection operator that projects the dynamics onto the tangent cone of the constraint set $S \subseteq \mathbb{R}^n$ in the direction specified by the image of the matrix $E \in \mathbb{R}^{n \times n_E}$. Without loss of generality we can assume E to have full column rank. In particular, this projection operator is given by

$$\Pi_{S,E}(x,v) = P_{T_S(x),E}(v) := \underset{\substack{a \in T_S(x) \\ a - v \in \operatorname{Im} E}}{\arg\min} \|a - v\|. \tag{3.3}$$

Note that ePDS have PDS as a special case. Indeed, with $\operatorname{Im} E = \mathbb{R}^n$, ePDS becomes the classical PDS formulation

$$\Pi_S(x,v) = P_{T_S(x)}(v) := \underset{a \in T_S(x)}{\arg\min} \|a - v\|. \tag{3.4}$$

Alternatively, (3.3) can be written as

$$\Pi_{S,E}(x,v) = v + E\eta^\star(x,v) \tag{3.5}$$

with

$$\eta^\star(x,v) = \underset{\eta\in\Lambda(x,v)}{\arg\min} \|E\eta(x,v)\| \tag{3.6}$$

and

$$\Lambda(x,v) = \{\eta \in \mathbb{R}^{n_E} \mid v + E\eta \in T_S(x)\}. \tag{3.7}$$

In Chapter 2, it is shown that under certain assumptions (see Assumption 2.3.1 in Chapter 2) (3.3) is equivalent to

$$\Pi_{S,E}(x,v) = \lim_{\delta\downarrow 0} \frac{P_{S,E}(x+\delta v) - x}{\delta}, \tag{3.8}$$

where, similarly to (3.3), we have $P_{S,E}(v) := \arg\min_{\substack{a\in S \\ a-v\in \operatorname{Im} E}} \|a - v\|$.

For now, we consider constraint sets that are convex polyhedral cones given by

$$S := \{x \in \mathbb{R}^n \mid Fx \geq 0\}, \tag{3.9}$$

for some matrix $F \in \mathbb{R}^{n_f\times n}$, although in the HIGS application (see Section 3.6) and also [57], more general (non-convex) constraint sets will be studied. Note that the tangent cone to S as in (3.9) is given by

$$T_S(x) = \{a \in \mathbb{R}^n \mid F_{I(x)}a \geq 0\}, \tag{3.10}$$

where

$$I(x) = \{i \in \{1,\dots,n_f\} \mid F_i x = 0\},$$

denotes the set of active constraints at $x \in S$.

Lemma 3.3.1. *$\Pi_{S,E}(x,v)$ is well-defined in the sense that the right-hand side of (3.3) consists of a single point, for all $x \in S$ and $v \in \mathbb{R}^n$, if and only if*

$$S + imE = \mathbb{R}^n. \tag{3.11}$$

Proof. Note that (3.11) implies that given any $v \in \mathbb{R}^n$, there exists an η such that $v + E\eta \in S \subseteq T_S(x)$, and thus, $\Lambda(x,v)$ (see (3.7)) is nonempty for all $x \in \mathbb{R}^n$ and all $v \in \mathbb{R}^n$. Moreover, using that $T_S(x)$ is a convex polyhedral cone (see (3.10)), implies that $\Lambda(x,v)$ is closed and convex. Combining this with the fact that square of the cost (3.6) $\eta^\top E^\top E\eta$ is a quadratic positive definite function as E has full column rank, (3.6) has a unique minimizer, and thus the right-hand side of (3.2) is well-defined. □

In this work the representation in (3.5) will be useful for establishing an equivalence between ePDS and oPDS.

3.3.2 Projected Dynamical Systems with Oblique Projections

Projected dynamical systems with oblique projections (oPDS) were introduced in [57] and are given by

$$\dot{x}(t) = \Pi_S^G(x(t), f(x(t), w(t))), \tag{3.12}$$

where $x(t) \in \mathbb{R}^n$ and $w(t) \in \mathbb{R}^{n_w}$ denote the state and exogenous inputs at time $t \in \mathbb{R}_{\geq 0}$, $f : \mathbb{R}^n \times \mathbb{R}^{n_w} \to \mathbb{R}^n$ is a vector field, as before, and Π_S^G is a projection operator given by

$$\Pi_S^G(x, v) = P^G_{T_S(x)}(v) := \underset{a \in T_S(x)}{\arg\min} \|a - v\|_G \tag{3.13}$$

with

$$\|a - v\|_G := \sqrt{(a - v)^\top G (a - v)}, \tag{3.14}$$

where $G \in \mathbb{R}^{n \times n}$ is symmetric positive definite, to make $\|.\|_G$ a well-defined norm. Note that with $G = I_n$, (3.13) also reduces to the classical PDS formulation (3.4).

It should be pointed out that (3.13) is well-defined for all $x \in S$ and all $v \in \mathbb{R}^n$ when constraint sets of the form (3.9) are considered, as the vector field is simply obtained through projection (with respect to a particular norm $\|.\|_G$, and without any restrictions as opposed to ePDS (c.f. (3.11))) onto the closed convex constraint set (3.9).

Remark 3.3.1. *Although in* (3.13) *we consider projections defined based on a constant matrix G, this need not be the case in general. In particular G could vary as a function of the state x by using the notion of Riemannian metrics to define a variable inner product on $T_S(x)$ that changes as a function of x (see [57] for more details).*

Our study of oPDS with a constant matrix G is motivated by the fact that they can be linked to the classical PDS (and thus ePDS) by means of similarity transformations and thus, the results available for PDS can be used for studying oPDS as in (3.12). We make this more explicit in Lemma 3.3.2.

Lemma 3.3.2. *Every oPDS of the form* (3.12)*, with a constant $G \succ 0$ can be written as a PDS and thus an ePDS.*

Proof. Let us introduce a similarity transformation of the system (3.12) by considering $\bar{x} = G^{\frac{1}{2}} x$. We then obtain

$$\begin{aligned} \dot{\bar{x}} = G^{\frac{1}{2}} \dot{x} &= G^{\frac{1}{2}} \underset{v \in T_S(G^{-\frac{1}{2}} \bar{x})}{\arg\min} \|v - f(G^{-\frac{1}{2}} \bar{x}, w)\|_G \\ &= G^{\frac{1}{2}} \underset{v \in T_S(G^{-\frac{1}{2}} \bar{x})}{\arg\min} \|G^{\frac{1}{2}} v - G^{\frac{1}{2}} f(G^{-\frac{1}{2}} \bar{x}, w)\|_{G^{-\frac{1}{2}\top} G G^{-\frac{1}{2}}}. \end{aligned} \tag{3.15}$$

Using Lemma 1 in [64], we get

$$\begin{aligned}\dot{\overline{x}} &= \underset{a\in T_{\overline{S}}(\overline{x})}{\arg\min}\|a - G^{\frac{1}{2}} f(G^{-\frac{1}{2}}\overline{x}, w)\| \\ &= \underset{a\in T_{\overline{S}}(\overline{x})}{\arg\min}\|a - \overline{f}(\overline{x}, w)\|\end{aligned} \tag{3.16}$$

with $a = G^{\frac{1}{2}} v$, and $\overline{S} = G^{\frac{1}{2}} S$, $\overline{f}(\overline{x}, w) = G^{\frac{1}{2}} f(G^{-\frac{1}{2}}\overline{x}, w)$. As such, we obtain

$$\dot{\bar{x}} = \Pi_{\bar{S}}(\bar{x}, \bar{f}(\bar{x}, w)), \tag{3.17}$$

Moreover, (3.17) is equivalent to the ePDS $\dot{\bar{x}} = \Pi_{\bar{S},E}(\bar{x}, \bar{f}(\bar{x}, w))$, with any E such that $\mathrm{im}E = \mathbb{R}^n$. This completes the proof. □

Note that (3.17) is in the well-studied classical PDS form considered in, e.g., [24, 40, 67, 102]. As presented in Lemma 3.3.2, the subclass of oPDS considered in this work are in fact PDS and since PDS are a special case of ePDS, (3.12) can always be written as an ePDS by means of a similarity transformation.

3.4 Sufficient Conditions For Equivalence

In this section, we present sufficient conditions for the equivalence of the ePDS (3.2) and the oPDS (3.12). As mentioned before, we consider constraint sets that are convex polyhedral cones described by (3.9), for which the tangent cone is given by (3.10).

Theorem 3.4.1. *Given a constraint set $S \subseteq \mathbb{R}^n$ of the form (3.9), a matrix $E \in \mathbb{R}^{n\times n_E}$ such that (3.11) holds, and a positive definite matrix $G \in \mathbb{R}^{n\times n}$,*

$$\Pi_{S,E}(x, v) = \Pi_S^G(x, v), \tag{3.18}$$

for all $x \in S$ and for all $v \in \mathbb{R}^n$, if

$$G^{-1}F^\top = E(E^\top E)^{-1}E^\top F^\top. \tag{3.19}$$

Proof. Consider $v^\star = \Pi_{S,E}(x, v)$. Using the alternative ePDS representation (3.7), we rewrite (3.18) as

$$v^\star := v + E\eta^\star \tag{3.20}$$

with

$$\eta^\star = \underset{\eta,\ v+E\eta\in T_S(x)}{\arg\min} \|E\eta\|. \tag{3.21}$$

It follows from (3.10) that

$$\begin{aligned}\eta^\star &= \underset{\eta, F_{I(x)}(v+E\eta)\geq 0}{\arg\min} ||E\eta|| \\ &= \underset{\eta, -F_{I(x)}(v+E\eta)\leq 0}{\arg\min} \frac{1}{2} E^\top \eta^\top \eta E.\end{aligned} \tag{3.22}$$

For solving (3.22), we resort to the Karush-Kuhn-Tucker (KKT) conditions [23, 78]. The stationarity and the dual feasibility conditions give

$$E^\top E\eta^\star - E^\top F_{I(x)}^\top \lambda_{I(x)} = 0 \text{ with } \lambda_{I(x)} \geq 0, \tag{3.23}$$

where $\lambda_{I(x)} \in \mathbb{R}_{\geq 0}^{|I(x)|}$ is a so-called Lagrangian multiplier and $|I(x)|$ denotes here the cardinality of the index set $I(x)$. Moreover, from the complementarity slackness condition as well as the constraint $F_{I(x)}(v + E\eta) \geq 0$, one obtains

$$0 \leq \lambda_{I(x)} \perp F_{I(x)}(v + E\eta^\star) \geq 0. \tag{3.24}$$

As a result of (3.23), we obtain

$$\eta^\star = (E^\top E)^{-1} E^\top F_{I(x)}^\top \lambda_{I(x)}. \tag{3.25}$$

As such, (3.20) becomes

$$v^\star = v + E(E^\top E)^{-1} E^\top F_{I(x)} \lambda_{I(x)}, \tag{3.26}$$

where $\lambda_{I(x)}$ should satisfy

$$0 \leq \lambda_{I(x)} \perp F_{I(x)}(v + E(E^\top E)^{-1} E^\top F_{I(x)}^\top \lambda_{I(x)}) \geq 0, \tag{3.27}$$

which as a result of (3.26), is equivalent to

$$0 \leq \lambda_{I(x)} \perp F_{I(x)} v^\star \geq 0. \tag{3.28}$$

Now, let us turn our attention to the right-hand side of (3.18). From (3.13) it follows that

$$\begin{aligned}\bar{v}^\star &:= \Pi_S^G(x, v) \\ &= \underset{a \in T_S(x)}{\arg\min} \frac{1}{2}(v-a)^\top G(v-a) \\ &= \underset{-F_{I(x)} a \leq 0}{\arg\min} \frac{1}{2}(v-a)^\top G(v-a).\end{aligned} \tag{3.29}$$

Writing the KKT conditions for (3.29), yields

$$\begin{aligned}\bar{v}^\star =& v + G^{-1} F_{I(x)}^\top \lambda_{I(x)}, \\ 0 \leq& \lambda_{I(x)} \perp F_{I(x)} \bar{v}^\star \geq 0.\end{aligned} \tag{3.30}$$

Note that (3.30) and the KKT conditions for the ePDS representation given by (3.26) and (3.28), have a similar structure. It follows from comparing these conditions that (3.18) holds if for all $x \in S$ it holds that

$$G^{-1}F_{I(x)}^{\top} = E(E^{\top}E)^{-1}E^{\top}F_{I(x)}^{\top}. \tag{3.31}$$

Condition (3.31) holding for all $x \in S$ is equivalent to (3.19) (note that $I(0) = \{1, 2, \ldots, n_f\}$), which concludes the proof. □

Given an ePDS of the form (3.2), Theorem 3.4.1 provides *sufficient* conditions that can be used to find a matrix G such that the system can be written as an oPDS (3.12). The following theorem, proposes an alternative, easy-to-check geometric condition for verifying whether an ePDS can be written as an oPDS.

Theorem 3.4.2. *Given matrices $E \in \mathbb{R}^{n\times n_E}$ and $F \in \mathbb{R}^{n_f\times n}$, there exists a positive definite matrix $G \in \mathbb{R}^{n\times n}$ satisfying* (3.19) *if and only if*

$$ker F + im E = \mathbb{R}^n. \tag{3.32}$$

Proof. For ease of notation, let $P := E(E^{\top}E)^{-1}E^{\top}$ and $R := G^{-1}$. Hence, finding $G \succ 0$ satisfying (3.19) is equivalent to finding a positive definite matrix R such that

$$RF^{\top} = PF^{\top}. \tag{3.33}$$

Note that (3.33) implies that for $x \in \mathrm{im}F^{\top}$, $Rx = Px$ and since $R \succ 0$, one has $x^{\top}Rx = x^{\top}Px > 0$, when $x \neq 0$ and $x \in \mathrm{im}F^{\top}$. It follows from the definition of P that $x^{\top}Px = x^{\top}E(E^{\top}E)^{-1}E^{\top}x$, and thus when $x \neq 0$ and $x \in \mathrm{im}F^{\top}$, then $E^{\top}x \neq 0$, i.e., $x \notin \ker E^{\top}$. In other words,

$$\mathrm{im}F^{\top} \cap \ker E^{\top} = \{0\}. \tag{3.34}$$

Taking the orthogonal complement on both sides of (3.34) yields

$$\ker F + \mathrm{im}E = \mathbb{R}^n.$$

This shows that (3.32) is a necessary condition for the existence of a $G = R^{-1}$ satisfying (3.19).

To see that (3.32) is also a sufficient condition, we have to show that if (3.32) holds then there exists a positive definite matrix $R = G^{-1} \succ 0$ satisfying (3.33). It follows from the reasoning above that (3.32) is equivalent to

$$x^{\top}Px > 0 \text{ when } x \neq 0 \text{ and } x \in \mathrm{im}F^{\top}. \tag{3.35}$$

To prove sufficiency of (3.32), consider an orthonormal basis $\{T_1, T_2, \ldots, T_n\}$ for $\mathrm{im}F^{\top} + \ker F = \mathbb{R}^n$, stacked in the matrix

$$T = \begin{bmatrix} T_1 & T_2 & \ldots & T_{n_1} & T_{n_1+1} & \ldots & T_n \end{bmatrix}, \tag{3.36}$$

where the first n_1 columns form an orthonormal basis for $\mathrm{im}F^\top$ and the remaining columns form an orthonormal basis for $\ker F$. Note that due to orthonormality it holds that $T^\top = T^{-1}$. Let us introduce a coordinate transformation $\bar{x} = Tx$ (and thus $x = T^{-1}\bar{x}$) and define

$$\tilde{R} := T^{-1}RT, \quad \tilde{P} := T^{-1}PT. \tag{3.37}$$

Note that $\tilde{R} \succ 0$ if and only if $R \succ 0$. It then follows that (3.33) is satisfied if and only if

$$T^{-1}RT \begin{bmatrix} I_{n_1} \\ 0 \end{bmatrix} = T^{-1}PT \begin{bmatrix} I_{n_1} \\ 0 \end{bmatrix}, \tag{3.38}$$

and thus

$$\tilde{R} \begin{bmatrix} I_{n_1} \\ 0 \end{bmatrix} = \tilde{P} \begin{bmatrix} I_{n_1} \\ 0 \end{bmatrix}. \tag{3.39}$$

Hence, the first n_1 columns of $\tilde{R}$ are specified by (3.39) (as P and thus $\tilde{P}$ are known). In addition, since $R = G^{-1}$ has to be symmetric this imposes that $\tilde{R}$ is a matrix of the form

$$\tilde{R} = \begin{bmatrix} A & B^\top \\ B & C \end{bmatrix}, \tag{3.40}$$

where A and B are fixed matrices (due to (3.39)) and C is a free variable. Also note that given a vector $y \in \mathbb{R}^{n_1} \setminus \{0\}$ it holds that

$$\begin{aligned} y^\top A y &= \begin{bmatrix} y \\ 0 \end{bmatrix}^\top \tilde{R} \begin{bmatrix} y \\ 0 \end{bmatrix} = \begin{bmatrix} y \\ 0 \end{bmatrix}^\top \tilde{P} \begin{bmatrix} y \\ 0 \end{bmatrix} \\ &= \begin{bmatrix} y \\ 0 \end{bmatrix}^\top T^{-1} P \underbrace{T \begin{bmatrix} y \\ 0 \end{bmatrix}}_{\in \mathrm{im}F^\top} > 0, \end{aligned} \tag{3.41}$$

where we have made use of (3.39) to replace $\tilde{R}$ with $\tilde{P}$ and used (3.35) to get the inequality at the end. Hence, $A \succ 0$. Thus, it is possible to find a matrix $R \succ 0$ that solves (3.33), if and only if there exists a matrix C such that (3.40) is positive definite. Note that the latter is always possible. Indeed, it follows from Schur's lemma [23], that (3.40) is positive definite if and only if

$$\begin{aligned} A &\succ 0, \\ A - B^\top C^{-1} B &\succ 0. \end{aligned} \tag{3.42}$$

By taking $C = \frac{1}{\epsilon} I$, with $\epsilon \in \mathbb{R}_{>0}$ sufficiently large, (3.42) can always be satisfied and thus (3.40) can be made positive definite. As such, we have shown that if (3.32) holds, or equivalently $x^\top P x > 0$ for $x \neq 0$ and $x \in \mathrm{im}F^\top$, it is always possible to find a matrix $R \succ 0$ satisfying (3.33). Hence, (3.32) is also a sufficient condition for (3.19). □

Remark 3.4.1. *Note that* (3.32) *implies* (3.11)*, as ker*$F \subseteq S$*. Hence, an ePDS satisfying Theorem 3.4.2, also satisfies the condition of Lemma 3.3.1 for being well-defined. This is natural as the equivalent oPDS is always well-defined.*

It should be noted that the equivalence conditions in Theorem 3.4.1 and Theorem 3.4.2 are independent of the particular vector fields and thus hold for all vector fields f in the ePDS (3.2) and the oPDS (3.12). However, if (3.19) does not hold, it may still be true that for *particular* vector fields the equivalence between (3.2) and (3.12) can be established. Corollary 3.4.1 proposes extensions of Theorem 3.4.1 and Theorem 3.4.2 that aim at exploiting knowledge of the vector field.

Corollary 3.4.1. *Let a vector field* $f : \mathbb{R}^n \times \mathbb{R}^{n_w} \to \mathbb{R}^n$*, a constraint set* $S \subseteq \mathbb{R}^n$ *of the form* (3.9)*, a matrix* $E \in \mathbb{R}^{n \times n_E}$ *such that* (3.11) *holds, and a positive definite matrix* $G \in \mathbb{R}^{n \times n}$ *be given. Moreover, denote by* $W \subseteq \mathbb{R}^{n_w}$ *the set of disturbance values of interest. Define*

$$\begin{aligned} J :=& \{i \in \{1, \dots, n_f\} \mid \exists x \in S \cap ker F_i, \exists w \in W \\ & \text{with } f(x,w) \notin T_S(x)\}. \end{aligned} \tag{3.43}$$

Then it holds for all $x \in S$ *and all* $w \in W$ *that*

$$\Pi_{S,E}(x, f(x,w)) = \Pi_S^G(x, f(x,w)),$$

if

$$G^{-1} F_J^\top = E(E^\top E)^{-1} E^\top F_J^\top. \tag{3.44}$$

Moreover, given $f : \mathbb{R}^n \times \mathbb{R}^{n_w} \to \mathbb{R}^n$*,* $S \subseteq \mathbb{R}^n$ *and* $E \in \mathbb{R}^{n \times n_E}$*, there exists* $G \succ 0$ *such that* (3.44) *holds, if and only if*

$$ker F_J + im E = \mathbb{R}^n. \tag{3.45}$$

Proof. If $i \notin J$, then it holds that $x \in S \cap \ker F_i$ and $w \in W$, implies $f(x,w) \in T_S(x)$. Hence, for the facet $S \cap \ker F_i$ of S there is no projection needed as $f(x,w) \in T_S(x)$ and thus $\Pi_{S,E}(x, f(x,w)) = \Pi_S^G(x, f(x,w)) = f(x,w)$, for any $G \succ 0$. As such, (3.19) and (3.32) reduce to (3.44) and (3.45), respectively. □

It follows from Theorem 3.4.2 that given an ePDS (3.2), if (3.32) holds, we can translate it into an oPDS (3.12). As such, the following two-step procedure is proposed for writing an ePDS as an oPDS:

1. Given an ePDS (3.2), check whether $\ker F + \mathrm{im} E = \mathbb{R}^n$.
2. If the first step is satisfied, find a matrix $G \succ 0$ satisfying (3.19). This problem can be formulated as a linear matrix inequality (LMI)-based feasibility test, subject to the constraint (3.19), which can be solved using available semi-definite programming solvers. Alternatively, the procedure in the proof of Theorem 3.4.2 can be followed.

If the above fails and particular knowledge of the vector field is available, one can use the results of Corollary 3.4.1 in the procedure above, as an alternative. Note that this procedure does not necessarily produce a unique matrix G. Thus, if needed, additional constraints on G could be imposed.

3.5 Some Implications of Equivalence: Incremental Stability and More

In this section, we showcase the usefulness of the results established in Section 3.4, by providing examples where utilizing the equivalence results are advantageous. In particular, we use Theorem 3.4.1 to propose sufficient conditions under which incremental stability of (3.2) can be established. Moreover, a discussion on other useful implications of the results in Section 3.4 is provided.

Definition 3.5.1. *[7],Consider a dynamical system $\dot{x} = g(x, w)$ with state $x \in \mathbb{R}^n$. Assume that for each exogenous disturbance $w \in L_\infty^{loc}$ and each initial condition $\xi = x(0)$ a locally absolutely continuous solution exists, whose value at time $t \in \mathbb{R}_{>0}$ is denoted by $x(t, \xi, w)$. The system is said to be incrementally asymptotically stable (δGAS), if there exists a $\mathcal{KL}-$function β such that for all ξ, $\eta \in \mathbb{R}^n$ and all $w \in L_\infty^{loc}$*

$$\|x(t, \xi, w) - x(t, \eta, w)\| \leq \beta(\|\xi - \eta\|, t) \quad \text{for all } t \in \mathbb{R}_{\geq 0}.$$

Definition 3.5.2. *A function $f : \mathbb{R}^m \to \mathbb{R}^n$, is called α-strongly G-monotone if there exists $\alpha > 0$ such that*

$$\langle f(x) - f(y), x - y\rangle_G \geq \alpha\|x - y\|_G^2, \quad \text{for all } x, y \in \mathbb{R}^m.$$

Theorem 3.5.1. *Given a constraint set $S \subseteq \mathbb{R}^n$ of the form (3.9), a matrix $E \in \mathbb{R}^{n \times n_E}$ such that (3.11) holds, and a vector field $f(x, w) = p(x) + h(w)$, with $p : \mathbb{R}^n \to \mathbb{R}^n$, and $h : \mathbb{R}^{n_w} \to \mathbb{R}^n$, the ePDS (3.2) is δGAS, if there exists a symmetric positive definite matrix $G \in \mathbb{R}^{n \times n}$, such that*

1. *G, F and E satisfy (3.19), and*
2. *The function $p : \mathbb{R}^n \to \mathbb{R}^n$ is continuous and α-strongly G-monotone for $\alpha > 0$.*

Proof. The first condition in the theorem ensures via Theorem 3.4.1 that (3.2) can be written as the oPDS (3.12). Using this oPDS-based representation, one can utilize condition (2) in the theorem in conjunction with Theorem 2 in [64] to prove δGAS of the system. □

Remark 3.5.1. *Other properties such as incremental input-to-state stability (δISS), as well as uniform/exponential and input-to-state convergence [110] and periodicity*

of steady-state solutions can be established for the ePDS (3.2) *under the conditions stated in Theorem 3.5.1. The proof for each case would also build upon first obtaining an equivalent oPDS representation for* (3.2)*, which is possible as a result of the first condition in Theorem 3.5.1, and then using the second condition in the theorem to prove these properties for the equivalent oPDS, which is possible as argued in Remark 1, [64].*

In addition to Theorem 3.5.1 and the results pointed out in Remark 3.5.1, as explained in Lemma 3.3.2, one can perform similarity transformations to turn (3.12) into a classical PDS. As such the equivalence results established in Section 3.4 enable one to rely on several existing results available for PDS. For example, for ePDS (3.2) with constraint sets of the form (3.9) one can conclude existence and uniqueness of solutions for all time $t \in \mathbb{R}_{\geq 0}$, if there exists $G \succ 0$ such that (3.19) (and the additional conditions required for well-posedness as stated in [102])is satisfied. All these results are based on the equivalence between ePDS and (o)PDS and thus, illustrate the usefulness of the equivalence results presented in Section 3.4, as they enable transferring relevant properties from the class of oPDS and PDS to the less studied class of ePDS.

3.6 Equivalent HIGS representations

In this section, we apply the results obtained in the previous sections to HIGS-controlled systems. HIGS are discontinuous dynamical systems introduced in [37] with the aim of realizing performance beyond levels attainable with LTI control, and have enjoyed considerable engineering success (see, for example, [73, 75]). To recall HIGS, we start by describing the closed-loop system under consideration leading to an ePDS-based formulation. Motivated by using the results available for oPDS, the ePDS-based representation together with the results of Section 3.4 are used to derive an alternative description for the closed-loop system in the oPDS framework of Section 3.3.2. This new representation of HIGS-controlled systems will then be used in Section 3.7, to propose conditions for incremental stability of HIGS-controlled systems.

3.6.1 System Description

We consider the interconnection in Fig. 3.1, consisting of an LTI plant $\mathscr{G}$ controlled in feedback with a single-input single-output (SISO) HIGS element $\mathscr{H}$. The plant $\mathscr{G}$ contains the linear part of the closed-loop system including the plant to be controlled and possibly an LTI controller, given by the state-space representation (where we have omitted time dependency for ease of notation)

$$\begin{cases} \dot{x}_g &= A_g x_g + B_{gv} v + B_{gw} w, \\ e &= C_g x_g, \end{cases} \tag{3.46}$$

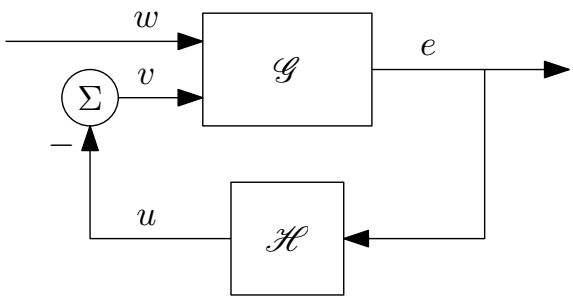

Figure 3.1. Closed-loop system in Lur'e form.

with states x_g taking values in $\mathbb{R}^{n_g}$, performance output e in $\mathbb{R}$, control input v in $\mathbb{R}$ and exogenous disturbances denoted by w taking values in $\mathbb{R}^{n_w}$. As the key area of application for HIGS is formed by motion systems containing floating masses, the following assumption is typically satisfied [37, 38].

Assumption 3.6.1. *The LTI system $\mathscr{G}$ as in Fig. 3.1 is such that $C_g B_{gw} = 0$ and $C_g B_{gv} = 0$.*

The HIGS element $\mathscr{H}$ considered in this chapter has as its primary mode of operation the first-order linear integrator dynamics

$$\begin{aligned} \dot{x}_h &= \alpha x_h + \omega_h e, \\ u &= -v = x_h, \end{aligned} \tag{3.47}$$

where the state x_h takes values in $\mathbb{R}$, the (HIGS) input e and the (HIGS) output u both take values in $\mathbb{R}$ and $\omega_h \in [0, \infty)$ denotes the integrator frequency. Moreover $\alpha \in \mathbb{R}$ is the pole location in this mode of operation. This mode of operation of the HIGS element is referred to as the *integrator mode*. Note that for $\alpha = 0$, (3.47) becomes equivalent to the integrator mode dynamics as considered in Chapter 2. With $\alpha \neq 0$, (3.47) resembles the integrator dynamics in a first order reset element (FORE) [29, 79]. The integrator mode (3.47) can only be used as long as the input-output pair (e, u) of $\mathscr{H}$ remains inside

$$\mathscr{F} := \left\{ (e, u) \in \mathbb{R}^2 \mid eu \geq \frac{1}{k_h} u^2 \right\}, \tag{3.48}$$

where $k_h \in (0, \infty)$ denotes the gain parameter of $\mathscr{H}$. Note that $(e, u) \in \mathscr{F}$ implies equal sign of the input e and the output u of the HIGS as $eu \geq 0$, see Fig. 3.2, which leads to performance enhancing properties due to reduced phase lag of the integrator (see [37] for more details).

At moments when the input-output pair (e, u) of $\mathscr{H}$ tends to leave the sector $\mathscr{F}$ the integrator dynamics in (3.47) are projected such that $(e, u) \in \mathscr{F}$ remains

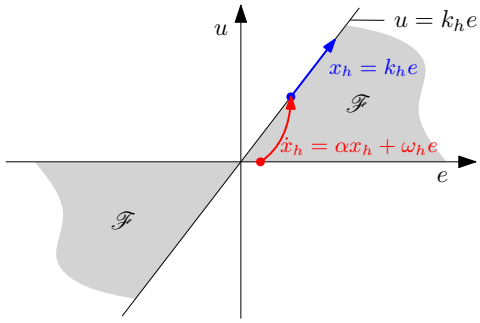

Figure 3.2. An example of a HIGS in operation.

true along the trajectories of the system. Note that we can only change (project) the controller dynamics to satisfy $(e, u) \in \mathscr{F}$, while we cannot change the physical plant dynamics by means of projection. This setup clearly and naturally is described by *partial* projection and thus ePDS, as shortly discussed next.

3.6.2 ePDS Based Representation

Consider the closed-loop interconnection in Fig. 3.1, with state $x = [x_g^\top \;\; x_h^\top]^\top \in \mathbb{R}^n$. By combining (3.46) and (3.47), we arrive at the following state space representation for the primary mode of operation for the closed-loop system:

$$\begin{aligned} \dot{x} &= A_{\text{int}} x + B w, \\ y &= C x, \end{aligned} \tag{3.49}$$

where $y = [e \;\; u]^\top$, and

$$\left[\begin{array}{c|c} A_{\text{int}} & B \\ \hline C & \end{array}\right] = \left[\begin{array}{cc|c} A_g & -B_{gv} & B_{gw} \\ \omega_h C_g & \alpha & 0_{1\times n_w} \\ \hline C_g & 0 & \\ 0_{1\times n_g} & 1 & \end{array}\right]. \tag{3.50}$$

Using the ePDS framework of Section 3.3.1, we can formally describe the dynamics of the system as

$$\begin{cases} \dot{x}(t) = \Pi_{S,E}(x(t), A_{\text{int}} x(t) + B w(t)), \\ y(t) = C x(t) \end{cases} \tag{3.51}$$

with

$$S = \mathscr{K} \cup -\mathscr{K}, \tag{3.52}$$

where $\mathscr{K}$ is a polyhedral cone given by

$$\mathscr{K} := \{x \in \mathbb{R}^n \mid Fx \geq 0\}, \tag{3.53}$$

where $F = \begin{bmatrix} F_1^\top & F_2^\top \end{bmatrix}^\top$ with $F_1 = [k_h C_g \ \ -1]$, and $F_2 = \begin{bmatrix} 0_{1\times n_g} & 1 \end{bmatrix}$. In fact, $F_1 x = k_h e - u$ and $F_2 x = u$ such that $(e, u) \in \mathscr{F}$ if and only if $x \in S$. Moreover, $E = [0_{1\times n_g}^\top \ \ 1]^\top$ such that the x_h-dynamics are projected and x_g (representing physical states that cannot be projected or controller states that should not be projected) is not changed by means of projection (see [38, 123] for more details). Note that

$$S + \mathrm{im}E = \mathbb{R}^n,$$

which makes the right-hand side of (3.51) well-defined. For a full proof of the well-posedness of the projection operator $\Pi_{S,E}$ in (3.51), see Chapter 2.

3.6.3 oPDS Based Representation

We will now present an alternative representation of HIGS-controlled systems in the oPDS framework discussed in Section 3.3.2. Prior to doing so, let us make note of the fact that in previous sections we considered convex polyhedral cones as constraint sets, while the constraint set (3.52) is a non-convex set and is given by a union of such cones. As a result, we can not directly use Theorem 3.4.1 and Theorem 3.4.2. Instead, we first consider the case where $x \in \mathscr{K}$ (see (3.53)) and subsequently use the symmetry of (3.52) to obtain a *switched* oPDS formulation for the HIGS-controlled system.

Let us turn our attention to

$$\begin{aligned} \dot{x}(t) &= \Pi_{\mathscr{K},E}(x(t), A_{\mathrm{int}}x(t) + Bw(t)) \\ &= P_{T_{\mathscr{K}}(x),E}(A_{\mathrm{int}}x(t) + Bw(t)). \end{aligned} \tag{3.54}$$

Note that even for (3.54), the results in Theorem 3.4.1 and Theorem 3.4.2 can not be directly used since

$$\ker F + \mathrm{im}E = \{x \in \mathbb{R}^n \mid x = [0^\top \beta \ \ ]^\top, \ \beta \in \mathbb{R}\}.$$

As such, it is not possible to obtain an oPDS representation of HIGS-controlled systems based on Theorem 3.4.1. However, note that the conditions in Theorem 3.4.1 and Theorem 3.4.2 guarantee equivalence of ePDS and oPDS irrespective of the actual vector field. It turns out that for HIGS-controlled systems we can exploit particular knowledge of the vector field in relation to the constraint set. In particular, for the HIGS-controlled system (3.51), exploiting the form of the vector field (3.49) in combination with Assumption 3.6.1 would enable us to make use of the results in Corollary 3.4.1. Indeed, let us make the observation that for

$$x \in \ker F_2 \cap \mathscr{K},$$

it can be verified by using Assumption 3.6.1, that $A_{\text{int}}x + Bw \in T_S(x)$. Indeed, for $x \in \ker F_2 \cap \mathscr{K}$, i.e., for $\{x \in \mathbb{R}^n \mid x_h = 0 \wedge C_g x_g \geq 0\}$, one has

$$F_2(A_{\text{int}}x + Bw) = \omega_h C_g x_g \geq 0.$$

This implies that when $F_2 x = 0$, the projections onto the tangent cone of S result in the integrator mode dynamics (regardless of the choice of E and G). Hence, to rewrite the ePDS (3.54) as an oPDS we only have to choose $G \succ 0$ to match the projections when $F_1 x = 0$, i.e., one of the facets of $\mathscr{K}$, as

$$\Pi_{\mathscr{K},E}(x, A_{\text{int}}x + Bw) = \Pi^G_{\mathscr{K}}(x, A_{\text{int}}x + Bw) = A_{\text{int}}x + Bw,$$

already holds for all points in $\{x \in \mathscr{K} \mid x \notin \ker F_1 \setminus \ker F_2\}$ and for all $w \in \mathbb{R}^{n_w}$, irrespective of the choice of G. As a result, (3.44) should only be satisfied when $F_1 x = 0$, i.e., if we can find a $G \succ 0$ satisfying

$$G^{-1}F_1^\top = E(E^\top E)^{-1}E^\top F_1^\top, \tag{3.55}$$

then for $x \in \mathscr{K}$, we can write the ePDS (3.54) as an oPDS (3.12). Note that F_1 and E do satisfy the condition (3.45) in Corollary 3.4.1, i.e.,

$$\ker F_1 + \text{im}E = \mathbb{R}^n, \tag{3.56}$$

which implies that it should be possible to find a $G \succ 0$ satisfying (3.55). Moreover, since $E = [0^\top_{n_g}\ 1]^\top$ is orthonormal, (3.55) simplifies to

$$G^{-1}F_1^\top = EE^\top F_1^\top \tag{3.57}$$

implying that G should satisfy the expression

$$F_1^\top = GEE^\top F_1^\top. \tag{3.58}$$

Equation (3.58) holds for any $G \succ 0$ of the form

$$G = \begin{bmatrix} G_{11} & -k_h C_g^\top \\ -k_h C_g & 1 \end{bmatrix}, \tag{3.59}$$

with $G_{11} \succ 0$, a free variable, sufficiently large such that $G_{11} - k_h^2 C_g^\top C_g \succ 0$ (to have $G \succ 0$ by Schur's lemma). As such, we have shown that for $x \in \mathscr{K}$, the HIGS-controlled system can be written as an oPDS. Next, we will use this result to obtain an oPDS representation of the system for $x \in S$.

Note that the tangent cone to the constraint set (3.52), is given by

$$T_S(x) = \begin{cases} T_{\mathscr{K}}(x), & \text{if } x \in \mathscr{K} \setminus -\mathscr{K} \\ -T_{\mathscr{K}}(-x), & \text{if } x \in -\mathscr{K} \setminus \mathscr{K} \\ \mathscr{K} \cup -\mathscr{K}, & \text{if } x \in \mathscr{K} \cap -\mathscr{K} \end{cases} \tag{3.60}$$

with

$$T_{\mathscr{K}}(x) = \{\nu \in \mathbb{R}^n \mid F_{I(x)}\nu \geq 0\}, \tag{3.61}$$

where

$$I(x) = \{i \in \{1,2\} \mid F_i x = 0\}$$

is the set of active constraints at $x \in \mathscr{K}$. Thus, when considering the complete constraint set (3.52), (3.51) can be alternatively written as the switched ePDS

$$\begin{aligned}\dot{x}(t) &= \Pi_{S,E}(x, A_{\text{int}}x + Bw) \\ &= \begin{cases} P_{T_{\mathscr{K}}(x),E}(A_{\text{int}}x + Bw), & \text{if } x \in \mathscr{K} \setminus -\mathscr{K} \\ P_{-T_{\mathscr{K}}(-x),E}(A_{\text{int}}x + Bw), & \text{if } x \in -\mathscr{K} \setminus \mathscr{K} \\ A_{\text{int}}x + Bw, & \text{if } x \in -\mathscr{K} \cap \mathscr{K}. \end{cases}\end{aligned} \tag{3.62}$$

Now, using the discussion above and the symmetry of (3.52), (3.51) (or equivalently (3.62)) can be alternatively written as

$$\begin{aligned}\dot{x}(t) &= \Pi_S^G(x, A_{\text{int}}x + Bw) \\ &= \begin{cases} P^G_{T_{\mathscr{K}}(x)}(A_{\text{int}}x + Bw), & \text{if } x \in \mathscr{K} \setminus -\mathscr{K} \\ P^G_{-T_{\mathscr{K}}(-x)}(A_{\text{int}}x + Bw), & \text{if } x \in -\mathscr{K} \setminus \mathscr{K} \\ A_{\text{int}}x + Bw, & \text{if } x \in -\mathscr{K} \cap \mathscr{K}, \end{cases}\end{aligned} \tag{3.63}$$

with G as in (3.59). Therefore, we have obtained a *switched* oPDS representation of the HIGS-controlled system (3.51).

In the next section, we will use the switched oPDS representation (3.63) of HIGS-controlled systems, to propose conditions under which the closed-loop system in Fig. 3.1 is guaranteed to be incrementally stable.

3.7 Incremental Stability of HIGS-controlled systems

In this section, we make use of the results in Section 3.6.3 to propose conditions for incremental stability of HIGS-controlled systems. As such, we consider the incremental closed-loop dynamics given by

$$\begin{aligned}\delta\dot{x}(t) &:= \frac{d}{dt}x_1(t) - \frac{d}{dt}x_2(t) \\ &\in \Pi_{S,E}(x_1(t), A_{int}x_1(t) + Bw(t)) - \Pi_{S,E}(x_2(t), A_{int}x_2(t) + Bw(t)) =: F(\delta x(t), w(t)),\end{aligned} \tag{3.64}$$

where $\delta x(t) \in \mathbb{R}^n$ is the difference between two solutions $x_1(t) = x(t, x_1(0), w)$ and $x_2(t) = x(t, x_2(0), w)$.

To study stability of (3.64), we make use of the following sufficient Lyapunov-based conditions for incremental stability.

Theorem 3.7.1. *[7, 140] Consider the closed-loop system in Fig. 3.1. If there exist a locally Lipschitz continuous function $V : \mathbb{R}^n \to \mathbb{R}_{\geq 0}$, class $\mathcal{K}_\infty$-functions α_1 and α_2 and class $\mathcal{K}$-function α, such that for any input $w \in PB \cap L_\infty^{loc}$, and all admissible solutions $x, \tilde{x}$ to the system, one has*

$$\alpha_1(\|\delta x\|) \leq V(\delta x) \leq \alpha_2(\|\delta x\|) \tag{3.65a}$$

$$\max_{\rho \in \partial V(\delta x)} \max_{f \in F(\delta x, w)} \langle \rho, f \rangle \leq -\alpha(\|\delta x\|) \tag{3.65b}$$

where $\delta x = x - \tilde{x}$, and ∂V is the generalized gradient of V at x, given by

$$\partial V(x) = \overline{\text{co}}\{\lim_{i \to \infty} \nabla V(x_i) \mid x_i \to x,\ x_i \notin \Omega\},$$

where $\overline{\text{co}}$ denotes the closed convex hull, ∇V denotes the gradient of V and Ω is the measure zero set where ∇V is not defined, then, the closed-loop system in Fig. 3.1 is δGAS.

Proof. The proof is similar to the proof of Theorem 6.2.8 in [140]. □

We are now ready to state the main result of this section.

Theorem 3.7.2. *Consider the HIGS controlled system* (3.51) *with $w \in PB \cap L_\infty^{loc}$, and suppose there exist a matrix $M = M^\top$, and a real constant $\tau > 0$, such that*

$$M \succ 0 \tag{3.66a}$$

$$M - k_h^2 C_g^\top C_g \succ 0 \tag{3.66b}$$

$$\begin{bmatrix} A_g^\top M + M A_g & -M B_{gv} \\ -B_{gv}^\top M & 0 \end{bmatrix} + \tau \begin{bmatrix} 0 & k_h C_g^\top \\ k_h C_g & -2 \end{bmatrix} \prec 0, \tag{3.66c}$$

$$A_{int}^\top P_1 + P_1 A_{int} \prec 0 \tag{3.66d}$$

$$A_{int}^\top P_2 + P_2 A_{int} \prec 0 \tag{3.66e}$$

where

$$P_1 = \begin{bmatrix} M + k_h^2 C_g^\top C_g & -k_h C_g^\top \\ -k_h C_g & 1 \end{bmatrix}, \tag{3.67}$$

$$P_2 = \begin{bmatrix} M & -k_h C_g^\top \\ -k_h C_g & 1 \end{bmatrix}, \tag{3.68}$$

then the HIGS-controlled system (3.51) *is δGAS.*

Proof. The proof is based on showing that under the conditions stated above, there exists an incremental Lyapunov function $V(\delta x)$ satisfying the conditions in Theorem 3.7.1. Note that with $w \in PB \cap L_\infty^{loc}$, similar arguments as used in Section 2.6 can be used to prove existence and forward completeness of solutions to (3.51), therefore existence of such an incremental Lyapunov function is sufficient for proving δGAS of (3.51). In particular, we consider the δGAS Lyapunov function

$$V(\delta x) = \begin{cases} \delta x_g^\top M \delta x_g, & \text{if } (\delta x_h, \delta e) \in \Omega_1, \\ \delta x^\top P_1 \delta x, & \text{if } (\delta x_h, \delta e) \in \Omega_2, \\ \delta x^\top P_2 \delta x, & \text{if } (\delta x_h, \delta e) \in \Omega_3, \end{cases} \tag{3.69}$$

where Ω_1, Ω_2, and Ω_3 are regions within the incremental input-output space of HIGS, as portrayed in Fig. 3.3. To show Lipschitz continuity of V, we have to show

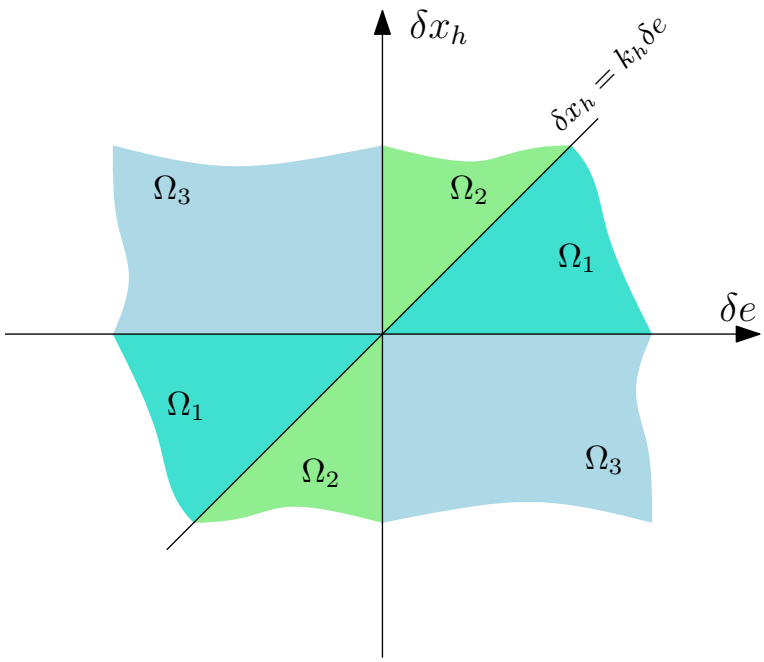

Figure 3.3. The incremental input-output space of HIGS.

that the different pieces of the Lyapunov functions are equal on the boundaries of the sets Ω_1, Ω_2 and Ω_3. Indeed, since $V(\delta x)$ is composed of locally Lipschitz functions, continuity of V implies that it is also Lipschitz continuous (see also the proof of Theorem 3.3 in [68]). Note that

$$\delta x^\top P_1 \delta x = \delta x_g^\top M \delta x_g + k_h^2 \delta x_g^\top C_g^\top C_g \delta x_g - k_h \delta x_g^\top C_g^\top \delta x_h - k_h \delta x_h^\top C_g \delta x_g + \delta x_h^2.$$

On the boundary between Ω_1 and Ω_2, one has $\delta x_h = k_h \delta e = k_h C_g \delta x_g$ leading to

$$\delta x^\top P_1 \delta x = W(\delta x) = \delta x_g^\top M \delta x_g,$$

showing that Lyapunov functions are the same at the boundary of Ω_1 and Ω_2.

Moreover, note that

$$\delta x^\top P_2 \delta x = \delta x_g^\top M \delta x_g - k_h \delta x_g^\top C_g^\top \delta x_h - k_h \delta x_h^\top C_g \delta x_g + \delta x_h^2.$$

On the boundary between the regions Ω_2 and Ω_3, one has $\delta e = C_g \delta x_g = 0$. Hence, on this boundary

$$\delta x^\top P_2 \delta x = \delta x^\top P_1 \delta x = \delta x_g^\top M \delta x_g + \delta x_h^2.$$

Lastly on the boundary between the regions Ω_3 and Ω_1, one has $\delta x_h = 0$ and thus

$$\delta x^\top P_2 \delta x = W(\delta x) = \delta x_g^\top M \delta x_g.$$

As such, the Lyapunov functions are the same at the respective boundaries between the regions Ω_i, $i \in \{1, 2, 3\}$, in the incremental input-output space of HIGS and thus V is Lipschitz continuous.

Next, we show the existence of functions $\alpha_1, \alpha_2 \in \mathcal{K}_\infty$, such that

$$\alpha_1(\|\delta x\|) \leq V(\delta x) \leq \alpha_2(\|\delta x\|). \tag{3.70}$$

Note that from (3.66a), one has

$$\tilde{\alpha}_1 \|\delta x_g\|^2 \leq \delta x_g^\top M \delta x_g = W(\delta x) \leq \tilde{\alpha}_2 \|\delta x_g\|^2, \tag{3.71}$$

with $\tilde{\alpha}_1 = \lambda_{\min}(M)$ and $\tilde{\alpha}_2 = \lambda_{\max}(M)$, where $\lambda_{\min}(M)$, and $\lambda_{\max}(M)$ denote the minimal and maximal eigenvalues of M, respectively. Next, note that for $(\delta x_h, \delta e) \in \Omega_1$, one has $\|\delta x_h\| \leq k_h \|\delta e\| = k_h \|C_g \delta x_g\| \leq k_h \|C_g\| \|\delta x_g\|$. Thus, $\|\delta x_h\|^2 - k_h^2 \|C_g\|^2 \|\delta x_g\|^2 \leq 0$. As such, from (3.71) one has

$$\tilde{\alpha}_1 \|\delta x_g\|^2 + \tilde{\alpha}_1 \tau (\|\delta x_h\|^2 - k_h^2 \|C_g\|^2 \|\delta x_g\|^2) \leq \delta x_g^\top M \delta x_g \tag{3.72}$$

for some $0 < \tau < \frac{1}{k_h^2 \|C_g\|^2}$. Therefore, it holds that

$$\tilde{\alpha}_3 \|\delta x\|^2 \leq \delta x_g^\top M \delta x_g \leq \tilde{\alpha}_4 \|\delta x\|^2, \tag{3.73}$$

with $\tilde{\alpha}_3 = \tilde{\alpha}_1 \min\left(1 - \tau k_h^2 \|C_g\|^2, \tau\right)$, and $\tilde{\alpha}_4 = \tilde{\alpha}_2$.

Moreover, when $(\delta x_h, \delta e) \in \Omega_2$, it holds that $V(\delta x) = \delta x^\top P_1 \delta x$. Note that it follows from (3.66b), (3.66a), together with Schur's Lemma that $P_1 \succ 0$, and therefore,

$$\tilde{\alpha}_5 \|\delta x\|^2 \leq \delta x^\top P_1 \delta x \leq \tilde{\alpha}_6 \|\delta x\|^2, \tag{3.74}$$

with $\tilde{\alpha}_5 = \lambda_{\min}(P_1)$. $\tilde{\alpha}_6 = \lambda_{\max}(P_1)$. Lastly, when $(\delta x_h, \delta e) \in \Omega_3$ and thus $V(\delta x) = \delta x^\top P_2 \delta x$, it follows from (3.66a), (3.66b) and Schur's Lemma that $P_2 \succ 0$, and thus

$$\tilde{\alpha}_7 \|\delta x\|^2 \leq \delta x^\top P_2 \delta x \leq \tilde{\alpha}_8 \|\delta x\|^2, \tag{3.75}$$

with $\tilde{\alpha}_7 = \lambda_{\min}(P_2)$. $\tilde{\alpha}_8 = \lambda_{\max}(P_2)$. Therefore, (3.70) holds with $\alpha_1(\|\delta x\|) = (\min(\tilde{\alpha}_3, \tilde{\alpha}_5, \tilde{\alpha}_7))\|\delta x\|^2$, and $\alpha_2(\|\delta x\|) = (\max(\tilde{\alpha}_4, \tilde{\alpha}_6, \tilde{\alpha}_8))\|\delta x\|^2$.

It now remains to show that there exists a function $\alpha \in \mathcal{K}_\infty$ such that (3.65b) holds. First, remark that with P_1 and P_2 as defined above, the system can be written as in (3.63) (with both $G = P_1$ or $G = P_2$) due to (3.66a) and (3.66b). Indeed, both P_1 and P_2 have the structure imposed in (3.59), and it follows from Schur's Lemma that (3.66a) and (3.66b) ensure P_1 and P_2 to be positive definite, respectively.

First, consider the case where $(\delta x, \delta e) \notin \Omega_1$, then one necessarily has both $(x_1 \in \mathscr{K} \wedge x_2 \in \mathscr{K})$ or $(x_1 \in -\mathscr{K} \wedge x_2 \in -\mathscr{K})$. Using P_1 and P_2 as defined above the HIGS-controlled system can be written in the form (3.63) where $G = P_1$ or $G = P_2$. Following the same reasoning as in Corollary 1 of [64], we get for $x_i,\ i \in \{1, 2\}$

$$\begin{aligned} \dot{x}_i &= \begin{cases} A_{int}x_i + Bw - P_1^{-1} n_{\mathscr{K}(x_i)}, & x_i \in \mathscr{K} \\ A_{int}x_i + Bw - P_1^{-1} n_{-\mathscr{K}(x_i)}, & x_i \in -\mathscr{K} \end{cases} \\ &= \begin{cases} A_{int}x_i + Bw - P_2^{-1} n_{\mathscr{K}(x_i)}, & x_i \in \mathscr{K} \\ A_{int}x_i + Bw - P_2^{-1} n_{-\mathscr{K}(x_i)}, & x_i \in -\mathscr{K} \end{cases} \end{aligned} \tag{3.76}$$

where $n_{\mathscr{K}(x_i)}$ is an element of the normal cone to the set $\mathscr{K}$ at point x_i. Consider now $\delta x = x_1 - x_2$ such that $(\delta x_h, \delta e) \in \Omega_2$. We then have

$$\begin{aligned} &\partial V(\delta x)\delta\dot{x} = \frac{d}{dt}|x_1 - x_2|^2_{P_1} = \frac{d}{dt}(x_1 - x_2)^\top P_1 (x_1 - x_2) \\ &= 2(x_1 - x_2)^\top (P_1 A_{int} + A_{int}^\top P_1)(x_1 - x_2) + (x_1 - x_2)^\top P_1 (-P_1^{-1} n_1 + P_1^{-1} n_2) \\ &= 2(x_1 - x_2)^\top (P_1 A_{int} + A_{int}^\top P_1)(x_1 - x_2) + (x_1 - x_2)^\top (n_2 - n_1), \end{aligned} \tag{3.77}$$

where $n_1 \in N_{\mathscr{K}(-\mathscr{K})}(x_1)$ and $n_2 \in N_{\mathscr{K}(-\mathscr{K})}(x_2)$. It follows from (3.66d) together with the monotonicity of the normal cone operator that $\partial V(\delta x)\delta\dot{x} = \frac{d}{dt}|x_1 - x_2|^2_{P_1} < -\varepsilon_1 \|\delta x\|^2$, for some $\varepsilon_1 \in \mathbb{R}_{>0}$ when $(\delta x_h, \delta e) \in \Omega_2$. For the case where $(\delta x_h, \delta e) \in \Omega_3$, by following a similar reasoning and as a result of (3.66e), we get $\partial V(\delta x)\delta\dot{x} = \frac{d}{dt}|x_1 - x_2|^2_{P_2} \leq -\varepsilon_2 \|\delta x\|^2$, for some $\varepsilon_2 \in \mathbb{R}_{>0}$.

Lastly, for $(\delta x_h, \delta e) \in \Omega_1$ which, covers $x_1 \in \mathscr{K}$ and $x_2 \in -\mathscr{K}$ (and vice versa) since if

$$Fx_1 \geq 0, \quad Fx_2 \leq 0$$

then

$$Fx_1 - Fx_2 = F\delta x \geq 0,$$

we consider the Lyapunov function $W(\delta x) = \delta x_g^\top M \delta x_g$. One has

$$\begin{aligned} \partial V(\delta x)\delta\dot{x} &= \delta\dot{x}_g^\top M\delta x_g + \delta x_g^\top M\delta\dot{x}_g \\ &= (A_g\delta x_g - B_{gv}\delta x_h)^\top M\delta x_g + \delta x_g M(A_g\delta x_g - B_{gv}\delta x_h) \\ &= \delta x_g^\top (A_g^\top M + MA_g)\delta x_g - \delta x_g^\top MB_{gv}\delta x_h - \delta x_h^\top B_{gv}^\top M\delta x_g. \end{aligned} \tag{3.78}$$

Additionally, for $(\delta x_h, \delta e) \in \Omega_1$, it holds that

$$\tau\delta x^\top \begin{bmatrix} 0 & k_h C_g^\top \\ k_h C_g & -2 \end{bmatrix} \delta x = 2\tau(k_h\delta x_h\delta e - \delta x_h^2) \geq 0. \tag{3.79}$$

for any $\tau \in \mathbb{R}_{\geq 0}$. As such, for $(\delta x_h, \delta e) \in \Omega_1$, by pre- and post-multiplication of (3.66c) with δx and by application of S-procedure relaxations we get $\partial V(\delta x)\delta\dot{x} \leq -\varepsilon_3\|\delta x\|^2$ for some $\varepsilon_3 \in \mathbb{R}_{\geq 0}$, due to (3.78) and (3.79). Therefore, (3.65b) holds with $\alpha = \min(\varepsilon_1, \varepsilon_2, \varepsilon_3)$. This completes the proof. □

Remark 3.7.1. *In Chapter 2, a proof of well-posedness in the sense of existence and forward completeness of Carathéodory solutions for HIGS-controlled systems was provided. Under the conditions in Theorem 3.7.2, one may also conclude uniqueness of solutions for these systems, as uniqueness of solutions is an immediate consequence of δGAS.*

Remark 3.7.2. *Under the conditions in Theorem 3.7.2, one may also conclude δISS of* (3.51) *based on the fact that the disturbances w in Fig. 3.1, enter the system* (3.46) *in an affine manner and using the same arguments as in Theorem 2 of [7].*

3.8 Summary and Conclusions

In this chapter, we have connected two classes of discontinuous dynamical systems consisting of extended projected dynamical systems (ePDS) and oblique projected dynamical systems (oPDS). We have presented two sets of sufficient conditions for establishing equivalence between these two recently introduced variations of PDS, thereby enabling the transfer of theoretical tools and properties from one class to the other.

The transfer of system-theoretic results, have been particularly highlighted for properties such as (incremental) stability, and periodicity of steady-state solutions

for periodic inputs. Moreover, the results have been used to obtain a new description for hybrid integrator-gain systems (HIGS)-based controllers in terms of (switched) oPDS. Based on this new description of HIGS-controlled systems conditions for incremental stability of HIGS-controlled systems are proposed, which make use of a novel construction of a piecewise quadratic Lyapunov function.

Future research directions include an in-depth study of properties of ePDS in general and HIGS-controlled systems in particular, further exploiting the equivalence established in this chapter.

4

Overcoming Performance Limitations of Linear Control with Hybrid Integrator-Gain Systems

Abstract - *It is well-known that the performance of linear time-invariant (LTI) feedback control is hampered by fundamental limitations. In this chapter, it is shown that by using a so-called hybrid integrator-gain system (HIGS) in the controller, important fundamental LTI performance limitations can be overcome. In particular, in this chapter, we show this for two well-known limitations, where overshoot in the step-response of the system has to be present for any stabilizing LTI controller. For each case, it is shown that by using HIGS-based control, one can avoid overshoot in the step-response of the system. Key design considerations for HIGS-based controllers as well as the stability of the resulting closed-loop interconnections are discussed.*

This chapter is based on [148].

4.1 Introduction

Linear control theory is a well-developed area of research equipped with numerous tools and methods to fit the needs of industry, including tools for the design and synthesis of linear controllers, as well as analysis of the stability and performance thereof. As such, the widespread use of linear control is often attributed to its design simplicity and predictability. However, all linear time-invariant (LTI) control systems suffer from fundamental limitations such as Bode's gain-phase relationship and the waterbed effect due to Bode's sensitivity integral. These limitations result in well-known design trade-offs in both the frequency- and time-domain [48, 100].

In terms of time-domain performance of LTI systems, restrictions on transient performance metrics such as overshoot, rise time, and settling time of the closed-loop system exist. More specifically, given certain classes of linear systems to be controlled, it is impossible to realize performance beyond particular limits with LTI control, regardless of the type or order of the LTI controller. As such, these constraints are called fundamental performance limitations of LTI control [119].

A potential solution to circumvent these fundamental performance limitations is to utilize hybrid or nonlinear control strategies, which by definition are not necessarily bound to the same limitations as LTI systems. Some examples include Variable Gain Control (VGC) [74], reset control [2, 79, 115], switched (hybrid) controllers [43], split-path nonlinear integrators [45, 126, 151], and more recently the works on hybrid integrator-gain systems (HIGS) [36].

In this chapter, we will focus on the latter, HIGS, which feature a nonlinear integrator that switches between an integrator- and a gain-mode. This controller was introduced in [37] to deal with the classical trade-off in linear control theory between low-frequency disturbance suppression by means of linear integral control and a desired transient response. Given an input signal, the switching behavior of this control element leads to an output signal, which has the same sign as its input at all times, thereby constantly forcing the output of the system towards the desired reference value. In frequency domain, a describing function analysis reveals that a HIGS element exhibits similar magnitude characteristics as a linear integrator while inducing only 38.15 degrees of phase lag (see for example [140]), as opposed to 90 degrees in the linear case. Similar desirable characteristics are found in the case of reset control elements [31, 79]. However, while reset integrators achieve these properties by producing *discontinuous* control signals, which can potentially excite high-frequency plant dynamics or amplify high-frequency noise, HIGS makes use of *continuous* output signals. This makes HIGS a powerful control element, especially in the context of high-precision mechatronics, where structural dynamics with numerous weakly damped resonances are present.

Multiple studies have already shown that it is possible to overcome fundamental LTI performance limitations by using hybrid and nonlinear control strategies. In particular, in [81] VGC has been used to overcome one of these limitations. Morever, in [18, 156], reset control has been used to overcome three fundamental

limitations of LTI control. These studies consider LTI control configurations, for which overshoot is guaranteed no matter the choice of the LTI controller and show that overshoot is eliminated in the step-response when employing nonlinear/hybrid controllers. More recently, in [143], it has been shown that a specific time-domain LTI performance limitation can be overcome, by employing a HIGS element.

In this chapter, the objective is to show that HIGS-based control can, in fact, overcome all the fundamental LTI performance limitations, related to overshoot, that have been overcome by any other type of nonlinear element, thereby underlining the strength of HIGS and HIGS-based control. In the process of overcoming these limitations, we reveal key design considerations for HIGS-based control and discuss the closed-loop stability analysis.

The remainder of this chapter is organized as follows. In Section 4.2, preliminary material related to fundamental limitations of LTI control will be presented. In Section 4.4, a general description of HIGS and the closed-loop system considered in the chapter, as well as a problem statement are provided. Section 4.5 and Section 4.6, are concerned with overcoming limitations of LTI control using HIGS-based designs, of which closed-loop stability will be established in Section 4.7. The chapter is concluded in Section 4.8, where the main conclusions and future directions of research are provided.

4.2 Preliminaries

In this section, we present some preliminary material that is used in the sections to follow.

4.2.1 Notation and definitions

The sets of reals, integers, and complex numbers are denoted by $\mathbb{R}$, $\mathbb{Z}$, and $\mathbb{C}$, respectively. Given a vector v, $\|v\|$ denotes its Euclidean norm. For a complex number $z \in \mathbb{C}$, we denote its real part by $\mathrm{Re}(z)$ and its imaginary part by $\mathrm{Im}(z)$.

Definition 4.2.1. *[88], A function $\alpha : [0, a) \to [0, \infty)$ is said to belong to class $\mathcal{K}$, if it is continuous, strictly increasing and $\alpha(0) = 0$. A function $\beta : [0, a) \times [0, \infty) \to [0, \infty)$ is said to belong to class $\mathcal{KL}$, if, it is continuous and for each fixed s, the mapping $r \mapsto \beta(r, s)$ belongs to class $\mathcal{K}$ with respect to r and, for each fixed r, the mapping $s \mapsto \beta(r, s)$ is decreasing with respect to s and $\beta(r, s) \to 0$ as $s \to \infty$.*

Definition 4.2.2. *[88], A system $\dot{x}(t) = f(x(t), w(t))$ with state $x(t) \in \mathbb{R}^n$, and disturbance input $w(t) \in \mathbb{R}^{n_w}$, at time $t \in \mathbb{R}_{\geq 0}$ is said to be input-to-state stable (ISS), if there exist a $\mathcal{KL}$-function β and a $\mathcal{K}$-function γ such that for any initial state $x(0) \in \mathbb{R}^n$ and any bounded input w, i.e., w such that $\sup_{t \geq 0} \|w(t)\| < \infty$,*

any corresponding solution $x : \mathbb{R}_{\geq 0} \to \mathbb{R}^n$ *satisfies for all* $t \in \mathbb{R}_{\geq 0}$

$$\|x(t)\| \leq \beta\left(\|x(0)\|, t\right) + \gamma\left(\sup_{0 \leq \tau \leq t} \|w(\tau)\|\right). \tag{4.1}$$

4.3 A recap on fundamental limitations of linear control

This section is concerned with the description of the fundamental limitations of LTI control considered in this chapter. To this end, let us consider the single-input single-output (SISO) closed-loop interconnection in Fig. 4.1. Here, the

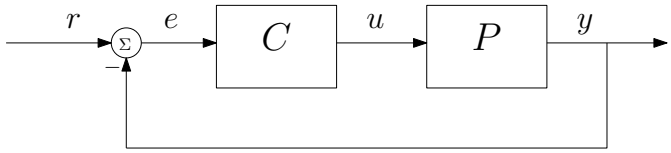

Figure 4.1. Linear closed-loop system configuration.

LTI plant and controller are represented by the transfer functions $P(s)$ and $C(s)$, respectively. The plant output $y(t) \in \mathbb{R}$ is subtracted from the reference signal $r(t) \in \mathbb{R}$, generating the error signal $e(t) = r(t) - y(t)$, at time $t \in \mathbb{R}_{\geq 0}$. This error signal is fed to the controller, which in turn generates the control output $u(t) \in \mathbb{R}$, at time $t \in \mathbb{R}_{\geq 0}$.

Assumption 4.3.1. *In the remainder of this chapter, unless stated otherwise, the reference signal* $r(t)$ *is assumed to be a unit-step, i.e.,* $r(t) = 1$ *for all* $t \in \mathbb{R}_{\geq 0}$. *Moreover, it is assumed that the plant* P *and the controller* C *have zero initial conditions.*

In what follows, we present some fundamental limitations of LTI control, which are unavoidable for certain classes of linear systems $P(s)$ when controlled by any stabilizing LTI controller $C(s)$. Prior to doing so, a few definitions from [119] are needed.

Definition 4.3.1. *[119], Let the open-loop LTI system in Fig. 4.1 be given by* $L(s) = P(s)C(s)$. *The closed-loop system in Fig. 4.1 is said to be internally stable if there are no unstable pole-zero cancellations in* $L(s)$, *and the transfer function* $S(s) = (1 + L(s))^{-1}$ *has all of its poles in the open left-half complex plane.*

In [119] the notion of internal stability as defined in Definition 4.3.1 is used for stating the limitations of LTI control. However, this definition is only applicable to LTI systems and can not be used to analyze the stability of hybrid closed-loop systems containing HIGS elements. Therefore, in this work we adopt the notion of ISS as in Definition 4.2.2, which can be used for both LTI and nonlinear systems.

Definition 4.3.2. *[119] The rise time of the step response of the closed-loop system in Fig. 4.1 with zero initial conditions (for P and C) is defined as*

$$t_r := \sup_{\delta \in \mathbb{R}_{>0}} \left\{ \delta : y(t) \leq \frac{t}{\delta} \text{ for all } t \in [0, \delta] \right\}. \tag{4.2}$$

Based on Definition 4.3.2, one can determine the rise time associated with the step response of a system by finding the maximal value of δ such that the step response falls below the line $y = \frac{t}{\delta}$, for $t \in [0, \delta]$.

Definition 4.3.3. *[119] The overshoot of the step response of the closed-loop system in Fig. 4.1 with zero initial conditions (for P and C), is the maximum value by which the output $y(t)$ exceeds its final setpoint value $r(t)$, i.e.,*

$$y_{\text{os}} := \sup_{t \in \mathbb{R}_{\geq 0}} \{-e(t)\}. \tag{4.3}$$

With the notions of rise time, overshoot, and ISS now defined, the fundamental limitations of LTI control considered in this chapter can be explicitly stated.

Proposition 4.3.1. *[119] Consider the closed-loop configuration in Fig. 4.1. Suppose that the LTI system $P(s)$, is stabilized (in the sense of ISS) by the LTI controller $C(s)$. Then*

(i) if $\lim_{s \to 0} sP(s)C(s) = c_1, 0 < |c_1| < \infty$, then

$$\lim_{t \to \infty} e(t) = 0, \text{ and}$$
$$\int_0^\infty e(t)\, \mathrm{d}t = \frac{1}{c_1};$$

(ii) if $\lim_{s \to 0} s^2 P(s)C(s) = c_2, 0 < |c_2| < \infty$, then

$$\lim_{t \to \infty} e(t) = 0, \text{ and} \tag{4.4}$$
$$\int_0^\infty e(t)\, \mathrm{d}t = 0. \tag{4.5}$$

Proof. See [119], Section 1.3. □

Remark 4.3.1. *Note that in the closed-loop interconnection of Fig. 4.1, when the transfer function of the open-loop system $P(s)C(s)$ has a single open-loop integrator, item (i) of Proposition 4.3.1 holds. This does not necessarily imply that the step response $y(t) = 1 - e(t)$, overshoots. However, as shown in Proposition 1 of [18], provided that the rise time t_r is sufficiently slow such that $t_r > \frac{2}{c_1}$, the*

unit-step response $y(t)$ overshoots, for any stabilizing LTI controller $C(s)$. Indeed, due to item (i) of proposition 4.3.1 one has

$$\int_0^\infty e(t)\,\mathrm{d}t = \frac{1}{c_1}$$

for some $c_1 \in \mathbb{R}$. Using Definition 4.3.2 we get

$$\begin{aligned}\int_0^\infty e(t)\,\mathrm{d}t = \frac{1}{c_1} &\geq \int_0^{t_r}\left(1-\frac{t}{t_r}\right)\mathrm{d}t + \int_{t_r}^\infty e(t)\,\mathrm{d}t \\ &= \frac{t_r}{2} + \int_{t_r}^\infty e(t)\,\mathrm{d}t,\end{aligned}$$

where t_r denotes the rise time. Therefore, we have

$$\int_{t_r}^\infty e(t)\,\mathrm{d}t \leq \frac{1}{c_1} - \frac{t_r}{2}.$$

Provided that, $t_r > \frac{2}{c_1}$, then $\int_{t_r}^\infty e(t)\,\mathrm{d}t < 0$, therefore $e(t) = 1 - y(t) < 0$ and thus $y(t) > 1$, for some $t \in (t_r, \infty)$, implying that there will be overshoot in the step response.

Remark 4.3.2. *In the closed-loop interconnection of Fig. 4.1, under zero initial conditions, the error signal $e(t)$ will be initially positive. Indeed for $y(t_0) = 0$, one has $e(t_0) = 1 - y(t_0) = 1$. If the transfer function of the open-loop plant $P(s)C(s)$ has two open-loop integrators, due to (4.5) in Proposition 4.3.1, the error $e(t)$ will have a change of sign. This implies that there has to be overshoot in the step-response $y(t)$ for any stabilizing LTI controller $C(s)$.*

Moreover, it is easy to show that (4.4) and (4.5) also hold when the open-loop plant $P(s)C(s)$ contains more than two integrators. Indeed, if

$$\lim_{s\to 0} s^n P(s)C(s) = c_n, 0 < |c_n| < \infty,$$

then one has $P(s)C(s) = \frac{\tilde{L}(s)}{s^n}$, where $\lim_{s\to 0}\tilde{L}(s) = c_n$. Additionally the Laplace transform of the error signal (to a unit step reference) is given by $E(s) = \frac{1}{s}\frac{1}{1+P(s)C(s)} = \frac{1}{s}\frac{s^n}{s^n+\tilde{L}(s)}$. With $n \geq 1$, by application of the final value theorem we obtain

$$\lim_{t\to\infty} e(t) = \lim_{s\to 0} sE(s) = \lim_{s\to 0}\frac{s^n}{s^n + \tilde{L}(s)} = 0,$$

thereby showing that (4.4) holds true. Furthermore, as a result of Lemma 1.3.1 in [119], we have for $n \geq 2$

$$\int_0^\infty e(t)\,\mathrm{d}t = \lim_{s\to 0} E(s) = \lim_{s\to 0}\frac{s^{n-1}}{s^n + \tilde{L}(s)} = 0,$$

showing that (4.5)*, also holds. As a result, for an open-loop plant containing two or more open-loop integrators, a non-zero overshoot is unavoidable in the step-response* $y(t)$ *for any stabilizing LTI controller* $C(s)$*.*

Proposition 4.3.2. *[119] Consider the interconnection in Fig. 4.1. Suppose that the open-loop plant* $P(s)$ *has a pole at* $s = p$*, such that* $\mathrm{Re}(p) > 0$*. Then, if the closed-loop system is ISS, it holds that*

$$\int_0^\infty e^{-pt} e(t)\,\mathrm{d}t = 0, \text{ and } \int_0^\infty e^{-pt} y(t)\,\mathrm{d}t = \frac{1}{p}. \tag{4.6}$$

Proof. See [119], Section 1.3. □

Remark 4.3.3. *As a result of Proposition 4.3.2, if the plant has an open-loop pole* p *in the right-half complex plane such that* $\mathrm{Im}(p) = 0$*, the unit-step response* $y(t)$ *necessarily overshoots for any internally stabilizing LTI controller* $C(s)$*. Moreover, as shown in [119] Remark 1.3.5, the overshoot satisfies*

$$y_{\mathrm{os}} \geq \frac{(pt_r - 1)e^{pt_r} + 1}{pt_r} \geq \frac{pt_r}{2}, \tag{4.7}$$

where t_r *is the rise time as defined in* (4.2)*.*

The limitations described in Remark 4.3.1, 4.3.2, and 4.3.3 have been previously shown to be overcome by hybrid and nonlinear control strategies such as VGC and reset control. In [143] a HIGS-based design is presented that is shown to overcome the limitation mentioned in Remark 4.3.3.

The aim of this chapter is to show that by using HIGS-based control, the limitations of LTI control as described in Remark 4.3.1 and Remark 4.3.2 can also be overcome, thereby showing that HIGS-based control can overcome all the limitations that have been previously overcome by other nonlinear/hybrid control strategies.

4.4 System description and problem statement

In this section, we describe the class of systems considered in this chapter. Additionally, the problem that we aim to address in this chapter is explicitly stated in this section.

4.4.1 Hybrid integrator-gain systems

A hybrid integrator-gain system (HIGS) element, denoted by $\mathscr{H}$, is described by the discontinuous piecewise linear (PWL) system

$$\mathscr{H}: \begin{cases} \dot{x}_h(t) = \omega_h z(t) & \text{if } (z(t), u(t), \dot{z}(t)) \in \mathscr{F}_1, \quad (4.8a) \\ x_h(t) = k_h z(t) & \text{if } (z(t), u(t), \dot{z}(t)) \in \mathscr{F}_2, \quad (4.8b) \\ u(t) = x_h(t), & \quad (4.8c) \end{cases}$$

with state $x_h(t) \in \mathbb{R}$, input $z(t) \in \mathbb{R}$, time-derivative of input $\dot{z}(t) \in \mathbb{R}$, and output $u(t) \in \mathbb{R}$, at time $t \in \mathbb{R}_{\geq 0}$. The parameters $\omega_h \in [0, \infty)$ and $k_h \in (0, \infty)$ denote the integrator frequency and gain value, respectively. Moreover, $\mathscr{F}_1$ and $\mathscr{F}_2$ denote the regions in $\mathbb{R}^3$ where the different subsystems are active. A HIGS element is designed to primarily operate in the so-called integrator mode given by (4.8a). However, the integrator-mode dynamics can be followed as long as the input-output pair (z, u) of $\mathscr{H}$ remain inside the sector

$$\mathscr{F} := \left\{ (z, u, \dot{z}) \in \mathbb{R}^3 \mid zu \geq \frac{1}{k_h} u^2 \right\}. \tag{4.9}$$

At moments when the input-output pair (z, u) tends to leave the sector $\mathscr{F}$, a switch is made to the so-called gain mode as given by (4.8b), so that the trajectories move along the sector boundary where $z = k_h u$ and thus remain in the sector $\mathscr{F}$. As such, the sets $\mathscr{F}_1$ and $\mathscr{F}_2$ are given by

$$\mathscr{F}_1 := \mathscr{F} \setminus \mathscr{F}_2, \tag{4.10}$$

$$\mathscr{F}_2 := \left\{ (z, u, \dot{z}) \in \mathbb{R}^3 \mid u = k_h z \wedge \omega_h z^2 > k_h \dot{z} z \right\}. \tag{4.11}$$

As a result of this construction, the input and output of a HIGS element have the same sign at all times. A visual interpretation of the sets $\mathscr{F}, \mathscr{F}_1$ and $\mathscr{F}_2$ can be found in Chapter 2. In the remainder of this chapter, it is assumed that the initial condition of a HIGS element is chosen as $x_h(0) = 0$.

The interested reader is referred to Chapter 2 and [38, 123], for a proof of existence and forward completeness of solutions as well as stability analysis of HIGS-controlled systems.

4.4.2 Closed-loop system description

We consider the general closed-loop interconnection in Fig. 4.2, where, as before,

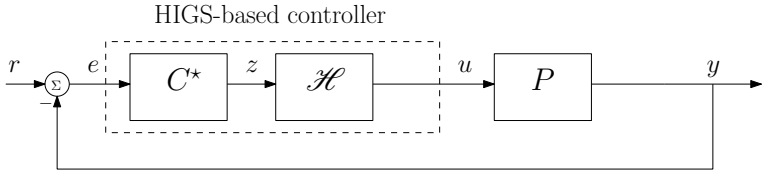

Figure 4.2. Closed-loop system configuration with HIGS-element.

the LTI plant to be controlled has transfer function $P(s)$. In contrast with the closed-loop interconnection in Fig. 4.1, the LTI controller has been replaced with a HIGS-based controller consisting of a HIGS element $\mathscr{H}$ as in (4.8) and an LTI controller with transfer function $C^\star(s)$.

Moreover, the state-space (minimal) realization of the plant's transfer function $P(s)$ is given by

$$\Sigma_p : \begin{cases} \dot{x}_p(t) = A_p x_p(t) + B_p u(t), \\ y(t) = C_p x_p(t), \end{cases} \tag{4.12}$$

where $x_p(t) \in \mathbb{R}^{n_p}$ is its state-vector, $u(t) \in \mathbb{R}$ is the input to the plant, $y(t) \in \mathbb{R}$ is the plant output at time $t \in \mathbb{R}_{\geq 0}$, and A_p, B_p, C_p are matrices of appropriate dimensions. Furthermore, the initial condition $x_p(0)$, is assumed to be zero. Similarly, let $(A_{C^\star}, B_{C^\star}, C_{C^\star}, D_{C^\star})$, be a state-space realization of the linear controller $C^\star(s)$. Due to the piecewise linear (PWL) nature of HIGS, the closed-loop interconnection, depicted in Fig. 4.2, can be represented as

$$\Sigma : \begin{cases} \dot{x} = A_i x + B_i w, & \text{if } (z, u, \dot{z}) \in \mathscr{F}_i, i \in \{1, 2\}, \\ y = Cx, \end{cases} \tag{4.13}$$

with state vector $x(t) = [x_p(t)^\top, x_{C^\star}(t)^\top, x_h(t)]^\top \in \mathbb{R}^n$, where x_p, $x_{C^\star}$, and x_h, denote the state of $P(s)$, $C^\star(s)$, and $\mathscr{H}$, respectively. Moreover, the performance output is denoted by $y(t)$, and $w(t) = [r(t)^\top, \dot{r}(t)^\top]^\top$ represents the vector of exogenous inputs. In addition, $\mathscr{F}_i, i \in \{1, 2\}$, denote the regions where integrator-mode and gain-mode dynamics are active, respectively. The state-space representation (4.13), will prove particularly useful for stability analysis of the closed-loop systems considered in the following sections (see also [38, 144], for more details). Explicit expressions of the matrices in (4.13) will be provided in subsequent sections, where deemed necessary.

4.4.3 Problem formulation

In this chapter, the objective is to design HIGS-based controllers overcoming the LTI performance limitations presented in Remark 4.3.1 and Remark 4.3.2. In particular, for each case a HIGS-based design as depicted in Fig. 4.2 is presented, that is capable of

i) achieving zero steady-state tracking error (as a linear integrator),

ii) eliminating overshoot,

iii) stabilizing the closed-loop system (in the sense of ISS).

thereby realizing performance objectives that are impossible to achieve with any stabilizing LTI controller.

4.5 Single open-loop integrator without overshoot

In this section, we present an example which illustrates that by using a HIGS-based design, the fundamental limitation in Remark 4.3.1 can be overcome. To

this end consider the interconnection in Fig. 4.2 with

$$P(s) = \frac{1}{s}, \quad C^\star(s) = 1.$$

As explained in Remark 4.3.1, for this choice of $P(s)$, the unit-step response of the system necessarily overshoots for any stabilizing LTI controller satisfying item (i) of Proposition 4.3.1, provided that the rise time t_r (see Definition 4.3.2) is sufficiently slow. More specifically, the step response overshoots if $t_r > 2/c_1$ with c_1 as defined in item (i) of Proposition 4.3.1. For determining the value of the constant c_1 we make use of the fact that the steady-state error of the closed-loop system to a unit-ramp input, i.e., $r(t) = t$, is given by $\lim_{t\to\infty} e_{\text{ramp}}(t) := \frac{1}{c_1}$, where e_{ramp} denotes the error signal to a unit-ramp input. Indeed, by application of the final value theorem to the closed-loop system in Fig. 4.1, the steady-state error to a unit-ramp input is found to be

$$\begin{aligned} \lim_{t\to\infty} e_{\text{ramp}}(t) &= \lim_{s\to 0}(s)(\frac{1}{s^2})\frac{1}{1+P(s)C(s)} \\ &= \lim_{s\to 0}\frac{1}{s+sP(s)C(s)}. \end{aligned} \tag{4.14}$$

Due to item (i) of Proposition 4.3.1, $\lim_{s\to 0} sP(s)C(s) = c_1$ and thus, for (4.14) we obtain

$$\lim_{s\to 0}\frac{1}{s+sP(s)C(s)} = \frac{1}{c_1}. \tag{4.15}$$

Therefore, the following performance objectives are impossible to achieve for any stabilizing linear controller $C(s)$:

i) no overshoot in the step response,

ii) steady state error not larger than 1, to a unit ramp reference,

iii) rise time in the step response larger than 2 seconds.

This is in fact the same set of objectives that are achieved by using reset control in [18]. Note that indeed the above objectives can not be achieved with any stabilizing LTI controller as objective ii) requires $c_1 \geq 1$, and since $t_r > 2 \geq 2/c_1$, the step response would necessary overshoot, thereby violating objective i).

For a HIGS-based design to overcome the limitation in Remark 4.3.1, it should achieve the same steady-state error to a unit-ramp input and a step response with a rise time satisfying $t_r > 2/c_1$, without any overshoot.

We start by computing the tracking error to a unit-ramp input for the closed-loop interconnection of $P(s)$ and a single HIGS element. The error signal can be

computed to be (for zero initial conditions)

$$e_{\text{ramp}}(t) = \begin{cases} \frac{1}{\sqrt{\omega_h}} \sin(\sqrt{\omega_h} t), & t \in [0, t_s), \\ \frac{1}{k_h} + \left(\frac{1}{\sqrt{\omega_h}} \sin(\sqrt{\omega_h} t_s) - \frac{1}{k_h} \right) e^{-k_h (t - t_s)}, & t \geq t_s, \end{cases} \tag{4.16}$$

where ω_h and k_h denote the integrator frequency and the gain parameter of the HIGS element, respectively. Moreover, $t_s = \frac{2}{\sqrt{\omega_h}} \arctan\left(\frac{k_h}{\sqrt{\omega_h}}\right)$ is the time instant when the HIGS switches from integrator mode to gain mode.

To see how (4.16) is derived, first note that for zero initial conditions the HIGS element $\mathscr{H}$ starts to operate in the integrator mode wherein the dynamics are given by the transfer function $\mathscr{H}_i(s) = \omega_h / s$, leading to the expression

$$E_{\text{ramp}}(s) = \frac{R(s)}{1 + \mathscr{H}_i(s) P(s)} = \frac{1/s^2}{1 + \omega_h / s^2} = \frac{1}{s^2 + \omega_h}, \tag{4.17}$$

for the error, in the complex domain. Here, $E_{\text{ramp}}(s)$ and $R(s)$ denote the Laplace transforms of the error $e_{\text{ramp}}(t)$ and the reference $r(t)$, respectively. By applying the inverse Laplace transform to (4.17) we obtain

$$e_{\text{ramp}}(t) = \frac{1}{\sqrt{\omega_h}} \sin(\sqrt{\omega_h} t), \quad \forall t \in [0, t_s). \tag{4.18}$$

To determine the switching instant t_s, note that at $t = t_s$, one has $k_h e_{\text{ramp}}(t_s) = u(t_s)$, and $\omega_h e_{\text{ramp}}(t_s) > k_h \dot{e}_{\text{ramp}}(t_s)$, such that at this time instant operation in the integrator mode leads to violation of the sector constraint of the HIGS element. The output of the HIGS element at time $t = t_s$ is given by

$$\begin{aligned} u(t_s) &= \int_0^{t_s} \omega_h e_{\text{ramp}}(t) dt = 1 - \cos(\sqrt{\omega_h} t_s) \\ &= k_h e_{\text{ramp}}(t_s) = \frac{k_h}{\sqrt{\omega_h}} \sin(\sqrt{\omega_h} t_s), \end{aligned} \tag{4.19}$$

where the last equality follows from (4.18). By solving (4.19) we obtain $t_s = \frac{2}{\sqrt{\omega_h}} \left(\arctan\left(\frac{k_h}{\sqrt{\omega_h}} \right) \right)$. Note that by using this expression for t_s together with (4.18), one can confirm that the switching condition $\omega_h e_{\text{ramp}}(t_s) > k_h \dot{e}_{\text{ramp}}(t_s)$ is satisfied. Indeed, by using the expression derived for t_s, together with the fact that $k_h > 0$, $\omega_h > 0$ as well as the trigonometric identities, $\sin(2 \arctan(x)) = \frac{2x}{1+x^2}$, and $\cos(2 \arctan(x)) = \frac{1-x^2}{1+x^2}$, one can confirm $\omega_h e_{\text{ramp}}(t_s) > k_h \dot{e}_{\text{ramp}}(t_s)$, such that a switch to the gain mode dynamics is required at $t = t_s$, in order to avoid violation of the sector constraint of the HIGS element.

Upon switching to the gain mode, the dynamics of the HIGS element are given by the transfer function $\mathscr{H}_g(s) = k_h$. To derive the expression for $e_{\text{ramp}}(t)$ after

the switching instance $t = t_s$, we define a shifted time parameter $t' = t - t_s$, and a shifted input $r(t') = t' + e(t_s) = t' + \frac{1}{\sqrt{\omega_h}}\sin(\sqrt{\omega_h}t_s)$, in order to compensate the trajectory movement between $t = 0$ and $t = t_s$, for all $t' \in \mathbb{R}_{\geq 0}$. When the HIGS element operates in the gain mode, we obtain the following expression for the error signal in the complex domain by application of the Laplace transform to $r(t')$ and using the same reasoning as in (4.17),

$$\begin{aligned} E_{\text{ramp}}(s) &= \frac{R(s)}{1 + \mathscr{H}_g(s)P(s)} \\ &= \frac{1}{k_h}\frac{1}{s} + \left(\frac{1}{\sqrt{\omega_h}}\sin(\sqrt{\omega_h}t_s) - \frac{1}{k_h}\right)\frac{1}{s + k_h}. \end{aligned} \tag{4.20}$$

Application of the inverse Laplace transform to (4.20) gives

$$\begin{aligned} e(t') &= \mathscr{L}^{-1}\{E\}(t') \\ &= \frac{1}{k_h} + \left(\frac{1}{\sqrt{\omega_h}}\sin(\sqrt{\omega_h}t_s) - \frac{1}{k_h}\right)e^{-k_h t'}. \end{aligned} \tag{4.21}$$

Using (4.21), one has $\dot{e}(t') = -k_h e(t')$ and thus $\omega_h e(t') \geq k_h \dot{e}(t')$, for all $t' \in \mathbb{R}_{\geq 0}$, $w_h > 0$, and $k_h > 0$. Hence, after $t = t_s$, no switch is made back to the integrator mode. By substituting $t' = t - t_s$ in (4.21), one obtains the second expression in (4.16) for $t \geq t_s$.

Building on the discussion above, the constant c_1 is given by

$$c_1 = \frac{1}{\lim_{t\to\infty} e_{\text{ramp}}(t)} = k_h. \tag{4.22}$$

Therefore, due to Remark 4.3.1, if we find a combination of k_h and ω_h such that the closed-loop system's step response does not overshoot and its rise time satisfies $t_r > 2/k_h$, we have overcome the limitation under consideration. To determine whether the step response of the closed-loop interconnection of $P(s)$ and a single HIGS element overshoots, we proceed by computing the error signal to a unit-step input, i.e., $r(t) = 1$, given by

$$e_{\text{step}}(t) = \begin{cases} \cos(\sqrt{\omega_h}t), & t \in [0, t_s), \\ \cos(\sqrt{\omega_h}t_s)e^{-k_h(t-t_s)}, & t \geq t_s, \end{cases} \tag{4.23}$$

where the switching time is given by $t_s = \frac{1}{\sqrt{\omega_h}}\arctan\left(\frac{k_h}{\sqrt{\omega_h}}\right)$. The derivation of (4.23) follows the same methodology used in the derivation of (4.16). Clearly the unit-step response of the system never overshoots, if $e_{\text{step}}(t)$ is non-negative for all $t \in \mathbb{R}_{\geq 0}$. Note that for e_{step} to be non-negative at all times, it is necessary that $\cos(\sqrt{\omega_h}t)$ is non-negative for all $t \in [0, t_s]$. Using the expression for t_s, this condition is equivalent to

$$\arctan\left(\frac{k_h}{\sqrt{\omega_h}}\right) \leq \frac{\pi}{2},$$

which is always satisfied since $\frac{-\pi}{2} < \arctan(\cdot) < \frac{\pi}{2}$. Moreover, for $t \geq t_s$, since $\cos(\sqrt{\omega_h} t_s) \geq 0$ and $k_h > 0$, it holds that $0 \leq \cos(\sqrt{\omega_h} t_s) e^{-k_h (t - t_s)} \leq \cos(\sqrt{\omega_h} t_s)$. Thus we conclude that $e_{\text{step}}(t) \geq 0$, for all $t \geq 0$ and therefore the unit-step response $y_{\text{step}}(t) = 1 - e_{\text{step}}(t)$ never overshoots, regardless of the choice of $\omega_h > 0$ and $k_h > 0$. Additionally, note that $\lim_{t \to \infty} e_{\text{step}}(t) = 0$, such that a steady-state tracking error of zero is achieved.

It remains to show that it is possible to find a combination of the parameters ω_h and k_h, such that the constraint on the rise time, i.e., $t_r > 2/c_1 = 2/k_h$, is satisfied. Based on Definition 4.3.2, the rise time t_r is determined from the tangency of the step response $y(t) = 1 - e_{\text{step}}(t)$, with the line $\hat{y}(t) := t/t_r$. Thus, we seek the pair $(t^\star, t_r)$, $t^\star > 0$, such that

$$y(t^\star) = \hat{y}(t^\star), \quad \dot{y}(t^\star) = \dot{\hat{y}}(t^\star). \tag{4.24}$$

For the particular choice of parameters $k_h = 1.5$, $\omega_h = 0.25$, using (4.24) leads to $t_r \approx 2.8 > \frac{2}{k_h} = \frac{4}{3}$. Hence, we have found a combination of the HIGS parameters k_h and ω_h which lead to no overshoot in the step response $y(t)$ while respecting the constraint $t_r > 2/k_h$.

Remark 4.5.1. *ISS of the closed-loop system considered in this section will be established in Section 4.7.*

The analysis presented thus far is verified with the simulation results in Fig. 4.3. As it can be seen in Fig. 4.3, a zero steady-state tracking error is achieved. Moreover, there is no overshoot in the step response $y(t)$, and the constraint on the rise time of the step response is satisfied. In Fig. 4.4, trajectories are shown that provide more insight into the switching behaviour of the HIGS element. It is observed that the element is initiated in integrator-mode and remains within that mode until reaching the sector boundary $u = k_h z$. Here, the integrator dynamics point out of the sector $[0, k_h]$, and thus a switch is made to the gain mode. From this point onward, the trajectories (exponentially) converge towards the origin, without any more mode switches.

4.6 Multiple open-loop integrators without overshoot

This section is concerned with using HIGS-based control for overcoming the limitation of LTI control discussed in Remark 4.3.2. To this end, consider the interconnection in Fig. 4.2 with $P(s) = (0.05s+1)/s^2$ (the choice of $C^\star(s)$ will be specified later). Note that, as explained in Remark 4.3.2, when the reference signal $r(t)$ is a unit-step, for this choice of $P(s)$ the step response of the system necessarily overshoots. In order to overcome this limitation, a stabilizing HIGS-based design that achieves a zero steady-state tracking error to a unit-step reference, while leading to

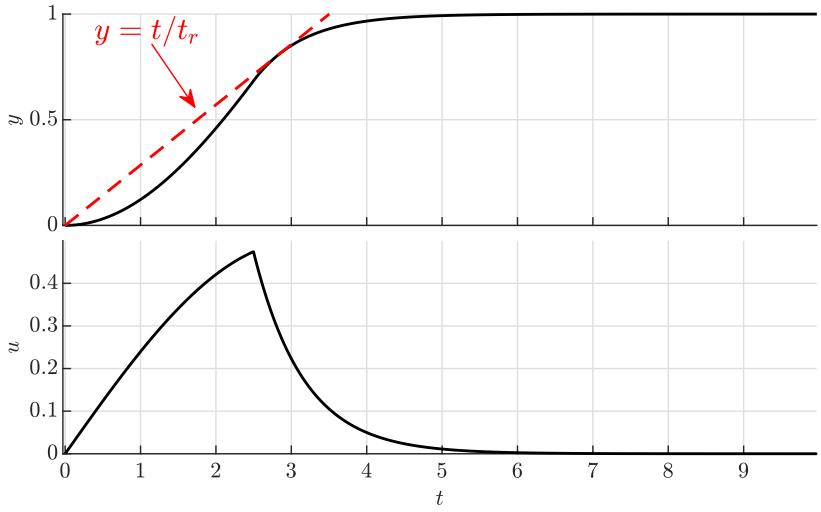

Figure 4.3. Step response $y(t)$ and control output $u(t)$ for the closed-loop system configuration with HIGS-based control and one open-loop integrator. The dashed line indicates the rise-time line $\hat{y}(t) = t/t_r$.

a error signal $e(t)$, which is non-negative for all time $t \in \mathbb{R}_{\geq 0}$, is desired. Achieving the latter objective results in a step response with no overshoot.

As mentioned in Section 4.4, the plant $P(s)$ is assumed to have zero initial conditions. As such, a positive initial control signal $u(t)$ is required to steer the output of the system toward the setpoint. Moreover, note that $P(s) = 1/s^2 + 0.05/s$, with the double integrator $1/s^2$ the more dominant term. Therefore, the system dominantly behaves as a double integrator (described by $\ddot{y}(t) = u(t)$). As a result, when the output $y(t)$ approaches the setpoint value, a sign change in the control input $u(t)$ is needed in order to decrease $\dot{y}(t)$ (and eventually make it zero), so that overshoot is avoided and a zero steady-state tracking error is achieved. However, note that $u(t)$ is the output of the HIGS element and as explained in Section 4.4.1, the input and output of a HIGS element always have the same sign. Thus, if the error signal $e(t)$ would be directly fed into the HIGS element, a sign change in $u(t)$ results in a change of sign in $e(t)$ which in turn, would lead to overshoot in the step response $y(t)$. In order to address this problem, we propose to place an LTI controller, denoted by $C^\star(s)$ in Fig 4.2, in front of the HIGS-element. In particular, $C^\star(s)$ is a PD filter given by

$$C^\star(s) = k_p \left(\frac{s}{\omega_c} + 1 \right), \tag{4.25}$$

where $\omega_c = |1 + 4j/\pi|\omega_h/k_h$ is the cross-over frequency of the describing function

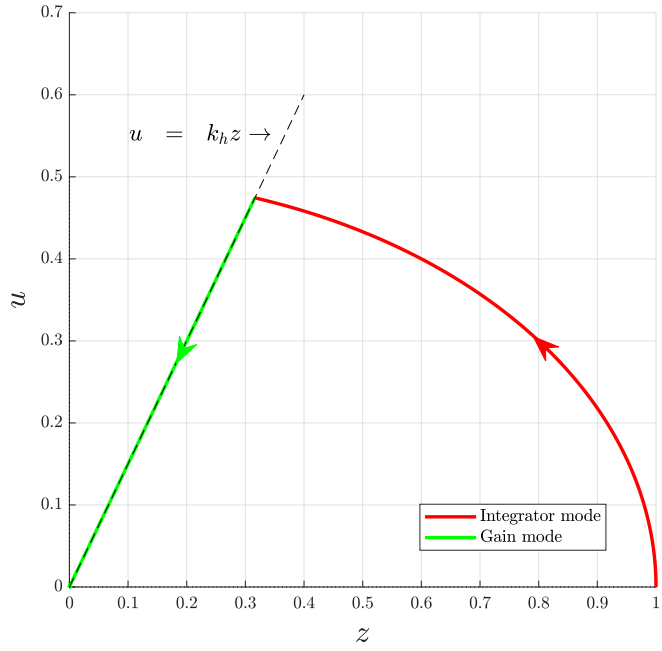

Figure 4.4. HIGS input $z(t)$ versus HIGS output $u(t)$.

of a HIGS-element (see [143], for an explicit expression of the describing function of the HIGS). By filtering the error signal with $C^\star(s)$ prior to feeding it to the HIGS element, the input to HIGS becomes

$$z(t) = k_p \left(e(t) + \frac{\dot{e}(t)}{\omega_c} \right). \tag{4.26}$$

With this choice of $C^\star(s)$, it is possible to have a sign change in the input $z(t)$ to the HIGS element, while avoiding a change of sign in $e(t)$. Indeed, it follows from (4.26) that $z(t) < 0$, if

$$\dot{e}(t) < -\omega_c e(t). \tag{4.27}$$

Hence, including the linear filter $C^\star(s)$ provides the possibility of changing the sign of the control signal $u(t)$, while avoiding a change of sign in $e(t)$. Therefore, by using (4.27) as a tuning guideline, a suitable value of ω_c (which can be tuned by changing the value of ω_h) can be obtained, which in turn leads to a control signal generated by the HIGS element that is initially positive and drives the system's output towards the setpoint value. At points when (4.27) holds true, the HIGS element changes the sign of its output, thereby slowing down the system's response

and thus potentially avoiding overshoot. As such, it is clear that the choice of ω_c (and thus ω_h) is crucial in the design of the HIGS-based controller. In particular, a suitable value of ω_h would lead to a change of sign in $u(t)$, fast enough to avoid overshoot. On the other hand, a too high ω_h value would result in a step response with overshoot. Indeed for $\omega_h \to \infty$, one has $z(t) \to k_p e(t)$. Therefore, as $\omega_h \to \infty$ a sign change in $z(t)$ implies a change of sign in $e(t)$ leading to overshoot.

Remark 4.6.1. *For practical implementation of the non-proper $C^\star(s)$ filter in (4.25), a proper high-pass filter is used for approximating the derivative term, which results in*

$$C^\star(s) = k_p \left(\frac{1}{\omega_c} \frac{s}{\tau s + 1} + 1 \right), \tag{4.28}$$

where $\tau > 0$ is chosen sufficiently small.

The unit-step response of the closed-loop system where the controller parameters are chosen as, $k_h = 1$, $\omega_h = 0.5$, and $k_p = 10$, is portrayed in Fig. 4.5. As it

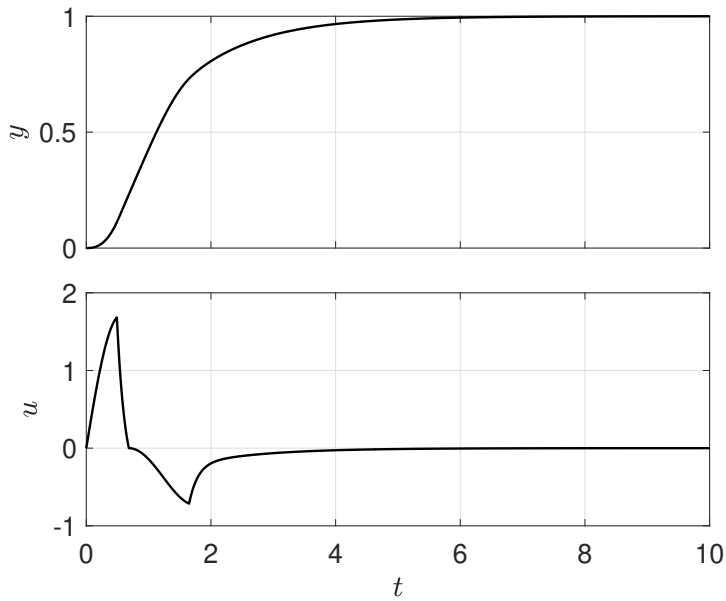

Figure 4.5. Step response $y(t)$ and control output $u(t)$ for the closed-loop system configuration with HIGS-based control and two open-loop integrators.

can be seen in Fig. 4.5, the step response y does not overshoot and a zero steady-state tracking error is achieved. Further insights into the mechanism leading to the absence of overshoot can be obtained by investigating the trajectories in Fig. 4.6. As shown in Fig. 4.6, the HIGS input $z(t)$ and output $u(t)$ show a change in

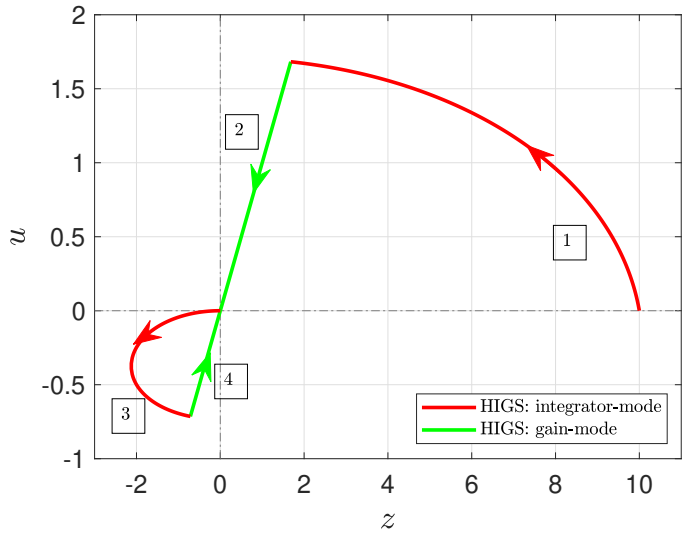

(a) HIGS input $z(t)$ versus HIGS output $u(t)$

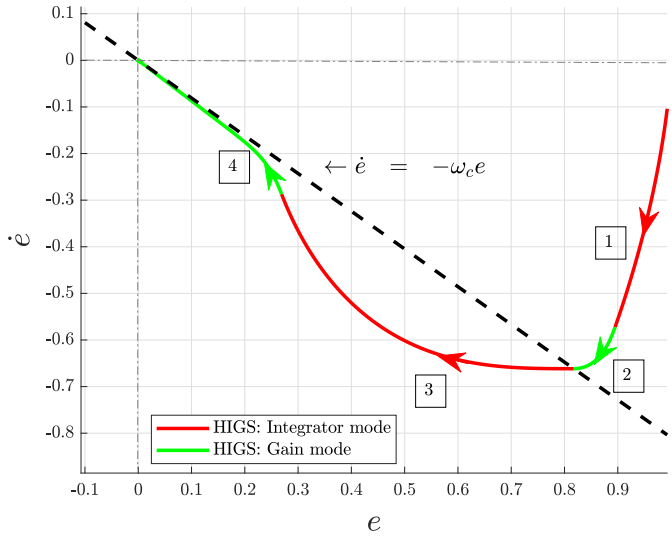

(b) Error $e(t)$ versus its derivative $\dot{e}(t)$

Figure 4.6. Trajectories of the HIGS-controlled system with two open-loop integrators.

sign, while $e(t) \geq 0$ for all $t \geq 0$. In particular, as shown in Fig. 4.6a, the HIGS element initially operates in integrator-mode. After some time, a switch is made to the gain-mode dynamics, resulting in trajectories that move towards the origin of the (z, u) plane. The operation of the HIGS element in the gain-mode leads to trajectories in the $(e, \dot{e})$ plane that cross the line $\dot{e} = -\omega_c e$ (see Fig. 4.6b), such that (4.27) holds and thus results in a sign change in $z(t)$. After this point, the trajectories in the $(e, \dot{e})$ plane eventually move towards the line $\dot{e} = -\omega_c e$, intersect it at the point $e = \dot{e} = 0$, and remain there. This leads to a steady-state error of zero without any overshoot in the step response.

The results presented in this section show that by using HIGS-based control, the limitation stated in Remark 4.3.2 can be overcome. In order to complete this claim, it remains to show that the closed-loop system is ISS. This will be done in Section 4.7.

4.7 Closed-loop stability

As remarked earlier, in order to complete the claims that the fundamental limitations considered in Remark 4.3.1 and Remark 4.3.2 are overcome, ISS of the closed-loop systems considered in Section 4.5 and Section 4.6 has to be established. In this section, we establish ISS (see Definition 4.2.2) for each interconnection, by solving linear matrix inequalities (LMIs), whose feasibility implies the existence of a quadratic ISS Lyapunov function.

Recall the general HIGS-controlled system in Fig. 4.2, described by piecewise linear representation (4.13) with state vector $x(t) = [x_p(t)^\top x_{C^\star}(t)^\top x_h(t)]^\top \in \mathbb{R}^n$. The matrices $A_i, B_i, i \in \{1, 2\}$ are given in (4.29), (4.30), where $(A_q, B_q, C_q, D_q), q \in \{P, C^\star\}$, denote the state-space matrices defined in Section 4.4. Moreover, the output matrix in (4.13), is given by $C = [C_p \ 0 \ 0]$.

$$A_1 = \begin{bmatrix} A_p & 0 & B_p \\ -B_{C^\star}C_p & A_{C^\star} & 0 \\ -\omega_h D_{C^\star}C_p & \omega_h C_{C^\star} & 0 \end{bmatrix}, \quad B_1 = \begin{bmatrix} 0 & 0 \\ B_{C^\star} & 0 \\ \omega_h D_{C^\star} & 0 \end{bmatrix}, \tag{4.29}$$

$$\begin{aligned} A_2 &= \begin{bmatrix} A_p & 0 & B_p \\ -B_{C^\star}C_p & A_{C^\star} & 0 \\ (-k_h C_{C^\star}B_{C^\star}C_p - k_h D_{C^\star}C_p A_p) & k_h C_{C^\star}A_{C^\star} & -k_h D_{C^\star}C_p B_p \end{bmatrix}, \\ B_2 &= \begin{bmatrix} 0 & 0 \\ B_{C^\star} & 0 \\ k_h C_{C^\star}B_{C^\star} & k_h D_{C^\star} \end{bmatrix}. \end{aligned} \tag{4.30}$$

In order to verify ISS of the closed-loop system (4.13), we employ Theorem 4.7.1 as stated below.

Theorem 4.7.1. *Consider the HIGS-controlled system* (4.13)*. Suppose there exists a matrix* $P = P^\top$*, symmetric matrices* W, Q*, and* U *with non-negative entries, and a real vector* Γ*, such that*

$$P - S^\top W S \succ 0, \tag{4.31}$$

$$A_1^\top P + P A_1 + S^\top U S \prec 0, \tag{4.32}$$

$$A_2^\top P + P A_2 + \Gamma G + G^\top \Gamma^\top + Z^\top Q Z \prec 0, \tag{4.33}$$

where the matrices S *and* Z *are given by*

$$S = \begin{bmatrix} 1 & 0 \\ k_h & -1 \end{bmatrix} \begin{bmatrix} 1 & 0 & 0 \\ 0 & 1 & 0 \end{bmatrix} E,$$

and

$$Z = \begin{bmatrix} -k_h & \omega_h \\ 0 & 1 \end{bmatrix} \begin{bmatrix} 0 & 0 & 1 \\ 1 & 0 & 0 \end{bmatrix} E,$$

with E*, such that for* $w = 0$*,* $Ex = [z, u, \dot{z}]^\top$*. Additionally,* $G = LE$*, with* $L = [k_h \ -1 \ 0]$*. Then* (4.13) *is ISS with respect to the disturbances* w*.*

Proof. Note that with S as defined above and $w = 0$, the sector boundedness of the input-output pair of the HIGS element, translates on the level of the state x to $x \in \mathcal{S}$, with

$$\mathcal{S} := \{x \in \mathbb{R}^n \mid Sx \geq 0 \vee Sx \leq 0\}, \tag{4.34}$$

wherein the inequalities are interpreted element-wise. Consider now the quadratic Lyapunov function $V(x) = x^\top P x$. Due to the non-negativity of the elements of W together with (4.34), by application of S-procedure relaxations we obtain from (4.31) that $P \succ 0$ and thus $V(x) > 0$, for all $x \in \mathcal{S}$ and hence for all $(z, u) \in \mathscr{F}$. Moreover, when the HIGS-element operates in the integrator mode, it follows from (4.32) together with (4.34) as well as the non-negativity of the elements of U and application of S-procedure relaxations that $\dot{V}(x) < 0$ along the trajectories of the system. Additionally, let us note that the gain mode condition $(z, u, \dot{z}) \in \mathscr{F}_2$, translates on the level of states to $x \in \mathcal{S}_g$, with

$$\mathcal{S}_g := \{x \in \mathbb{R}^n \mid Gx = 0 \wedge (Zx > 0 \vee Zx < 0)\} \tag{4.35}$$

with Z and G as defined in the Theorem and where, once again, the inequalities are interpreted element-wise. Therefore, as a result of the non-negativity of the elements in Q and by application of Finsler's Lemma [22] together with S-procedure relaxations we have $\dot{V}(x) < 0$ along the trajectories of the system in the gain mode. This proves stability of (4.13) with $w = 0$. Next, using the fact that w is an affine input to (4.13), one can utilize the same arguments as in [88], Section 4.9, to show that $V(x)$ is an ISS-Lyapunov function [129] for (4.13) and thus, the system is ISS with respect to all bounded exogenous inputs w. □

The above stability analysis result has been applied to the closed-loop systems considered in Section 4.5 and Section 4.6, i.e., (4.13), where the matrices in (4.29) and (4.30) are computed based on the parameters specified in these sections. For solving the LMIs, use has been made of the MATLAB toolbox `Yalmip` [96] and the solver `MOSEK` [5]. For the example in Section 4.5, a feasible solution with

$$P = \begin{bmatrix} 0.2521 & 0.3592 \\ 0.3592 & 0.8331 \end{bmatrix}, \; W \begin{bmatrix} 3.264 & 1.04 \\ 1.04 & 0.7449 \end{bmatrix},$$
$$U = \begin{bmatrix} 0.6017 & 3.647 \\ 3.647 & 0.72 \end{bmatrix}, \; V = \begin{bmatrix} 0.5641 & 0.5501 \\ 0.5501 & 1.038 \end{bmatrix},$$
$$\Gamma = \begin{bmatrix} 0.0472 & -0.2521 \end{bmatrix}.$$

is found for the LMIs. Moreover for the system considered in Section 4.6, the LMIs are rendered feasible with

$$P = \begin{bmatrix} 6863.0 & 1092.0 & 7617.0 & 4259.0 \\ 1092.0 & 644.3 & -881.7 & 1048.0 \\ 7617.0 & -881.7 & 20999.0 & 3833.0 \\ 4259.0 & 1048.0 & 3833.0 & 3569.0 \end{bmatrix},$$
$$W = \begin{bmatrix} 53.15 & 97.99 \\ 97.99 & 84.31 \end{bmatrix},$$
$$U = \begin{bmatrix} 13.0 & 12433.0 \\ 12433.0 & 195.4 \end{bmatrix}, \; V = \begin{bmatrix} 3.064 & 5593.0 \\ 5593.0 & 4.902\,10^6 \end{bmatrix},$$
$$\Gamma = \begin{bmatrix} -5.428\,10^6 & -2.457\,10^6 & -5.058\,10^6 & 1.019\,10^7 \end{bmatrix}.$$

As a result of the feasibility of the LMIs, we conclude ISS of the closed-loop systems in Section 4.5 and Section 4.6.

With this, we claim that the HIGS-based designs proposed in the previous sections overcome the fundamental limitations of LTI control, described in Remarks 4.3.1 and 4.3.2.

4.8 Summary and Conclusion

In this chapter, we have employed HIGS-based control for overcoming two well-known fundamental time-domain performance limitations of LTI control. In particular, we have shown that by using HIGS-based control, fundamental overshoot limitations inherent to LTI systems with one or multiple open-loop integrators can be overcome. Together with the work presented in [143], the results in this chapter show that all overshoot limitations of LTI control that have been previously overcome by nonlinear and hybrid control strategies, can also be overcome by HIGS-based control, thereby highlighting the strength of HIGS-based control design.

Future research directions include the extension of our results to more complex and industrially relevant examples. Additionally, systematic procedures for design/synthesis of HIGS-based controllers that overcome fundamental performance limitations of linear control are of interest.

5

Analysis of Sampled-Data Hybrid Integrator-Gain Systems: A Discrete-Time Approach

Abstract - *Hybrid integrator-gain systems (HIGS) are hybrid control elements used to overcome fundamental performance limitations of linear time-invariant feedback control, and have enjoyed early successes in engineering applications such as control of high-precision motion systems. However, the creation of discretized versions of HIGS and their sampled-data analysis have not been addressed in the literature so far. Given that nowadays almost all controllers are implemented digitally and thus in discrete time, this forms a highly relevant topic of research for HIGS and HIGS-based control. In this chapter, we address these open issues by presenting discrete-time HIGS elements, which preserve the main philosophy behind the operation of HIGS in continuous time. Moreover, stability criteria are presented that can be used to certify input-to-state stability of discrete-time and sampled-data HIGS-controlled systems based on both (i) (measured) frequency response data, and (ii) linear matrix inequalities (LMIs). A numerical case study is provided to illustrate the use of the main results.*

This chapter is based on [121] and [120].

5.1 Introduction

Hybrid integrator-gain systems (HIGS) are hybrid control elements that have been shown to be effective tools in realizing performance beyond the limitations of linear time-invariant (LTI) control [143, 148]. Extensive research has led to several fruitful results for HIGS and HIGS-based control design in terms of mathematical formalization, well-posedness and stability analysis [38, 122, 123, 142], overcoming fundamental limitations of LTI control [143, 148], and improving closed-loop performance of control systems [37, 75, 141, 144].

However, thus far the literature related to HIGS has mainly focused on *continuous-time* (CT) HIGS-controlled systems. In practice, while the plant to be controlled, e.g., a high precision motion system, is a CT system, almost all controllers are implemented digitally and thus, in *discrete-time* (DT). Such a construction leads to an overall *sampled-data* (SD) control system consisting of CT plants to be controlled and DT controllers. In this chapter, we aim to address important aspects related to the creation of proper SD implementations of SD HIGS-based controllers and their analysis.

Generally speaking, as illustrated in Fig. 5.1, three main approaches can be distinguished for SD control. These are namely [105]:

i) the continuous-time design approach (abbreviated as CTD), in which CT controllers are designed based on a CT model of the plant and the obtained CT controllers are subsequently discretized and implemented;

ii) the discrete-time approach (abbreviated as DTD), in which a discrete-time (DT) controller is designed based on a DT model of the plant;

iii) the sampled-data design approach (abbreviated as SDD), in which a discrete-time controller is directly designed based on a CT model of the plant.

In the CTD approach, while one can benefit from CT (physical)design/analysis insights and tools, the digital controller implementation is not considered. This results in a need for implementation with a (i) fast sampling rate and (ii) a *consistent* discretization of the controller [4, 62] such that the solutions to the DT controller converge to the solutions of the controller designed in CT, under fast sampling. While fast sampling could be achieved by (expensive) hardware, consistent discretization of HIGS being a hybrid controller with a discontinuous vector field is not straightforward. The DTD approach on the other hand, in principle does not require fast sampling to maintain stability [90]. However, this approach ignores the inter-sample behavior of the plant and thus desirable overall performance of the SD system is not automatically guaranteed. Lastly, the SDD approach (see e.g. [39, 65]) neither considers a CT model of the controller nor ignores the inter-sample plant behavior. However, it is the most complex approach among the three due to the hybrid nature of the system it considers, consisting of CT plant and DT controller dynamics. Additionally, given that SDD methods consider CT

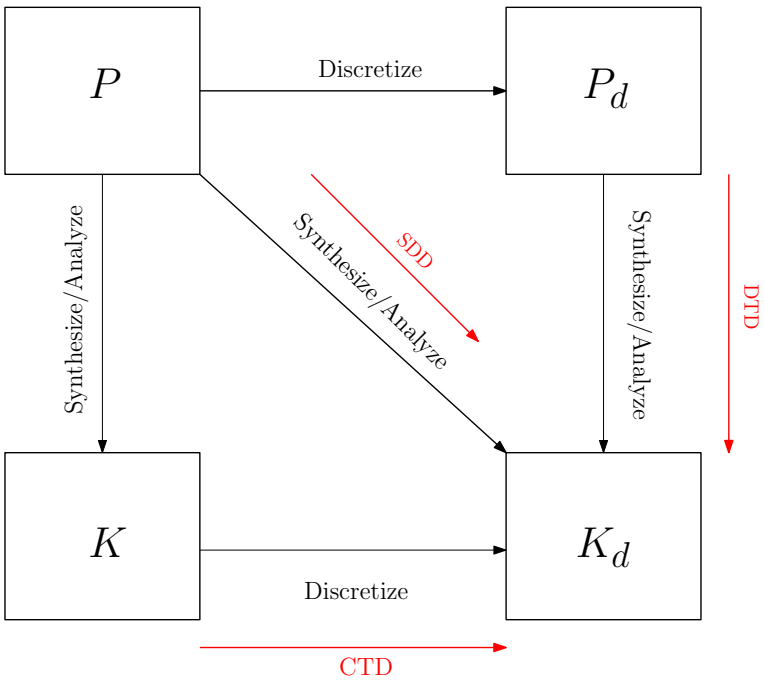

Figure 5.1. The three main approaches for SD control of CT plant P with a DT controller K_d.

plant models, utilization of such methods for applications, such as control of high precision motion systems, wherein the plant model is often obtained by means of data-driven methods such as system identification and thus evolves in DT, is not a well justified choice [108].

In this chapter, we present tools for analysis of SD HIGS-controlled systems in the DTD approach, which is typically easier to apply in practice compared to the SDD approach, and can be used in conjunction with DT models obtained from system identification which are used in many applications where HIGS-based controller have been utilized. Moreover, DTD methods have the advantage of providing direct guarantees on DT closed-loop behavior (in contrast to the CTD approach) that, under appropriate conditions, can also be used to provide guarantees when taking the inter-sample behavior into account [106].

Our contributions are fourfold. As a first contribution, we present DT versions of HIGS, which preserve the essential characteristics and the main philosophy behind the operation of HIGS in continuous time. The presented DT HIGS can be used for analysis and design of HIGS-based SD controllers following the three approaches (DTD, CTD, and SDD) for SD control design. We present two sets of stability criteria that can be used to certify input-to-state stability (ISS) of systems

consisting of DT HIGS-based controllers and a DT LTI plant. These two sets of ISS criteria are based on (i) (measured) frequency response data, and (ii) linear matrix inequalities (LMIs), forming the second and third contributions of this chapter, respectively. We also show that the LMIs are guaranteed to provide less conservative results compared to the frequency-domain criterion as satisfaction of the latter implies feasibility of a special case of the LMIs. As a fourth contribution, it is shown that DT ISS guarantees imply also ISS of sampled-data HIGS-controlled systems consisting of DT HIGS-based controllers and a CT LTI plant (including the inter-sample behavior). A numerical case study is also provided, to illustrate the results.

The remainder of this chapter is organized as follows. Section 5.2 contains preliminary material and a short introduction to CT HIGS and its main motivation. Section 5.3 introduces DT HIGS. In Section 5.4 the closed-loop system under consideration as well as Stability criteria in frequency and time-domain are presented. Section 5.5 extends the DT stability analysis to sampled-data HIGS-controlled systems. This is followed by a numerical example and conclusions in Sections 5.6 and 5.7, respectively.

5.2 Preliminaries

In this section, we present some preliminary material that is used in the sections to follow.

5.2.1 Notation and definitions

The following notation conventions will be used. We denote a real, symmetric matrix $A \in \mathbb{R}^{n\times n}$ by $A \in \mathbb{S}^{n\times n}$. Given a symmetric matrix $A \in \mathbb{S}^{n\times n}$ we say that it is positive (negative)-definite, denoted by $A \succ (\prec) 0$, if $x^\top Ax > (<)\ 0$ for all $x \in \mathbb{R}^n \setminus \{0\}$. We write $A \in \mathbb{S}^{n\times n}_{\geq 0}$, if A is symmetric and all its elements are non-negative. The inequality symbols $>$, $\geq$, $<$, $\leq$ for a vector are understood component-wise. For a vector $x \in \mathbb{R}^n$ we denote its p norm by $\|x\|_p$. We write $\|x\|$ for the standard Euclidean norm. For a matrix $A \in \mathbb{R}^{n\times m}$ we use $\|A\|_\infty = \max_{1\leq i\leq m} \sum_{j=1}^{n} |a_{ij}|$, where $|a_{ij}|$ denotes the absolute value of the element in the i^{th} row and j^{th} column of A. For a bounded function $u : \mathbb{R}_{\geq 0} \to \mathbb{R}^n$, we write $\|u\|_\infty = \sup_{t\in\mathbb{R}_{\geq 0}} \|u(t)\|$. Similarly for a bounded function $w : \mathbb{N} \to \mathbb{R}^n$ we use the notation $\|w\|_\infty = \sup_{k\in\mathbb{N}} \|w(k)\|$.

Definition 5.2.1. *[88] A function $\alpha : [0, a) \to [0, \infty)$ is said to belong to class $\mathcal{K}$, if it is continuous, strictly increasing and $\alpha(0) = 0$, it is a $\mathcal{K}_\infty$ function if it belongs to class $\mathcal{K}$ and $\alpha(s) \to \infty$ as $s \to \infty$. A function $\beta : [0, a) \times [0, \infty) \to [0, \infty)$ is said to belong to class $\mathcal{KL}$, if, it is continuous and for each fixed s, the mapping $r \mapsto \beta(r, s)$ belongs to class $\mathcal{K}$ with respect to r and, for each fixed r, the mapping $s \mapsto \beta(r, s)$ is decreasing with respect to s and $\beta(r, s) \to 0$ as $s \to \infty$.*

Consider a system of the form

$$x[k] = f(x[k-1], w[k-1]) \tag{5.1}$$

with $x[k]$ taking values in $\mathbb{R}^n$ and $w[k]$ taking values in $\mathbb{R}^m$, denoting the state and input, respectively, of the system at time instant $t = kT_s$, where $k \in \mathbb{N}$ and $T_s \in \mathbb{R}_{>0}$ denote the discrete time instant and the sampling period, respectively. Moreover, $f : \mathbb{R}^n \times \mathbb{R}^m \to \mathbb{R}^n$ is a function satisfying $f(0,0) = 0$.

Definition 5.2.2. *[85] System* (5.1) *is said to be input-to-state stable (ISS) with respect to w, if there exist a $\mathcal{KL}$-function $\beta : \mathbb{R}_{\geq 0} \times \mathbb{R}_{\geq 0} \to \mathbb{R}_{\geq 0}$ and a $\mathcal{K}$-function γ such that, for each bounded input $w : \mathbb{N} \to \mathbb{R}^m$ and each initial condition x_0, it holds that*

$$\|x[k, x_0, w]\| \leq \beta(\|x_0\|, k) + \gamma(\|w\|_\infty),$$

for each $k \in \mathbb{N}$, where $x[k, x_0, w]$ denotes the state of system (5.1)*, for initial state $x[0] = x_0$ and input w at discrete-time instant k.*

Definition 5.2.3. *[54, 85] A function $V : \mathbb{R}^n \to \mathbb{R}$ is called an ISS Lyapunov function for the system* (5.1)*, if the following holds:*

1. *There exists $\mathcal{K}_\infty$-functions α_1 and α_2 such that for all $x \in \mathbb{R}^n$*

$$\alpha_1(\|x\|) \leq V(x) \leq \alpha_2(\|x\|). \tag{5.2}$$

2. *There exist a $\mathcal{K}_\infty$-function α_3 and a $\mathcal{K}$-function γ, such that*

$$V(f(x,w)) - V(x) \leq -\alpha_3(\|x\|) + \gamma(\|w\|) \tag{5.3}$$

for all $x \in \mathbb{R}^n$ and all $w \in \mathbb{R}^m$.

Theorem 5.2.1. *The system* (5.1) *is ISS in the sense of Definition 5.2.3, if it admits an ISS Lyapunov function as defined in Definition 5.2.3.*

Proof. See [54, 85, 93], for the proof. □

5.2.2 Continuous-time HIGS

A CT HIGS element [37], denoted by $\mathscr{H}$, is described by

$$\mathscr{H} : \begin{cases} \dot{x}_h(t) = \omega_h e(t) & \text{if } (e(t), u(t), \dot{e}(t)) \in \mathscr{F}_1, \quad (5.4a) \\ x_h(t) = k_h e(t) & \text{if } (e(t), u(t), \dot{e}(t)) \in \mathscr{F}_2, \quad (5.4b) \\ u(t) = x_h(t) & \quad (5.4c) \end{cases}$$

with state $x_h(t) \in \mathbb{R}$, input $e(t) \in \mathbb{R}$, time-derivative $\dot{e}(t) \in \mathbb{R}$ of the input, and output $u(t) \in \mathbb{R}$, at time $t \in \mathbb{R}_{\geq 0}$. The parameters $\omega_h \in [0, \infty)$, $k_h \in (0, \infty)$ denote

the integrator frequency and the gain parameter of the HIGS element, respectively. Moreover, $\mathscr{F}_1$ and $\mathscr{F}_2$ denote the regions in $\mathbb{R}^3$, where the different subsystems are active. A HIGS element primarily operates in the so-called integrator mode (5.4a). However, the integrator mode dynamics can only be followed as long as the input-output pair (e, u) of $\mathscr{H}$ remains inside the sector

$$\mathcal{S} := \left\{ (e, u) \in \mathbb{R}^2 \mid eu \geq \frac{1}{k_h} u^2 \right\}. \tag{5.5}$$

When the pair (e, u) tends to leave $\mathcal{S}$, a switch is made to the so-called gain mode (5.4b), keeping the trajectories on the sector boundary, where $u = k_h e$, and thus in $\mathcal{S}$. In particular, the sets $\mathscr{F}_1$ and $\mathscr{F}_2$, are given by

$$\mathscr{F}_1 := \{(e, u, \dot{e}) \in \mathbb{R}^3 \mid (e, u) \in \mathcal{S}\} \setminus \mathscr{F}_2, \tag{5.6}$$

$$\begin{aligned} \mathscr{F}_2 :=& \{(e, u, \dot{e}) \in \mathbb{R}^3 \mid (e, u) \in \mathcal{S} \wedge u = k_h e \\ & \wedge \omega_h e^2 > k_h \dot{e} e\}. \end{aligned} \tag{5.7}$$

As a result of this construction, the input and output of a HIGS element have the same sign at all times, and, even more, its input and output remain inside $\mathcal{S}$. This leads to favorable properties in terms of a reduced phase lag of 38.15 degrees from a describing function perspective [38], in contrast to the 90 degrees phase lag of a standard linear integrator. In [143, 148], it was shown how these features of sign equivalence can be used to overcome fundamental overshoot performance limitations present in LTI control [119], making HIGS a promising control element. Additionally, HIGS has been shown to offer performance enhancing properties, for applications such as high-precision mechatronics [37, 141, 144], and active vibration isolation systems [75].

5.3 Discrete-Time HIGS

In this section, we present DT versions of HIGS, which preserve the main characteristics and the working principle of CT HIGS elements as in (5.4). In particular, we present DT variants of HIGS that

i) predominantly operate as a linear DT integrator;

ii) switch to other operating regimes when required to generate an output which satisfies (together with their input) the same sector constraint as in CT HIGS, cf. (5.5);

iii) given an input, produce an output that is (in DT) similar to the output of CT HIGS.

For the proposed DT HIGS versions, we will provide formal analysis tools in Sections 5.4 and 5.5.

5.3.1 DT HIGS: A bimodal version

In this section we present a first DT HIGS, which is given by

$$\tilde{\mathscr{H}}: \begin{cases} x_h[k] = x_h[k-1] + \omega_h T_s e[k], & \text{if } \tilde{\xi}[k] \in \tilde{\mathscr{F}}_1, \quad (5.8a) \\ x_h[k] = k_h e[k], & \text{if } \tilde{\xi}[k] \in \tilde{\mathscr{F}}_2, \quad (5.8b) \\ u[k] = x_h[k], & \quad (5.8c) \end{cases}$$

where $e[k] \in \mathbb{R}$, $x_h[k] \in \mathbb{R}$, and $u[k] \in \mathbb{R}$ denote the input, state and output of the system, respectively, at time instant $t = kT_s$, with $k \in \mathbb{N}$ the discrete time-step, and $T_s \in \mathbb{R}_{>0}$ the sampling period. The decision of which mode of operation is active is based on the decision variable $\tilde{\xi}[k] := (e[k], u^-[k], e^-[k]) := (e[k], u[k-1], e[k-1])$, while the regions where different subsystems are active, are denoted by $\tilde{\mathscr{F}}_1$, $\tilde{\mathscr{F}}_2 \subseteq \mathbb{R}^3$, which will be specified below.

The DT integrator mode dynamics are given by (5.8a), obtained by backward Euler discretization of (5.4a). Moreover, the DT gain-mode dynamics are given by (5.8b). Note that since (5.8a) has integrator dynamics, both its backward and forward Euler integration are exact with respect to the integration of the state (since $e^0 = I$), and thus, the choice between backward and forward Euler discretization, only influences the approximation of the input term used on the right-hand-side of (5.8a), i.e., $e[k]$ for backward Euler and $e[k-1]$ for forward Euler.

As in the case of CT HIGS, given an input e, a DT HIGS element is designed to primarily operate in the integrator mode (5.8a), while generating an output u such that $(e[k], u[k]) \in \mathcal{S}$, for all $k \in \mathbb{N}$, with $\mathcal{S}$ as defined in (5.5). We assume that $(e[0], u[0]) \in \mathcal{S}$, which, given $e[0]$, can always be arranged by a proper choice of $u[0] = x_h[0]$ (e.g., $u[0] = 0$ is always a viable choice). At moments when the integrator-mode dynamics lead to input-output trajectories that do not belong to $\mathcal{S}$, as in (5.5), a switch is made to the other mode such that $(e[k], u[k]) \in \mathcal{S}$, for all $k \in \mathbb{N}$.

Thereto, we define

$$\tilde{\mathscr{F}}_1 := \{\tilde{\xi} \in \mathbb{R}^3 \mid (e^-, u^-) \in \mathcal{S} \ \wedge (u^- + \omega_h T_s e)e \geq \frac{1}{k_h}(u^- + \omega_h T_s e)^2\}, \quad (5.9)$$

as the region where the integrator-mode dynamics (5.8a) are active. Note that the second condition defining the set in (5.9) can be perceived as a one-step ahead prediction of the output u, according to the integrator-mode dynamics (5.8a). In particular, with $\tilde{\mathscr{F}}_1$ as defined in (5.9), given $(e[k-1], u[k-1]) \in \mathcal{S}$ and a new sample $e[k]$ of the input, the integrator mode dynamics are active, if the output $u[k]$ to be generated by operation in the integrator mode satisfies $(e[k], u[k]) \in \mathcal{S}$, as computed in $(u^- + \omega_h T_s e)e \geq \frac{1}{k_h}(u^- + \omega_h T_s e)^2$, in (5.9).

Using a similar reasoning as above, the region where the gain-mode dynamics

are active is chosen as the complement

$$\tilde{\mathscr{F}}_2 := \{\tilde{\xi} \in \mathbb{R}^3 \mid (e^-, u^-) \in \mathcal{S} \wedge (u^- + \omega_h T_s e)e < \frac{1}{k_h}(u^- + \omega_h T_s e)^2\}, \tag{5.10}$$

as it results in operation in the gain-mode (5.8b) only if the trajectories resulting from the integrator mode (5.8a) would violate (5.5). With the choice of sets $\tilde{\mathscr{F}}_1$ and $\tilde{\mathscr{F}}_2$ as in (5.9) and (5.10), the DT HIGS element (5.8) predominantly operates in the integrator mode and generates an output u such that $(e[k], u[k]) \in \mathcal{S}$, for all $k \in \mathbb{N}$, thereby preserving the main philosophy behind the operation of CT HIGS (5.4).

Assumption 5.3.1. *The parameters ω_h, k_h, and T_s, are such that the inequality*

$$0 < T_s \leq \frac{k_h}{\omega_h},$$

is satisfied.

Assumption 5.3.1 can be easily satisfied by design and ensures that (5.8) always operates in the integrator mode from zero initial conditions. This is an important property, as otherwise, given an input e, a DT HIGS element would only operate in the integrator mode if there has been a sign change in successive input samples. This is clearly undesirable as the integrator mode should be the primary mode of operation of DT HIGS. Indeed for $x_h[k-1] = u[k-1] = 0$, the output of the integrator mode is given by $u[k] = \omega_h T_s e[k]$, which under Assumption 5.3.1 satisfies $(e[k], u[k]) \in \mathcal{S}$.

An illustration of the regions $\tilde{\mathscr{F}}_1$, and $\tilde{\mathscr{F}}_2$, when $k_h = \omega_h = 1$, $T_s = 0.5$, is provided in Fig. 5.2. Note that while the gain-mode dynamics (5.4b) of a CT HIGS element are active on a lower-dimensional subspace of the $(e, u, \dot{e})$ (see Fig. 2.4 in Chapter 2) space (due to the condition $u = k_h e$ in (5.7)), as shown in Fig. 5.2, both modes of (5.8) are active on sets with non-empty interiors.

The responses of a bimodal DT HIGS element as in (5.8) and a CT HIGS element as in (5.4), to a sinusoidal input, are compared with each other in Fig. 5.3. As it can be seen in Fig. 5.3, at discrete time instances kT_s with $k \in \mathbb{N}$, the response of (5.8) is initially similar to the response of (5.4). However, upon a zero crossing in the input e, the responses become considerably different. This can be explained as follows. As explained in Chapter 2 (e.g. in the proof of Theorem 2.6.1), upon a zero crossing in the input $e(t)$, a CT HIGS element (5.4) resumes operation in the integrator mode (5.4a). However, in DT when there is a zero crossing in the input e, i.e., when $e[k]e[k-1] < 0$, since $x_h[k-1]e[k-1] \geq 0$ (due to sector boundedness of the input-output pair of HIGS), then one necessarily has $x_h[k-1]e[k] \leq 0$. Therefore, if $|x_h[k-1]| > |\omega_h T_s e[k]|$, then the integrator mode dynamics (5.8a) generate an output $u_{int}[k] = x_h[k-1] + \omega_h T_s e[k]$ satisfying $(x_h[k-1] + \omega_h T_s e[k])e[k] < 0 < \frac{1}{k_h}(x_h[k-1] + \omega_h T_s e[k])^2$, and thus violating the

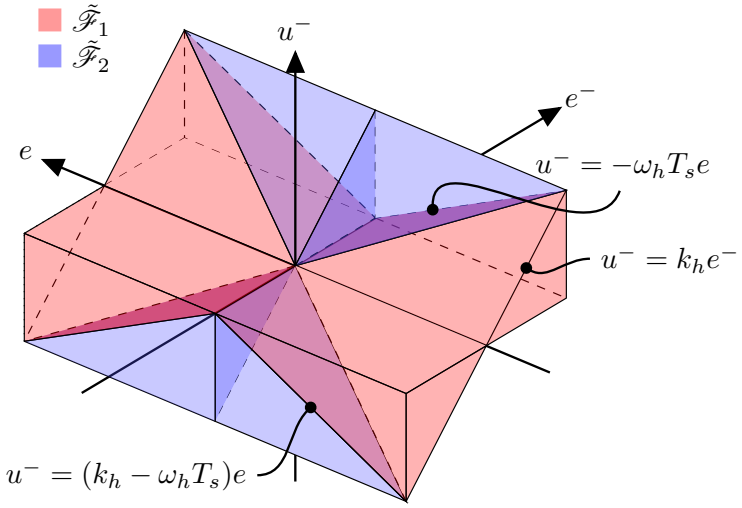

Figure 5.2. Regions $\tilde{\mathscr{F}}_1$, and $\tilde{\mathscr{F}}_2$, in the (e, u^-, e^-) space.

sector condition (5.5). Therefore, in such cases (5.8) operates in the gain mode (5.8b), which, as illustrated in Fig. 5.3, results in an offset between the outputs of (5.8) and (5.4) (which disappears if T_s goes to zero).

Therefore, in the next subsection, we also present a DT HIGS, which generates an output similar to CT HIGS (5.4) also in cases where a zero crossing in the input can cause a significant difference between the output u of (5.8) and (5.4), at sampling instances $t = kT_s$.

5.3.2 DT HIGS: A trimodal version

In this section we introduce a DT HIGS element, which, as in the case of DT HIGS (5.8) presented in Section 5.3.1, predominantly operates as a DT integrator and produces trajectories, respecting the sector constraint (5.5). Contrary to (5.8) however, this DT HIGS produces an output more similar to a CT HIGS, also in cases where zero-crossings in the input could lead to large deviations between the output of (5.8) and (5.4).

The proposed DT HIGS is given by

$$\overline{\mathscr{H}}: \begin{cases} x_h[k] = x_h[k-1] + \omega_h T_s e[k], & \text{if } \overline{\xi}[k] \in \overline{\mathscr{F}}_1, \quad (5.11a) \\ x_h[k] = k_h e[k], & \text{if } \overline{\xi}[k] \in \overline{\mathscr{F}}_2, \quad (5.11b) \\ x_h[k] = 0, & \text{if } \overline{\xi}[k] \in \overline{\mathscr{F}}_3, \quad (5.11c) \\ u[k] = x_h[k], & \quad (5.11d) \end{cases}$$

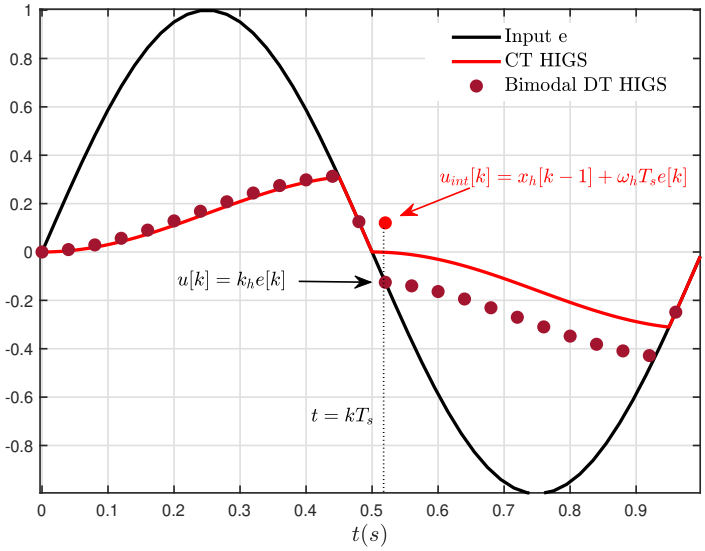

Figure 5.3. Response of (5.4) and (5.8) with $k_h = \omega_h = 1$, $T_s = 0.04s$, to a sinusoidal input.

where, as before, $e[k] \in \mathbb{R}$, $x_h[k] \in \mathbb{R}$, and $u[k] \in \mathbb{R}$ denote the input, state and output of the system, respectively, at time instant $t = kT_s$, with $k \in \mathbb{N}$ the discrete time-step, and $T_s \in \mathbb{R}_{>0}$ the sampling period. Similar to (5.8), the decision of which mode of operation is active is based on the decision variable $\bar{\xi}[k] := (e[k], u^-[k], e^-[k]) := (e[k], u[k-1], e[k-1])$, while the regions where different subsystems are active, are denoted by $\overline{\mathscr{F}}_1$, $\overline{\mathscr{F}}_2, \overline{\mathscr{F}}_3 \subseteq \mathbb{R}^3$.

Just as in the case of (5.8), (5.11) is designed to primarily operate according to (5.11a) for as along as the resulting input-output trajectories remain inside the sector (5.5). As such the set $\overline{\mathscr{F}}_1$, is taken the same as $\tilde{\mathscr{F}}_1$ in (5.9), i.e., $\overline{\mathscr{F}}_1 = \tilde{\mathscr{F}}_1$. To generate input-output trajectories that always reside in (5.5), the gain mode dynamics (5.11b) should be followed when $\bar{\xi}[k] \in \mathscr{F} \setminus \overline{\mathscr{F}}_1 = \tilde{\mathscr{F}}_2$, where $\tilde{\mathscr{F}}_2$ is as defined in (5.10). Moreover, in order to generate an output similar to CT HIGS, when there is a zero crossing in the input e, the set $\overline{\mathscr{F}}_2$ is given by

$$\overline{\mathscr{F}}_2 := \{\bar{\xi} \in \mathbb{R}^3 \mid \bar{\xi} \in \tilde{\mathscr{F}}_2 \wedge ee^- \geq 0\}. \tag{5.12}$$

Note that the construction in (5.12) ensures that (5.11b) is only followed when the integrator mode dynamics produce trajectories that violate the sector constraint (5.5), and it holds that $ee^- \geq 0$, meaning that the last two samples of the input have a similar sign, i.e., no zero crossings in the input e has been detected. For cases where $\bar{\xi}[k] \notin \overline{\mathscr{F}}_1 \wedge \bar{\xi}[k] \notin \overline{\mathscr{F}}_2$, implying that neither the integrator mode

(5.11a) nor the gain mode (5.11b) is followed, the third mode of operation called the zeroing mode, given by (5.11c) is used. The zeroing mode is active when

$$\overline{\xi}[k] \in \overline{\mathscr{F}}_3 := \{\overline{\xi} \in \mathbb{R}^3 \mid \overline{\xi} \in \tilde{\mathscr{F}}_2 \wedge ee^- < 0\}. \tag{5.13}$$

An illustration of the regions $\overline{\mathscr{F}}_1$, $\overline{\mathscr{F}}_2$, and $\overline{\mathscr{F}}_3$ when $k_h = \omega_h = 1,\ T_s = 0.5s$, is provided in Fig. 5.4. As in the case of (5.8), the parameters T_s, ω_h and k_h, are

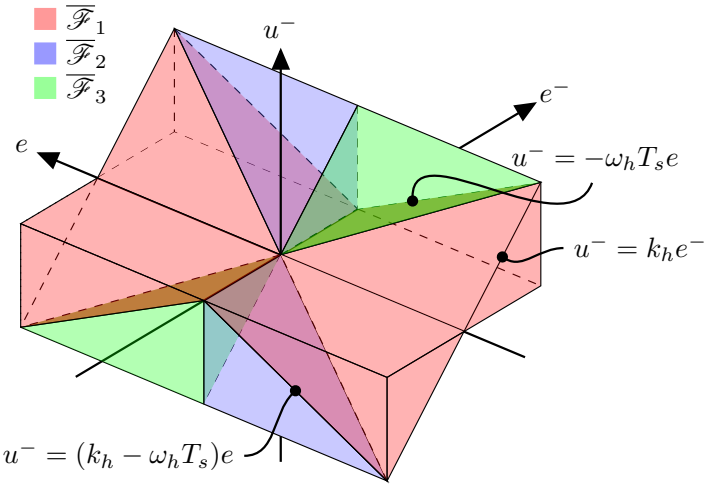

Figure 5.4. Regions $\overline{\mathscr{F}}_1$, $\overline{\mathscr{F}}_2$, and $\overline{\mathscr{F}}_3$ in the (e, u^-, e^-) space.

assumed to satisfy Assumption 5.3.1. Note that, with this assumption satisfied, the trimodal DT HIGS element always operates in the integrator mode (5.11a) upon operating in the zeroing mode (5.11c).

The response of a CT HIGS element (5.4) to a sinusoidal input, is compared to those of DT HIGS elements as in (5.8) and (5.11) in Fig. 5.5. As it can be seen in Fig. 5.5, initially the three responses are similar to each other. After a zero crossing in the input e, as discussed before, the bimodal DT HIGS element (5.8) generates an output $u_{gain}[k] = k_h e[k]$, which is different from the response of the CT HIGS element, and results in an offset (the size of which is dependent on T_s) between the two responses. The trimodal DT HIGS (5.11) element on the other hand, generates an output $u_{zeroing}[k] = 0$, which is much closer to the output of the CT HIGS (5.4) element, and thus produces an output similar to the output of (5.4), at all times $t = kT_s$, $k \in \mathbb{N}$.

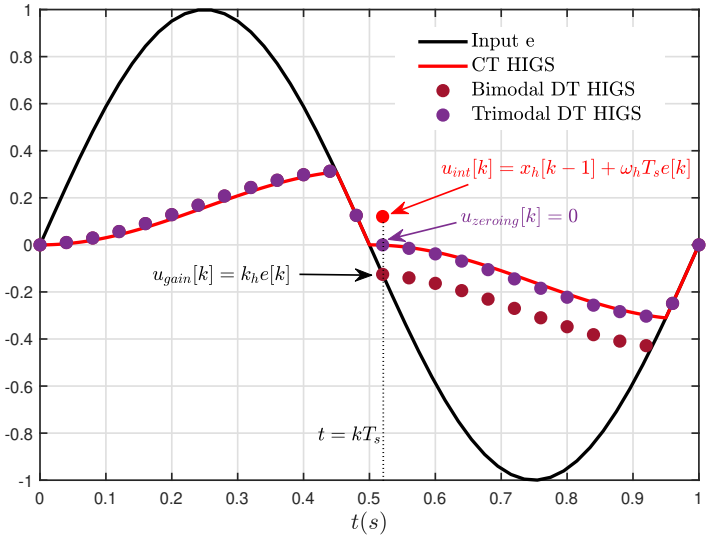

Figure 5.5. Response of CT and the different DT HIGS elements with $k_h = \omega_h = 1$, $T_s = 0.04s$, to a sinusoidal input.

5.3.3 A projection-based perspective on DT HIGS-controlled systems

In Chapters 2 and 3 projection-based formalizations of CT HIGS-controlled systems have been presented, in the class of *extended projected dynamical systems* (ePDS). In this section, we shortly introduce DT ePDS, obtained by applying time-stepping techniques [62] to CT ePDS. A projection-based description of DT HIGS-controlled systems is also presented and compared with DT HIGS as presented in the previous subsections.

Prior to introducing DT ePDS, let us first shortly recall a well-established iterative scheme for discretization of PDS, as presented in [102]. Consider the PDS

$$\dot{x}(t) = \Pi_K(x, f(x, u)) \tag{5.14}$$

with state $x(t) \in \mathbb{R}^n$, input $u(t) \in \mathbb{R}^m$, at $t \in \mathbb{R}_{\geq 0}$, $f : \mathbb{R}^n \times \mathbb{R}^m \to \mathbb{R}^n$, constraint set $K \subseteq \mathbb{R}^n$, and projection operator $\Pi : K \times \mathbb{R}^n \to \mathbb{R}^n$. As presented in [102], the *projected Euler discretization* of (5.14) takes the form

$$x[k] = P_K(x[k-1] + \tau f(x[k-1], u[k-1])), \tag{5.15}$$

where $\tau \in \mathbb{R}_{>0}$ is the time-step size, and for a vector $v \in \mathbb{R}^n$

$$P_K(v) := \arg\min_{a \in K} \|v - a\| \tag{5.16}$$

is the projection of v onto K. Here, an unconstrained Euler integration step is followed by a projection onto the constraint set K. Note that other numerical integration schemes such as Heun or Runge-Kutta methods can be used in a similar setting as in (5.15), i.e., an unconstrained numerical integration step followed by a projection onto the feasible set (see [102] for more details). Consider now the ePDS

$$\dot{x}(t) = \Pi_{K,E}(x, f(x,u)) \tag{5.17}$$

with $E \in \mathbb{R}^{n \times n_E}$ and $K \subseteq \mathbb{R}^n$, such that Assumption 2.3.1 in Chapter 2 is satisfied. Inspired by (5.15), we formulate the projected Euler discretization of (5.17) as

$$x[k] = P_{K,E}(x[k-1] + \tau f(x[k-1], u[k-1])) \tag{5.18}$$

with

$$P_{K,E}(v) := \arg\min_{\substack{a \in K \\ a - v \in \mathrm{im}E}} \|a - v\|. \tag{5.19}$$

With the operator $P_{K,E}$ as defined in (5.19), the sequence of solutions $x[k]$, $k \in \mathbb{N}$, to (5.18) is obtained by first following an unconstrained Euler integration scheme, and then projecting it onto the constraint set K in the direction given by $\mathrm{im}E$.

Lemma 5.3.1. *Consider the projection operator $P_{K,E}$, as defined in* (5.19) *with the constraint set K and the matrix E, satisfying Assumption 2.3.1 in Chapter 2. The projection $P_{K,E}(v)$ is well-defined in the sense that it provides a unique outcome for each $v \in \mathbb{R}^n$.*

Proof. The proof is based on similar arguments as used in Section 2.3.2 in Chapter 2 and is included here for completeness. In particular, we start by noting that (5.18) can be equivalently written as

$$x[k] = x[k-1] + \tau f(x[k-1], u[k-1]) + E\eta^\star, \tag{5.20}$$

with

$$\eta^\star = \arg\min_{\eta \in \Lambda(x,\tau)} \|E\eta\|, \tag{5.21}$$

where

$$\Lambda(x,\tau) = \{\eta \in \mathbb{R}^{n_E} \mid x[k-1] + \tau f(x[k-1], u[k-1]) + E\eta \in K\}.$$

Next, using the same arguments as in the proof of Lemma 2.3.1 we can show that under Assumption 2.3.1, $\Lambda(x,\tau)$ is a non-empty, closed, polyhedral set. This, together with the fact that E has full column rank, and thus, square of the cost function (5.21) being $\eta^\top E^\top E\eta$ is a quadratic positive definite function, imply that a unique minimizer exists, thereby concluding the proof. □

Let us now consider again the HIGS-controlled system in Fig. 2.3 of Chapter 2 described by

$$\dot{x}(t) = \Pi_{S,E}(x(t), A_1 x(t) + Bw(t)) \tag{5.22}$$

with the matrices A_1 and B as described in (2.31), the state $x = [x_g^\top \quad x_h]^\top$ with $x_g \in \mathbb{R}^{n_g}$ the state of the linear part of the system, satisfying Assumption 2.5.1, and $x_h \in \mathbb{R}$ the state of the HIGS element. Moreover, $E = [0_{n_g}^\top, \quad 1]^\top$ and $S = \mathscr{K} \cup -\mathscr{K}$, where

$$\mathscr{K} = \{x \in \mathbb{R}^n \mid Fx \geq 0\}$$

and $F = [F_1^\top \quad F_2^\top]^\top$, as defined in (2.29). Using the formulation in (5.18) we discretize (5.22) as

$$x[k] = P_{S,E}(x[k-1] + T_s(A_1 x[k-1] + Bw[k-1])). \tag{5.23}$$

Interestingly, solving (5.23) shows that the system has three modes of operation, analogous to the integrator mode, gain mode and the zeroing mode (when $F_1 x < (>)0 \wedge F_2 x \geq (\leq)0$). As such, by applying time-stepping techniques to ePDS, one also obtains a third mode of operation (as in the trimodal DT HIGS (5.11)) in DT, which is not present in CT. The DT ePDS-based representation (5.23) is of interest for studying topics such as consistency of discretization and robust numerical integration of ePDS for simulation of HIGS-controlled systems. However, in the sections to follow, we focus on (5.8) and (5.11) and this representation is not explored further.

5.4 Stability analysis of DT HIGS-controlled systems

In this section we present stability conditions for DT HIGS-controlled systems. In particular, conditions are presented that can be used to certify ISS of DT HIGS-controlled systems based on both (measured) frequency response functions and LMIs.

5.4.1 DT Closed-loop system description

We consider the closed-loop system in Fig. 5.6, consisting of a DT LTI system $\overline{\mathscr{G}}$ and a DT HIGS element $\mathcal{H}_{DT}$. Here, $\overline{\mathscr{G}}$ contains the linear part of the loop, consisting of the plant to be controlled and possibly LTI parts of the controller. The system $\overline{\mathscr{G}}$ is given by

$$\overline{\mathscr{G}} : \begin{cases} x_g[k] & = A_g x_g[k-1] + B_{gv} v[k-1] + B_{gw} w[k-1], \\ e[k] & = C_g x_g[k] \end{cases} \tag{5.24}$$

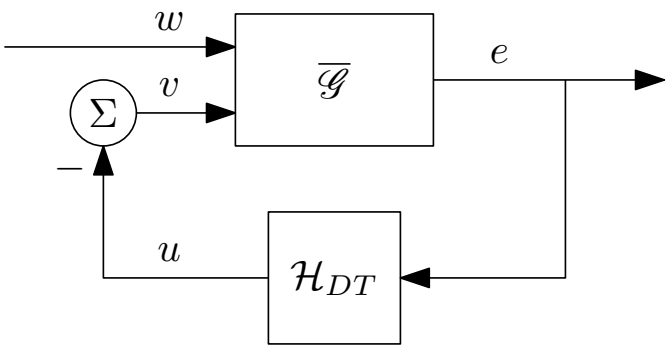

Figure 5.6. DT HIGS-controlled closed-loop system.

with state $x_g[k]$ taking values in $\mathbb{R}^{n_g}$, output $e[k]$ taking values in $\mathbb{R}$, control input $v[k]$ in $\mathbb{R}$ and exogenous disturbances $w[k]$ in $\mathbb{R}^{n_w}$, $k \in \mathbb{N}$. Moreover, A_g, B_{gv}, B_{gw}, and C_g are real matrices of appropriate dimensions. The DT HIGS element $\mathcal{H}_{DT}$ is given by either (5.8) or (5.11). For the closed-loop interconnection in Fig. 5.6, we have the state $x[k] = [x_g^\top[k]\ x_h^\top[k]]^\top \in \mathbb{R}^n$, where $n = n_g + 1$. In the case where $\mathcal{H}_{DT}$ is given by (5.8), by combining (5.8) and (5.24), we arrive at the state-space representation

$$\Sigma : \begin{cases} x[k] = A_i x[k-1] + B_i w[k-1], \text{ if } \tilde{\xi}[k] \in \tilde{\mathscr{F}}_i, i \in \{1,2\} \\ e[k] = Cx[k] \end{cases} \tag{5.25}$$

for the closed-loop dynamics with $\tilde{\mathscr{F}}_i$, $i \in \{1,2\}$, as defined in (5.9) and (5.10), and

$$\left[\begin{array}{c|c} A_1 & B_1 \end{array}\right] = \left[\begin{array}{cc|c} A_g & -B_{gv} & B_{gw} \\ \omega_h T_s C_g A_g & 1 - \omega_h T_s C_g B_{gv} & \omega_h T_s C_g B_{gw} \end{array}\right], \tag{5.26}$$

$$\left[\begin{array}{c|c} A_2 & B_2 \end{array}\right] = \left[\begin{array}{cc|c} A_g & -B_{gv} & B_{gw} \\ k_h C_g A_g & -k_h C_g B_{gv} & k_h C_g B_{gw} \end{array}\right], \tag{5.27}$$

$$C = \left[\begin{array}{cc} C_g & 0 \end{array}\right]. \tag{5.28}$$

In the case where the HIGS element $\mathcal{H}_{DT}$ is given by (5.11), we obtain

$$\Sigma : \begin{cases} x[k] = A_i x[k-1] + B_i w[k-1], \text{ if } \bar{\xi}[k] \in \overline{\mathscr{F}}_i, i \in \{1,2,3\} \\ e[k] = Cx[k] \end{cases} \tag{5.29}$$

with $\overline{\mathscr{F}}_i$, $i \in \{1,2,3\}$, as defined in (5.9), (5.12), and (5.13), the matrices A_i, B_i, C, $i \in \{1,2\}$ as defined in (5.26), (5.27), (5.28), and

$$\left[\begin{array}{c|c} A_3 & B_3 \end{array}\right] = \left[\begin{array}{cc|c} A_g & -B_{gv} & B_{gw} \\ 0 & 0 & 0_{1\times n_w} \end{array}\right]. \tag{5.30}$$

In the next subsections, we study the stability of (5.25) and (5.29). In doing so the notion of ISS as in Definition 5.2.2 is adopted.

5.4.2 Frequency-domain stability conditions

In this section results are presented, which guarantee ISS of (5.25) and (5.29), using simple-to-check graphical conditions based on frequency response functions of the plant model (5.24). As frequency response functions are generally easy to measure in practice (e.g., in mechatronic positioning systems), such frequency-based conditions for ISS are appealing to control practitioners.

Theorem 5.4.1. *Consider systems* (5.25) *and* (5.29) *with* (A_g, B_{gv}, C_g) *being a minimal realization. The systems are ISS, if*

i) The system matrix A_g *of the plant* (5.24) *is Schur;*

ii) $\frac{1}{k_h} + Re\{W(z)\} > 0$, *for all* $z \in \mathbb{C}$, $|z| = 1$, *with*

$$W(z) = C_g(zI - A_g)^{-1}B_{gv}. \tag{5.31}$$

Proof. The proof is based on showing that under the conditions stated in the theorem, there exists an ISS Lyapunov function for the systems under consideration, which by the virtue of Theorem 5.2.1 then implies ISS of the underlying systems. The proof is divided into the following steps:

1. Initially we use stability of $\overline{\mathscr{G}}$, implied by i), positive realness of $C_g(zI - A_g)^{-1}B_{gv} + \frac{1}{k_h}$, following from ii), minimality of (A_g, B_{gv}, C_g), and the fact that $u[k]e[k] \geq \frac{1}{k_h}u^2[k]$ for all $k \in \mathbb{N}$, to construct a quadratic ISS Lyapunov function $V_g(x_g) = x_g^\top P_g x_g$, with $P_g \succ 0$ for $\overline{\mathscr{G}}$, with input $v = -x_h$, by application of the DT KYP Lemma [25, 113].

2. For both cases where $\mathcal{H}_{DT}$ is given by (5.8) or (5.11), a quadratic Lyapunov-like function $V_h(x_h)$ is constructed for the DT HIGS $\mathcal{H}_{DT}$ in isolation with input $e[k-1] = C_g x_g[k-1]$. By explicit use of the sector constraint of $\mathcal{H}_{DT}$ it is shown that the Lyapunov function decreases along the trajectories of the DT-HIGS element.

3. The functions V_g and V_h constructed in the previous steps are combined into a single quadratic ISS Lyapunov function for the overall closed-loop systems, thereby proving the theorem.

Throughout the proof we have dropped time dependence, where clear from the context, to lighten the notation.
Step 1: It follows from the DT KYP Lemma [25, 50] (sometimes also referred to as the Kalman-Szegö-Popov Lemma), that the minimality of (A_g, B_{gv}, C_g), together

with the hypotheses in the Theorem imply the existence of a symmetric positive definite matrix P_g, a matrix L and a positive constant ε such that

$$\begin{aligned} A_g^\top P_g A_g - P_g &= -L^\top L - \varepsilon P_g, \\ B_{gv}^\top P_g A_g &= C_g - \sqrt{\frac{2}{k_h} - B_{gv}^\top P_g B_{gv}} \;\; L. \end{aligned} \tag{5.32}$$

Consider now the Lyapunov function $V_g(x_g) = x_g^\top P_g x_g$. One has

$$\begin{aligned} \Delta V_g &:= V_g(A_g x_g + B_{gv} v + B_{gw} w) - V_g(x_g) \\ &= (A_g x_g + B_{gv} v + B_{gw} w)^\top P_g (A_g x_g + B_{gv} v + B_{gw} w) - x_g^\top P_g x_g \\ &= x_g^\top (A_g^\top P_g A_g - P_g) x_g + 2 x_g^\top A_g^\top P_g B_{gv} v + 2 x_g^\top A_g^\top P_g B_{gw} w + \\ & v^\top B_{gv}^\top P_g B_{gv} v + 2 v^\top B_{gv}^\top P_g B_{gw} w + w^\top B_{gw}^\top P_g B_{gw} w. \end{aligned} \tag{5.33}$$

Using (5.32) and $v = -x_h$, we obtain

$$\begin{aligned} \Delta V_g &= x_g^\top (-L^\top L - \varepsilon P_g) x_g - 2 x_g^\top (C_g^\top - \sqrt{\frac{2}{k_h} - B_{gv}^\top P_g B_{gv}} \;\; L^\top) x_h \\ &+ 2 x_g^\top A_g^\top P_g B_{gw} w + x_h^\top B_{gv}^\top P_g B_{gv} x_h - 2 x_h^\top B_{gv}^\top P_g B_{gw} w \\ &+ w^\top B_{gw}^\top P_g B_{gw} w. \end{aligned} \tag{5.34}$$

By using now the sector constraint of $\mathcal{H}_{DT}$, i.e., $\|x_h\| \leq k_h \|C_g x_g\|$ and reworking (5.34), we get

$$\begin{aligned} \Delta V_g &\leq -\varepsilon V_g(x_g) - \left(L x_g - \sqrt{\frac{2}{k_h} - B_{gv}^\top P_g B_{gv}} \;\; x_h \right)^\top \left(L x_g - \sqrt{\frac{2}{k_h} - B_{gv}^\top P_g B_{gv}} \;\; x_h \right) \\ &+ \left(2 x_g^\top A_g^\top P_g B_{gw} - 2 x_h^\top B_{gv}^\top P_g B_{gw} + w^\top B_{gw}^\top P_g B_{gw} \right) w \\ &\leq -\varepsilon V_g(x_g) + \left(2 x_g^\top A_g^\top P_g B_{gw} - 2 x_h^\top B_{gv}^\top P_g B_{gw} + w^\top B_{gw}^\top P_g B_{gw} \right) w. \end{aligned}$$

Moreover, note that

$$\begin{aligned} &\left(2 x_g^\top A_g^\top P_g B_{gw} - 2 x_h^\top B_{gv}^\top P_g B_{gw} + w^\top B_{gw}^\top P_g B_{gw} \right) w \\ &\leq 2 \lambda_{\max}(P_g) \|A_g\| \|B_{gw}\| \|x_g\| \|w\| + 2 \lambda_{\max}(P_g) \|B_{gv}\| \|B_{gw}\| \|x_h\| \|w\| \\ &+ \lambda_{\max}(P_g) \|B_{gw}\|^2 \|w\|^2 \leq \alpha_1 \|x_g\| \|w\| + \alpha_2 \|x_g\| \|w\| + \alpha_3 \|w\|^2 \\ &= \alpha_4 \|x_g\| \|w\| + \alpha_3 \|w\|^2, \end{aligned} \tag{5.35}$$

with $\alpha_1 = 2\lambda_{\max}(P_g)\|A_g\|\|B_{gw}\|$, $\alpha_2 = 2\lambda_{\max}(P_g) k_h \|B_{gv}\| \|B_{gw}\| \|C_g\|$, $\alpha_3 = \lambda_{\max}(P_g)\|B_{gw}\|^2$, $\alpha_4 = \alpha_1 + \alpha_2$, and where we have used the sector condition $\|x_h\| \leq k_h \|C_g\| \|x_g\|$. By using Young's inequality, we get

$$\Delta V_g \leq -\underbrace{\left(\varepsilon \lambda_{\min}(P_g) - \frac{\alpha_4}{2\delta_1} \right)}_{c_1} \|x_g\|^2 + \underbrace{\left(\frac{\alpha_4 \delta_1}{2} + \alpha_3 \right)}_{c_2} \|w\|^2. \tag{5.36}$$

Note that both c_1 and c_2 are positive, if δ_1 is taken sufficiently large.

Step 2: Consider the quadratic Lyapunov-like function $V_h(x_h) = x_h^2$, for the isolated DT HIGS element $\mathcal{H}_{DT}$. When $\mathcal{H}_{DT}$ operates in the integrator mode, i.e., according to (5.8a) or (5.11a), we have

$$\begin{aligned}
&\Delta V_{h,i} := V_h(x_h[k-1] + \omega_h T_s e[k]) - V_h(x_h[k-1]) \\
&= (x_h[k-1] + \omega_h T_s e[k])^2 - x_h^2[k-1] = 2\omega_h T_s e[k] x_h[k-1] \\
&+ (\omega_h T_s)^2 e^2[k] \\
&\leq \omega_h T_s x_h^2[k-1] + (\omega_h T_s + (\omega_h T_s)^2) e^2[k] = -c_3 x_h^2[k-1] \\
&+ (c_3 + \omega_h T_s) x_h^2[k-1] + (\omega_h T_s + (\omega_h T_s)^2) e^2[k]
\end{aligned} \tag{5.37}$$

for some $c_3 > 0$, and where we have made use of Young's inequality. Once again using the sector constraint of $\mathcal{H}_{DT}$, i.e., $\|x_h\| \leq k_h \|C_g\| \|x_g\|$ and applying Young's inequality for products, together with $e = C_g x_g$ yields

$$\begin{aligned}
&\Delta V_{h,i} \leq -c_3 x_h^2[k-1] + (c_3 k_h + \omega_h T_s k_h) \|C_g\|^2 \|x_g[k-1]\|^2 + \\
&\underbrace{(\omega_h T_s + (\omega_h T_s)^2)}_{\tilde{\alpha}} \|e[k]\|^2.
\end{aligned}$$

Note that by using $e = C_g x_g$, and $\|v\| = \|x_h\| \leq k_h \|C_g x_g\|$, and application of Young's inequality we get

$$\|e[k]\|^2 \leq (\tilde{\alpha}_1 + \tilde{\alpha}_2 (k_h \|C_g\|^2) \|x_g[k-1]\|^2 + \tilde{\alpha}_3 \|w[k-1]\|^2, \tag{5.38}$$

with $\tilde{\alpha}_1 = \|C_g A_g\|^2 + \|C_g A_g\| \|C_g B_{gv}\| + \|C_g A_g\| \|C_g B_{gw}\|$, $\tilde{\alpha}_2 = \|C_g A_g\| \|C_g B_{gv}\| + \|C_g B_{gv}\|^2 + \|C_g A_g\| \|C_g B_{gw}\|$, $\tilde{\alpha}_3 = \|C_g A_g\| \|C_g B_{gw}\| + \|C_g B_{gw}\|^2 + \|C_g A_g\| \|C_g B_{gv}\|$. Therefore, we have

$$\begin{aligned}
&\Delta V_{h,i}(x_h) \leq -c_3 \|x_h\|^2 + \underbrace{\left((c_3 k_h + \omega_h T_s k_h) \|C_g\|^2 + \tilde{\alpha}\tilde{\alpha}_1 + \tilde{\alpha}\tilde{\alpha}_2 k_h \|C_g\|^2\right)}_{\beta_1} \|x_g\|^2 + \\
&\underbrace{\tilde{\alpha}\tilde{\alpha}_3}_{\gamma_1} \|w\|^2,
\end{aligned}$$

where we have dropped time arguments for ease of notation.

When $\mathcal{H}_{DT}$ operates in the gain mode, i.e., either according to (5.8b) or (5.11b), we have

$$\begin{aligned}
&\Delta V_{h,g} := x_h^2[k] - x_h^2[k-1] = k_h^2 e^2[k] - x_h^2[k-1] \\
&\leq -x_h[k-1]^2 + k_h^2 \tilde{\alpha}_1 \|x_g[k-1]\|^2 + k_h^2 \tilde{\alpha}_2 k_h^2 \|C_g\|^2 \|x_g[k-1]\|^2 + k_h^2 \tilde{\alpha}_3 \|w\|^2
\end{aligned} \tag{5.39}$$

with $\tilde{\alpha}_i$, $i \in \{1,2,3\}$, as defined above. As such, we get

$$\begin{aligned}&\Delta V_{h,g} \leq \\ &-x_h^2 + \underbrace{\left(k_h^2\tilde{\alpha}_1 + k_h^4\tilde{\alpha}_2\|C_g\|^2\right)}_{\beta_2}\|x_g\|^2 + \underbrace{k_h^2\tilde{\alpha}_3}_{\gamma_2}\|w\|^2.\end{aligned} \tag{5.40}$$

Lastly, when $\mathcal{H}_{DT}$ is given by (5.11), and it operates in the zeroing mode (5.11c), we have

$$\Delta V_{h,z} := V(0) - V(x_h[k-1]) = -x_h^2[k-1]. \tag{5.41}$$

Hence, for both cases wherein $\mathcal{H}_{DT}$ is given by the bimodal (5.8) or the trimodal (5.11) setting, one has

$$\Delta V_h(x_h) \leq -\overline{\alpha}\|x_h\|^2 + \overline{\beta}\|x_g\|^2 + \overline{\gamma}\|w\|^2, \tag{5.42}$$

along all modes of operation, where $\overline{\alpha} = \min(1, c_3)$, $\overline{\beta} = \max(\beta_1, \beta_2)$, and $\overline{\gamma} = \max(\gamma_1, \gamma_2)$.

Step 3: Let us now consider the closed-loop system in Fig. 5.6. Consider the Lyapunov function

$$V(x_g, x_h) = V_g(x_g) + \mu V_h(x_h) = x^\top P x,$$

with $x = \begin{bmatrix} x_g^\top & x_h^\top \end{bmatrix}^\top$, $P = \begin{bmatrix} P_g & 0 \\ 0 & \mu \end{bmatrix}$, and some $\mu > 0$. Note that $P \succ 0$ due to P_g being positive define and $\mu > 0$. As a result of (5.36) and (5.42), for the closed-loop system (5.25) and (5.29), the one-step difference in the Lyapunov function $V(x_g, x_h)$, given by $\Delta V(x) := V(A_i x + B_i w) - V(x)$ with $i \in \{1,2\}$ for $\mathcal{H}_{DT}$ as in (5.8a) and $i \in \{1,2,3\}$ for $\mathcal{H}_{DT}$ as in (5.11a), satisfies

$$\begin{aligned}\Delta V(x) &= \Delta V_g + \mu \Delta V_h \\ &\leq -(c_1 - \mu\overline{\beta})\|x_g\|^2 - \mu\overline{\alpha}\|x_h\|^2 + (c_2 + \mu\overline{\gamma})\|w\|^2 \\ &\leq -\kappa_1\|x\|^2 + \kappa_2\|w\|^2,\end{aligned} \tag{5.43}$$

with $\kappa_1 := \min\left((c_1 - \mu\overline{\beta}), \mu\overline{\alpha}\right)$, $\kappa_2 := c_2 + \mu\overline{\gamma}$, and μ sufficiently small such that $c_1 - \mu\overline{\beta} > 0$. This shows that $V(x_g, x_h)$ is an ISS Lyapunov function for both (5.25) and (5.29), thereby concluding the proof. □

The conditions in Theorem 5.4.1 resemble the Tsypkin criterion [92], which is the DT analog of the CT circle criterion [88] for the study of DT absolute stability. However, while the Tsypkin criterion is concerned with static, memoryless nonlinearities, DT HIGS is a dynamical system, thereby requiring additional steps and arguments in the proof.

Theorem 5.4.1 can be verified using easy-to-measure frequency response functions (FRFs). In particular, condition i) can be checked using standard linear control arguments. For a given value of $k_h \in \mathbb{R}_{>0}$, checking condition ii), boils down to checking whether the Nyquist plot of $W(e^{j\omega})$ lies to the right of the vertical line passing through the point $\frac{-1}{k_h} + j0$ in the complex plane, for all $\omega \in [0, 2\pi]$.

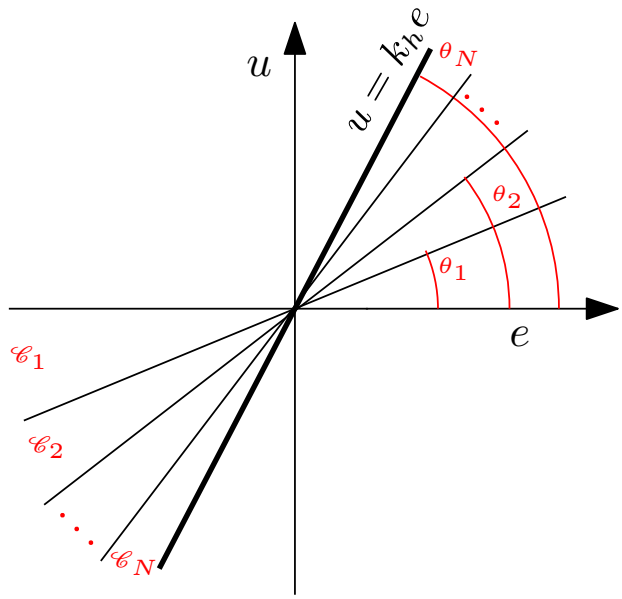

Figure 5.7. Partitioning of the input-output space of the DT HIGS element $\mathcal{H}_{DT}$.

5.4.3 Time-domain stability analysis

In this section we present LMI-based conditions that guarantee ISS of (5.25) and (5.29) using a multiple Lyapunov function approach [42]. In doing so, we exploit the fact that the input-output pairs of the proposed DT HIGS elements (5.8) and (5.11) belong to the set (5.5), for all $k \in \mathbb{N}$. In particular, in each case we partition the input-output space of the DT HIGS element $\mathcal{H}_{DT}$ and allow different Lyapunov functions to be active within each region of the partition. The partitioning employed in this work is similar to the one used in [2, 144, 155] for reset control systems and CT HIGS-controlled systems. More specifically, the input-output $e-u$ plane is partitioned into N sub-sectors $\mathscr{C}_i$, $i \in \{1, 2, \ldots, N\}$, by choosing $N+1$ equidistantly spaced angles $0 = \theta_0 < \theta_1 < \cdots < \theta_N = \arctan(k_h)$, as shown in Fig. 5.7. Loosely speaking, $\mathscr{C}_i$ is related to the sector $[\theta_{i-1}, \theta_i]$ in the $e-u$ plane. As shown in [2, 144, 155], for every pair (e, u) located in $\mathscr{C}_i$ one has

$$\underbrace{\begin{bmatrix} -\sin\theta_{i-1} & \cos\theta_{i-1} \\ \sin\theta_i & -\cos\theta_i \end{bmatrix}}_{E_i} \begin{bmatrix} e \\ u \end{bmatrix} \geq 0 \tag{5.44}$$

for all (e, u) in the first quadrant of the $e-u$ plane, and $E_i \begin{bmatrix} e \\ u \end{bmatrix} \leq 0$, for all (e, u) in the third quadrant of the $e-u$ plane. Moreover, note that the state of the closed-loop system in Fig. 5.6, can be mapped to the input-output pair of $\mathcal{H}_{DT}$ according to

$$\begin{bmatrix} e[k] \\ u[k] \end{bmatrix} = \underbrace{\begin{bmatrix} C_g & 0 \\ 0 & 1 \end{bmatrix}}_{\overline{C}} \begin{bmatrix} x_g[k] \\ x_h[k] \end{bmatrix}. \tag{5.45}$$

Therefore, $(e, u) \in \mathscr{C}_i$, $i \in \{1, 2, \ldots, N\}$, translates on the level of states to $x \in \mathcal{S}_i$, $i \in \{1, 2, \ldots, N\}$, with

$$\mathcal{S}_i = \{x \in \mathbb{R}^n \mid E_i \overline{C} x \geq 0 \vee E_i \overline{C} x \leq 0\} \tag{5.46}$$

with E_i and $\overline{C}$ defined as in (5.44) and (5.45), respectively.

Note that while a CT HIGS element (5.4) operates in the gain mode (5.4b) when $u = k_h e$ (see (5.7)) and thus, when x lies on the boundary of $\mathcal{S}_N$, it is possible for a DT HIGS to operate in all modes when $x \in \mathcal{S}_i$, for all $i \in \{1, ..., N\}$. However, after operation in the gain mode, the trajectories do lie on the boundary of $\mathcal{S}_N$. In addition, in case $\mathcal{H}_{DT}$ is given by (5.11), after operation in the zeroing mode, the trajectories lie on the boundary of $\mathcal{S}_1$. Moreover, another subtlety that arises in the DT setting is that due to the discrete-time nature of the dynamics, the solutions to the system can jump over sub-sectors, e.g., at $t = kT_s$ $x[k] \in \mathcal{S}_1$, and at $t = (k+1)T_s$, $x[k+1] \in \mathcal{S}_3$. Such a scenario is not encountered in CT due to the continuity of the solutions.

We are now ready to state the main results of this section.

Theorem 5.4.2. *Consider the system* (5.25). *Suppose there exist symmetric matrices* $W_i, U_{1,ij}, U_{2,i}, Y_{1,ij}, Y_{2,i} \in \mathbb{S}^{2\times 2}_{\geq 0}$ *and* $P_i \in \mathbb{S}^{n\times n}$ *, for* $i, j \in \{1, 2, \ldots, N\}$, *such that*

$$P_i - \overline{C}^\top E_i^\top W_i E_i \overline{C} \succ 0, \tag{5.47}$$

$$A_1^\top (P_j + \overline{C}^\top E_j^\top Y_{1,ij} E_j \overline{C}) A_1 - P_i + \overline{C}^\top E_i^\top U_{1,ij} E_i \overline{C} \prec 0, \tag{5.48}$$

$$A_2^\top (P_N + \overline{C}^\top E_N^\top Y_{2,i} E_N \overline{C}) A_2 - P_i + \overline{C}^\top E_i^\top U_{2,i} E_i \overline{C} \prec 0. \tag{5.49}$$

Then the closed-loop system (5.25) *is ISS.*

Proof. Due to (5.46) together with the non-negativity of the elements in W_i, (5.47) implies that $V(x) = x^\top P_i x > 0$, when $x \in \mathcal{S}_i$, $i \in \{1, 2, \ldots, N\}$ and $x \neq 0$, ensuring positive definiteness of V. Furthermore, in integrator-mode, one has

$$\begin{aligned} &\Delta V_1^{ij} := V(A_1 x + B_1 w) - V(x) = \\ &x^\top (A_1^\top P_j A_1 - P_i) x + 2 x^\top A_1^\top P_j B_1 w + w^\top B_1^\top P_j B_1 w, \end{aligned} \tag{5.50}$$

$i, j \in \{1, \ldots, N\}$, when $x \in \mathcal{S}_i$ and $A_1 x + B_1 w \in \mathcal{S}_j$. Note that when $x \in \mathcal{S}_i$ it holds that $x^\top \overline{C}^\top E_i^\top U_{1,ij} E_i \overline{C} x \geq 0$ for $U_{1,ij} \in \mathbb{S}^{2\times 2}_{\geq 0}$, and when $A_1 x + B_1 w \in \mathcal{S}_j$, it holds that

$$\begin{aligned} 0 \leq & (A_1 x + B_1 w)^\top \overline{C}^\top E_j^\top Y_{1,ij} E_j \overline{C} (A_1 x + B_1 w) = \\ & x^\top A_1^\top \overline{C}^\top E_j^\top Y_{1,ij} E_j \overline{C} A_1 x + 2 x^\top A_1^\top \overline{C}^\top E_j^\top Y_{1,ij} E_j \overline{C} B_1 w \\ & + w^\top B_1^\top \overline{C}^\top E_j^\top Y_{1,ij} E_j \overline{C} B_1 w, \end{aligned} \tag{5.51}$$

and thus

$$\begin{aligned} & - x^\top A_1^\top \overline{C}^\top E_j^\top Y_{1,ij} E_j \overline{C} A_1 x \leq 2 x^\top A_1^\top \overline{C}^\top E_j^\top Y_{1,ij} E_j \overline{C} B_1 w \\ & + w^\top B_1^\top \overline{C}^\top E_j^\top Y_{1,ij} E_j \overline{C} B_1 w \end{aligned} \tag{5.52}$$

for $Y_{1,ij} \in \mathbb{S}^{2\times 2}_{\geq 0}$. Due to (5.48), (5.50), (5.52) as well as non-negativity of the elements of $\tilde{Y}_{1,ij}$, and $U_{1,ij}$, by application of S-procedure relaxations [22], we obtain for $x \in \mathcal{S}_i$, $A_1 x + B_1 w \in \mathcal{S}_j$,

$$\begin{aligned} \Delta V_1^{ij} \leq & -\epsilon_1 \|x\|^2 \\ & + 2 x^\top (A_1^\top P_j B_1 + A_1^\top \overline{C}^\top E_j^\top Y_{1,ij} E_j \overline{C} B_1) w \\ & + w^\top (B_1^\top P_j B_1 + B_1^\top \overline{C}^\top E_j^\top Y_{1,ij} E_j \overline{C} B_1) w, \end{aligned} \tag{5.53}$$

for some $\epsilon_1 > 0$. Young's inequality for products yields now

$$\begin{aligned} \Delta V_1^{ij} \leq & (-\epsilon_1 + \frac{1}{\delta_1}) \|x\|^2 \\ & + (\delta_1 \|A_1^\top (P_j + \overline{C}^\top E_j^\top Y_{1,ij} E_j \overline{C}) B_1\|^2 \\ & + \|B_1^\top (P_j + \overline{C}^\top E_j^\top Y_{1,ij} E_j \overline{C}) B_1\|) \|w\|^2, \end{aligned} \tag{5.54}$$

with $\delta_1 > 0$, sufficiently large ($\delta_1 > \frac{1}{\epsilon_1}$, when $x \in \mathcal{S}_i$, and $A_1 x + B_1 w \in \mathcal{S}_j$, $i, j \in \{1, 2, \ldots, N\}$).

Next, note that after operating in gain mode, the state x lies within the last sub-sector $\mathcal{S}_N$, i.e., one always has $A_2 x + B_2 w \in \mathcal{S}_N$. Therefore, in the gain mode, one has for $x \in \mathcal{S}_i$

$$\begin{aligned} & \Delta V_2^{iN} := V(A_2 x + B_2 w) - V(x) = \\ & x^\top (A_2^\top P_N A_2 - P_i) x + 2 x^\top A_2^\top P_N B_2 w + w^\top B_2^\top P_N B_2 w, \end{aligned} \tag{5.55}$$

for $i \in \{1, \ldots, N\}$. As a result of (5.49), noting that $x \in \mathcal{S}_i$ implies $x^\top \overline{C}^\top E_i^\top U_{2,i} E_i \overline{C} x \geq 0$ for $U_{2,j} \in \mathbb{S}^{2\times 2}_{\geq 0}$, and $A_2 x + B_2 w \in \mathcal{S}_N$ implies $(A_2 x + B_2 w)^\top \overline{C}^\top E_N^\top Y_{2,i} E_N \overline{C} (A_2 x +$

$B_2w) \geq 0$, for $Y_{2,j} \in \mathbb{S}^{2\times 2}_{\geq 0}$, using similar arguments as in (5.51)- (5.53) and by application of S-procedure relaxations and Young's inequality for products we get

$$\begin{aligned}\Delta V_2^{iN} \leq & (-\epsilon_2 + \frac{1}{\delta_2})\|x\|^2 \\ & + (\delta_2 \|A_2^\top (P_N + \overline{C}^\top E_N^\top Y_{2,i} E_N \overline{C}) B_2\|^2 \\ & + \|B_2^\top (P_N + \overline{C}^\top E_N^\top Y_{2,i} E_N \overline{C}) B_2\|) \|w\|^2\end{aligned} \tag{5.56}$$

for some $\epsilon_2 > 0$ and $\delta_2 > \frac{1}{\epsilon_2}$.

Combining (5.54) and (5.56) yields

$$\Delta V := V(A_i x + B_i w) - V(x) \leq -\alpha \|x\|^2 + \sigma \|w\|^2, \tag{5.57}$$

for $i \in \{1, 2\}$ with $\alpha = \min_j(\epsilon_j - \frac{1}{\delta_j})$, $j \in \{1, 2\}$ and $\sigma = \max(\beta, \gamma)$, where

$$\begin{aligned}\beta = & \max_{(i,j)} \{ \delta_1 \|A_1^\top (P_j + \overline{C}^\top E_j^\top Y_{1,ij} E_j \overline{C}) B_1\|^2 \\ & + \|B_1^\top (P_j + \overline{C}^\top E_j^\top Y_{1,ij} E_j \overline{C}) B_1\| \}\end{aligned}$$

$$\begin{aligned}\gamma = & \max_i \{ \delta_2 \|A_2^\top (P_N + \overline{C}^\top E_N^\top Y_{2,i} E_N \overline{C}) B_2\|^2 \\ & + \|B_2^\top (P_N + \overline{C}^\top E_N^\top Y_{2,i} E_N \overline{C}) B_2\| \}\end{aligned}$$

with $i, j \in \{1, \ldots, N\}$. We thus conclude that V is an ISS Lyapunov function for (5.25), thereby completing the proof. □

Theorem 5.4.2 provides sufficient LMI conditions for certifying ISS of the closed-loop system in Fig. 5.6, when $\mathcal{H}_{DT}$ is given by the bimodal DT HIGS (5.8).

Next, we provide similar conditions for the case where $\mathcal{H}_{DT}$ is given by the trimodal DT HIGS (5.11).

Theorem 5.4.3. *Consider the system* (5.29). *Suppose there exist symmetric matrices* $W_i, U_{1,ij}, U_{2,i}, U_{3,i}, Y_{1,ij}, Y_{2,i}, Y_{3,i} \in \mathbb{S}^{2\times 2}_{\geq 0}$ *with non-negative elements, non-negative scalars* $\tau_{2i}, \tau_{3i} \in \mathbb{R}_{\geq 0}$, *and* $P_i \in \mathbb{S}^{n\times n}$, *for* $i, j \in \{1, 2, \ldots, N\}$, *such that*

$$P_i - \overline{C}^\top E_i^\top W_i E_i \overline{C} \succ 0, \tag{5.58}$$

$$A_1^\top (P_j + \overline{C}^\top E_j^\top Y_{1,ij} E_j \overline{C}) A_1 - P_i + \overline{C}^\top E_i^\top U_{1,ij} E_i \overline{C} \prec 0, \tag{5.59}$$

$$A_2^\top (P_N + \overline{C}^\top E_N^\top Y_{2,i} E_N \overline{C}) A_2 - P_i + \overline{C}^\top E_i^\top U_{2,i} E_i \overline{C} + \tau_{2i} Q \prec 0, \tag{5.60}$$

$$A_3^\top (P_1 + \overline{C}^\top E_1^\top Y_{3,i} E_1 \overline{C}) A_3 - P_i + \overline{C}^\top E_i^\top U_{3,i} E_i \overline{C} - \tau_{3i} Q \prec 0 \tag{5.61}$$

with $Q = \Xi + \Xi^\top$ *where* $\Xi = \begin{bmatrix} C_q^\top C_g A_g & \frac{-1}{2} C_g^\top C_g B_{gv} \\ (\frac{-1}{2} C_g^\top C_g B_{gv})^\top & 0 \end{bmatrix}$. *Then* (5.29) *is ISS.*

Proof. As in the case of Theorem 5.4.2, due to (5.46) and the non-negativity of the elements in W_i, $i \in \{1, \dots, N\}$, (5.58) implies that the Lyapunov function $V(x) = x^\top P_i x > 0$, when $x \in \mathcal{S}_i$, $i \in \{, \dots, N\}$, and $x \neq 0$, and is thus positive definite within the sector of $\mathcal{H}_{DT}$. Following similar arguments as in the proof of Theorem 5.4.2, we get

$$\begin{aligned}\Delta V_1^{ij} &:= V(A_1 x + B_1 w) - V(x) \\ &\leq (-\epsilon_1 + \frac{1}{\delta_1})\|x\|^2 + (\delta_1 \|A_1^\top (P_j + \overline{C}^\top E_j^\top Y_{1,ij} E_j \overline{C}) B_1\|^2 \\ &+ \|B_1^\top (P_j + \overline{C}^\top E_j^\top Y_{1,ij} E_j \overline{C}) B_1\|)\|w\|^2,\end{aligned} \tag{5.62}$$

with $\epsilon_1 > 0$ and $\delta_1 > \frac{1}{\epsilon_1}$ such that $\epsilon_1 - \frac{1}{\delta_1}$ is positive.

In the gain mode, we have for $x \in \mathcal{S}_i$,

$$\begin{aligned}&\Delta V_2^{iN} := V(A_2 x + B_2 w) - V(x) = \\ &x^\top (A_2^\top P_N A_2 - P_i) x + 2 x^\top A_2^\top P_N B_2 w + w^\top B_2^\top P_N B_2 w,\end{aligned} \tag{5.63}$$

for $i \in \{1, \dots, N\}$. Note that according to (5.12), the gain mode is followed when

$$\begin{aligned}e[k]e[k-1] = \frac{1}{2} x^\top [k-1] Q x[k-1] \\ + x^\top [k-1] \underbrace{\begin{bmatrix} I_{n_g} \\ 0 \end{bmatrix} C_g^\top B_{gw}}_{\overline{S}} w[k-1] \geq 0.\end{aligned} \tag{5.64}$$

Using (5.64), and following the same reasoning as in (5.51)-(5.53) in the proof of Theorem 5.4.2, we obtain

$$\begin{aligned}\Delta V_2^{iN} \leq &-(\epsilon_2 - \frac{1}{\delta_2})\|x\|^2 \\ &+ (\delta_2 \|A_2^\top \left(P_N + \overline{C}^\top E_N Y_{2,i} E_N \overline{C}\right) B_2 + \tau_{2,i} \overline{S}\|^2 \\ &+ \|B_2^\top P_N B_2 + B_2^\top E_N^\top Y_{2,i} E_N \overline{C} B_2\|)\|w\|^2\end{aligned} \tag{5.65}$$

for some $\epsilon_2 > 0$ and $\delta_2 > \frac{1}{\epsilon_2}$ such that $\epsilon_2 - \frac{1}{\delta_2} > 0$.

In the zeroing mode, we have for $x \in \mathcal{S}_i$,

$$\begin{aligned}&\Delta V_3^{i1} := V(A_3 x + B_3 w) - V(x) = \\ &x^\top (A_3^\top P_1 A_3 - P_i) x + 2 x^\top A_3^\top P_1 B_3 w + w^\top B_3^\top P_1 B_3 w,\end{aligned} \tag{5.66}$$

for $i \in \{1, \dots, N\}$. According to (5.13), the zeroing mode is followed when

$$\begin{aligned}e[k]e[k-1] = \frac{1}{2} x^\top [k-1] Q x[k-1] \\ + x^\top [k-1] \underbrace{\begin{bmatrix} I_{n_g} \\ 0 \end{bmatrix} C_g^\top B_{gw}}_{\overline{S}} w[k-1] < 0.\end{aligned} \tag{5.67}$$

Using the same reasoning as in (5.65) we get (also noting that after operation in the zeroing mode $A_3x + B_3w \in \mathcal{S}_1$),

$$\begin{aligned}\Delta V_3^{i1} \leq & -(\epsilon_3 - \frac{1}{\delta_3})\|x\|^2 \\ & + (\delta_3 \|A_3^\top \left(P_1 + \overline{C}^\top E_1 Y_{3,i} E_1 \overline{C} - \tau_{3,i}\overline{S}\right) B_3 - \tau_{3,i}\overline{S}\|^2 \\ & + \|B_3^\top P_1 B_3 + B_3^\top E_1^\top Y_{3,i} E_N \overline{C} B_3\|)\|w\|^2,\end{aligned} \tag{5.68}$$

for some $\epsilon_3 > 0$ and $\delta_3 > \frac{1}{\epsilon_3}$ such that $\epsilon_3 - \frac{1}{\delta_3} > 0$.

Combining (5.62) and (5.65) and (5.68) yields

$$\Delta V := V(A_i x + B_i w) - V(x) \leq -\alpha\|x\|^2 + \sigma\|w\|^2, \tag{5.69}$$

for $i \in \{1, 2, 3\}$, $\alpha = \min_j(\epsilon_j - \frac{1}{\delta_j})$, $j \in \{1, 2, 3\}$, and $\sigma = \max(\beta, \gamma, \zeta)$ with

$$\begin{aligned}\beta =& \max_{(i,j)}\{\delta_1 \|A_1^\top (P_j + \overline{C}^\top E_j^\top Y_{1,ij} E_j \overline{C}) B_1\|^2 \\ & + \|B_1^\top (P_j + \overline{C}^\top E_j^\top Y_{1,ij} E_j \overline{C}) B_1\|\}\end{aligned}$$

$$\begin{aligned}\gamma =& \max_i\{\delta_2 \|A_2^\top (P_N + \overline{C}^\top E_N^\top Y_{2,i} E_N \overline{C}) B_2 + \tau_{2,i}\overline{S}\|^2 \\ & + \|B_2^\top (P_N + \overline{C}^\top E_N^\top Y_{2,i} E_N \overline{C}) B_2\|\},\end{aligned}$$

$$\begin{aligned}\zeta =& \max_i\{\delta_3 \|A_3^\top (P_1 + \overline{C}^\top E_1^\top Y_{2,1} E_1 \overline{C}) B_3 - \tau_{3,i}\overline{S}\|^2 \\ & + \|B_3^\top (P_1 + \overline{C}^\top E_1^\top Y_{3,i} E_1 \overline{C}) B_3\|\},\end{aligned}$$

where $i, j \in \{1, \ldots, N\}$. We thus conclude that V is an ISS Lyapunov function for (5.29), thereby completing the proof. □

5.4.4 The link between the two criteria

Considering the closed-loop system in Fig.5.6, we have thus far presented two sets of stability results for both (5.25) and (5.29). In particular, Theorem 5.4.1 presents frequency-domain conditions for certifying ISS (for both (5.25) and (5.29)), while Theorem 5.4.2 and Theorem 5.4.3, provide LMI-based conditions for certifying ISS of (5.25) (consisting of bimodal DT HIGS) and (5.29) (consisting of trimodal DT HIGS), respectively.

The strength of Theorem 5.4.1 lies in the fact that it can be verified based on graphical evaluations of FRF measurements. However, this theorem only makes use of sector boundedness of the input-output pair of the HIGS element $\mathcal{H}_{DT}$ and does not exploit specific knowledge related to the internal dynamics of the HIGS element, making it possibly conservative. Moreover, Theorem 5.4.1 concludes stability of the closed-loop system on the basis of the existence of a common quadratic

Lyapunov function (see Step 3 in the proof of Theorem 5.4.1). Theorems 5.4.2 and 5.4.3 on the other hand make extensive use of specific knowledge related to the internal HIGS dynamics and conclude stability on the basis of the existence of multiple Lyapunov functions. Consequently, Theorems 5.4.2 and 5.4.3 are expected to produce less conservative results when compared to Theorem 5.4.1. The downside of the LMI-based stability conditions with respect to the frequency-domain condition is that they rely on parametric models of the underlying system which are not always easy to obtain. Additionally, in case the LMIs are infeasible, it is not clear how the controller parameters should be tuned to render the LMIs feasible.

We now state results relating the satisfaction of the frequency-domain conditions in Theorem 5.4.1 to the feasibility of the LMIs in Theorems 5.4.2 and 5.4.3. In particular, we prove that satisfaction of the frequency-domain conditions implies feasibility of a special case of the LMIs. Therefore, the frequency-domain conditions are guaranteed to be more conservative.

Theorem 5.4.4. *Under minimality of (A_g, B_{gv}, C_g), satisfaction of the conditions in Theorem 5.4.1 implies feasibility of the LMIs in Theorem 5.4.2 with $N \in \mathbb{N}_{\geq 1}$, $W_i = Y_{1,ij} = Y_{2,i} = 0_{2\times 2}$, $U_{1,ij} = U_{2,i} = U = \frac{1}{\alpha}\begin{bmatrix} 0 & 1 \\ 1 & 0 \end{bmatrix}$, and $P_i = \begin{bmatrix} P_g & 0 \\ 0 & \mu \end{bmatrix}$, where $P_g \in \mathbb{S}^{n_g \times n_g}$ is a positive-definite matrix and $\mu \in \mathbb{R}_{>0}$, $\alpha = \sin(\arctan(k_h))$.*

Proof. As shown in Step 3 of the proof of Theorem 5.4.1, this theorem concludes ISS of the closed-loop system on the basis of the existence of a Lyapunov function of the form $V(x) = x^\top P x$ with

$$P = \begin{bmatrix} P_g & 0 \\ 0 & \mu \end{bmatrix}, \tag{5.70}$$

wherein $\mu > 0$ and $P_g \in \mathbb{S}^{n_g \times n_g}$ is a positive definite matrix. Therefore, $P_i = P$ is also positive definite and thus satisfies (5.47) with $W_i = 0$.

Let us now turn our attention to (5.48). Note that with $P_1 = P$ as defined above and A_1 as defined in (5.26), we have

$$A_1^\top P_1 A_1 - P_1 = \mathcal{I}_1 + \mu Q_1, \tag{5.71}$$

with

$$\mathcal{I}_1 = \begin{bmatrix} A_g^\top P_g A_g - P_g & -A_g^\top P_g B_{gv} \\ -B_{gv}^\top P_g A_g & B_{gv}^\top P_g B_{gv} \end{bmatrix},$$

$$Q_1 = \begin{bmatrix} (\omega_h T_s)^2 A_g^\top C_g^\top C_g A_g & \omega_h T_s A_g^\top C_g^\top (1 - \omega_h T_s C_g B_{gv}) \\ \omega_h T_s (1 - \omega_h T_s B_{gv}^\top C_g^\top) C_g A_g & (1 - \omega_h T_s C_g B_{gv})(1 - \omega_h T_s B_{gv} C_g)^\top - 1 \end{bmatrix}.$$

Also note that with $N = 1$ and the choice of U as specified above we have

$$\overline{C}^\top E_1^\top U E_1 \overline{C} = \begin{bmatrix} 0 & C_g^\top \\ C_g & \frac{-2}{k_h} \end{bmatrix}.$$

By application of the DT KYP lemma (see (5.32)), we have

$$\mathcal{I}_1 = \begin{bmatrix} -L^\top L - \varepsilon P_g & \sqrt{\frac{2}{k_h} - B_{gv}^\top P_g B_{gv}} L^\top - C_g^\top \\ \sqrt{\frac{2}{k_h} - B_{gv}^\top P_g B_{gv}} L - C_g & B_{gv} P_g B_{gv} \end{bmatrix} \tag{5.72}$$

for some matrix L and a positive constant ε. Therefore, under the conditions stated in the theorem, (5.48) is given by

$$\begin{aligned} &\mathcal{I}_1 + \mu Q_1 + \overline{C}^\top E_1^\top U E_1 \overline{C} \\ &= \underbrace{\begin{bmatrix} -L^\top L - \varepsilon P_g & \sqrt{\frac{2}{k_h} - B_{gv}^\top P_g B_{gv}} L^\top \\ \sqrt{\frac{2}{k_h} - B_{gv}^\top P_g B_{gv}} L & B_{gv} P_g B_{gv} - \frac{2}{k_h} \end{bmatrix}}_{\overline{\mathcal{I}}} + \mu Q_1. \end{aligned} \tag{5.73}$$

By Schur's lemma, the matrix $\overline{\mathcal{I}}$, is negative definite if and only if

$$-L^\top L - \varepsilon P_g + \frac{\left(\frac{2}{k_h} - B_{gv}^\top P_g B_{gv}\right) L^\top L}{\left(-B_{gv}^\top P_g B_{gv} + \frac{2}{k_h}\right)} = -\varepsilon P_g \prec 0$$

and $-L^\top L - \varepsilon P_g \prec 0$, which indeed holds given that P_g is positive definite, and $\varepsilon > 0$. Consequently, (5.73) is negative definite for $\mu = m_1 > 0$ sufficiently small. Similar reasoning can be used to rewrite (5.49) as

$$\overline{\mathcal{I}} + \mu \tilde{Q} \tag{5.74}$$

with

$$\tilde{Q} = \begin{bmatrix} k_h^2 C_g^\top C_g & -k_h^2 C_g^\top C_g B_{gv} \\ -k_h^2 B_{gv}^\top C_g^\top C_g & k_h^2 B_{gv}^\top C_g^\top C_g B_{gv} \end{bmatrix}.$$

Once again, (5.74) is negative definite for $\mu = m_2 > 0$, sufficiently small. Therefore, under the conditions stated in the theorem, the LMIs (5.47)- (5.49) are satisfied with $\mu = \min(m_1, m_2)$, thereby concluding the proof for $N = 1$. Let us now note that for $N > 1$, choosing $P_i = P$, would to lead the satisfaction of the LMIs. This completes the proof. □

Next, we state a similar result, linking Theorems 5.4.1 and 5.4.3.

Theorem 5.4.5. *Under minimality of (A_g, B_{gv}, C_g), satisfaction of the conditions in Theorem 5.4.1 implies feasibility of the LMIs in Theorem 5.4.2 with $N \in \mathbb{N}_{\geq 1}$, $W_i = Y_{1,ij} = Y_{2,i} = Y_{3,i} = 0_{2\times 2}$, $U_{1,ij} = U_{2,i} = U_{3,i} = U = \frac{1}{\alpha}\begin{bmatrix} 0 & 1 \\ 1 & 0 \end{bmatrix}$, and $P_i = \begin{bmatrix} P_g & 0 \\ 0 & \mu \end{bmatrix}$, $\tau_{2i} = \tau_{3i} = 0$ where $P_g \in \mathbb{S}^{n_g \times n_g}$ is a positive-definite matrix and $\mu \in \mathbb{R}_{>0}$, $\alpha = \sin(\arctan(k_h))$.*

Proof. Satisfaction of the LMIs (5.58), (5.59), and (5.60) follows from the exact same arguments as in the proof of Theorem 5.4.4. For the satisfaction of (5.61), we note that under the conditions stated in the theorem, for $N = 1$, (5.61) can be written as

$$\overline{\mathcal{I}} + \mu \overline{Q}, \tag{5.75}$$

with $\overline{\mathcal{I}}$ as defined in (5.73) and

$$\overline{Q} = \begin{bmatrix} 0 & 0 \\ 0 & -1 \end{bmatrix}.$$

Following the same reasoning as in the proof of Theorem 5.4.4, we conclude that all the LMIs in Theorem 5.4.3 are satisfied for μ sufficiently small, thereby concluding the proof. □

With Theorem 5.4.4 and Theorem 5.4.5, we have shown that satisfaction of the conditions in Theorem 5.4.1 implies feasibility of a specific case of the LMIs. Consequently, the frequency-domain conditions in Theorem 5.4.1 are guaranteed to yield more conservative results when compared to the LMIs in Theorems 5.4.2 and 5.4.3.

5.5 Sampled-data ISS Guarantees

In the previous section, stability criteria were presented that can be used to guarantee ISS for closed-loop HIGS-controlled systems in DT (ignoring inter-sample behavior). In this section we show that DT ISS, implies ISS of sampled-data HIGS-controlled systems, thus also taking into account the inter-sample behavior, building on ideas in [130].

Consider the interconnection in Fig. 5.8 consisting of a CT linear plant $\mathscr{P}$, and a general DT nonlinear controller ϕ (e.g., a HIGS-based controller), interconnected via a sampler and a zero-order hold device. Here, the plant is given by

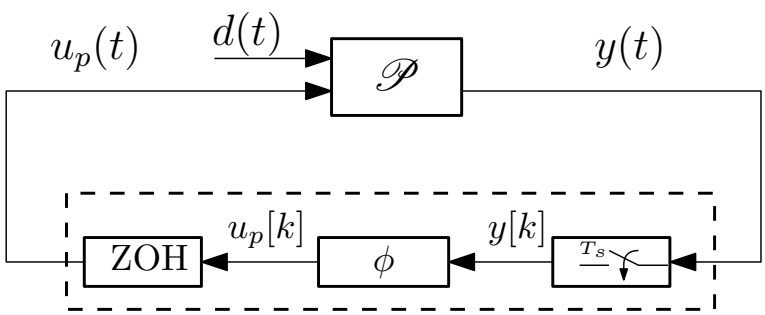

Figure 5.8. CT plant $\mathscr{P}$ and sampled-data nonlinear controller.

$$\mathscr{P}: \begin{cases} \dot{x}_p(t) = \mathcal{A}_p x_p(t) + \mathcal{B}_{pu} u_p(t) + \mathcal{B}_{pd} d(t), \\ y(t) = \mathcal{C}_p x_p(t) \end{cases} \tag{5.76}$$

with $\mathcal{A}_p$, $\mathcal{B}_{pu}$, $\mathcal{B}_{pd}$, $\mathcal{C}_p$ real matrices of appropriate dimensions, $x_p(t) \in \mathbb{R}^{n_p}$ the state of the plant, $u_p(t) \in \mathbb{R}^{n_u}$ and $d(t) \in \mathbb{R}^{n_d}$ the control input and the input disturbances, respectively, and $y(t) \in \mathbb{R}^{n_y}$ the plant output, at time $t \in \mathbb{R}_{\geq 0}$. The nonlinear controller ϕ is of the general form

$$\phi: \begin{cases} x_\phi[k] = f(y[k], y[k-1], x_\phi[k-1]), \\ u_p[k] = h(x_\phi[k]) \end{cases} \tag{5.77}$$

with $f: \mathbb{R}^{n_y} \times \mathbb{R}^{n_y} \times \mathbb{R}^{n_\phi} \to \mathbb{R}^{n_\phi}$, $h: \mathbb{R}^{n_\phi} \to \mathbb{R}^{n_y}$, and $x_\phi[k] \in \mathbb{R}^{n_\phi}$, $u_p[k] \in \mathbb{R}^{n_u}$, $y[k] \in \mathbb{R}^{n_y}$ denoting its state, output and input, respectively, at discrete time $k \in \mathbb{N}$, corresponding to time instants $t = kT_s$ with T_s the sampling period, as before. For the interconnection in Fig.5.8, we choose the state $x_{sd}(t) = [x_p^\top(t) \;\; x_\phi^\top(t)]^\top \in \mathbb{R}^n$. Note that $\dot{x}_\phi(t) = 0$, for $t \in [kT_s, (k+1)T_s)$. In this section we investigate ISS of the closed-loop system in Fig.5.8, as defined in Definition 5.5.1 below.

Definition 5.5.1. *[106] The interconnection in Fig.5.8 is said to be input-to-state stable if there exists $\beta \in \mathcal{KL}$ and $\gamma \in \mathcal{K}$, such that for all $x_{sd}(t_0) \in \mathbb{R}^n$ and $\|d\|_\infty \leq \infty$,*

$$\|x_{sd}(t)\| \leq \beta(\|x_{sd}(t_0)\|, t - t_0) + \gamma(\|d\|_\infty), \quad \forall t \geq t_0. \tag{5.78}$$

Note that the class of systems described by (5.77) includes as a particular case, HIGS-based controllers as shown in Fig. 5.9, consisting of a DT HIGS element and DT LTI controllers $\mathcal{C}_i$, $i \in \{1, 2, 3\}$.

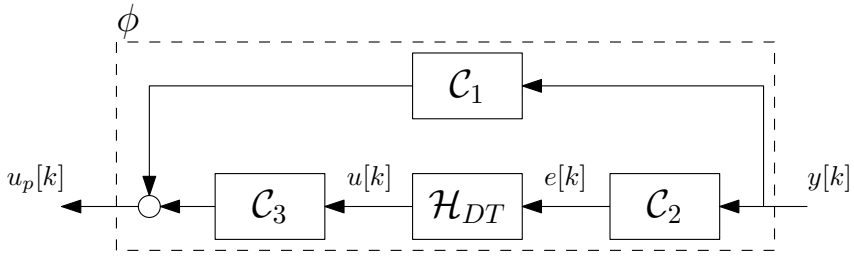

Figure 5.9. The controller ϕ in the case of HIGS-based control.

Analysis of the system in Fig. 5.8 by following the DTD approach, requires a DT model of the plant $\mathscr{P}$ (5.76), which can be obtained via exact ZOH discretization of (5.76), leading to

$$\overline{\mathscr{P}}: \begin{cases} x_p[k] &= A_p x_p[k-1] + B_p u_p[k-1] + w[k-1], \\ y[k] &= C_p x_p[k] \end{cases} \tag{5.79}$$

with $A_p := e^{\mathcal{A}_p T_s}$, $B_p := \int_0^{T_s} e^{\mathcal{A}_p \tau} d\tau \mathcal{B}_{pu}$, $w[k-1] := \int_{(k-1)T_s}^{kT_s} e^{\mathcal{A}_p(kT_s-\tau)} \mathcal{B}_{pd} d(\tau) d\tau$, $C_p := \mathcal{C}_p$. Considering (5.79), we obtain the exact DT model

$$\begin{aligned} x_{sd}[k] &= \begin{bmatrix} A_p x_p[k-1] + B_p h(x_\phi[k-1]) + w[k-1] \\ f(C_p x_p[k], C_p x_p[k-1], x_\phi[k-1]) \end{bmatrix}, \\ y[k] &= \begin{bmatrix} C_p & 0 \end{bmatrix} x_{sd}[k] \end{aligned} \tag{5.80}$$

with $x_{sd}[k] = \begin{bmatrix} x_p^\top[k] & x_\phi^\top[k] \end{bmatrix}^\top$ for the system in Fig. 5.8.

Using this exact model, we can formulate a corollary of Theorem 6 in [106], which can be used for concluding (CT) ISS of the sampled-data system under consideration, based on DT ISS of (5.80).

Corollary 5.5.1. *Suppose the DT system* (5.80) *is ISS with respect to the DT disturbance w. Then, the sampled-data system in Fig. 5.8, is ISS with respect to the CT disturbance d, in the sense of Definition 5.5.1.*

Proof. Note that in between sampling instances, the system dynamics are linear since $\dot{x}_\phi(t) = \dot{u}_p(t) = 0$ for $t = (k-1)T_s + \lambda T_s$, $0 < \lambda < 1$ (due to ZOH), and thus the inter-sample behavior of states $x_{sd}(t) = [x_p^\top(t) \; x_\phi^\top(t)]^\top$ can be readily computed and shown to satisfy the boundedness property

$$\|x_{sd}(t)\| \leq \gamma_1(\|x_{sd}((k-1)T_s)\|) + \gamma_2(\|d\|_\infty) \tag{5.81}$$

for all $t \in [(k-1)T_s \;\; T_s]$, $k \in \mathbb{N}\backslash\{0\}$ and $\gamma_1, \gamma_2 \in \mathcal{K}_\infty$. Moreover, note that for $(k-1)T_s \leq t \leq kT_s$, $\|w[k-1]\|_\infty \leq c\|d\|_\infty$, with $c = \int_{(k-1)T_s}^{kT_s} \|e^{\mathcal{A}_p(kT_s-\tau)} \mathcal{B}_{pd}\|_\infty d\tau = \int_0^{T_s} \|e^{\mathcal{A}_p(T_s)} \mathcal{B}_{pd}\|_\infty d\tau$. Thus ISS of the DT system (5.80) with respect to w, implies its ISS with respect to the CT disturbance d. It follows now from Theorem 6 of [106], that the boundedness property (5.81), and ISS of (5.80) with respect to the DT disturbance w, implies ISS of the sampled-data system in Fig. 5.8 with respect to the CT disturbance d. □

For the case where ϕ is a HIGS-based controller as in Fig. 5.9, (5.80) is given by (5.25) or (5.29). Thus, as a result of Corollary 5.5.1, one may conclude ISS of the resulting sampled-data HIGS-controlled system using Theorem 5.4.1 and Theorem 5.4.2 or Theorem 5.4.3.

Remark 5.5.1. *For a stabilizing controller of* (5.76) *to exist, stabilizability of $(\mathcal{A}_p, \mathcal{B}_{pu})$ as well as detectability of $(\mathcal{A}_p, \mathcal{C}_p)$ are required [77]. Moreover, as shown in [30, 99], in order to avoid the loss of these properties as a result of sampling, and thus for the existence of a DT stabilizing controller of* (5.76)*, the sampling period T_s should be non-pathological (see [30, 99] for a detailed explanation on this topic) with respect to $\mathcal{A}_p$. In particular, let the i^{th} eigenvalue $\lambda_i(\mathcal{A}_p)$ of $\mathcal{A}_p$, be given by*

$$\lambda_i(\mathcal{A}_p) = \sigma_i + j\omega_i.$$

The sampling period T_s is called non-pathological with respect to $\mathcal{A}_p$ if there exist no eigenvalues $\lambda_i(\mathcal{A}_p)$, $\lambda_j(\mathcal{A}_p)$, $i \neq j$, such that $\sigma_i = \sigma_j$ and $\omega_i = \omega_j + l\frac{2\pi}{T_s}$, for some $l \in \mathbb{Z} \setminus \{0\}$.

As such, these conditions are necessary for the satisfaction of the stability criteria in Section 5.4. Lastly, remark that as shown in [108], in high precision motion control applications (forming one of the main areas of application for HIGS-based control), the sampling is non-pathological for all $T_s \in \mathbb{R}_{>0}$.

Remark 5.5.2. *The work presented so far in this chapter provides the tooling to certify ISS of SD HIGS-controlled systems via the DTD approach. Let us shortly elaborate on concluding stability of SD HIGS controlled systems via the CTD approach, based on our results here. Theorem 6.1 of [38], provides frequency-domain conditions that resemble the conditions in Theorem 5.4.1, but for CT HIGS-controlled systems. In particular, given a CT HIGS-controlled system as in Fig. 5.10, with $\mathscr{G}$, the linear part of the loop, satisfying assumptions typically made in HIGS-based control (see Assumption 2.5.1 in Chapter 2), and $\mathscr{H}$ a CT HIGS element as in (5.4), verifying whether the conditions in Theorem 6.1 in [38] are satisfied amounts to checking the stability of the linear system $\mathscr{G}$ and whether the transfer function $\mathscr{G}_{ev}(j\omega)$ from the control input v to the output e, lies on the right side of the vertical line intersecting the real axis at the point $\frac{-1}{k_h}$ for all $\omega \in \mathbb{R}$. Note that these conditions are only related to the linear part of the loop $\mathscr{G}$ and are*

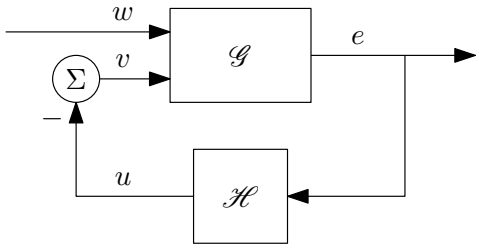

Figure 5.10. CT closed-loop HIGS-controlled system.

in fact similar conditions as in Theorem 5.4.1, the only difference being that while in Theorem 5.4.1 the DT transfer function $W(z)$ is considered, the result in [38] is concerned with the CT transfer function $\mathscr{G}_{ev}(s)$.

Let us now consider the interconnection in Fig. 5.11, wherein the input to v is generated by a zero-order-hold device and the output e is sampled by a sampler. As shown in Chapter 3 of [30], the relation between the DT transfer function W from $\overline{v}$ to $\overline{e}$, and the CT transfer function $\mathscr{G}_{ev}$ from v to e, is given by (see [30] Chapter 3 for the derivations)

$$W(e^{j\omega T_s}) = \sum_{k=-\infty}^{\infty} \mathscr{G}_{ev}(j\omega + k\omega_s) r(j\omega + k\omega_s), \tag{5.82}$$

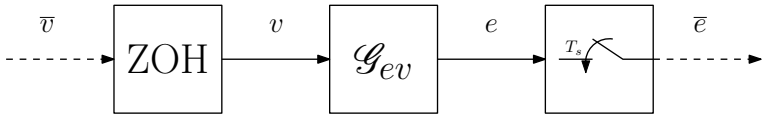

Figure 5.11. Discretization of $\mathscr{G}_{ev}$ using zero-order-hold.

with $\omega_s = \frac{2\pi}{T_s}$, *and*

$$r(j\omega) = e^{-j\omega\frac{T_s}{2}} \frac{\sin(\omega\frac{T_s}{2})}{\omega\frac{T_s}{2}}.$$

Note that if $\mathscr{G}_{ev}(j\omega)$ *is band limited to frequencies below the Nyquist frequency* $\omega_N = \frac{\pi}{T_s}$, *based on* (5.82) *we have*

$$W(e^{j\omega T_s}) = \mathscr{G}_{ev}(j\omega)r(j\omega), \quad \omega_N < \omega < \omega_N. \tag{5.83}$$

Let us now make the observation that

$$\lim_{T_s \to 0} r(j\omega) = 1, \tag{5.84}$$

and thus, for $T_s \to 0$, $W(e^{j\omega T_s}) \approx \mathscr{G}_{ev}(j\omega)$. *Therefore, provided that* $\mathscr{G}_{ev}(j\omega)$ *is band limited to* $-\omega_N < \omega < \omega_N$, *satisfaction of the conditions in Theorem 6.1 of [38], implies satisfaction of the conditions in Theorem 5.4.1 for* $T_s \to 0$, *which in turn through Corollary 5.5.1 certifies ISS of SD HIGS-controlled systems.*

5.6 Numerical Example

In this section, we present an illustrative example whereby the different stability criteria presented in Section 5.4 are compared with each other.

Consider the interconnection in Fig. 5.8, where $\mathscr{P}$ is a mass-spring-damper system with transfer function

$$\mathscr{P}(s) = \frac{1}{ms^2 + bs + k}, \tag{5.85}$$

and mass $m = 1$ kg, damping coefficient $b = 0.0564$ Ns/m and stiffness coefficient $k = 1$ N/m. Moreover, the controller ϕ is as depicted in Fig. 5.9, with $\mathcal{C}_1(z) = 0$, $\mathcal{C}_2(z) = 1$ and $\mathcal{C}_3(z) = C(z)$ a linear lead filter, obtained by discretization of $C(s) = 1.4\frac{s+5}{s+6.95}$, using zero-pole matching. Let us first consider a sampling time of $T_s = 0.001s$ (also used for the discretization of $C(s)$). To evaluate ISS of the DT closed-loop system using Theorem 5.4.1, note that the poles of the linear part of the system $P_{\text{lin}}(z) = P(z)C(z)$, with $P(z)$ the ZOH discretization of (5.85), are within the unit circle and thus condition i) in Theorem 5.4.1 is satisfied. Checking

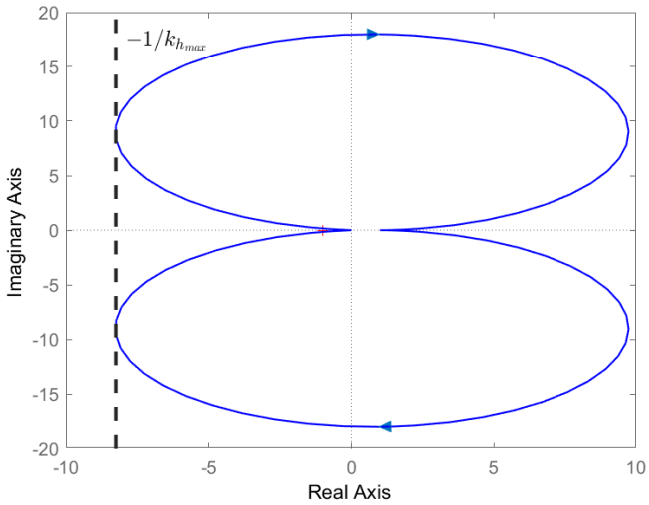

Figure 5.12. Nyquist diagram of $P(z)C(z)$.

condition ii) in Theorem 5.4.1, amounts to inspecting the Nyquist diagram of $P_{\text{lin}}(e^{j\omega})$ as shown in Fig. 5.12, from which it follows that the closed-loop system is guaranteed to be ISS for any $\omega_h \in (0, \infty)$ and $k_h \leq 0.12$, by Theorem 5.4.1. Indeed, 0.12 is the maximal k_h value for which the Nyquist diagram in Fig. 5.12 falls to the right side of the vertical line passing through $\frac{-1}{k_h} + j0$, in the complex plane, and thus satisfies condition ii) in Theorem 5.4.1.

In addition, the results obtained from Theorem 5.4.2 using LMI-based ISS guarantees for the case where $\mathcal{H}_{DT}$ is given by (5.48), are portrayed in Fig. 5.13a as a function of the number N of partitions, $N \in \{1, 2, 4\}$. Note that Fig. 5.13a also shows the range of parameters for which the system is estimated to be ISS based on extensive time-series simulations. As it can be seen in Fig. 5.13a, by using Theorem 5.4.2, one concludes stability of (5.25) for a range of (k_h, ω_h) well beyond the values found by application of the frequency-domain conditions in Theorem 5.4.1. This is indeed expected as a result of Theorem 5.4.4 and the discussions in Section 5.4.4.

To illustrate the effect of the sampling period, Fig. 5.13b portrays the analysis results obtained with a sampling time of $T_s = 0.1s$. Note that for $T_s = 0.1s$, the simulation-based estimated ISS region (the grey area) is smaller than for $T_s = 0.001s$. This indicates the general need for the analysis tools presented in this chapter as pure CT analysis (see for example [38]) completely ignores the role of sampling, which in turn could cause wrong conclusions regarding stability. Let us also make the observation that even with a single quadratic Lyapunov function,

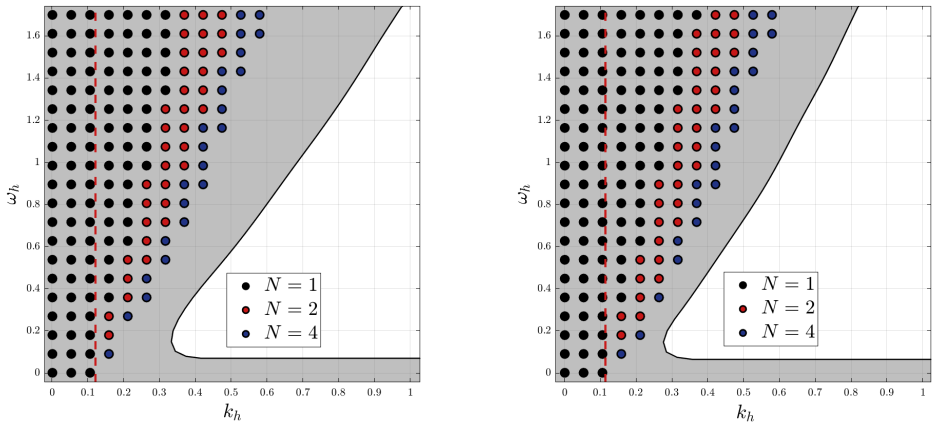

Figure 5.13. ISS region found by time-series simulations ■, ISS (k_h, ω_h) values returned by Theorem 5.4.2 (as a function of the number of partitions N), the k_h value obtained from Theorem 5.4.1 ▬, for a sampling time of (a) $T_s = 0.001s$, and (b) $T_s = 0.1s$.

i.e., for $N = 1$, Theorem 5.4.2 provides a feasible range of (k_h, ω_h) values extending well beyond those obtained by Theorem 5.4.1, which indicates the strength of the relaxation terms introduced in Theorem 5.4.2.

The results obtained from application of Theorem 5.4.3 for the case where $\mathcal{H}_{DT}$ is given by (5.11) are presented in Fig. 5.14. Similar observations as in the case of Fig. 5.13 can be made. Namely, the results obtained from the LMIs are less conservative (even with $N = 1$) compared to the frequency domain conditions, as expected due to Theorem 5.4.5. Moreover, the stability region is smaller for the case with slower sampling, thereby indicating the need for the tooling presented in this chapter.

Lastly note that by virtue of Theorem 5.5.1, the results presented regarding stability of the closed-loop system in DT, are also valid for the SD system consisting of the CT plant (5.85) and the DT HIGS-based controllers.

5.7 Summary and Conclusions

In this chapter, we have proposed two DT versions of HIGS, which preserve the main characteristics of CT HIGS, namely predominant operation in the integrator-mode while guaranteeing sign equivalence (sector boundedness) of its input-output pair. For the DT HIGS elements we have presented novel stability criteria that

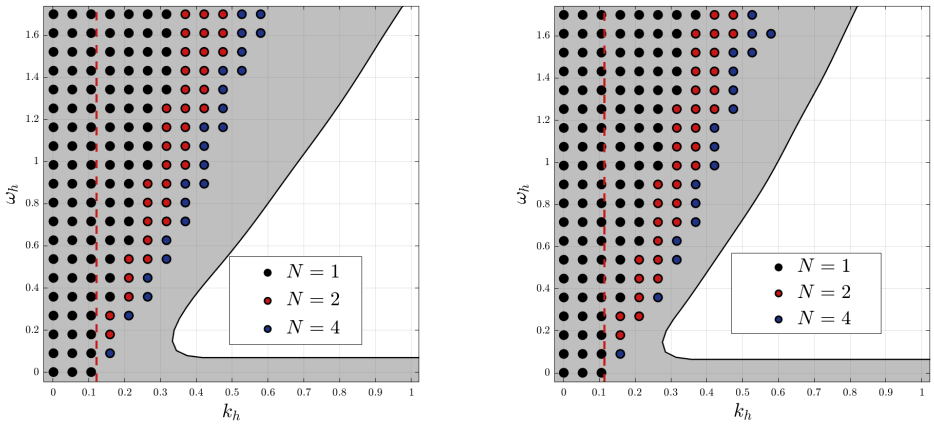

Figure 5.14. ISS region found by time-series simulations ■, ISS (k_h, ω_h) values returned by Theorem 5.4.3 (as a function of the number of partitions N), the k_h value obtained from Theorem 5.4.1 ▬, for a sampling time of (a) $T_s = 0.001s$, and (b) $T_s = 0.1s$.

can be used to conclude ISS using (i) (measured) frequency response conditions and (ii) LMI-based conditions. We have also shown that satisfaction of these stability criteria imply ISS of sampled-data systems consisting of a CT plant and DT HIGS-based controllers (including the inter-sample behavior). While the frequency-domain criteria do not require parametric models and can be evaluated using easy-to-obtain frequency response data, we have formally proven that their satisfaction implies feasibility of a special case of the LMI-based conditions and thus are more conservative. This has been further illustrated by a numerical example showing that the LMIs are significantly less conservative than the frequency-domain criteria. Future research directions include reduction of the conservatism associated with the stability analysis, as well as transforming the presented stability criteria for synthesis of sampled-data HIGS-based controllers.

6

A Hybrid Integrator-Gain Based Bandpass Filter for Active Vibration Isolation with Improved Skyhook Damping

Abstract - *In this chapter a nonlinear filter with bandpass characteristics is presented for active vibration isolation with enhanced skyhook damping properties. The new nonlinear filter consists of two so-called hybrid integrator-gain systems, which are control elements recently introduced, aiming to overcome fundamental limitations of linear time-invariant control. The effectiveness of the novel control design is illustrated by means of experiments performed on an industrial active vibration isolation system. In particular, it is shown that the favorable properties of hybrid integrator-gain systems which are mainly expressed by reduced phase lag, allow for significantly larger active damping gain values, thereby enabling superior active vibration isolation. Additionally, improvements in closed-loop transient behavior in terms of overshoot and settling time are obtained. Moreover, no undesired effects of nonlinearity in the form of amplification of high-frequency dynamics of the plant are measured under normal operating conditions.*

This chapter is based on: [75] and [125].

6.1 Introduction

Linear time-invariant (LTI) control is a well-developed area of research, and usage of LTI control techniques is commonplace in many industrial sectors, such as high-precision mechatronics. However, LTI control theory suffers from fundamental limitations such as Bode's gain-phase relationship and the waterbed effect, due to Bode's sensitivity integral. Such fundamental limitations typically lead to design trade-offs which affect closed-loop performance both in time-domain as well as in frequency-domain. This, has led to increased attention to nonlinear and hybrid control elements, which have proven to be effective tools in realizing performance beyond the limitations of LTI control. Examples of such control elements include switching controllers [69], variable gain controllers (VGC) [70, 80], split-path nonlinear integrators (SPANI) [45, 151], filtered split-path nonlinear integrators (F-SPANI) [126], reset controllers [2, 19, 31, 155], and the more recently introduced hybrid integrator-gain systems (HIGS) [37].

HIGS consist of an integrator mode and a gain mode that together with switching logic guarantee that the input and output of the hybrid integrator are constrained to a sector at all times, thereby always having the same sign. As a result of this construction, a HIGS element's describing function [128] exhibits similar amplitude characteristics to that of a linear lowpass filter while only having 38.15° of phase lag (as opposed to 90° in the linear case) [38]. A similar phase advantage is found in the case of reset control elements [19]. However, while reset control gives rise to discontinuous control signals that can potentially excite high frequency dynamics of the plant, HIGS achieve their favorable phase properties with continuous signals. The improvement obtained in terms of phase lag for both the HIGS and reset control systems, suggests the possibility of designing a compensator capable of supplying the required bandwidth for a closed-loop system, with reduced gain at high frequencies [29], as a result of requiring less phase lead to be generated by differential action. Additionally, the reduced phase lag of these controllers, also may prove useful in improving transient performance of control systems [19, 143, 148, 156]. HIGS were introduced in [37], where tools for frequency domain design and stability analysis of HIGS-based controllers were presented. Moreover [37, 145], present experimental demonstrations of HIGS outperforming linear controllers, when applied to high-precision mechatronics. In [38, 120, 121, 139, 142], stability analysis results are presented for continuous time, discrete time and sampled-data HIGS-controlled systems. Mathematical formalization and well-posedness analysis of HIGS-controlled systems are discussed in [38, 122, 123]. Moreover in [143, 148], it is shown that HIGS-based control can be used to overcome some well-known fundamental limitations of LTI control.

In this chapter, a HIGS-based design is presented and compared to its linear counterpart regarding its effectiveness in the context of active vibration isolation. Vibration isolation systems are widely used in high precision mechatronic systems such as wafer scanners [26, 109] which are indispensable in the production

of integrated circuits (ICs), and electron microscopes that are key enablers for advances in many fields such as nanotechnology, material science and life science [84, 134]. In such applications, there are ever increasing requirements on accuracy and throughput of the machines. In order to achieve accurate measurements which are crucial for meeting the extreme performance requirements of such high-precision systems, sensors and other sensitive equipment are placed on so-called metrology frames which are isolated from external disturbances [41, 84], such as floor vibrations and acoustic excitation, by means of vibration isolation. In active vibration isolation, for damping of suspension modes (often through skyhook damping, see, for example, [95]) linear bandpass filters are frequently utilized to allow for

1. avoiding the usage of poor low-frequency sensor information,

2. active damping by means of high-gain feedback in the frequency interval containing the suspension modes of the system,

3. restoring the passive isolation properties of the system at high frequencies.

This makes such systems an interesting test case for hybrid control designs since such designs can be used to potentially improve vibration isolation properties as shown in [69], due to their enhanced phase properties, which may enable one to do high-gain feedback without compromising stability of the system. However, such controllers are also likely to induce more high-frequency disturbances as a result of generating non-smooth control signals.

In this chapter, a HIGS-based bandpass filter is constructed by interconnecting two HIGS-based filters in series. The phase advantage of the HIGS-based filter over a linear bandpass filter, as observed from describing function analysis, is then exploited to achieve superior skyhook damping with improved transient performance. The effectiveness of the proposed design is tested by experimental validation on an industrial vibration isolation system. In doing so, the performance of the controller is compared with its linear counterpart, which is frequently used in industrial practice. We also present stability criteria that can be used to verify stability of the closed-loop system under consideration, based on measurements of frequency response functions. Our design and analysis approach is similar to one often followed in high-precision motion industries. In particular, while the design of the controllers are based on continuous-time reasoning, the sampled-data nature of the system under consideration, consisting of continuous-time dynamics of the plant to be controlled as well as the discrete-time dynamics of the digitally implemented controller, is addressed in the stability analysis, thereby providing stability guarantees for the closed-loop system.

The remainder of this chapter is organized as follows. In Section 6.2, a brief introduction of HIGS is provided. In Section 6.3, the design, working principle and properties (both in time domain and frequency domain) of the HIGS-based

bandpass filter are discussed. Section 6.4 recalls the concept of active vibration isolation through skyhook damping. Section 6.5 is concerned with the experimental validation of our work, where first a description of the industrial active vibration isolation system is provided, followed by a discussion of the control strategy and stability analysis as well as measurement results obtained both in frequency and time domain. The chapter is concluded in Section 6.6, where the main contributions of our work as well as future directions for research are highlighted.

6.2 Hybrid Integrator-Gain Systems

A HIGS element $\mathscr{H}$, is given by

$$\mathscr{H} := \begin{cases} \dot{x}_h(t) = \omega_h e(t), & \text{if } (e(t), u(t), \dot{e}(t)) \in \mathscr{F}_1 \quad (6.1a) \\ x_h(t) = k_h e(t), & \text{if } (e(t), u(t), \dot{e}(t)) \in \mathscr{F}_2 \quad (6.1b) \\ u(t) = x_h(t), & \quad (6.1c) \end{cases}$$

where $x_h(t) \in \mathbb{R}$ is the state and $e(t) \in \mathbb{R}$ and $\dot{e}(t) \in \mathbb{R}$ denote the input to $\mathscr{H}$ and its time derivative, respectively, at time $t \in \mathbb{R}_{\geq 0}$. Moreover, $u(t) \in \mathbb{R}$ is the output of $\mathscr{H}$, the parameters $\omega_h \in [0, \infty)$ and $k_h \in (0, \infty)$ denote the integrator frequency and gain value, respectively, and $\mathscr{F}_1$ and $\mathscr{F}_2$ denote the regions, where the two different subsystems are active. The initial condition of the state x_h is assumed to be zero, i.e., $x_h(0) = 0$ and thus $u(0) = 0$. A HIGS element $\mathscr{H}$ in (6.1) is designed to mainly operate in integrator mode (6.1a), however, by design, the input-output pair (e, u) of $\mathscr{H}$ is constrained to lie in a $[0, k_h]$-sector, i.e., $(e, u, \dot{e}) \in \mathscr{F}$, with

$$\mathscr{F} := \left\{ (e, u, \dot{e}) \in \mathbb{R}^3 \mid eu \geq \frac{1}{k_h} u^2 \right\}, \quad (6.2)$$

at all times $t \in \mathbb{R}_{\geq 0}$. Note that with $u(0) = 0$, $(e(0), u(0), \dot{e}(0)) \in \mathscr{F}$ for all $e(0) \in \mathbb{R}$. When the integrator dynamics (6.1a) result in trajectories that tend to violate the constraint $(e, u, \dot{e}) \in \mathscr{F}$, the dynamics of $\mathscr{H}$ switch to the gain mode given by (6.1b) such that $(e, u, \dot{e}) \in \mathscr{F}$ remains true along the trajectories of the system. In particular, $\mathscr{H}$ switches its dynamics from (6.1a) to (6.1b) when $(e, u, \dot{e}) \in \mathscr{F}_2$. To be precise, we have

$$\mathscr{F}_1 := \mathscr{F} \setminus \mathscr{F}_2, \quad (6.3)$$

$$\mathscr{F}_2 := \left\{ (e, u, \dot{e}) \in \mathscr{F} \mid u = k_h e \ \wedge \ \omega_h e^2 > k_h \dot{e} e \right\}. \quad (6.4)$$

Note that $u = k_h e$ implies that the trajectories are on the boundary of $\mathscr{F}$ and $\omega_h e^2 > k_h \dot{e} e$ suggests that vector field in the integrator mode points outside $\mathscr{F}$, in which case the system should operate in the gain mode such that sector violation is avoided. A graphical illustration of the sets $\mathscr{F}$, $\mathscr{F}_1$ and $\mathscr{F}_2$ is provided in Fig. 6.1.

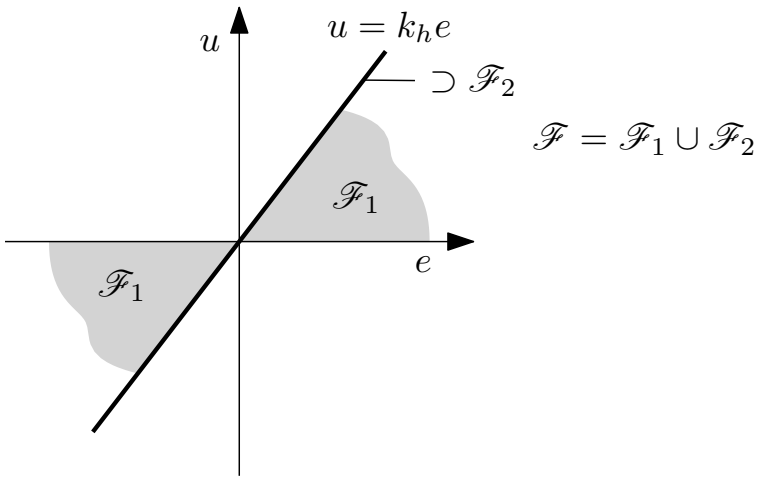

Figure 6.1. Schematic representation of the sector $\mathscr{F}$ and the regions $\mathscr{F}_1$ and $\mathscr{F}_2$.

In addition to the time-domain properties of $\mathscr{H}$ resulting from (6.1), its frequency-domain properties can be studied in an approximative manner by means of describing function analysis. To this end, consider a sinusoidal input $e(\tau)$

$$e(\tau) = \hat{e}\sin(\tau), \tag{6.5}$$

with $\tau = \omega t,\ \omega \geq 0,\ t \in \mathbb{R}_{\geq 0}$ and amplitude $\hat{e} \in \mathbb{R}$. In [36] it is shown that the describing function $\mathcal{D}(j\omega)$ of $\mathscr{H}$ in (6.1) between the input e and output u is given by

$$\mathcal{D}(j\omega) = \frac{a_1 + b_1 j}{\hat{e}}, \tag{6.6}$$

where a_1, b_1 are the Fourier coefficients of the fundamental harmonic and are given by

$$\begin{aligned} a_1 &= \frac{\hat{e}}{2\pi}\left\{\frac{\omega_h}{\omega}\left(\cos(2\gamma) - 4\cos(\gamma) + 3\right) + k_h\left(2(\pi - \gamma) + \sin(2\gamma)\right)\right\} \\ b_1 &= \frac{\hat{e}}{2\pi}\left\{\frac{\omega_h}{\omega}\left(4\sin(\gamma) - \sin(2\gamma) - 2\gamma\right) - k_h\left(1 - \cos(2\gamma)\right)\right\}. \end{aligned} \tag{6.7}$$

Here γ denotes the switching instant from integrator mode to the gain mode and is given by

$$\gamma = 2\arctan(\omega k_h/\omega_h). \tag{6.8}$$

Note that as $\omega \to \infty$, and thus $\gamma \to \pi$ one has

$$\lim_{\gamma \to \pi} \mathcal{D}(j\omega) = \frac{\omega_h}{j\omega}\left\{1 + \frac{4j}{\pi}\right\}, \tag{6.9}$$

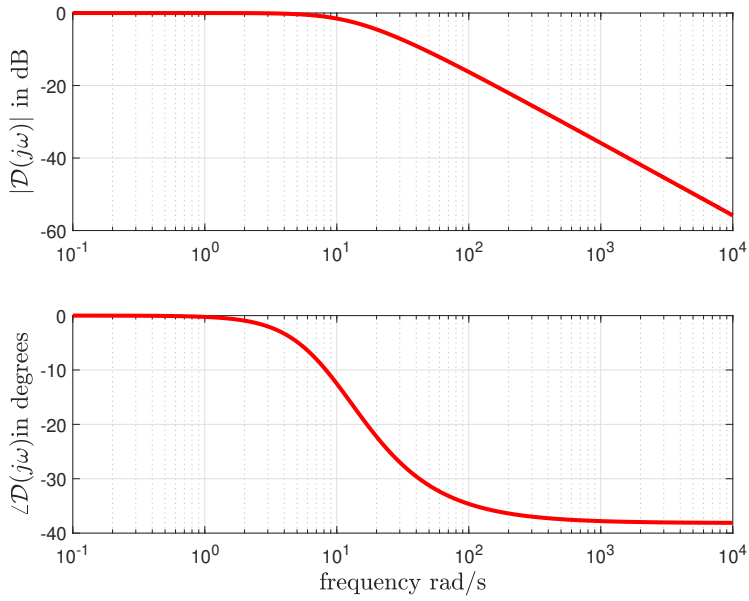

Figure 6.2. Bode plot of describing function of a single HIGS element with $\omega_h = 10$ rad/s and $k_h = 1$.

which resembles a 20dB/decade amplitude decay similar to magnitude characteristics of a linear integrator, but with a phase lag of only 38.15 degrees (as opposed to 90 degrees in the linear case) due to the extra imaginary-valued constant $4/\pi$. It is this phase advantage over linear integrators that is exploited in HIGS-based control design, for enhancing frequency-domain characteristics such as closed-loop bandwidth as well as time-domain transient performance. The Bode plot of $\mathcal{D}(j\omega)$ as defined in (6.6) is portrayed in Fig. 6.2, for the case where $\omega_h = 10$ rad/s and $k_h = 1$. As it can be seen in Fig. 6.2, $\mathcal{D}(j\omega)$ has magnitude characteristics similar to a linear lowpass filter, while only having 38.15 degrees of phase lag. Next, using the insights obtained from the describing function analysis presented above, we construct the HIGS-based bandpass filter.

6.3 HIGS-based Bandpass Filter

In this section, we present the HIGS-based bandpass filter design and investigate its open-loop time domain behavior and properties. In addition, an approximative frequency domain analysis of the HIGS-based filter based on describing function

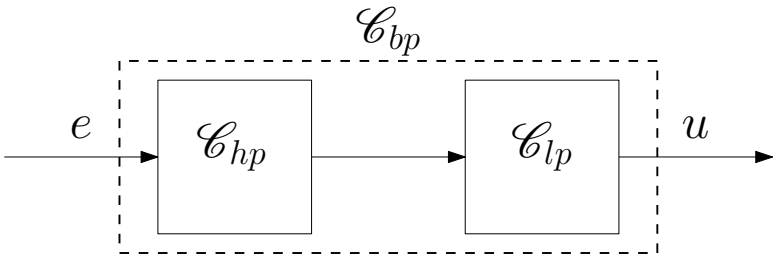

Figure 6.3. Block diagram of a linear bandpass filter.

analysis is provided.

6.3.1 Design and working principle

As explained in Section 6.1, bandpass filters are frequently utilized for active vibration isolation via skyhook damping. In this section, the design and working principle of the HIGS-based bandpass filter is discussed. Prior to presenting the HIGS-based bandpass filter, let us first consider a linear bandpass filter $\mathscr{C}_{bp}$, in Fig. 6.3, constructed by the series interconnection of a linear highpass filter $\mathscr{C}_{hp}$ and a linear lowpass filter $\mathscr{C}_{lp}$. The transfer function $\mathscr{C}_{bp}(s)$ of the bandpass filter in Laplace domain is given by

$$\mathscr{C}_{bp}(s) = \frac{u(s)}{e(s)} = \overbrace{\frac{\omega_{lp}}{s+\omega_{lp}}}^{lowpass} \cdot \underbrace{\frac{s}{s+\omega_{hp}}}_{highpass} \tag{6.10}$$

with $\omega_{hp} = 2\pi \times 0.1$ rad/s and $\omega_{lp} = 2\pi \times 10$ rad/s the filter's cut-off frequencies. In high-precision mechatronic applications bandpass filters of the form (6.10) are frequently utilized, with ω_{hp} chosen at a frequency beyond which the sensor gives useful and reliable information. Moreover, $\omega_{lp} > \omega_{hp} > 0$ can be used for maintaining passive isolation properties of the plant as well as reducing the sensitivity of the closed-loop system to noise and high-frequency (un-modelled) dynamics by lowering the gain, at high frequencies. Note that in the interval $[\omega_{hp}, \omega_{lp}]$, (6.10) approximates unity gain and thus, in this frequency interval the input of the filter is passed through to its output. The bandpass filter $\mathscr{C}_{bp}$ can also be described in state space form by

$$\begin{aligned} \dot{x}_{bp}(t) &= \begin{bmatrix} -\omega_{hp} & 0 \\ -\omega_{hp} & -\omega_{lp} \end{bmatrix} x_{bp}(t) + \begin{bmatrix} 1 \\ 1 \end{bmatrix} e(t), \\ u(t) &= \begin{bmatrix} 0 & \omega_{lp} \end{bmatrix} x_{bp}(t), \end{aligned} \tag{6.11}$$

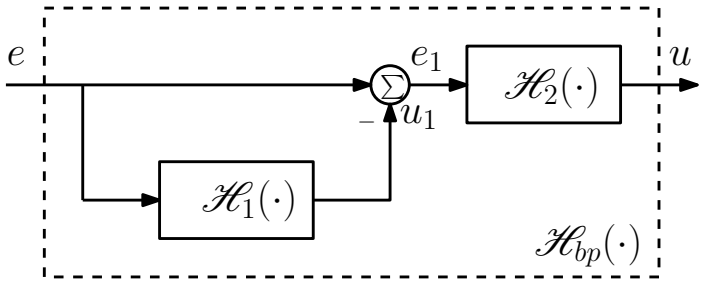

Figure 6.4. Block diagram of a HIGS-based bandpass filter.

with state $x_{bp}(t) = \begin{bmatrix} x_{hp}^\top(t) & x_{lp}^\top(t) \end{bmatrix}^\top$, where $x_{hp}(t) \in \mathbb{R}$ and $x_{lp}(t) \in \mathbb{R}$, denote the state of $\mathscr{C}_{hp}$ and $\mathscr{C}_{lp}$, respectively, at time $t \in \mathbb{R}_{\geq 0}$.

Given the linear bandpass filter $\mathscr{C}_{bp}$ in Fig. 6.3, consider the block diagram in Fig. 6.4, which represents a hybrid bandpass filter $\mathscr{H}_{bp}$, i.e., the HIGS-based equivalent of (6.10), with $\mathscr{H}_1, \mathscr{H}_2$ as defined in (6.1), where $k_{h1} = k_{h2} = 1$, $\omega_{h1} = \omega_{hp}/(2\alpha)$ rad/s, $\omega_{h2} = \omega_{lp}/\alpha$ rad/s, and $\alpha = |1 + 4j/\pi|$ is a scaling constant that follows from (6.9), ensuring that the cut-off frequencies of the HIGS-based filters match that of their linear counterpart. As show in Fig. 6.2, the describing function of a HIGS element has magnitude characteristics similar to a linear lowpass filter. Therefore, $\mathscr{H}_2$ in Fig. 6.4, acts as a lowpass filter. With the particular configuration in Fig. 6.4, by subtracting the output of the HIGS element $\mathscr{H}_1$ from its input, a HIGS-based highpass filter is constructed.

The Bode diagram of both this HIGS-based highpass filter and its linear equivalent are provided in Fig. 6.5. The series interconnection of this HIGS-based highpass and the HIGS element $\mathscr{H}_2$ (having lowpass characteristics), leads to the construction of the HIGS-based bandpass filter, the properties of which will be studied next.

The HIGS-based bandpass filter has four modes of operation and can be de-

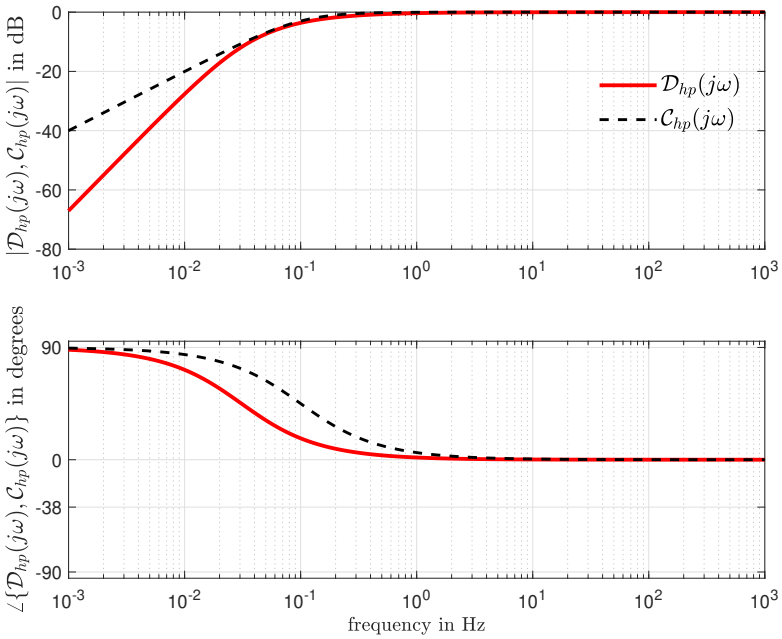

Figure 6.5. Bode plot of describing function of $\mathcal{D}_{hp}(j\omega) = 1 - \mathcal{D}_1(j\omega)$ and $C_{hp}(j\omega) = \frac{s}{s+\omega_{hp}}$, $\omega_{hp} = (0.1 \times 2\pi)/2\alpha$ rad/s, $\alpha = |1 + 4j/\pi|$, and $k_h = 1$.

scribed by

$$\dot{x}_{hbp} := \begin{bmatrix} \dot{x}_{h1} \\ \dot{x}_{h2} \end{bmatrix} = \begin{cases} \begin{bmatrix} \omega_{h1} e \\ \omega_{h2} e_1 \end{bmatrix}, & \text{if } (e, u_1, \dot{e}) \in \mathscr{F}_1^1 \wedge (e_1, u, \dot{e}_1) \in \mathscr{F}_1^2 \\ \begin{bmatrix} \omega_{h1} e \\ k_{h2} \dot{e}_1 \end{bmatrix}, & \text{if } (e, u_1, \dot{e}) \in \mathscr{F}_1^1 \wedge (e_1, u, \dot{e}_1) \in \mathscr{F}_2^2 \\ \begin{bmatrix} k_{h1} \dot{e} \\ \omega_{h2} e_1 \end{bmatrix}, & \text{if } (e, u_1, \dot{e}) \in \mathscr{F}_2^1 \wedge (e_1, u, \dot{e}_1) \in \mathscr{F}_1^2 \\ \begin{bmatrix} k_{h1} \dot{e} \\ k_{h2} \dot{e}_1 \end{bmatrix}, & \text{if } (e, u_1, \dot{e}) \in \mathscr{F}_2^1 \wedge (e_1, u, \dot{e}_1) \in \mathscr{F}_2^2 \\ u = x_{h2}, \end{cases} \tag{6.12}$$

where we have omitted time-dependency to lighten the notation. Here, $x_{h1} \in \mathbb{R}$ and $x_{h2} \in \mathbb{R}$, denote the states of $\mathscr{H}_1$ and $\mathscr{H}_2$, respectively, and $\mathscr{F}_i^j$, $i \in \{1, 2\}$, $j \in \{1, 2\}$, denote the regions where the i^{th} mode ($i = 1$ for integrator mode, and $i = 2$ for gain mode) of HIGS element j are active. By using $e_1 = e - u_1 = e - x_{h1}$, we get

$$\begin{bmatrix} \dot{x}_{h1} \\ \dot{x}_{h2} \end{bmatrix} = \begin{cases} \begin{bmatrix} \omega_{h1} e \\ \omega_{h2}(e - x_{h_1}) \end{bmatrix}, & \text{if } (e, u_1, \dot{e}) \in \mathscr{F}_1^1 \wedge (e - u_1, u, \dot{e} - \dot{u}_1) \in \mathscr{F}_1^2 \\ \begin{bmatrix} \omega_{h1} e \\ k_{h2}(\dot{e} - \omega_{h1} e) \end{bmatrix}, & \text{if } (e, u_1, \dot{e}) \in \mathscr{F}_1^1 \wedge (e - u_1, u, \dot{e} - \dot{u}_1) \in \mathscr{F}_2^2 \\ \begin{bmatrix} k_{h1} \dot{e} \\ \omega_{h2}(e - x_{h1}) \end{bmatrix}, & \text{if } (e, u_1, \dot{e}) \in \mathscr{F}_2^1 \wedge (e - u_1, u, \dot{e} - \dot{u}_1) \in \mathscr{F}_1^2 \\ \begin{bmatrix} k_{h1} \dot{e} \\ k_{h2}(\dot{e} - k_{h1} \dot{e}) \end{bmatrix}, & \text{if } (e, u_1, \dot{e}) \in \mathscr{F}_2^1 \wedge (e - u_1, u, \dot{e} - \dot{u}_1) \in \mathscr{F}_2^2 \\ u = x_{h2}. \end{cases}$$

Note that the derivative of the input e to the bandpass filter is required, for both deciding which mode of operation is active, as well as computation of dynamics in modes where either HIGS element operate in the gain mode. As a result, the input e is assumed to be continuous and differentiable.

6.3.2 Time domain characteristics

To describe the open-loop time-domain behavior of both the linear and HIGS-based bandpass filters, $\mathscr{C}_{bp}$ and $\mathscr{H}_{bp}$, consider the time responses shown in Fig. 6.6, which are the result of sinusoidal inputs (gray curves) as in (6.5) with $\hat{e} = 1$ and $\omega \in \{2\pi \times 1/20, 2\pi, 2\pi \times 20\}$ rad/s. First observe that by choice of its parameter ω_{h1}, the integrator in $\mathscr{H}_1$ is fast enough to invoke the integrator mode for the

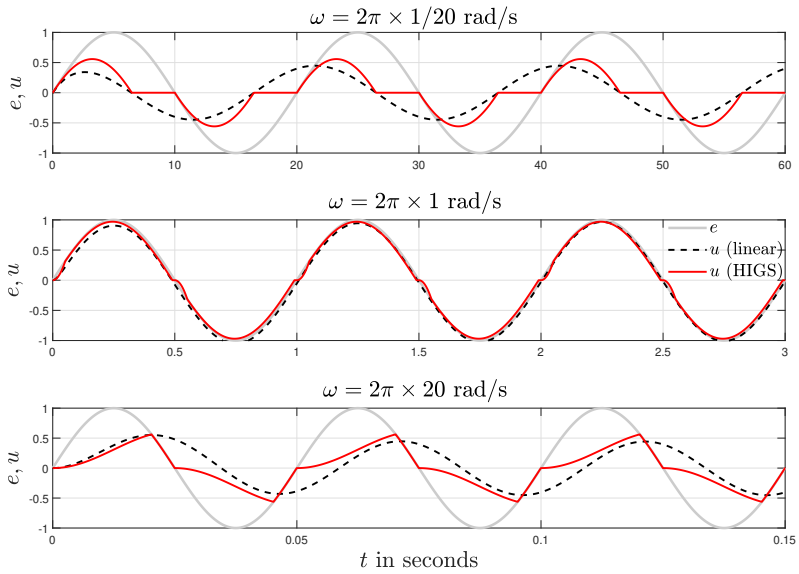

Figure 6.6. Time series simulations of the output u of a linear bandpass filter in (6.10) (dashed-black) and the HIGS-based bandpass filter from Figure 6.4 (red) to a sinusoidal input e (gray) with $\omega \in \{2\pi \times 1/20, 2\pi, 2\pi \times 20\}$ rad/s.

case $\omega = 2\pi \times 1/20$ rad/s, which is shown in the upper part of the figure. At $t \approx 6.4$ seconds, $\mathscr{H}_1$ switches from integrator mode to gain mode, which means its output becomes equal to its input e, i.e., the input to $\mathscr{H}_2$ becomes zero, which subsequently yields the output u to be zero too. At $t = 10$ seconds, e changes sign and $\mathscr{H}_1$ switches back to integrator mode. For the cases $\omega = 2\pi$ rad/s and $\omega = 2\pi \times 20$ rad/s, the input signal to $\mathscr{H}_2$, i.e., $e - u_1 \approx e$, reflects a too slow contribution of $\mathscr{H}_1$. Conversely, by choice of its parameter ω_{h2}, the integrator in $\mathscr{H}_2$ is too fast for the cases $\omega = 2\pi \times 1/20$ rad/s and $\omega = 2\pi$ rad/s. As a result, $\mathscr{H}_2$ largely operates in gain mode. For the case $\omega = 2\pi$ rad/s, i.e., the middle part of the figure, this means that since $e - u_1 \approx e$ and because $\mathscr{H}_2 \approx 1$, the output $u \approx e$. For the case $\omega = 2\pi \times 20$ rad/s, i.e., the lower part of the figure, it can be seen that for $t \in [0.05, 0.07]$ seconds, $\mathscr{H}_2$ operates in integrator mode, whereas during $t \in (0.07, 0.08)$ seconds, it operates in gain mode. For all responses, observe that the hybrid behavior of the HIGS-based bandpass filter (red curves) effectively results in mimicking either phase lead (upper part) or phase lag (lower part) while avoiding unequal signs of the input-output pair (e, u). The latter is clearly not the case for the response of the linear bandpass filter (dashed black curves).

To be more precise, we can show that the input-output pair (e, u) of the HIGS-based bandpass filter satisfies the same sector constraint as a single HIGS element, cf. (6.2). More particularly, for $k_{h,1} = k_{h,2} = 1$, one has

$$u^2(t) \leq e(t)u(t) \leq e^2(t), \tag{6.13}$$

for all $t \in \mathbb{R}_{\geq 0}$. To see this, first note that by design, the input $e(t)$ to the first HIGS element $\mathscr{H}_1$ and its output $u_1(t)$ have the same sign and satisfy the relation $|u_1(t)| \leq |e(t)|$. Therefore, the input to $\mathscr{H}_2$ given by $e_1(t) = e(t) - u_1(t)$, always has the same sign as $e(t)$, and thus $e(t)e_1(t) \geq 0$. Let us now turn our attention to the input-output pair of $\mathscr{H}_2$, i.e., $e_1(t)$ and $u(t)$. By design, these signals satisfy

$$e_1(t)u(t) = (e(t) - u_1(t))u(t) = e(t)u(t) - u_1(t)u(t) \geq u^2(t). \tag{6.14}$$

Moreover, note that $u(t)$ and $u_1(t)$ have the same sign. Indeed, since $e(t)$ and $e_1(t)$ have the same sign for all $t \in \mathbb{R}_{\geq 0}$ and $e(t)$ and $u_1(t)$ have the same sign, it follows that $e_1(t)$ and $u_1(t)$ also have the same sign. Furthermore, as $e_1(t)$ and $u(t)$ have similar signs, it holds that $u_1(t)$ and $u(t)$ have equal sign and thus, $u(t)u_1(t) \geq 0$. As such, it follows from (6.14) that

$$e(t)u(t) \geq e(t)u(t) - u_1(t)u(t) \geq u^2(t), \tag{6.15}$$

which indeed shows that the lower bound in (6.13) holds. To also see that the upper bound in (6.13), i.e., $e(t)u(t) \leq e^2(t)$ is satisfied, note that by virtue of the design of $\mathscr{H}_2$, $|u(t)| \leq |e_1(t)|$. Moreover, $|e_1(t)| \leq |e(t)|$ since $e(t)$ and $u_1(t)$ have the same sign and $|e(t)| \geq |u_1(t)|$. As a result, one has $|u(t)| \leq |e_1(t)| \leq |e(t)|$ and thus $e^2(t) \geq u^2(t)$ which indeed shows that the upper bound in (6.13) holds.

As it will become clear in subsequent sections, the sector boundedness of the input-output pair of the HIGS-based band pass filter is useful for stability analysis.

6.3.3 Frequency domain characteristics

In the frequency domain, the behavior of the HIGS-based bandpass filter can be evaluated in an approximate manner using the following describing function

$$\mathcal{D}_{bp}(j\omega) \approx (1 - \mathcal{D}_1(j\omega))\mathcal{D}_2(j\omega), \tag{6.16}$$

where $\mathcal{D}_1(j\omega), \mathcal{D}_2(j\omega)$ follow from (6.6) and (6.7) with the parameter values given in the discussion related to Fig. 6.4. Note that (6.16) does not necessarily represent the true describing function $\bar{\mathcal{D}}_{bp}$ of $\mathscr{H}_{bp}$ and only approximates it. However, note that $\mathscr{H}_1$ and $\mathscr{H}_2$, are used in the construction of the HIGS-based highpass and lowpass filters, respectively, and thus one has $\omega_{h2} \gg \omega_{h1}$. In other words, one has $\omega_{h2} \geq \gamma\omega_{h1}$ for some large constant $\gamma \in \mathbb{R}_{>0}$. Therefore, given a sinusoidal input $e = \hat{e}\sin(\omega t)$, as also shown in Fig. 6.6, for $\omega \to 0$, while $\mathscr{H}_1$ exhibits switching behavior, $\mathscr{H}_2$ largely operates in gain mode and thus, exhibits linear dynamics. In addition, for $\omega \to \infty$, the integrator in $\mathscr{H}_1$ is too slow and thus $\mathscr{H}_1$ largely operates in the integrator mode, while $\mathscr{H}_2$ exhibits switching behavior. As a result, the nonlinear behaviors of the two HIGS elements show limited interference with each other and thus, $\mathcal{D}_{bp}(j\omega)$ as defined in (6.16) is a good approximation of $\bar{\mathcal{D}}_{bp}(j\omega)$. The frequency responses of $\mathcal{C}_{bp}(j\omega)$, the approximated describing function $\mathcal{D}_{bp}(j\omega)$ and the true describing function $\bar{\mathcal{D}}_{bp}(j\omega)$, obtained from time-series simulations and computation of the first Fourier coefficients, are provided in the Bode diagram of Fig. 6.7. A few observations can be made from Fig. 6.7. Firstly, let us make the observation that $\mathcal{D}_{bp}(j\omega)$ provides an excellent approximation of $\bar{\mathcal{D}}_{bp}(j\omega)$. At low frequencies, it is observed that while $\mathcal{C}_{bp}(j\omega)$ has a 20 dB/decade increase in magnitude, $\mathcal{D}_{bp}(j\omega)$ has a 40 dB/decade increase in magnitude, i.e., an additional 20dB/decade. At low frequencies both $\mathcal{D}_{bp}(j\omega)$ and $\mathcal{C}_{bp}(j\omega)$ have 90 degrees of phase lead, which is a clear manifestation of defying Bode's gain-phase relationship, in the case of the HIGS-based bandpass filter. The additional 20 dB/decade suppression at low frequencies, seen in the case of $\mathcal{D}_{bp}(j\omega)$, can be explained as follows. At low frequencies, one has

$$\lim_{\omega\to 0} \mathcal{D}_{bp}(j\omega) = \lim_{\omega\to 0}(1 - \mathcal{D}_1(j\omega)), \tag{6.17}$$

with $\mathcal{D}_1(j\omega)$ as defined in (6.6). By using the power series expansions of $\sin(\gamma)$, $\sin(2\gamma)$, $\cos(\gamma)$, $\cos(2\gamma)$ in the expressions of the Fourier coefficients in (6.7) and taking the limit for $\omega \to 0$, for the Fourier coefficient a_1 one obtains

$$\lim_{\omega\to 0} a_1 = \frac{-4\hat{e}}{3\pi} k_{h1}^3 \frac{\omega^2}{\omega_{h1}^2}, \tag{6.18}$$

and for the Fourier coefficient b_1, we get

$$\lim_{\omega\to 0} b_1 = \hat{e}k_{h1}. \tag{6.19}$$

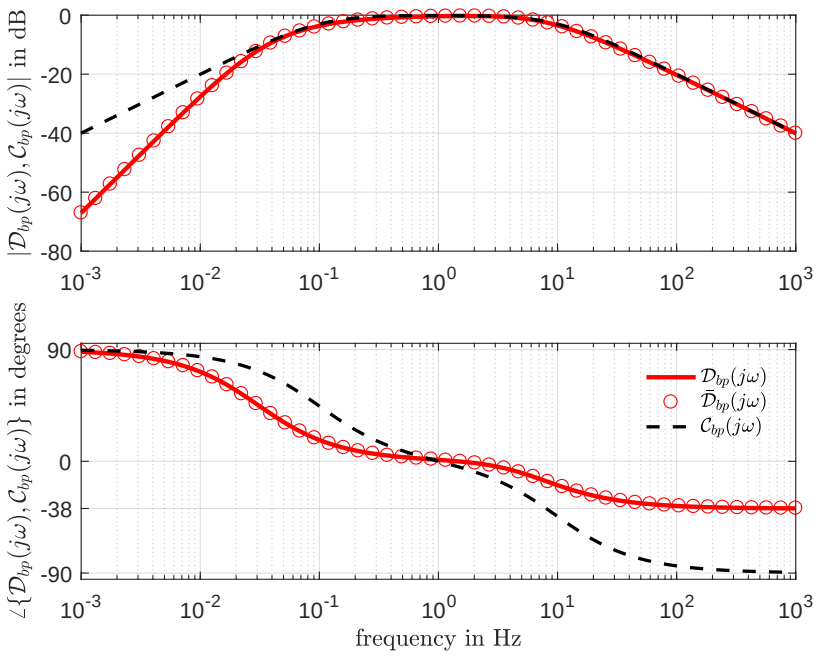

Figure 6.7. Bode diagram of linear bandpass filter $\mathcal{C}_{bp}(j\omega)$ (dashed black), the approximated describing function of the HIGS-based bandpass filter $\mathcal{D}_{bp}(j\omega)$ (solid red line), and the actual describing function of the HIGS-based bandpass filter $\bar{\mathcal{D}}_{bp}(j\omega)$(red circles).

Therefore

$$\lim_{\omega\to 0}(1-\mathcal{D}_1(j\omega)) = \lim_{\omega\to 0}(1-\frac{a_1+b_1 j}{\hat{e}}) = 1-k_{h1}+\frac{4}{3\pi}k_{h1}^3\frac{\omega^2}{\omega_{h1}^2}. \tag{6.20}$$

By substituting $k_{h1}=1$, we get $\lim_{\omega\to 0}(1-\mathcal{D}_1(j\omega)) = j\frac{4\omega^2}{3\pi\omega_h^2}$. Note that this is a positive imaginary number proportional to ω^2, which indeed clarifies the 40 dB/decade amplification as well as the 90 degrees of phase lead at low frequencies. In the frequency range $\omega \in 2\pi\times[0.1,10]$ rad/s, both filters have unity gain and thus this frequency interval forms the passband of both $\mathcal{C}_{bp}(j\omega)$ and $\mathcal{D}_{bp}(j\omega)$. Beyond $\omega = 2\pi\times 10$ rad/s both $\mathcal{D}_{bp}(j\omega)$ and $\mathcal{C}_{bp}(j\omega)$ exhibit 20dB/decade amplitude decay, while the favorable phase properties of the HIGS element $\mathscr{H}_2$ becomes apparent over its linear counterpart. In particular, one observes 51.85 degrees less phase lag in the case of $\mathcal{D}_{bp}(j\omega)$ compared to $\mathcal{C}_{bp}(j\omega)$. Once again, this is a clear manifestation of defying the Bode gain-phase relationship in the case of $\mathcal{D}_{bp}(j\omega)$.

The HIGS-based bandpass filter introduced in this section, will be used in the context of active vibration isolation, in particular the application of skyhook damping, in Section 6.5. Next, we shortly introduce the concept of skyhook damping for active vibration isolation.

6.4 Active Vibration Isolation by Skyhook Damping

In order to explain the concept of skyhook damping, consider the 1-degree of freedom (DOF) mass-spring-damper system in Fig. 6.8a, which represents a simplified 1-DOF model of an industrial vibration isolation system in the vertical direction z. The displacement of the payload, with mass m, to be isolated from external disturbances, is denoted by z_1 and the system is supported by a structure whose displacement, is denoted by z_0. Generally speaking, there exist two types of disturbances acting on the payload :(i) floor vibrations, and (ii) direct disturbances, denoted in Fig. 6.8a by F_d. A performance indicator used to investigate the sensitivity of the payload with respect to floor vibrations, is the transfer function from z_0 to z_1, also known as the transmissibility function $\mathcal{T}$, which in the Laplace domain is given by

$$\mathcal{T}(s) = \frac{Z_1(s)}{Z_0(s)} = \frac{bs+k}{ms^2+bs+k}, \tag{6.21}$$

with s the Laplace variable, and m ,b, k, the mass, damping coefficient and stiffness coefficient, respectively. In order to investigate the sensitivity of the payload to direct disturbances, the transfer from F_d to z_1, called the compliance function $\mathcal{C}$, given by

$$\mathcal{C}(s) = \frac{Z_1(s)}{F_d(s)} = \frac{1}{ms^2+bs+k}, \tag{6.22}$$

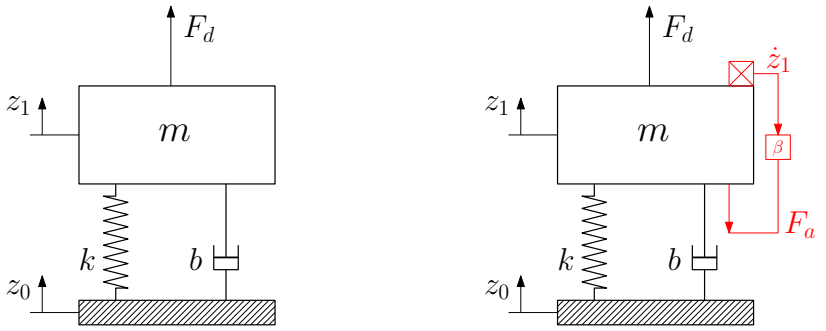

(a) Mass-spring-damper system with mass m, spring k, and damper b.

(b) Mass-spring-damper system with skyhook damping.

Figure 6.8. Mass-spring-damper system.

is considered. The magnitude characteristics of $\mathcal{T}$ and $\mathcal{C}$ as defined above, are shown in Fig. 6.9, where $m = 1300$ kg, $k = 170$ kN/m, $b = 1100$ Ns/m, correspond to the parameter values of the industrial active vibration isolation system studied later in Section 6.5.

As it can be seen in Fig. 6.9, there exists a weakly damped resonance, in both $\mathcal{C}$ and $\mathcal{T}$ at the natural frequency of the system given by $\omega = \sqrt{\frac{k}{m}}$. One strategy to provide extra damping to this resonance peak, is skyhook damping, as portrayed in Fig. 6.8b, wherein multiplication of vertical velocity $\dot{z}_1$ of the payload with an active damping gain β produces an active damping force $F_a = \beta \dot{z}_1$, proportional to the velocity of the payload. In particular, this construction results in transmissibility and compliance functions that are given by

$$\mathcal{T}(s) = \frac{bs + k}{ms^2 + (b + \beta)s + k}, \tag{6.23}$$

and

$$\mathcal{C}(s) = \frac{1}{ms^2 + (b + \beta)s + k}, \tag{6.24}$$

respectively. The magnitude characteristics of $\mathcal{T}$, and $\mathcal{C}$, as in (6.23) and (6.24), are shown in Fig. 6.10, for a range of active damping gain values β.

The following observations can be made from Fig. 6.10. First, note that, as expected from (6.23) and (6.24), with an increase in the value of β, better damping of the suspension mode is achieved. Additionally, note that this strategy is only

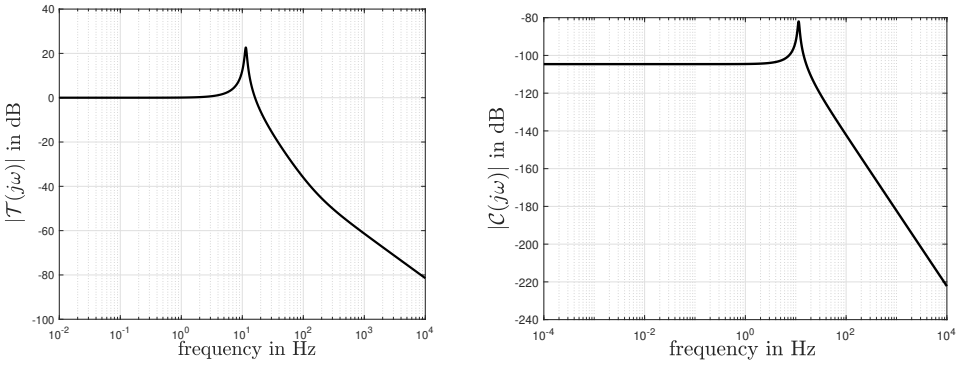

(a) **(b)**

Figure 6.9. Vibration isolation performance indicators (a) transmissibility, and (b) compliance.

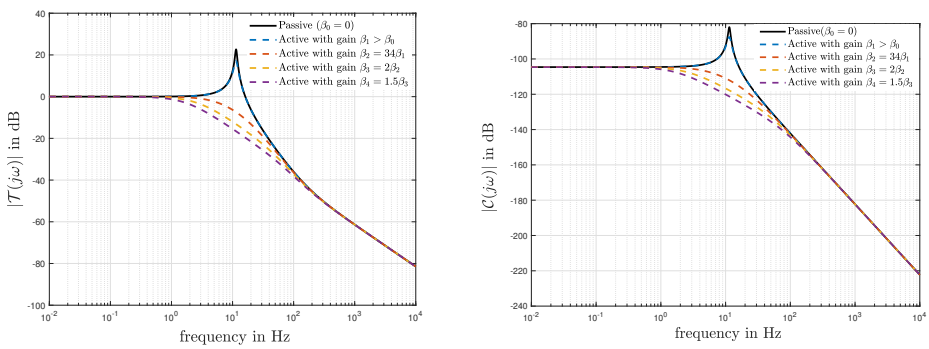

(a) **(b)**

Figure 6.10. Vibration isolation performance indicators (a) transmissibility, and (b) compliance, with skyhook damping

beneficial in a limited frequency range. In particular one has

$$\lim_{s\to 0} \mathcal{T}(s) = 1, \quad \lim_{s\to 0} \mathcal{C}(s) = \frac{1}{k},$$
$$\lim_{s\to \infty} \mathcal{T}(s) = \frac{b}{ms}, \quad \lim_{s\to \infty} \mathcal{C}(s) = \frac{1}{ms^2},$$

and thus at low, and high frequencies, the magnitude characteristics of $\mathcal{T}$ and $\mathcal{C}$, are independent of the active damping gain β.

In practice, the velocity $\dot{z}_1$ is obtained by either integrating output of accelerometers or direct measurements using e.g. geophones, which do not provide accurate measurements at low frequencies. In addition, high-frequency control effort should be minimized as to preserve the passive vibration isolation properties. This also means keeping the sensitivity of the closed-loop system low, to high frequency noise. In the frequency interval containing the suspension mode(s) of the system, it is desired to do high-gain feedback (i.e., to have a high β value) to allow for better damping of the suspension modes. Therefore, for application of skyhook damping, velocity measurements are typically fed to a bandpass filter, in order to allow for skyhook damping in a limited frequency range, thereby enabling damping of suspension modes without affecting performance at other frequencies.

In the next section, we make use of the HIGS-based bandpass filter as introduced in Section 6.3, for active vibration isolation by means of skyhook damping. In particular, the favorable phase properties of the HIGS-based bandpass filter over its linear counter part as shown in Fig. 6.7 will be used to allow for higher active damping-gains without compromising stability of the system, thereby improving vibration isolation properties of the system.

6.5 HIGS-based Skyhook Damping

In this section, we show the usefulness of the HIGS-based bandpass filter in the context of active vibration isolation. In particular, a HIGS-based skyhook damping strategy is applied to an industrial active vibration isolation system (AVIS), and its performance is compared with its linear counterpart.

6.5.1 System description

We consider the industrial vibration isolation system depicted in Fig. 6.11. This system consists of a 6 degrees of freedom movable metrology frame, a base frame and three vibration isolation modules. The isolation modules are placed between the base frame and the metrology frame and contain pneumatically controlled air mounts that provide gravity compensation, damping and a low suspension stiffness [17]. In addition, each isolation module is also equipped with Lorentz actuators to enable active vibration isolation. Lastly, both the base as well as the metrology frames are equipped with accelerometers that provide measurements of absolute

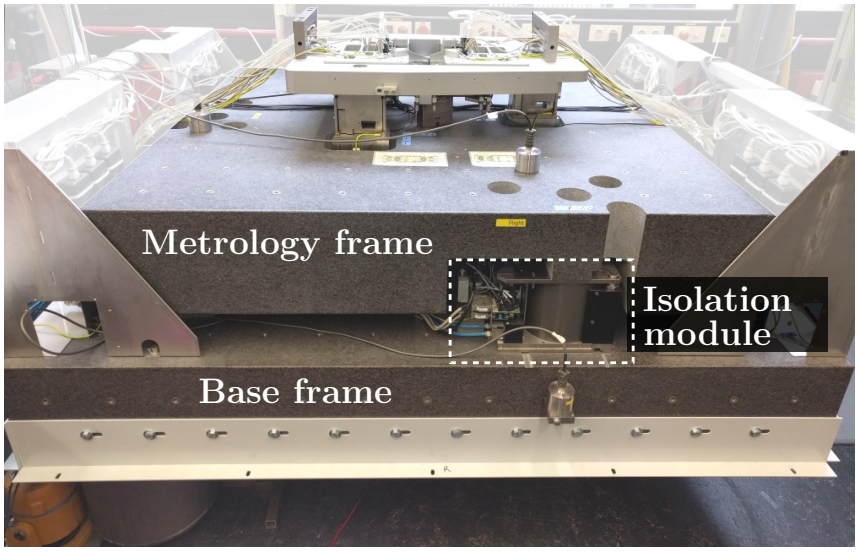

Figure 6.11. Industrial active vibration isolation system, consisting of the base frame, the isolated metrology frame and isolation modules.

acceleration in the vertical direction, at the location of the isolation modules. A schematic representation of the system is provided in Fig. 6.12.

Considering the center of the mass of the metrology frame as the frame of reference, as shown in Fig. 6.12, the metrology frame can move either in the vertical direction by moving along the principal coordinates (z, θ_x, θ_y) or in the horizontal directions by moving along the principal coordinates (x, y, θ_z). In this chapter we consider vertical movement, i.e., movement along (z, θ_x, θ_y). The relative gain array (RGA) number [127] of the system dynamics in the vertical direction calculated based on measured frequency response data, and used as a measure for interaction between the different input and output directions is shown in Fig. 6.13. It is observed that the dynamics in the principal coordinates (z, θ_x, θ_y) are strongly decoupled (up to 100 Hz), and thus one can approach the problem of controlling the multi-input multi-output plant under consideration, as a multi-loop single-input single-output (SISO) control problem. In addition, as previously explained, the system is equipped with sensors and actuators at the location of each isolation module. The mappings from the sensor measurements/control inputs at the location of the individual isolation module to the center of mass of the metrology frame can be found in Section 2.2 of [17].

Since, as explained above, the plant dynamics in the principal coordinates (z, θ_x, θ_y) are strongly we can obtain a (simplified) decentralized plant model in

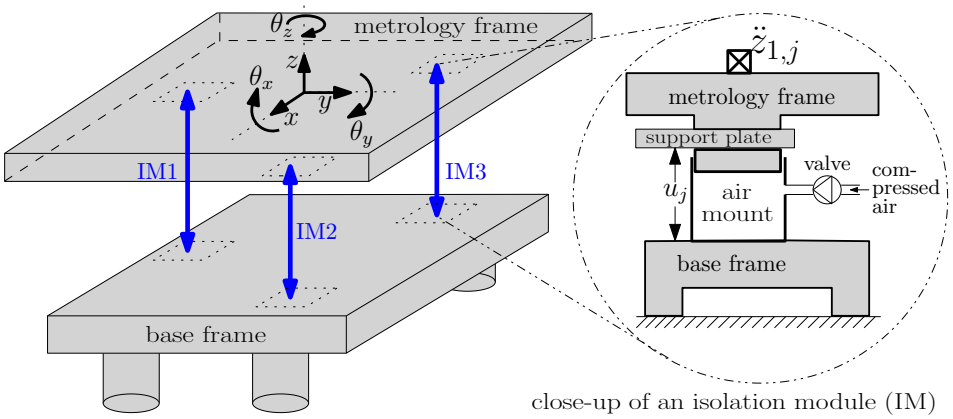

Figure 6.12. Schematic representation of the system, where the index j denotes the j^{th} isolation module.

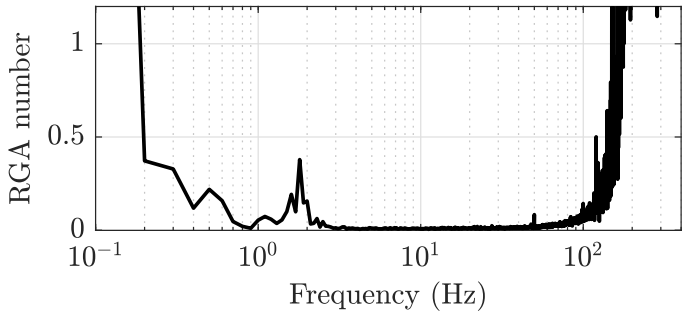

Figure 6.13. Relative gain array number calculated using frequency response measurements.

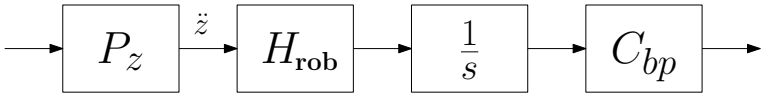

Figure 6.14. Open-loop system in the z direction.

Laplace domain, given by

$$P(s) = \begin{bmatrix} P_z(s) & 0 & 0 \\ 0 & P_{\theta_x}(s) & 0 \\ 0 & 0 & P_{\theta_y}(s) \end{bmatrix} = \begin{bmatrix} \frac{s^2}{ms^2+b_z s+k_z} & 0 & 0 \\ 0 & \frac{s^2}{J_x s^2+b_{\theta_x} s+k_{\theta_x}} & 0 \\ 0 & 0 & \frac{s^2}{J_y s^2+b_{\theta_y} s+k_{\theta_y}} \end{bmatrix}, \tag{6.25}$$

where the plant parameters can be found in Appendix A of [17]. In the remainder of this chapter, we focus on the control problem in the z direction noting that linear feedback controllers designed with the methods described for example in [17], are utilized in the θ_x and θ_y directions.

Note that in the model (6.25), the system's transfer function in the z direction neither models higher-order plant dynamics, nor contains information regarding actuator delays. Therefore, following the same logic as in [17], to obtain a more realistic model of the plant, a robustness filter H_{rob} given by

$$H_{\text{rob}}(s) = \frac{\omega_{lp}^2}{s^2 + 2\xi_{lp}\omega_{lp}s + \omega_{lp}^2} \times \frac{s + \omega_z}{\omega_z}, \tag{6.26}$$

with $\omega_{lp} = 1.8 \times 2\pi$ rad/s, $\xi_{lp} = 0.7$, and $\omega_z = 2\pi \times 16$ rad/s, is designed and included in the open-loop model of the plant.

To get an initial indication regarding the usefulness of the HIGS-based bandpass filter in the context of skyhook damping, let us consider the open-loop system in Fig. 6.14, consisting of the system's transfer function in the z direction, the robustness filter H_{rob}, an integrator, used to obtain velocity information and a bandpass filter C_{bp}. The Bode diagram of the open-loop system in Fig. 6.14 for both cases where C_{bp} is given by the linear filter (6.10) and the describing function (6.16) of the HIGS-based bandpass filter is provided in Fig. 6.15. Here, the passbands of both bandpass filters are chosen to be $\omega \in 2\pi \times [0.2, 20]$rad/s. The rationale behind this choice will be explained in Section 6.5.3, below. As it can be seen in Fig. 6.15, due to the favorable phase properties of the HIGS-based bandpass filter, the frequency at which the open-loop system with the HIGS-based bandpass filter has a phase lag of 180 degrees is higher than that of the linear open-loop system. Moreover, at these frequencies the gain of the HIGS-controlled system is 5.5dB less than that of the linear case, resulting in a gain margin with

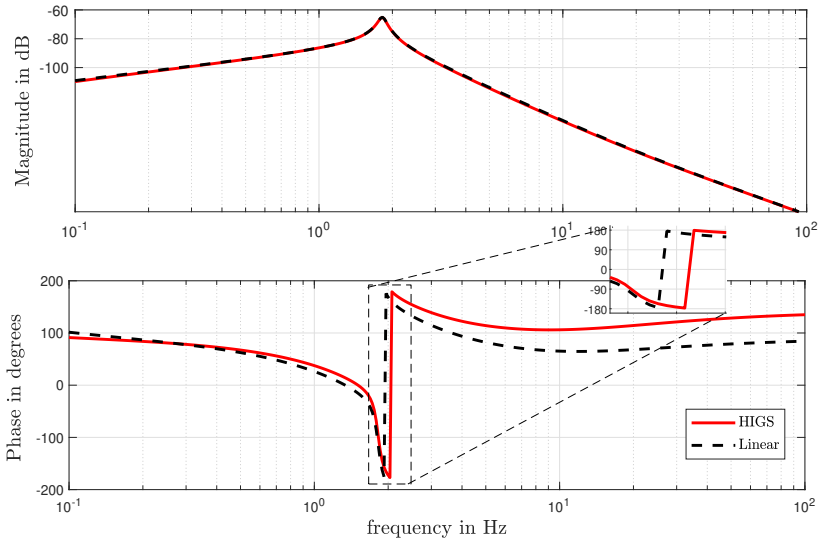

Figure 6.15. Frequency response of the open-loop system for both linear and HIGS-based controllers.

a factor 1.8 higher in the case of HIGS-based control. This in turn suggests the possibility of increasing the active damping gain with almost a factor 2 higher, in case of HIGS-based control (from a describing function perspective) when compared to the linear case, thereby enabling superior active vibration isolation. In what follows, this will be shown with measurement results, obtained from implementation of both linear and HIGS-based control strategies on the system in Fig. 6.11.

For the system in Fig. 6.11 a skyhook damping control strategy as shown in Fig. 6.16 is used in the z direction. Herein the vertical velocity $\dot{z}$ is obtained by integrating vertical acceleration $\ddot{z}$, which is measured by the accelerometers and fed to a bandpass filter C_{bp}. The output of the bandpass filter is subsequently multiplied with a gain β, which results in an active damping force, $F_{sky} = \beta\dot{z}$, proportional to the velocity of the metrology frame. Note that in addition to the skyhook damper, the feedback loop also contains a proportional feedback controller with gain K_a, which has the physical interpretation of virtual mass added to the metrology frame. The proportional controller is given by $K_a = 2.10\times10^{6}$Ns/m and is designed with the same rationale as explained in [17]. In what follows, we focus on the skyhook damper $\mathcal{C}_z^{sky}$ and compare the results obtained when, (i) C_{bp} is a linear bandpass filter of the form (6.10), (ii) C_{bp} is a HIGS-based bandpass filter with the structure shown in Fig. 6.4. Prior to doing so, we formulate conditions

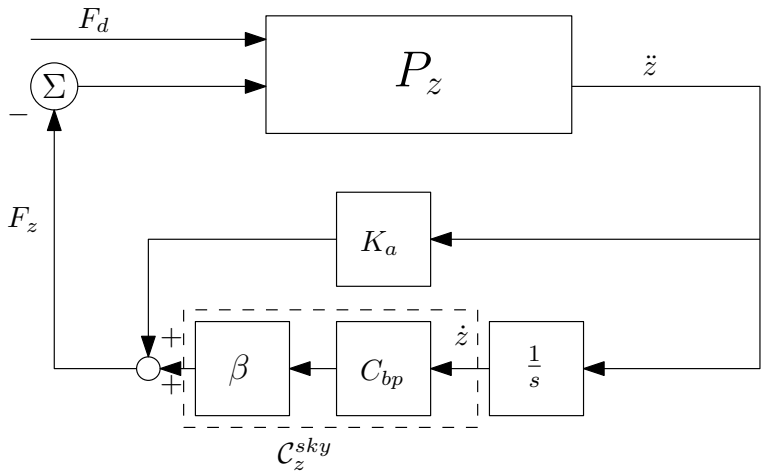

Figure 6.16. Block diagram of AVIS in the z direction, using acceleration feedback.

that can be used to certify stability of the system, considering both the discrete-time implementation of the nonlinear HIGS-based controller and the interaction between the dynamics in the principal coordinates (z, θ_x, θ_y).

6.5.2 Stability Analysis

Although in the design procedure, the interaction between the dynamics in the (z, θ_x, θ_y) coordinates are negligible, they should be taken into account for a rigorous stability analysis. Indeed, as shown in Fig. 6.17, while the system dynamics are strongly decoupled in the vertical directions of motion, measurements of frequency response functions reveal that there exists some interaction between the different input and output directions.

Noting that linear feedback controllers designed using the methodologies presented in [17], are used for stabilization of the dynamics in the θ_x and θ_y directions, it remains to investigate the stability of the system in the z direction, upon closing the loop with the skyhook HIGS-based controller. To this end, consider the interconnection in Fig. 6.18, where the effect of the plant inputs in the θ_x and θ_y directions denoted by $M_\theta := [M_x^\top \quad M_y^\top]^\top + [d_{\theta_x}^\top \quad d_{\theta_y}^\top]^\top$, is considered on the output in the z direction. In particular, one has

$$\dot{z} = \mathcal{P}_{zz}(u_z + d_z) + \underbrace{\begin{bmatrix}\mathcal{P}_{z\theta_x} & \mathcal{P}_{z\theta_y}\end{bmatrix}}_{\mathcal{P}_{\theta z}} \underbrace{\left(\begin{bmatrix}M_x \\ M_y\end{bmatrix} + \begin{bmatrix}d_{\theta_x} \\ d_{\theta_y}\end{bmatrix}\right)}_{M_\theta},$$

where $\mathcal{P}_{z\theta_x}$ and $\mathcal{P}_{z\theta_y}$, and $\mathcal{P}_{zz}$, denote the (closed-loop) transfers from $M_x + d_{\theta_x}$

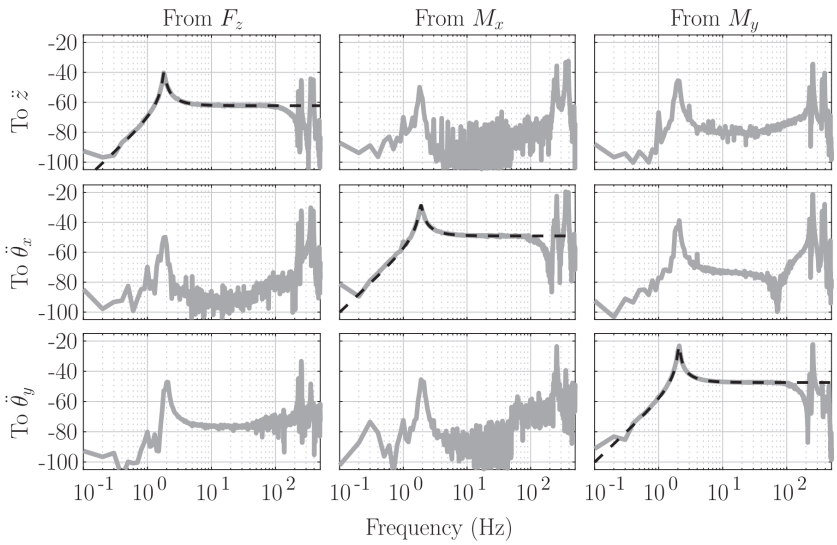

Figure 6.17. Measured (solid gray) and modelled (dashed black) plant dynamics in the vertical direction.

, $M_y + d_{\theta_y}$ and $u_z + d_z$ to the output in the z direction. Based on this reasoning, the linear plant $\mathcal{P}_z^{eq}$ seen by the skyhook damper in the z direction, denoted by $\mathcal{C}_z^{sky}$, which includes the dynamics in the z direction as well as interaction with other loops, is given by the transfer $\frac{\dot{z}}{u_z}$ for which the frequency response function (FRF) can be obtained from system identification [111].

In case $\mathcal{C}_z^{sky}$ is the HIGS-based skyhook damper as shown in Fig. 6.19, stability analysis of the closed-loop system should be handled with care given (i) the nonlinear HIGS-based controller is implemented in discrete-time and (ii) FRF measurements of $\mathcal{P}_z^{eq}$, are obtained by means of system identification and thus provide a discrete-time model of the underlying system. Note that $\mathcal{P}_z^{eq}$ contains dynamics of both the continuous-time plant to be controlled as well as linear discrete-time controllers. Therefore, the FRF measurements of $\mathcal{P}_z^{eq}$ do not contain information on the inter-sample behavior of the plant.

For the discrete-time implementation of the HIGS-based bandpass filter introduced in Section 6.3, use is made of the discrete-time HIGS element introduced in Section 5.3.2 of Chapter 5. As explained in there, the input-output pair of this discrete-time HIGS element satisfies the same sector bound as a continuous-time HIGS element and thus, the input-output pair of a HIGS-based bandpass filter as in Fig. 6.4, with $\mathscr{H}_1$ and $\mathscr{H}_2$, discrete-time HIGS elements, also satisfies the sector condition (6.13) (in discrete-time). This sector boundedness property, will play a key role in the main results of this section, stated in Theorem 6.5.1 below.

In analyzing stability of the system, we adopt the notion of input-to-state

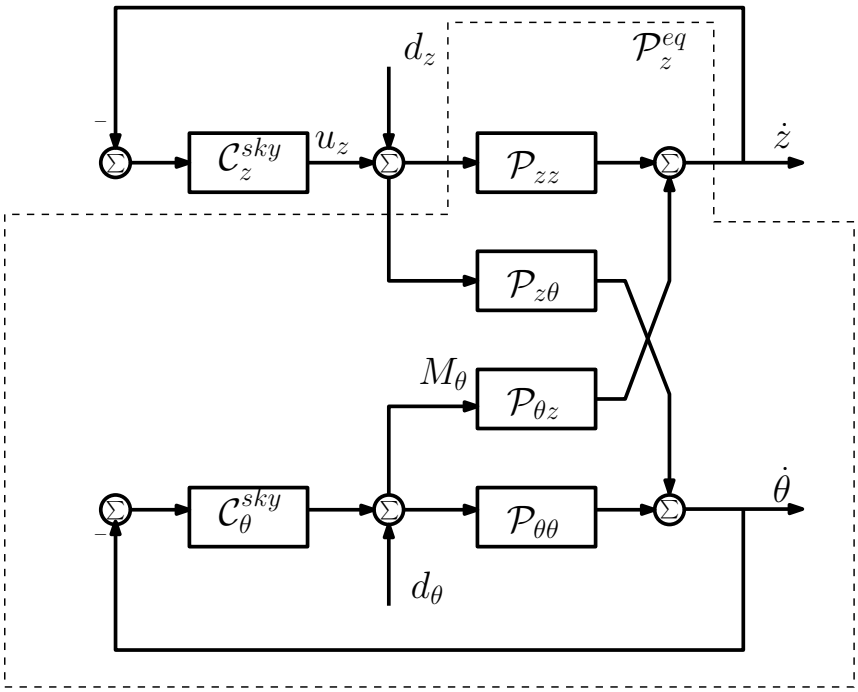

Figure 6.18. Block diagram of the system where the effect of the input M_θ (consisting of M_x and M_y) on the output in z direction is taken into account through the plant $\mathcal{P}_{\theta z}$ (consisting of $\mathcal{P}_{z\theta_x}$ and $\mathcal{P}_{z\theta_y}$).

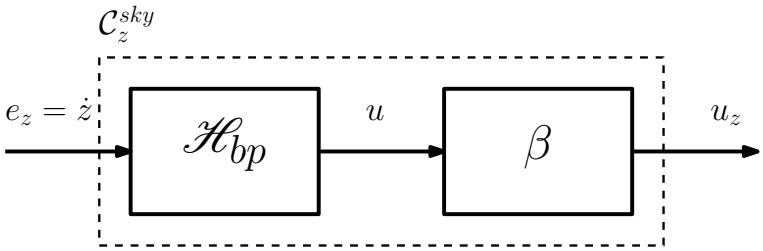

Figure 6.19. HIGS-based skyhook damper.

stability (ISS) as defined in [105].

Theorem 6.5.1. *Consider the system in Fig. 6.18 where $\mathcal{C}_z^{sky}$ is the HIGS-based skyhook damper in Fig. 6.19, constructed by the interconnection of discrete-time HIGS elements $\mathscr{H}_1$ and $\mathscr{H}_2$. Moreover $\mathcal{P}_z^{eq}$, contains the continuous-time plant to be controlled as well as discrete-time linear controllers, in the loop. The system is ISS with respect to bounded disturbances d_z if the following conditions are satisfied*

i) $\mathcal{P}_z^{eq}$ is stable;

ii) The FRF $\mathcal{P}_z^{eq}(e^{j\omega})$ satisfies

$$\frac{1}{\beta} + Re(\mathcal{P}_z^{eq}(e^{j\omega})) > 0 \text{ for all } \omega \in [0\ , 2\pi]. \tag{6.27}$$

Proof. The proof builds on similar arguments as used in proving Theorems 5.4.1 and 5.5.1 in Chapter 5 and can be summarized in the following main steps:

(i) First note that input-output pair (e_z, u_z) of the HIGS-based skyhook damper in Fig. 6.19 satisfies the sector condition

$$\frac{1}{\beta}u_z^2 \leq e_z u_z.$$

Indeed, it follows from (6.13) that $u^2 \leq e_z u$, and since $u = \frac{1}{\beta}u_z$, one has $\frac{1}{\beta}u_z^2 \leq e_z u_z$. Now consider a minimal state space realization of the discrete-time system $\mathcal{P}_z^{eq}(z)$, given by $(A_z^{eq}, B_z^{eq}, C_z^{eq})$, such that

$$\mathcal{P}_z^{eq}(z) = C_z^{eq}(zI - A_z^{eq})^{-1}B_z^{eq}.$$

with z a complex indeterminate. Note that condition ii) in the Theorem implies positive realness of $C_z^{eq}(zI-A_z^{eq})^{-1}B_z^{eq}+\frac{1}{\beta}$. This, together with the stability of $\mathcal{P}_z^{eq}$ due to item i), the minimality of the realization $(A_z^{eq}, B_z^{eq}, C_z^{eq})$, as well as the sector boundedness of the input-output pair of the HIGS-based skyhook damper, implies the existence of a quadratic ISS Lyapunov function $V_p(x_p) = x_p^\top P_p x_p$, with x_p the state of $\mathcal{P}_{eq}^z$, and $P_p \succ 0$ for $\mathcal{P}_{eq}^z$, with input u_z, by the virtue of the discrete-time Kalman Yakubovich Popov Lemma [25, 50, 113].

(ii) A quadratic Lyapunov-like function $V_h(x_{hbp}) = \frac{1}{2}x_{hbp}^2$, where x_{hbp} denotes the state of $\mathscr{H}_{bp}$ is constructed for $\mathscr{H}_{bp}$ in isolation, with $e_z = C_z^{eq}x_p$. By explicit use of the sector constraint of $\mathscr{H}_{bp}$ it is shown that the Lyapunov function decreases along the trajectories of the HIGS-based bandpass filter.

(iii) It can be shown that the functions V_g and V_h can be combined to construct an ISS Lyapunov function $V(x) = V_p(x_p) + \alpha V_h(x_{hbp}) = x^\top P_f x$, with $x = [x_p^\top \;\; x_{hbp}^\top]^\top$, and $P_f = \begin{bmatrix} P_p & 0 \\ 0 & \frac{1}{2}\alpha \end{bmatrix}$, with $0 < \alpha$ small enough, for the closed-loop system, thereby proving ISS of the system in discrete-time according to [85].

(iv) Lastly, given that in between sampling instances, the system has linear dynamics (since the nonlinear controller is only active in discrete-time), the intersample behavior of the plant can be bounded, thereby proving ISS of the sampled-data system consisting of the continuous-time plant to be controlled and the discrete-time controllers, in view of Theorem 6 in [106], thus completing the proof.

□

Note that condition i) in Theorem 6.5.1 is satisfied by design of the stabilizing controllers in the θ_x and θ_y directions. Thus, for verification of the stability of the system the system in Fig. 6.18, one has to verify condition ii) in the theorem.

For a given value of $\beta \in \mathbb{R}_{>0}$, checking condition ii), boils down to checking whether the Nyquist plot of $\mathcal{P}_{eq}^z(e^{j\omega})$ lies to the right of the vertical line passing through the point $\frac{-1}{\beta} + j0$ in the complex plane, for all $\omega \in [0, 2\pi]$. This is in fact a similar result as the Tsypkin-like criterion stated in Theorem 5.4.1 of Chapter 5 for a discrete time HIGS-controlled system containing a single HIGS element, extended to the case of the HIGS-based bandpass filter which contains two HIGS elements. While this Theorem offers the possibility of verifying stability based on measurements of frequency response data, and can be checked without a parametric model, it is expected to provide conservative results as it solely uses sector boundedness of the nonlinear HIGS-based controller and essentially discards its internal dynamics.

The Nyquist diagram of $\mathcal{P}_z^{eq}$ is shown in Fig 6.20 which depicts measured frequency response data of $\mathcal{P}_z^{eq}$. Based on Fig. 6.20 one concludes that condition ii) of Theorem 6.5.1 is satisfied for any $\beta < \frac{-1}{-0.1948} = 5.13$, and thus the system is ISS for any $\beta < 5.13$.

6.5.3 Experimental Results

In this section, we present experimental results obtained by HIGS-based skyhook damping applied to the industrial active vibration isolation system in Fig. 6.11, and compare the obtained performance with the case where a linear skyhook damper is utilized. Throughout the section, the passband of both the HIGS-based and the linear bandpass filters are designed to be $\omega \in 2\pi \times [0.2, 20]$ rad/s. Note that this frequency range is chosen, as it includes the natural frequency of the system in the vertical direction, given by $\omega = \sqrt{k/m}$ with k and m, the

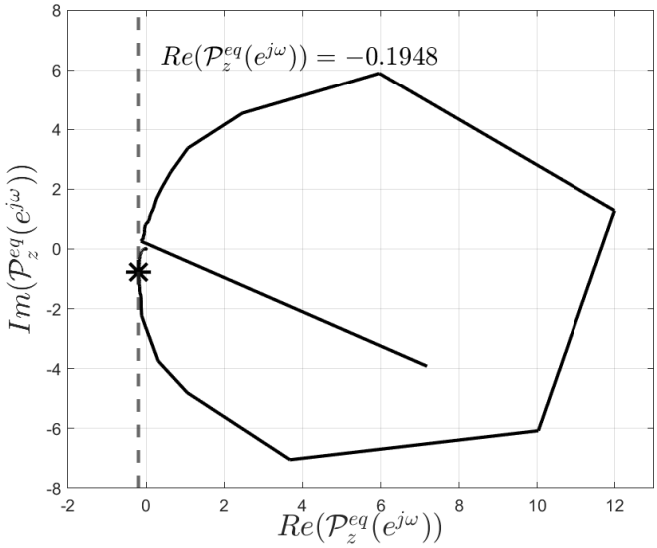

Figure 6.20. Nyquist diagram of $\mathcal{P}_z^{eq}$.

stiffness coefficient and mass, with the numerical values provided in Section 6.4, thereby enabling damping of the suspension mode present at this frequency. In addition, as shown in [17], the accelerometers suffer from measurement noise below $0.2 \times 2\pi$ rad/s, and thus, the passband of the filters are chosen such that frequency content below this value is not passed through to the output of the filters.

For ease of exposition, let us define the dimensionless skyhook damping gain $\zeta = (\beta/(2m\sqrt{k/m})) \times \alpha$, where β is the skyhook damping gain, m and k, denote the mass and stiffness of the system, respectively, and $\alpha = 148$ is a dimensionless gain, used in the implementation of the skyhook damper.

To investigate the sensitivity of the metrology frame with respect to floor vibrations, the ever present vibrations from the floor are used as an input source. The power spectral density (PSD) [111] of these input disturbances are then compared with the PSD of the accelerations of the metrology frame in the vertical direction, in order to investigate isolation of the metrology frame with respect to floor vibrations. The PSDs have been obtained using spectral analysis performed on data obtained with a sampling frequency of 4 kHz and a data record of ten minutes, split into sub-records of ten seconds. Each sub-record is then filtered using a Hanning window with a 50% overlap factor to compensate for data loss due to windowing. In Fig. 6.21, the total measured power in the accelerations of the base frame and metrology frame are shown as a function of the dimensionless skyhook damping gain ζ, for both the linear as well as the HIGS-based skyhook

damper. Note that for each ζ value, the measurements have been performed four times and averaged. The variance levels associated with the measurements are in the order of magnitude of 10^{-17} (m/s^2), indicating high repeatability of the results. Also let us note that while we present measurements for the HIGS-based skyhook damper up to a damping gain value of $\zeta = 7$, the measurements for the linear controller do not go beyond a gain of $\zeta = 4$. This is because, in case of the linear skyhook damper, the system becomes unstable beyond a value of $\zeta = 4$, while in case of HIGS-based control, the gain can be increased up to $\zeta = 7$, without compromising stability of the system. This indicates that with HIGS-based control one can use an active damping gain which is a factor 1.75 higher than the possibilities offered by linear control. Interestingly, a similar ratio of 1.8 was found based on the describing function of HIGS (see Fig. 6.14 and the related analysis), which demonstrates the anticipatory power of describing function analysis. This result is a clear consequence of the advantageous phase properties of the HIGS-based control expressed through increased gain margins. The ability to increase the value of active damping gain beyond levels possible in case of linear skyhook damping, suggests the possibility of obtaining superior skyhook damping using HIGS-based control (see also the discussion in Section 6.4). This observation also reveals that Theorem 6.5.1, used for stability analysis is, as expected, rather conservative as it guarantees stability for a maximum active damping gain value of $\beta = 5.13$, which is equivalent to $\zeta = 3.33$. Let us also remark that the noticeable difference between the total power of the accelerations of the base frame, in case of $\zeta = 7$, compared to the other active damping gain values is due to the experiments being done on a different day and thus under different environmental conditions. The measurements shown in Fig. 6.21 suggest no negative expression of non-linearity in the form of amplification of high-frequency dynamics of the plant. To enable a more detailed analysis, the cumulative PSD of accelerations of base, and metrology frames are shown in Fig. 6.22, for a fixed $\zeta = 4$.

As it can be seen from Fig. 6.22b, there is indeed no negative expression of nonlinearity, in the form of amplification of high-frequency dynamics of the plant, in the case of HIGS-based control. As a matter of fact, while in the case of HIGS-based control, the base frame has more input power, the power of the accelerations of the metrology frame are less in the HIGS-controlled system compared to linear case, indicating better isolation performance in the case of HIGS-based control.

To assess the sensitivity of system with respect to direct disturbances, an input disturbance, the cumulative power spectral density (PSD) of which is shown in Fig. 6.23, is used as an input to the system. The measured PSD of the accelerations of the metrology frame in the z direction, when $\zeta = 4$, are shown in Fig. 6.24, for both the linear and the HIGS-based skyhook damper. As it can be seen in Fig. 6.24, the HIGS-based skyhook damper achieves a better damping of the suspension mode, which can be attributed to the advantageous phase properties of the HIGS-based controller. To further study the performance of the different control strategies, the response of the system to a pulse input, applied to the metrology frame, as shown

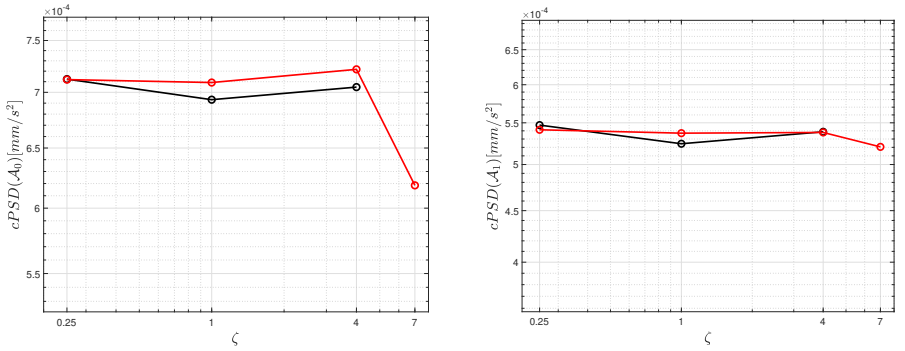

(a) **(b)**

Figure 6.21. Total power of measurements of the accelerations of (a) the base frame and (b) the metrology frame as a function of the dimensionless active damping gain ζ for, linear skyhook damper (black) and HIGS-based skyhook damper (red).

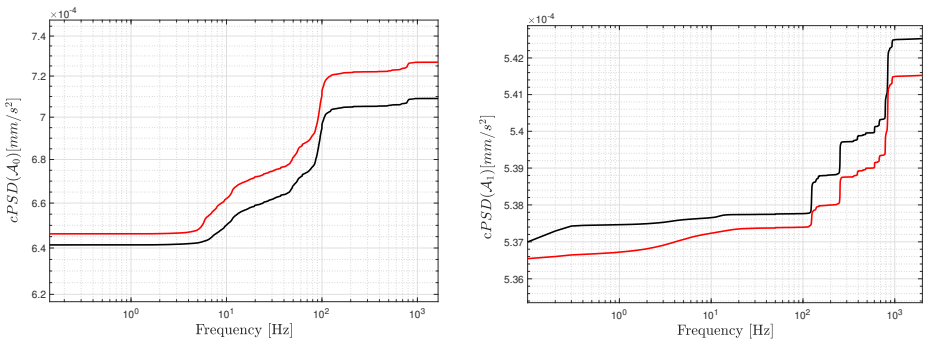

(a) **(b)**

Figure 6.22. Measured cumulative PSD of accelerations of (a) the base frame and (b) the metrology frame, for both linear skyhook damper (black) and HIGS-based skyhook damper (red), where $\zeta = 4$.

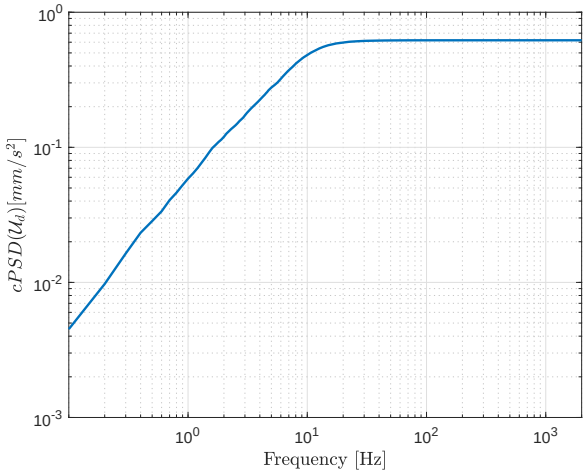

Figure 6.23. cPSD of direct disturbances put into the system.

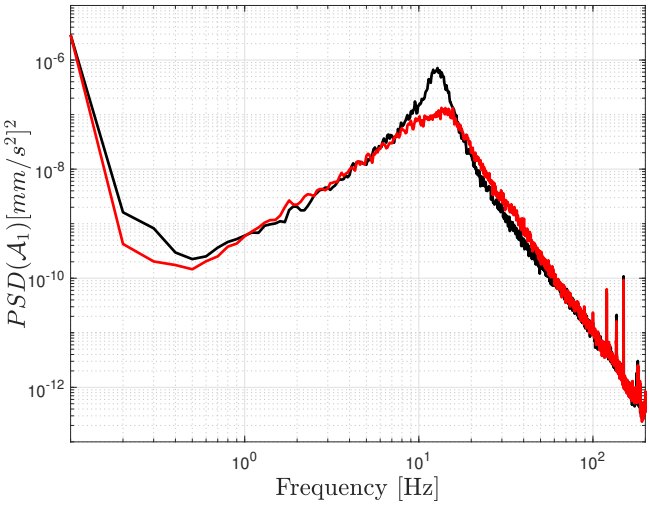

Figure 6.24. PSD of accelerations of the metrology frame for both linear (black) and HIGS-based (red) skyhook damper, with $\zeta = 4$.

by the dashed lines in Fig. 6.25 is studied, for dimensionless skyhook damping gain values $\zeta \in \{1, 4, 7\}$. Note that since with the linear control design, the

system becomes unstable beyond a dimensionless active damping gain of $\zeta = 4$, the experiments with $\zeta = 7$ are only performed with HIGS-based skyhook damper. As observed from Fig. 6.25, with $\zeta = 1$, similar responses are obtained for the

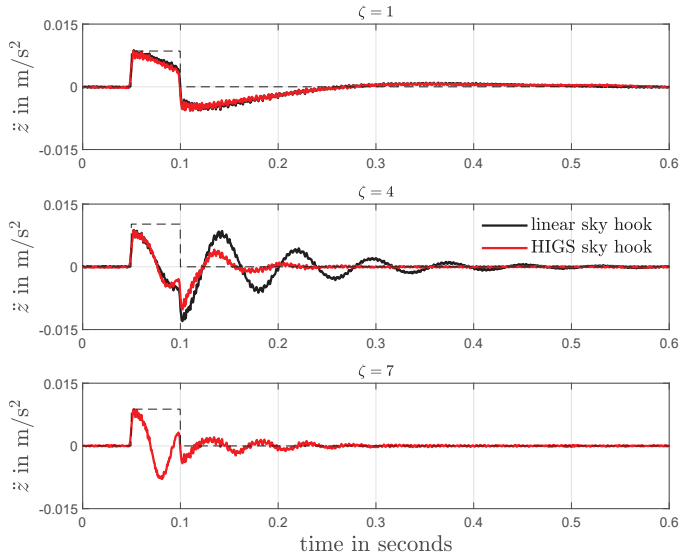

Figure 6.25. Measured responses of the system in Figure 6.11 in the vertical direction, when controlled with a linear skyhook damper (black) and a HIGS-based skyhook damper (red) to a pulse (dashed black) input.

HIGS-controlled and the linearly controlled case. As the skyhook damping gain is increased to $\zeta = 4$, the HIGS-based controller clearly outperforms the linear controller in terms of both overshoot and settling time, and also achieves better damping. In particular, the contribution of the peak around the frequency of 10 Hz, as seen in Fig. 6.24, is clearly visible in the response of the linear controller while in case of the HIGS-based skyhook damper a much better damped response is observed. Lastly, with $\zeta = 7$, an even better damped response is obtained, which clearly indicates the benefit of using the HIGS-based control strategy.

A more detailed analysis of the relation between the value of ζ and transient performance in terms of overshoot and settling time is performed and presented in Fig. 6.25. The upper and lower parts of the figure depict overshoot and settling time, respectively. Here, overshoot is defined as the percentage by which the maximum value $|\ddot{z}(t_o)|$, exceeds the final value $\ddot{z}(t_f)$ with $t_o \in [0, t_f)$ the instant of time at which $\ddot{z}(t_o)$ is reached. Moreover, settling time is defined as the time $t_s \in [0, t_f)$, such that $|\ddot{z}(t)|$ remains within 5% of $|\ddot{z}(t_f)|$ for all $t \in [t_s, t_f)$.

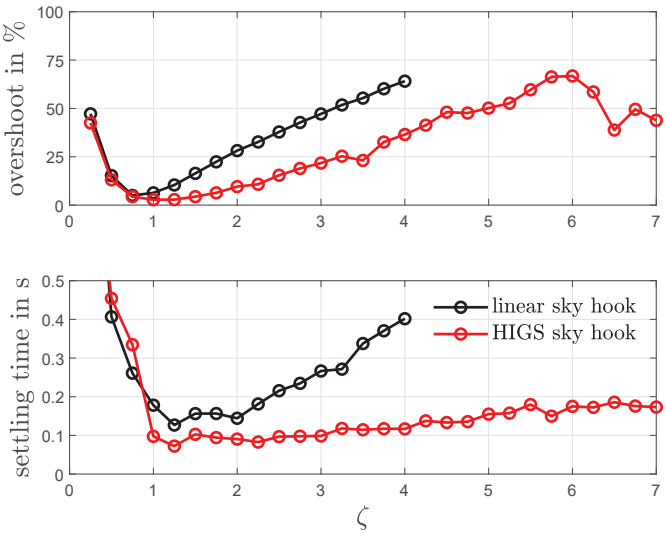

Figure 6.26. Overshoot and settling time as a function of active damping gain ζ.

A few observations can be made from Fig. 6.26. Firstly, for low values of the active damping gain $\zeta < 1$, the HIGS-based controller does not seem to outperform the linear controller. Thus for low values of ζ, utilizing a linear controller seems to be more natural as it avoids the complexities of design/analysis associated with the nonlinear HIGS element. However, for $\zeta \geq 1$ both metrics seem to improve by using the HIGS-based controller. As previously mentioned, beyond $\zeta = 4$, it is not possible to use the linear controller as the resulting closed loop becomes unstable, while with the HIGS-based design, one can increase the value of the skyhook damping gain as high as $\zeta = 7$ without destabilizing the closed-loop system. It should, however, be mentioned that although for $\zeta \geq 1$ both metrics of transient performance are more desirable with the HIGS-based design, it does not seem to be beneficial for transient performance to increase ζ beyond 1.25, as both overshoot and settling are minimal at $\zeta = 1.25$. However, as shown earlier the disturbance rejection properties are significantly enhanced by increasing skyhook damping gain values (see Fig. 6.24 and Fig. 6.25). As a result, it is concluded that with the HIGS-based design, one can obtain an enhanced vibration isolation by skyhook damping, while maintaining an adequate transient performance.

6.6 Summary and Conclusions

In this chapter, a novel hybrid control design for active vibration isolation by means of skyhook damping is presented. The proposed controller has been successfully implemented on an industrial active vibration isolation system and the resulting closed-loop performance has been compared to that of a linear controller, which is frequently used in such applications. We have also presented frequency-domain tools for analysis of stability of the system.

The experimental results indicate that for large enough active damping gain values, the hybrid controller offers the possibility of improving transient performance in terms of overshoot and settling time. For small active damping gain values, it is recommended to utilize linear controllers as the HIGS-based design does not seem to offer any performance improvements and would only add to the complexity of analysis and design of the closed loop system due to its nonlinear nature. Our results also indicate that the HIGS-based design yields larger stability margins, when compared to the linear controller, which in turn enables one to increase the active damping gain beyond what is possible with the linear controller, thereby enabling enhanced vibration isolation by means of skyhook damping without compromising stability and maintaining a reasonable transient behavior. Moreover, no negative expressions of nonlinearity in the form of amplification of high-frequency plant dynamics are observed, which favors utilization of HIGS-based control for active vibration isolation industries.

Future work will be focused on using HIGS-based controllers in multiple control loops, in order to further improve closed-loop performance.To this end, we intend to develop tools with low conservativeness for systematic analysis and design of controllers comprised of interconnections of HIGS elements.

7 Conclusions and recommendations

7.1 Conclusions

The central focus in this thesis is formed by so-called *Hybrid integrator-gain systems* (HIGS), which are hybrid control elements, recently introduced with the aim of overcoming fundamental performance limitations of LTI control. The introduction of HIGS was motivated by the desire to have a controller that offers similar performance enhancing benefits as reset control, while avoiding discontinuous control signals and hard resets. The presented results on HIGS vary from answering fundamental system theoretic questions to application-oriented work. The main conclusions related to the contributions presented in this dissertation are provided below.

7.1.1 Mathematical formalization and well-posedness

In Chapter 2 a new class of discontinuous dynamical systems called *extended projected dynamical systems* (ePDS) was introduced, which includes as a special case the class of projected dynamical systems (PDS) and broadens it by facilitating partial projection of dynamics onto constraint sets not previously considered in the PDS literature. While the introduction of ePDS is of interest on its own, it is, also instrumental in and, in fact, motivated by mathematical formalization of HIGS-controlled systems. Indeed, ePDS naturally capture the engineering philosophy behind the operation of HIGS. In addition, in Chapter 2, it was shown

that HIGS-controlled systems are well-posed in the sense of existence and forward completeness of solutions, under some regularity conditions on the exogenous inputs, thereby laying down a proper mathematical framework for formal studies of HIGS-controlled systems.

In Chapter 3 sufficient conditions were presented under which the introduced ePDS are equivalent to another recently introduced variant of PDS, namely oblique projected dynamical systems (oPDS), that allow for using non-Euclidean norms for projection of the dynamics. This equivalence is established in order to enable the transfer of system-theoretical tools and properties from one class to the other. It was shown how this equivalence can be used for obtaining sufficient conditions for properties such as incremental stability and convergence of ePDS. The equivalence conditions were also used for obtaining an oPDS-type representation for HIGS-controlled systems. Using this new oPDS representation, sufficient conditions were proposed for incremental stability of HIGS-controlled systems, using a novel construction of piece-wise quadratic Lyapunov functions. While such conditions were already established in [140], our results serve as an alternative that exploits the "projection-based" nature of HIGS-controlled systems.

7.1.2 Overcoming fundamental limitations of LTI control

One of the main motivations of using nonlinear/hybrid control strategies is to overcome fundamental performance limitations inherently connected with LTI control techniques. As such, with the introduction of a new hybrid control element such as HIGS, the question naturally arises whether one can overcome (some or all of) these limitations using HIGS-based control. In Chapter 4, we considered some fundamental limitations of LTI feedback control and showed that by using HIGS, these limitations can be overcome, which clearly illustrates the strength and potential of HIGS-based control. The results presented in Chapter 4 aid the adoption of HIGS by control practitioners as they show genuine, performance enhancing advantages over LTI control.

7.1.3 Discrete-time and sampled-data HIGS

In Chapter 5, motivated by the fact that nowadays controllers are implemented digitally, and thus, in discrete-time, discrete-time HIGS elements were introduced. These discrete-time HIGS elements share the same philosophy of operation as continuous-time HIGS elements and preserve their main characteristics. For discrete-time HIGS-controlled systems consisting of linear plants to be controlled and discrete-time HIGS-based controllers, stability criteria were presented that can be used to certify discrete-time input-to-state stability. These criteria are based on (i) (easy to measure) frequency response data, and (ii) feasibility of a set of linear matrix inequalities (LMIs). While the frequency-domain conditions can be verified graphically and without the need for parametric models, the LMIs pro-

vide much less conservative results. In fact, the frequency domain conditions are guaranteed to be more conservative since their satisfaction implies feasibility of a special case of the LMIs.

Additionally, following a discrete-time design approach, it was shown that the satisfaction of the presented discrete-time stability criteria, implies ISS of sampled-data systems, consisting of continuous-time LTI plants to be controlled and discrete-time HIGS-based controllers, interfaced with sampler and zero-order-hold (ZOH) devices. Moreover, in Chapter 5 , it was shown that the presented frequency-domain stability criterion can be used in a continuous-time design approach as well, to conclude stability of sampled-data HIGS-controlled systems. That is, if the continuous-time plant model satisfies the required conditions, under fast sampling, the ZOH discretization of the plant also satisfies them and thus the conditions can also be used for verifying stability using the continuous-time model of the plant.

7.1.4 HIGS-based active vibration control

In order to demonstrate the potential of HIGS-based control design beyond theoretical and simulation-based studies, in Chapter 6, we presented a novel HIGS-based controller design and illustrated its effectiveness in the context of active vibration control. In particular, a HIGS-based skyhook damping strategy was presented, which was shown to have superior performance compared to its LTI counterpart, as illustrated by experimental results obtained from an industrial active vibration isolation system. Key in achieving this superior performance were the advantageous phase properties of HIGS, which in turn allow for providing more active damping to the system without compromising stability. The performance of the controllers was assessed in terms of frequency-domain metrics as is commonly used in active vibration isolation control, as well as in metrics of transient performance. The results clearly reflect the superiority of the HIGS-based controller in achieving higher gains for active damping while showing no negative expression of nonlinearity, in the form of additional excitation of high-frequency dynamics of the plant.

The design approach followed in Chapter 6 is similar to one often followed in industrial practice. In particular, although the design of the controller was done based on continuous-time tools and insights, tools were provided for stability analysis of the sampled-data system under consideration, such that rigorous stability guarantees were obtained.

7.2 Recommendations

Although several important research questions were answered in this thesis, there are still many unexplored research directions related to HIGS and HIGS-based control. In addition, based on the work presented in this thesis, there might be

possible extensions and generalizations worth working towards. The objective of this section is to provide recommendations for future work and to propose possible starting points.

7.2.1 Recommendations for Mathematical formalization and well-posedness

In Chapter 2, the new class of ePDS was introduced and used for formalization of HIGS-controlled systems. There are several future directions of research worth delving into for ePDS. To start with, in Chapter 2, we consider constraint sets that satisfy certain assumptions (as listed in Assumption 2.3.1). While the conditions in Assumption 2.3.1 are capable of describing constraint sets such as sector conditions that are needed in the context of HIGS and similar control elements, in order to enable the study of a broader range of systems in the ePDS framework, relaxation of these assumptions forms an interesting direction of future research. In addition, in Chapter 2, we presented the ePDS formalization of HIGS-controlled systems consisting of a single HIGS element. As it has been shown, e.g., in Chapter 6, HIGS-based controllers consisting of multiple HIGS elements can lead to improved performance (see also [140] for more examples of HIGS-based controllers consisting of multiple HIGS elements), and thus it is also of interest to consider projection-based formalizations of control loops consisting of multiple HIGS elements.

The introduction of the class of ePDS, was motivated by capturing the engineering philosophy of HIGS, i.e., combining the operation of an LTI integrator with a projection operator, to enhance performance. It is also of interest to study the combination of other LTI control elements with projection operators and further explore the performance enhancing properties of such "projection-based" control schemes.

The work presented in Chapter 2 provides a formal mathematical framework for studying closed-loop systems that contain a HIGS element. Formalization of open-loop HIGS is also of interest, as it may prove instrumental for, e.g., formalization of closed-loop systems containing multiple HIGS elements.

The well-posedness results presented in Chapter 2 considered exogenous inputs that belong to the class of piecewise Bohl (PB) functions. Establishing well-posedness beyond PB inputs, e.g., for Lebesgue measurable inputs, is an interesting topic of future research. In addition, uniqueness of solutions, with the exception of cases where incremental stability can be established, remains a completely open issue. Note that in Chapter 2 solutions are considered in Carathéodory sense. One interesting direction of research would be to consider the Krasovskii regularization of HIGS-controlled systems for broader input classes and investigate whether the resulting Krasvoskii solutions coincide with the Carathéodory solutions of the system.

For establishing equivalence between ePDS and oPDS, the work presented in Chapter 3 considered constraint sets that are convex polyhedral cones. A clear

future direction of research is establishing equivalence conditions for more general classes of constraint sets. Regarding the conditions presented for incremental stability of HIGS-controlled systems, where we have utilized this equivalence result, reducing the conservatism associated with the conditions is an important topic of future research.

7.2.2 Recommendations for overcoming fundamental limitations of LTI control

Overcoming fundamental performance limitations of LTI control using HIGS, as presented in Chapter 4 is done by considering examples wherein certain performance objectives are impossible to achieve with any LTI controller, and subsequently demonstrating that by employing HIGS-based control these objectives can be accomplished. Although our work does include design insights and working principles, it would be of interest to develop systematic design/synthesis procedures for overcoming fundamental limitations of LTI control using hybrid control in general, and HIGS in particular.

7.2.3 Recommendations for sampled-data HIGS

Regarding discrete-time and sampled-data HIGS-controlled systems, there are several directions for future work. The work presented in Chapter 5, mainly focuses on stability analysis of sampled-data HIGS-controlled systems via the discrete-time design approach. However, the proposed discrete-time HIGS can be used in all the other approaches for sampled-data control design/analysis, being continuous-time design (CTD) and sampled-data design (SDD), as well (see Fig. 7.1 below). For CTD, one important direction of research would be proving consistency of the discrete-time HIGS elements, in the sense that the interpolated solutions of discrete-time HIGS converge to a solution to continuous-time HIGS, as the sampling time goes to zero [62]. As the analysis results presented in Chapter 5 are concerned with stability, it would also be interesting to propose tools for assessing performance of sampled-data HIGS-based control, wherein the effect of intersample behavior of the plant on the performance is considered. A potentially interesting direction would be multirate control [44, 108, 152] with HIGS. It is also of interest to develop tools for direct synthesis of sampled-data HIGS-based controllers which provide stability and performance guarantees in the sampled-data setting.

7.2.4 Recommendations for HIGS-based control design

The design of the HIGS-based active vibration isolation control strategy presented in Chapter 6 was done in the frequency domain, based on the describing function approximation of HIGS. In order to further facilitate frequency-domain design of

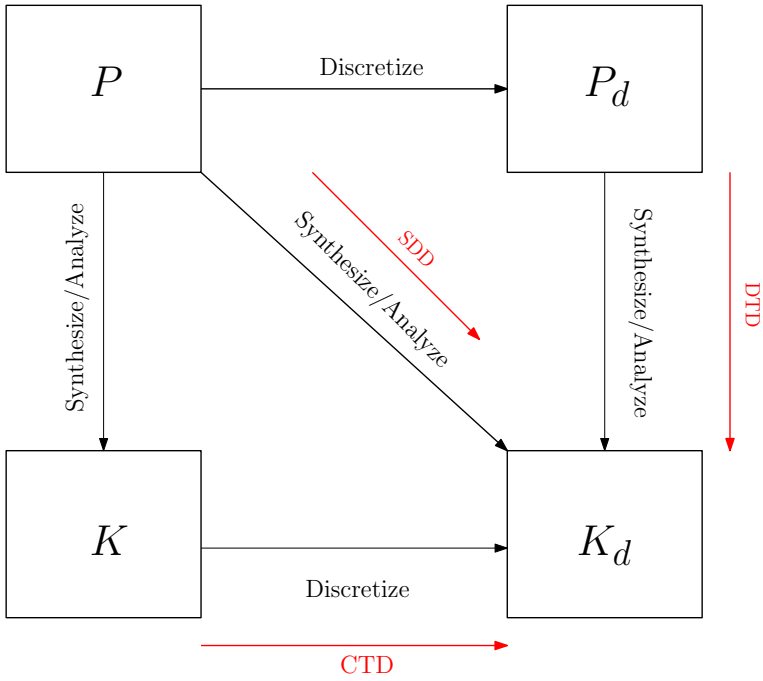

Figure 7.1. The three main approaches for sampled-data control.

HIGS-based controllers in a manner, which is easy to integrate in current industrial practice, it is highly interesting to develop more rigorous tools for nonlinear loopshaping designs. A potentially interesting approach in developing such tools would be using the notion of scaled relative graphs which has been shown to be useful in creation of graphical analysis tools for nonlinear systems [28]. In Chapter 6 we also presented a stability result, which exploits knowledge of the particular structure used in the creation of the HIGS-based bandpass filter, being a controller comprised of multiple HIGS elements. It is also of interest to develop stability analysis methodologies for more general interconnections consisting of multiple HIGS elements that scale well and are computationally tractable. One possible direction for development of such scalable tools is compositional analysis [8, 98], wherein dissipativity properties of individual sub-systems in an interconnection and the interconnection properties, are used to conclude on the dissipativity properties of the overall system.

In Chapter 6, we have considered HIGS-based control in a multi-loop SISO control context. Developing dedicated design/synthesis tools for multivariabe HIGS-based control is a highly interesting and challenging topic of future research too. A potential approach would be developing design/synthesis tools by adopting the

frequency domain approximation of HIGS, based on describing function analysis, along with an additional uncertainty model that captures the effect of higher-order harmonics.

7.2.5 Final words

Automatic control is an essential technology for the optimisation, regulation and stabilization of vital engineering systems in the modern society. In several industrial sectors, LTI control techniques are widely utilized to ensure desired operation of the involved processes and systems. These control techniques, while powerful, suffer from fundamental limitations that can be potentially overcome by hybrid and nonlinear control strategies. The work presented in this dissertation, has focused on a particular hybrid control element called HIGS and contains contributions with respect to a number of important topics of research for this new control element. The author closes the thesis with the hope that the presented contributions spark the interest of the scientific control community for future research on HIGS, and lead to the adoption of HIGS-based control techniques in control engineering practice.

Bibliography

[1] W. Aangenent and R. de Jong. Time domain performance based nonlinear state feedback control of constrained linear systems. (October):1–3, 2007.

[2] W. H. T. M. Aangenent, G. Witvoet, W.P.M.H. Heemels, M.J.G. van de Molengraft, and M. Steinbuch. Performance analysis of reset control systems. *International Journal of Robust and Nonlinear Control*, 20:1213–1233, June 2010.

[3] K. Abidi and A. Sabanovic. Sliding-mode control for high-precision motion of a piezostage. *IEEE Transactions on Industrial Electronics*, 54(1):629–637, 2007.

[4] V. Acary and B. Brogliato. *Numerical methods for nonsmooth dynamical systems: applications in mechanics and electronics*. Springer Science & Business Media, 2008.

[5] E. D. Andersen, C. Roos, and T. Terlaky. On implementing a primal-dual interior-point method for conic quadratic optimization. *Mathematical Programming*, 95(2):249–277, 2003.

[6] K.H. Ang, G. Chong, and Y. Li. PID control system analysis, design, and technology. *IEEE Transactions on Control Systems Technology*, 13(4):559–576, 2005.

[7] D. Angeli. A Lyapunov approach to incremental stability properties. *IEEE Transactions on Automatic Control*, 47(3):410–421, 2002.

[8] M. Arcak, C. Meissen, and A.K. Packard. *Networks of dissipative systems: compositional certification of stability, performance, and safety*. Springer, 2016.

[9] K. Åström and B. Wittenmark. *Computer-controlled systems: theory and design*. Prentice Hall, Information and System Sciences Series, 1997.

[10] K. J. Åström. Automatic control—the hidden technology. In *Advances in control*, pages 1–28. Springer, 1999.

[11] J.P. Aubin and A. Cellina. *Differential inclusions: set-valued maps and viability theory*. Springer-Verlag Berlin Heidelberg New York Tokyo, 1984.

[12] A. Baños and A. Barreiro. *Reset Control Systems*. Advances in Industrial Control. Springer London, London, 2012.

[13] A. Baños, F. Perez, and J. Cervera. Network-based reset control systems with time-varying delays. *IEEE Transactions on Industrial informatics*, 10(1):514–522, 2013.

[14] A. Barreiro and A. Baños. Delay-dependent stability of reset systems. *Automatica*, 46(1):216–221, 2010.

[15] R. Beerens, A. Bisoffi, L. Zaccarian, W.P.M.H. Heemels, H. Nijmeijer, and N. van de Wouw. Reset integral control for improved settling of pid-based motion systems with friction. *Automatica*, 107:483–492, 2019.

[16] R. Beerens, A. Bisoffi, L. Zaccarian, H. Nijmeijer, W.P.M.H. Heemels, and N. van de Wouw. Reset PID design for motion systems with stribeck friction. *IEEE Transactions on Control Systems Technology*, 30:294–310, January 2022.

[17] M. A. Beijen, M. F. Heertjes, H. Butler, and Maarten Steinbuch. Mixed feedback and feedforward control design for multi-axis vibration isolation systems. *Mechatronics*, 61:106–116, 8 2019.

[18] O. Beker, C.V. Hollot, and Y. Chait. Plant with integrator: an example of reset control overcoming limitations of linear feedback. *IEEE Transaction on Automatic Control*, 46(11):1797–1799, 2001.

[19] O. Beker, C.V. Hollot, Y. Chait, and H. Han. Fundamental properties of reset control systems. *Automatica*, 40(6):905–915, 2004.

[20] R. Bertollo, A.R. Teel, and L. Zaccarian. Soft-reset control with max-of-quadratics Lyapunov certificates. *IEEE Transactions on Automatic Control*, pages 1–13, 2022.

[21] O. Bosgra, H. Kwakernaak, and G. Meinsma. Design methods for control systems. *Notes for a Course of the Dutch Institute of Systems and Control*, 2001.

[22] S. Boyd, L. El Ghaoui, E. Feron, and V. Balakrishnan. *Linear Matrix Inequalities in System and Control Theory*. Society for Industrial and Applied Mathematics, 1994.

[23] S. Boyd and L. Vandenberghe. *Convex optimization*. Cambridge university press, 2004.

[24] B. Brogliato, A. Daniilidis, C. Lemaréchal, and V. Acary. On the equivalence between complementarity systems, projected systems and differential inclusions. *Systems & Control Letters*, 55(1):45–51, 2006.

[25] B. Brogliato, R. Lozano, B. Maschke, and O. Egeland. Dissipative systems analysis and control. *Theory and Applications*, 2:2–5, 2007.

[26] H. Butler. Position control in lithographic equipment [applications of control]. *IEEE Control Syst. Mag.*, 31(5):28–47, 2011.

[27] J. Carrasco and E. Navarro-López. Towards l_2-stability of discrete-time reset control systems via dissipativity theory. *Systems & Control Letters*, 62(6):525–530, 2013.

[28] T. Chaffey, F. Forni, and R. Sepulchre. Graphical nonlinear system analysis. *arXiv preprint arXiv:2107.11272*, 2021.

[29] Y. Chait and C. V. Hollot. On Horowitz's contributions to reset control. *International Journal of Robust and Nonlinear Control*, 12(4):335–355, 2002.

[30] T. Chen and B. Francis. *Optimal sampled-data control systems*. Springer, 1995.

[31] J.C. Clegg. A nonlinear integrator for servomechanisms. *Transactions of the American Institute of Electrical Engineers, Part II: Applications and Industry*, 77(1):41–42, 1958.

[32] A.T.J.R. Cobbenhagen, D.J. Antunes, M.J.G. van de Molengraft, and W.P.M.H. Heemels. Opportunities for control engineering in arable precision agriculture. *Annual Reviews in Control*, 51:47–55, 2021.

[33] B. Cornet. Existence of slow solutions for a class of differential inclusions. *Journal of mathematical analysis and applications*, 96(1):130–147, 1983.

[34] J. Cortes. Discontinuous dynamical systems. *IEEE Control Systems Magazine*, 28(3):36–73, 2008.

[35] A. Ahmadi Dastjerdi, A. Astolfi, N. Saikumar, N. Karbasizadeh, D. Valerio, and S. H. HosseinNia. Closed-loop frequency analysis of reset control systems. *IEEE Transactions on Automatic Control*, pages 1–8, 2022.

[36] D.A. Deenen. Design and analysis of the hybrid integrator with gain-switching functionality. Master Thesis, Eindhoven University of Technology.

[37] D.A. Deenen, M.F. Heertjes, W.P.M.H. Heemels, and H. Nijmeijer. Hybrid integrator design for enhanced tracking in motion control. In *2017 American Control Conference*, pages 2863–2868. IEEE, 2017.

[38] D.A. Deenen, B. Sharif, S.J.A.M. van den Eijnden, H. Nijmeijer, W.P.M.H. Heemels, and M.F. Heertjes. Projection-Based Integrators for Improved Motion Control: Formalization, Well-posedness and Stability of Hybrid Integrator-Gain Systems. *Automatica*, 2021.

[39] H.J. Dreef and M.C.F. Donkers. H_∞ and H_2 optimal sampled-data controller synthesis: A hybrid systems approach with mixed discrete/continuous specifications. *Automatica*, 125:109382, 2021.

[40] P. Dupuis and A. Nagurney. Dynamical systems and variational inequalities. *Annals of Operations Research*, 44(1):7–42, 1993.

[41] M. A. Echter, C. D. Roll, A. D. Keene, and J. D. Ellis. Carrier fringe analysis algorithms for three degree of freedom optical probing. *Precision Engineering*, 38(4):893–902, 2014.

[42] G. Ferrari-Trecate, F.A. Cuzzola, D. Mignone, and M. Morari. Analysis of discrete-time piecewise affine and hybrid systems. *Automatica*, 38(12):2139–2146, 2002.

[43] A. Feuer, G. Goodwin, and M. Salgado. Potential benefits of hybrid control for linear time invariant plants. In *1997 American Control Conference*, pages 2790–2794. IEEE, 1997.

[44] A. Feuer and G. C. Goodwin. *Multirate Control*, pages 477–500. Birkhäuser Boston, Boston, MA, 1996.

[45] W.C. Foster, D.L. Gieseking, and W.K. Waymeyer. A nonlinear filter for independent gain and phase (with applications). *Journal of Basic Engineering*, 88(2):457–462, 1966.

[46] G.F. Franklin, J.D. Powell, and A. Emami-Naeini. *Feedback control of dynamic systems*, volume 3.

[47] J. Freudenberg and D. Looze. *Frequency domain properties of scalar and multivariable feedback systems*. Springer.

[48] J. Freudenberg, R. Middleton, and A. Stefanpoulou. A survey of inherent design limitations. In *2000 American Control Conference ACC*, pages 2987–3001. IEEE, 2000.

[49] P. Gahinet and P. Apkarian. A linear matrix inequality approach to H_∞ control. *International journal of robust and nonlinear control*, 4(4):421–448, 1994.

[50] W. Gao and Y. Zhou. *Some necessary and sufficient conditions for discrete-time postive real matrices*. Department of mathematics, Stockholm University, 2006.

[51] A. Gelb and W.E. Vander Velde. *Multiple-Input Describing Functions and Nonlinear System Design*. McGraw Hill, 1968.

[52] R. Goebel, R.G. Sanfelice, and A.R. Teel. *Hybrid Dynamical Systems: modeling, stability, and robustness*. Princeton University Press, 2012.

[53] J. Groenewegen. The unknown potential of the dutch economy. *Rabobank*, 2016.

[54] L. Grüne and C.M. Kellett. ISS-Lyapunov functions for discontinuous discrete-time systems. *IEEE Transactions on Automatic Control*, 59(11):3098–3103, 2014.

[55] K. Gruntjens, M.F. Heertjes, S. van Loon, N. van De Wouw, and W.P.M.H. Heemels. Hybrid integral reset control with application to a lens motion system. In *American Control Conference 2019, Philadelphia, USA*, pages 2408–2413, 2019.

[56] Y. Guo, Y. Wang, L. Xie, and J. Zheng. Stability analysis and design of reset systems: Theory and an application. *Automatica*, 45(2):492–497, 2009.

[57] A. Hauswirth, S. Bolognani, and F. Dorfler. Projected dynamical systems on irregular, non-Euclidean domains for nonlinear optimization. *SIAM Journal on Control and Optimization*, 59(1):635–668, 2021.

[58] A. Hauswirth, S. Bolognani, G. Hug, and F. Dörfler. Projected gradient descent on riemannian manifolds with applications to online power system optimization. In *2016 54th Annual Allerton Conference on Communication, Control, and Computing (Allerton)*, pages 225–232. IEEE, 2016.

[59] A. Hauswirth, I. Subotić, S. Bolognani, G. Hug, and F. Dörfler. Time-varying projected dynamical systems with applications to feedback optimization of power systems. In *2018 IEEE Conference on Decision and Control (CDC)*, pages 3258–3263. IEEE, 2018.

[60] L. Hazeleger, M.F. Heertjes, and H. Nijmeijer. Second-order reset elements for stage control design. In *2016 American Control Conference*, pages 2643–2648. IEEE, 2016.

[61] W. Heemels. *Linear complementarity systems: a study in hybrid dynamics*. PhD thesis, 1999.

[62] W. P. M. H. Heemels, V. Sessa, F. Vasca, and M. K. Camlibel. Computation of periodic solutions in maximal monotone dynamical systems with guaranteed consistency. *Nonlinear Analysis: Hybrid Systems*, 24:100–114, 2017.

[63] W.P.M.H. Heemels, P. Bernard, K. Scheres, R. Postoyan, and R.G. Sanfelice. Hybrid systems with continuous-time inputs: Subtleties in solution concepts and existence results. In *IEEE Conference on Decision and Control (CDC) 2021, Austin (Texas), USA*, 2021.

[64] W.P.M.H. Heemels, M.K. Camlibel, and M.F. Heertjes. Oblique projected dynamical systems and incremental stability under state constraints. *IEEE Control Systems Letters*, 4:1060–1065, 2020.

[65] W.P.M.H. Heemels, G.E. Dullerud, and A.R. Teel. L2-gain analysis for a class of hybrid systems with applications to reset and event-triggered control: A lifting approach. *IEEE Trans. Automat. Contr.*, 61:2766–2781, 2016.

[66] W.P.M.H. Heemels, J.M. Schumacher, and S. Weiland. Linear complementarity systems. *SIAM Journal on Applied Mathematics*, 60:1234–1269, 2000.

[67] W.P.M.H. Heemels, J.M. Schumacher, and S. Weiland. Projected dynamical systems in a complementarity formalism. *Operations Research Letters*, 27:83–91, 2000.

[68] W.P.M.H. Heemels and S. Weiland. Input-to-state stability and interconnections of discontinuous dynamical systems. *Automatica*, 44(12):3079–3086, 2008.

[69] M. F. Heertjes, I. H. Sahin, N. van de Wouw, and W. P. M. H. Heemels. Switching control in vibration isolation systems. *IEEE Transactions on Control Systems Technology*, 21(3):626–635, 2012.

[70] Marcel F. Heertjes and Yasemin Vardar. Self-tuning in Sliding Mode Control of High-Precision Motion Systems. In *Proceedings of the 6th IFAC Symposium on Mechatronic Systems*, pages 13–19, Hangzhou, China, 2013.

[71] M.F. Heertjes, K.G.J. Gruntjens, S.J.L.M. van Loon, N. Kontaras, and W.P.M.H. Heemels. Design of a variable gain integrator with reset. In *American Control Conference (ACC) 2015, Chicago, USA*, pages 2155–2160, 2015.

[72] M.F. Heertjes, K.G.J. Gruntjens, S.J.L.M. van Loon, N. van de Wouw, and W.P.M.H. Heemels. Experimental evaluation of reset control for improved stage performance. In *12th IFAC International Workshop on Adaptation and Learning in Control and Signal Processing 2016, Eindhoven, Netherlands*, pages 93–98, 2016.

[73] M.F. Heertjes, N. Irigoyen Perdiguero, and D.A. Deenen. Robust control and data-driven tuning of a hybrid integrator-gain system with applications to wafer scanners. *International Journal of Adaptive Control and Signal Processing*, 2018.

[74] M.F. Heertjes and M. Steinbuch. Stability and performance of a variable gain controller with application to a dvd storage drive. *Automatica*, 40(4):591–602, apr 2004.

[75] M.F. Heertjes, S.J.A.M. van den Eijnden, B. Sharif, W.P.M.H. Heemels, and H. Nijmeijer. Hybrid integrator-gain system for active vibration isolation with improved transient response. *IFAC-PapersOnLine*, 52(15):454–459, 2019.

[76] C. Henry. An existence theorem for a class of differential equations with multivalued right-hand side. *Journal of Mathematical Analysis and Applications*, 41(1):179–186, 1973.

[77] J. P. Hespanha. *Linear systems theory*. Princeton university press, 2009.

[78] J.B. Hiriart-Urruty and C. Lemaréchal. *Convex analysis and minimization algorithms I: Fundamentals*, volume 305. Springer science & business media, 2013.

[79] I. Horowitz and P. Rosenbaum. Non-linear design for cost of feedback reduction in systems with large parameter uncertainty. *International Journal of Control*, 21(6):977–1001, 1975.

[80] B. Hunnekens, N. van De Wouw, M.F. Heertjes, and H. Nijmeijer. Synthesis of variable gain integral controllers for linear motion systems. *IEEE Trans. Control Syst. Technol.*, 23(1):139–149, 2015.

[81] B. G. B. Hunnekens, N. van de Wouw, and D. Nešić. Overcoming a fundamental time-domain performance limitation by nonlinear control. *Automatica*, 67:277–281, May 2016.

[82] B.G.B. Hunnekens. *Performance optimization of hybrid controllers for linear motion systems*. PhD thesis, Mechanical Engineering, 2015.

[83] J. Imura and A. van der Schaft. Characterization of well-posedness of piecewise-linear systems. *IEEE Transactions on Automatic Control*, 45(9):1600–1619, 2000.

[84] K. Iwaya, R. Shimizu, T. Hashizume, and T. Hitosugi. Systematic analyses of vibration noise of a vibration isolation system for high-resolution scanning tunneling microscopes. *Review of Scientific Instruments*, 82(8):083702, 2011.

[85] Z. Jiang and Y. Wang. Input-to-state stability for discrete-time nonlinear systems. *Automatica*, 37(6):857–869, 2001.

[86] A. Jokic, M. Lazar, and P.P.J. van den Bosch. On constrained steady-state regulation : Dynamic KKT controllers. *IEEE Transactions on Automatic Control*, 54(9):2250–2254, 2009.

[87] C.G. Kang. Origin of stability analysis: " on governors" by JC Maxwell [historical perspectives]. *IEEE Control Systems Magazine*, 36(5):77–88, 2016.

[88] H.K. Khalil. *Nonlinear systems*, volume 3. Prentice hall, Upper Saddle River, 2002.

[89] K.R. Krishnan and I.M. Horowitz. Synthesis of a non-linear feedback system with significant plant-ignorance for prescribed system tolerances†. *Int. J. Control*, 19(4):689–706, apr 1974.

[90] D.S. Laila, D. Nešić, and A. Astolfi. Sampled-data control of nonlinear systems. In *Advanced topics in control systems theory*, pages 91–137. Springer, 2006.

[91] F. Lamnabhi-Lagarrigue, A. Annaswamy, S. Engell, A. Isaksson, P. Khargonekar, Richard M. Murray, H. Nijmeijer, T. Samad, D. Tilbury, and P. Van den Hof. Systems control for the future of humanity, research agenda: Current and future roles, impact and grand challenges. *Annual Reviews in Control*, 43:1–64, 2017.

[92] M. Larsen and P. V. Kokotović. A brief look at the Tsypkin criterion: from analysis to design. *Int. J. Adapt. Control and Signal Processing*, 15(2):121–128, 2001.

[93] M. Lazar, W.P.M.H. Heemels, and A.R. Teel. Further input-to-state stability subtleties for discrete-time systems. *IEEE Transactions on Automatic Control*, 58:1609–1613, June 2013.

[94] J.H. Le and A. R. Teel. Passive soft-reset controllers for nonlinear systems. In *2021 60th IEEE Conference on Decision and Control (CDC)*, pages 5320–5325. IEEE, 2021.

[95] H. Li and R. M. Goodall. Linear and non-linear skyhook damping control laws for active railway suspensions. *Control Engineering Practice*, 7(7):843–850, 1999.

[96] J. Lofberg. YALMIP : a toolbox for modeling and optimization in MATLAB. In *2004 IEEE International Conference on Robotics and Automation*, pages 284–289, 2004.

[97] T. Loquen, S. Tarbouriech, and C. Prieur. Stability analysis for reset systems with input saturation. In *2007 46th IEEE Conference on Decision and Control*, pages 3272–3277. IEEE, 2007.

[98] C. Meissen, L. Lessard, M. Arcak, and A. K. Packard. Compositional performance certification of interconnected systems using admm. *Automatica*, 61:55–63, 2015.

[99] R. Middleton and J. Freudenberg. Non-pathological sampling for generalized sampled-data hold functions. *Automatica*, 31(2):315–319, 1995.

[100] R.H. Middleton. Trade-offs in linear control system design. *Automatica*, 27(2):281–292, mar 1991.

[101] J. Mokyr. The next age of invention: Technology's future is brighter than pessimists allow. *City Journal*, 24(1):12–21, 2014.

[102] A. Nagurney and D. Zhang. *Projected dynamical systems and variational inequalities with applications*, volume 2. Springer Science & Business Media, 2012.

[103] D. Nesic, A.R. Teel, and L. Zaccarian. Stability and performance of siso control systems with first-order reset elements. *IEEE Transactions on Automatic Control*, 56(11):2567–2582, 2011.

[104] D. Nešić, L. Zaccarian, and A.R. Teel. Stability properties of reset systems. *Automatica*, 44(8):2019–2026, 2008.

[105] D. Nešić, A.R. Teel, and P.V. Kokotović. Sufficient conditions for stabilization of sampled-data nonlinear systems via discrete-time approximations. *Syst. Control Lette.*, 38(4):259–270, 1999.

[106] D. Nešić, A.R. Teel, and E.D. Sontag. Formulas relating $\mathscr{KL}$ stability estimates of discrete-time and sampled-data nonlinear systems. *Syst. Control Lett.*, 38(1):49–60, 1999.

[107] N.Karbasizadeh and S. H.HosseinNia. Continuous reset element: Transient and steady-state analysis for precision motion systems. *Control Engineering Practice*, 126:105232, 2022.

[108] T. Oomen, M. van de Wal, and O. Bosgra. Design framework for high-performance optimal sampled-data control with application to a wafer stage. *International Journal of Control*, 80(6):919–934, 2007.

[109] T.A.E. Oomen, R.M.A. Herpen, van, S.J. Quist, M.M.J. Wal, van de, O.H. Bosgra, and M. Steinbuch. Connecting system identification and robust control for next-generation motion control of a wafer stage. *IEEE Transactions on Control Systems Technology*, 22(1):102–118, 2014.

[110] A. Pavlov, N. van de Wouw, and H. Nijmeijer. *Uniform output regulation of nonlinear systems: a convergent dynamics approach*. Springer Science & Business Media, 2006.

[111] R. Pintelon and J. Schoukens. *System identification: a frequency domain approach*. John Wiley & Sons, 2012.

[112] A.Yu. Pogromsky, W.P.M.H. Heemels, and H. Nijmeijer. On solution concepts and well-posedness of linear relay systems. *Automatica*, 39(12):2139–2147, 2003.

[113] A. Rantzer. On the Kalman—Yakubovich—Popov lemma. *Systems & control letters*, 28(1):7–10, 1996.

[114] R. T. Rockafellar and R. J. B. Wets. *Variational analysis*, volume 317. Springer Science & Business Media, 1997.

[115] N. Saikumar and H. Hosseinnia. Generalized Fractional Order Reset Element (GFrORE). In *European Nonlinear Dynamics Conference*, 2017.

[116] Y. Sam, J. Osman, and Ruddin M. Ghani, A. A class of proportional-integral sliding mode control with application to active suspension system. *Systems & control letters*, 51(3-4):217–223, 2004.

[117] R.G. Sanfelice, R. Goebel, and A.R. Teel. Generalized solutions to hybrid dynamical systems. *ESAIM: Control, Optimisation and Calculus of Variations*, 14(4):699–724, 2008.

[118] M. M. Seron and G. C. Goodwin. Sensitivity limitations in nonlinear feedback control. *Syst. Control Lett.*, 27(4):249–254, apr 1996.

[119] M.M. Seron, J.H. Braslavsky, and G.C. Goodwin. *Fundamental Limitations in Filtering and Control*. Communications and Control Engineering. Springer London, London, 1997.

[120] B. Sharif, D.W.T. Alferink, M.F. Heertjes, H. Nijmeijer, and W.P.M.H. Heemels. Analysis of sampled-data hybrid integrator-gain sytems: A discrete-time approach. *In prepration for journal submission*, 2022.

[121] B. Sharif, D.W.T. Alferink, M.F. Heertjes, H. Nijmeijer, and W.P.M.H. Heemels. A discrete-time approach to analysis of sampled-data hybrid integrator-gain systems. In *IEEE Conference On Decision and Control, Cancun, Mexico*, 2022.

[122] B. Sharif, M. Heertjes, H. Nijmeijer, and W.P.M.H. Heemels. On the equivalence of extended and oblique projected dynamics with applications to hybrid integrator-gain systems. In *American Control Conference (ACC) 2021, New Orleans, USA*, pages 3434–3439, 2021.

[123] B. Sharif, M.F. Heertjes, and W.P.M.H. Heemels. Extended projected dynamical systems with applications to hybrid integrator-gain systems. In *2019 IEEE Conference on Decision and Control (CDC)*, pages 5773–5778, 2019.

[124] B. Sharif, M.F. Heertjes, H. Nijmeijer, and W.P.M.H. Heemels. Extended projected dyanmical systems. *In preparation for journal submission.*

[125] B. Sharif, S.J.A.M. van den Eijnden, M. Beijen, S.P. Achten, H. Nijmeijer, W.P.M.H. Heemels, and M.F. Heertjes. A hybrid integrator-gain based bandpass filter for active vibration isolation with improved skyhook damping. *In Prepration for journal submission*, 2022.

[126] B. Sharif, A. van der Maas, N. van de Wouw, and W.P.M.H. Heemels. Filtered split-path nonlinear integrator: A hybrid controller for transient performance improvement. *IEEE Transactions on Control Systems Technology*, 2021.

[127] S. Skogestad and I. Postlethwaite. *Multivariable feedback control: Analysis and design*. John Wiley & Sons, 2001.

[128] Slotine and Li. *Applied nonlinear control*. 1991.

[129] E. D. Sontag. On the Input-to-State Stability Property. *European Journal of Control*, 1(1):24–36, 1995.

[130] E.D. Sontag. Smooth stabilization implies coprime factorization. *IEEE Transactions on Automatic Control*, 34(4):435–443, 1989.

[131] E.D. Sontag. *Mathematical control theory: deterministic finite dimensional systems*, volume 6. Springer Science & Business Media, 1990.

[132] G. Stein. Respect the unstable. *IEEE Control Systems Magazine*, 23(4):12–25, 2003.

[133] M. Steinbuch and M.L. Norg. Advanced motion control: An industrial perspective. *European Journal of Control*, 4(4):278–293, 1998.

[134] N. Strijbosch, E. Verschueren, K. Tiels, and T. Oomen. High precision sample positioning in electron microscopes. *Mikroniek*, 4:26–31, 2021.

[135] A. R. Teel. Continuous-time implementation of reset control systems. *Trends in Nonlinear and Adaptive Control*, pages 27–41, 2022.

[136] R. Tóth. APROCS-Automated linear parameter-varying modeling and control synthesis for nonlinear complex systems-erc. *Impact*, 2018(1):98–100, 2018.

[137] V. I. Utkin. Sliding mode control design principles and applications to electric drives. *IEEE transactions on industrial electronics*, 40(1):23–36, 1993.

[138] M. van de Wal, G. van Baars, F. Sperling, and O. Bosgra. Multivariable H_∞/μ feedback control design for high-precision wafer stage motion. *Control Engineering Practice*, 10(7):739–755, 2002.

[139] S. van den Eijnden, M. Heertjes (23277), W.P.M.H. Heemels, and H. Nijmeijer. Frequency-domain tools for stability analysis of hybrid integrator-gain systems. In *European Control Conference, Rotterdam, The Netherlands, 2021*, 2021.

[140] S. J. A. M. van den Eijnden. *Hybrid Integrator-Gain Systems: Analysis, Design, and Applications*. PhD thesis, Mechanical Engineering, June 2022. Proefschrift.

[141] S.J.A.M. van den Eijnden, M. Francke, H. Nijmeijer, and M.F. Heertjes. Improving wafer stage performance with multiple hybrid integrator-gain systems. *IFAC-PapersOnLine*, 53(2):8321–8326.

[142] S.J.A.M van den Eijnden, W.P.M.H. Heemels, H. Nijmeijer, and M. Heertjes. Stability and performance analysis of hybrid integrator-gain systems: A linear matrix inequality approach. *Nonlinear Analysis: Hybrid Systems*, 45:101192, 2022.

[143] S.J.A.M. van den Eijnden, M.F. Heertjes, W.P.M.H. Heemels, and H. Nijmeijer. Hybrid integrator-gain systems: A remedy for overshoot limitations in linear control? *IEEE Control Systems Letters*, 4:1042 – 1047, 2020.

[144] S.J.A.M. van den Eijnden, M.F. Heertjes, and H. Nijmeijer. Robust stability and nonlinear loop-shaping design for hybrid integrator-gain-based control systems. In *2019 American Control Conference*, pages 3063–3068. IEEE, 2019.

[145] S.J.A.M. Van den Eijnden, Y. Knops, and MF Heertjes. A hybrid integrator-gain based low-pass filter for nonlinear motion control. In *2018 IEEE Conference on Control Technology and Applications (CCTA)*, pages 1108–1113. IEEE, 2018.

[146] A. van der Maas, N. Van De Wouw, and W.P.M.H. Heemels. Filtered split-path nonlinear integrator (f-spani) for improved transient performance. In *American Control Conference 2017, Seattle (WA), USA.*, pages 3500–3505, 2017.

[147] A.J. van der Schaft and J.M. Schumacher. Complementarity modeling of hybrid systems. *IEEE Transactions on Automatic Control*, 43(4):483–490, 1998.

[148] D. van Dinther, B. Sharif, S. J. A. M. van den Eijnden, H. Nijmeijer, M. F. Heertjes, and W. P. M. H. Heemels. Overcoming performance limitations of linear control with hybrid integrator-gain systems. In *IFAC Conf. Anal. Design of Hybrid Systems (ADHS), Brussels, Belgium*, 2021.

[149] S.J.L.M. van Loon. *Hybrid control for performance improvement of linear systems.* PhD thesis, Mechanical Engineering, January 2016. Proefschrift.

[150] S.J.L.M. van Loon, K. Gruntjens, M.F. Heertjes, N. van de Wouw, and W.P.M.H. Heemels. Frequency-domain tools for stability analysis of reset control systems. *Automatica*, 82:101–108, 2017.

[151] S.J.L.M. van Loon, B. Hunnekens, W.P.M.H. Heemels, N. van de Wouw, and H. Nijmeijer. Split-path nonlinear integral control for transient performance improvement. *Automatica*, 66:262–270, April 2016.

[152] J. van Zundert, T. Oomen, J. Verhaegh, W. Aangenent, Duarte J. Antunes, and W. P. M. H. Heemels. Beyond performance/cost tradeoffs in motion control: A multirate feedforward design with application to a dual-stage wafer system. *IEEE Transactions on Control Systems Technology*, 28(2):448–461, 2020.

[153] A. Vidal and A. Banos. QFT-based design of PI+ CI reset compensators: application in process control. In *2008 Mediterranean Conference on Control and Automation*, pages 806–811. IEEE, 2008.

[154] L. Zaccarian, D. Nešić, and A. R. Teel. Analytical and numerical Lyapunov functions for SISO linear control systems with first-order reset elements. *International Journal of Robust and Nonlinear Control*, 21(10):1134–1158, 2011.

[155] L. Zaccarian, D. Nešić, and A.R. Teel. First order reset elements and the Clegg integrator revisited. In *2005 American Control Conference*, pages 563–568. IEEE, 2005.

[156] G. Zhao, D. Nešić, Y. Tan, and C. Hua. Overcoming overshoot performance limitations of linear systems with reset control. *Automatica*, 101:27–35, 2019.

[157] K.J. Åström and T. Hägglund. The future of PID control. *Control Engineering Practice*, 9(11):1163–1175, 2001.

List of publications

Peer-reviewed journal articles

- D.A. Deenen, B. Sharif, S.J.A.M. van den Eijnden, H. Nijmeijer, W.P.M.H. Heemels, and M.F. Heertjes. Projection-Based Integrators for Improved Motion Control: Formalization, Well-posedness and Stability of Hybrid Integrator-Gain Systems. *Automatica*, Volume 133, 109830, 2021.
- B. Sharif, A . van der Maas, N. van de Wouw, and W.P.M.H. Heemels. IEEE Transactions on Control Systems Technology 30(2), p. 451-463.
- B. Sharif, M.F. Heertjes, H. Nijmeijer, and W.P.M.H. Heemels. Extended projected dynamical systems. *In preparation for journal submission.*
- B. Sharif, D.W.T. Alferink, M.F. Heertjes, H. Nijmeijer, and W.P.M.H. Heemels. Analysis of sampled-data hybrid integrator-gain systems: A discrete-time approach. *Submitted for publication in journal.*
- B. Sharif, S.J.A.M. van den Eijnden, M. Beijen, S.P. Achten, H. Nijmeijer, W.P.M.H. Heemels, and M.F. Heertjes. A hybrid integrator-gain based bandpass filter for active vibration isolation with improved skyhook damping. *In prepration for journal submission.*
- A. Sadeghzadeh, B. Sharif , R.Tóth. Affine Linear Parameter-Varying Embedding of Nonlinear Models with Complexity Reduction and Minimal Overbounding. IET Control Theory & Applications, Volume 14, Issue 20, (2020) pp. 3363 – 3373.

Peer-reviewed articles in conference proceedings

- B. Sharif, M.F. Heertjes, and W.P.M.H. Heemels. Extended projected dynamical systems with applications to hybrid integrator-gain systems. In *2019 IEEE Conference on Decision and Control (CDC)*, Nice, France, pages 5773–5778, 2019.

- B. Sharif, M. Heertjes, H. Nijmeijer, and W.P.M.H. Heemels. On the equivalence of extended and oblique projected dynamics with applications to hybrid integrator-gain systems. In *2021 American Control Conference (ACC)*, New Orleans, USA, pages 3434–3439, 2021.
- D. van Dinther, B. Sharif, S. J. A. M. van den Eijnden, H. Nijmeijer, M. F. Heertjes, and W. P. M. H. Heemels. Overcoming performance limitations of linear control with hybrid integrator-gain systems. In *IFAC-Papers OnLine*, Volume 54, Issue 5, 2021, Pages 289-294.
- B. Sharif, D.W.T. Alferink, M.F. Heertjes, H. Nijmeijer, and W.P.M.H. Heemels. A discrete-time approach to analysis of sampled-data hybrid integrator-gain systems. In *2022 IEEE Conference On Decision and Control (CDC)*, Cancun, Mexico, pages 7612-7617, 2022.
- M.F. Heertjes, S.J.A.M. van den Eijnden, B. Sharif, W.P.M.H. Heemels, and H. Nijmeijer. Hybrid integrator-gain system for active vibration isolation with improved transient response. *IFAC-PapersOnLine*, volume 52, issue 15, pages 454–459, 2019.
- S.J.A.M. van den Eijnden, B. Sharif, M.F. Heertjes, and W.P.M.H. Heemels, Frequency-domain stability conditions for split-path nonlinear Systems, *in the 12th IFAC Symposium on Nonlinear Control Systems (NOLOCS)*, Canberra, Australia, 2023.
- M.F. Heertjes, S.J.A.M. van den Eijnden, and B. Sharif, An Overview on Hybrid Integrator-Gain Systems with applications to Wafer Scanners, *In 2023 IEEE International Conference on Mechatronics (ICM)*, Loughborough, UK, 2023.

Non peer-reviewed abstracts in conference proceedings

- B. Sharif, S.J.A.M. van den Eijnden, W.P.M.H. Heemels, H. Nijmeijer, M.F. Heertjes. Hybrid Integrator-Gain System for Active Vibration Control with Improved Transient Response, in *Book of Abstracts of* 38^{th} *Benelux Meeting on Systems and Control,* Lomel, Belgium, 2019.
- B. Sharif, M.F. Heertjes, W.P.M.H. Heemels. Extended Projected Dynamical Systems: A Framework for Analysis of Hybrid Integrator-Gain Systems, in *Book of Abstracts of* 39^{th} *Benelux Meeting on Systems and Control,* Elspeet, The Netherlands, 2020.
- B. Sharif, M.F. Heertjes, H. Nijmeijer, W.P.M.H. Heemels. Analysis of Sampled-Data Hybrid Integrator-Gain-Based Control Systems, in *Book of Abstracts of* 41^{st} *Benelux Meeting on Systems and Control,* Brussels, Belgium, 2022.

- B. Sharif, M.F. Heertjes, H. Nijmeijer, W.P.M.H. Heemels. Hybrid integrator-gain systems: An overview of some recent results, in Euspen special interest group meeting on precision motion systems & control, 's-Hertogenbosch, The Netherlands, 2022.

Acknowledgements

The completion of this dissertation marks the end of an important era in my life. I came to the Netherlands in August 2013 and ever since I have been, in one way or another, affiliated with TU Eindhoven (TUe). From 2013-2016 B.Sc. student in Electrical Engineering, 2016-2018 M.Sc. student in Electrical Engineering and 2018-present PhD candidate in Mechanical Engineering. For reasons of practicality I am going to focus on this last part (2018-present) but all these years are filled with memories the sweet ones of which were shared with amazing people, who also made the bitter ones surmountable. Throughout the past four years many people have enriched my life some of whom I would like to particularly mention.

Firstly, I would like to thank my promotors Marcel and Maurice who presented me with the opportunity to continue with a PhD after my M.Sc. studies and together formed a supervision team that any PhD candidate would be lucky to have.

Marcel, I still vividly remember the first talk I had with you in GEM Z -1.145. From this very first meeting you got me hooked on HIGS. Your enthusiasm and positive attitude never changed throughout these years and I really appreciate the freedom that you gave me in pursuing the research directions that interested me. I should also say that without a doubt you are one of the most humble people that I have come across in my life. Your investment in industry-relevant research while keeping the importance of theoretical soundness in mind, therefore not looking for shortcuts or aiming for low-hanging fruits, makes you a rather unique person in my opinion. During most of my time as a university student I was told about the gap between control in university and control in industry. Thanks to you, I did not feel the severity of this gap during my PhD. Indeed your mindset is what ensures that with the ever increasing complexity in the engineering systems around us, it is still safe to say " everything is under control ".

Maurice, for me it was easy to see why your work receives the attention that it does, after our very first meeting. The topics that we worked on together gave me a lot of energy and motivation and I thank you for presenting me with the opportunity to do so (not many people in the engineering community know about projected dynamical systems, variational inequalities etc...). Your enthusiasm, sharpness, easy-to-approach persona, and energetic attitude was essential in get-

ting things going at the earlier stages of my PhD and for this I am very grateful. I also really appreciate your investment in reading and providing me with detailed feedback on almost any document that I produced. Although deciphering them was sometimes a challenge, the impact they had on the quality of the work was immense.

All in all, I can not thank my promotors enough for all their support during the past four years. Working with you makes me feel privileged.

Next, I would like to thank my co-promotor. Henk, I was really happy when you joined Marcel and Maurice in the team of supervisors I had. Your view on things were at points truly eye opening. The alternative perspective that you provided on how I saw things was amazing and really taught me that sometimes it is necessary to take a step back and see how things tie together in the bigger picture. Our one-on-one discussions about your feedback on my drafts were an absolute pleasure and I really appreciate the time you allocated to doing this.

I also want to express my gratitude to Andy Teel, Luca Zaccarian, Siep Weiland and Hassan HossainNia, for both agreeing to be in my defense committee as well as taking the time to read and asses my thesis.

Next, I want to thank the members of the CLOC project for both the financial support of the project as well as the enjoyable user-committee meetings we had. A big shout out goes to our project partners in TU Delft, namely Hassan, Joost, Niranjan, Nima and Ali. I enjoyed both learning about your work as well as presenting my results to you during our meetings.

I would like to also thank Roland Tóth and Bahadir Saltik, working with whom as a master student convinced me of continuing with a PhD after completion of my M.Sc. studies.

The work presented in this dissertation has largely benefited from contributions made by wonderful master students whom I had the pleasure of co-supervising. Dorus, Sef and Dirk, you have all made your marks on this dissertation and I consider myself blessed for having the opportunity to be involved in your graduation projects. I know that I am far from an ideal supervisor but my shortcomings where made up for by your own hard work.

Next, it is time to thank all my (former) CST and D & C colleagues for creating a friendly yet intellectually stimulating atmosphere to work at. There are a few names that I would like mention in particular. Sven, Koen, Fahim, Frans, Sajad, Mohammad, Alex, and Wouter thank you for all the fun interactions and occasional chats during the coffee breaks. Rishi, thank you for the welcoming attitude and for the refreshing times we spent both inside and outside the university talking about/watching football. I know we are footballing arch rivals but that made our interactions even more fun. Koen (Scheres), it was great to get to know you in the last year of my PhD. I am sure if it was not for the Corona lockdown period, we would have known each other a lot sooner but , as the saying goes, better late than never. Thanks for all the interesting chats (about all sorts of things), the nice discussions and interactions both inside and outside of the university. Hadi,

I remember that you voluntarily came by our office on my first day to give me a tour and helped me familiarize myself with the group dynamics. I really appreciate this. Having you around as a fellow Iranian colleague was very nice at points and I truly enjoyed our interactions.

A big shout out goes to my (former) office mates at GEM Z -1.144 Chyannie, Tomas, Sebastiaan, Redmer, Ricky and Giannis. Chyannie, I was pleasantly suprised to see your familiar face on my first day in the office. It was a great joy to have you around and thank you for all the fun discussions, inviting me to the pub quizzes at the Irish pub and the occasional delicious vegan dishes you shared with us. Tomas, it was great to have one of my closest friends in the Netherlands also as an office mate. I enjoyed all our interactions including the delicious dinners, the hiking trips and the inside jokes about all sorts of things. I wish you all the best in completing your thesis and I am sure our friendship will outlive our time at the university. Ricky, having you as an office mate once a week was a great pleasure specially given that after the Corona period hardly anyone used to come to GEM Z -1.144. I enjoyed the talks about PhD life, the lunch walks and the stimulating discussions about various topics. I also really enjoyed our time at the CDC in Cancun. It is great that we are going to remain to be colleagues after you defend your PhD. I already look forward to our walks around the high tech campus. Redmer, you started your PhD in the second half of the last year of my time as a PhD candidate. Thanks for all the discussions in the office. Writing can sometimes be a boring task and your presence helped me in escaping this boredom (sorry if I talked too much at points). Your perspective on life outside the university was extremely useful. I also really enjoyed our conversations about Basketball. I wish you all the best with your journey as a PhD candidate and look forward to seeing your thesis in a few years from now. Giannis, having someone to discuss hardcore PDS literature with (aside from my promotors) was rather refreshing, albeit for a short while towards the end of my PhD journey. I also really enjoyed our conversations about politics and philosophy and look forward to the time when you move to Eindhoven where we could have more such interactions.

There is one last office mate who deserves a paragraph all to himself. Sebastiaan, as if my fantastic team of promotors were not enough for spoiling me, I was blessed with an outstanding HIGS sparring partner in you. Our conversations played a crucial role in shaping my thoughts and without our discussions many of the results in this dissertation would not have materialized as they did. Without any degree of exaggeration you have also produced what I think is the most complete PhD dissertation (fantastic theory and fantastic practice) that I have seen during my time at the university. I am also happy that we continue to be colleagues and look forward to our potential future collaborations.

A special mention goes out to Daniel (Deenen). Daniel, your great work on HIGS as an M.Sc. student lead to the initiation of not one but two PhD projects. This alone, shows how good you are as a researcher. Aside from our collaboration about HIGS and the hybrid systems and control course, which I really enjoyed, I

am grateful that you helped me in finding a position in industry that I am very excited about. I am very happy that we are going to be collaborating once more.

Nancy and Roos, thank you for all your support with the administrative side of things. I am sorry that we bugged you so many times with the water issue near our office. Hopefully it will not come back again.

There are also many people who made my life enjoyable outside of the university. Mahmood, Amin, Maryam, Hossein, Mahsa, Tomas, Fatima, Shah, Amirhossein, Mozhgan, Kolsoom, Arash, thank you all for the nice memories that we share.

True friendship is gem that is not easy to find. I sincerely thank Mr. Sheikholmolouki, Dr. Hedayat and Dr. Roushan for their lessons in true friendships and support during some of the toughest moments in my life.

I would like to thank my family for being there for me in all stages of my life. Baba and Maman, thank you for being the teachers anyone would be lucky to have in life. Baba, without your leadership, larger than life personality and life lessons I would not be where I am today. Maman, there is nothing I can say or do to make up for your unconditional love, support, and all the sacrifices that you have made over the years. Thank you for everything. Khashayar, when we left our home country, having you by my side made many struggles easier to surmount. Although I was born only minutes after you, you were truly the bigger brother that I needed in many occasions. I also want to thank my extended family, particularly my in-laws, for their love and support over the past years.

Last but certainly not least, Negar, my better half. You entered my life shortly before I started my PhD and your presence made my life a million times better. With you the joyful moments were much sweeter and I knew that I can count on your support and compassion during the tougher moments. Thank you for being there for me, giving me the best memories I have had in the past years, and for putting up with me during my (not so few) cranky moments. Having you in my life makes me feel blessed.

Bardia Sharif,
Eindhoven, February 2023.

About the author

Bardia Sharif was born on April 21, 1993, in Esfahan, Iran. After finishing high school, he studied Electrical Engineering at Eindhoven University of Technology (TUe), the Netherlands. After finishing his Bachelor of Science in Electrical engineering in 2016, he continued with pursuing a Master of Science degree in Electrical Engineering, at the same institution from which he graduated in 2018 (Cum Laude). During his Masters education, he specialized in systems and control, and performed his graduation project titled " Linear Parameter Varying Control of Nonlinear Systems", in the control systems group of the department of Electrical Engineering at TUe, under the supervision of Roland Tóth.

In October 2018, Bardia started his PhD research in the Control Systems Technology section, at the department of Mechanical Engineering of TUe, under the supervision of Marcel Heertjes, Maurice Heemels and Henk Nijmeijer. His research was part of the project "from PID to complex order control (CLOC)" and was funded by the Dutch research council (NWO). The research performed during his PhD was about a new class of control elements called Hybrid Integrator-Gain Systems (HIGS) and focused on mathematical formalization, analysis and sampled-data design of controllers containing HIGS. This dissertation contains the main results of his research.